Selective Hydrogenation of Butadiene with Carbon-Supported Palladium Catalysts

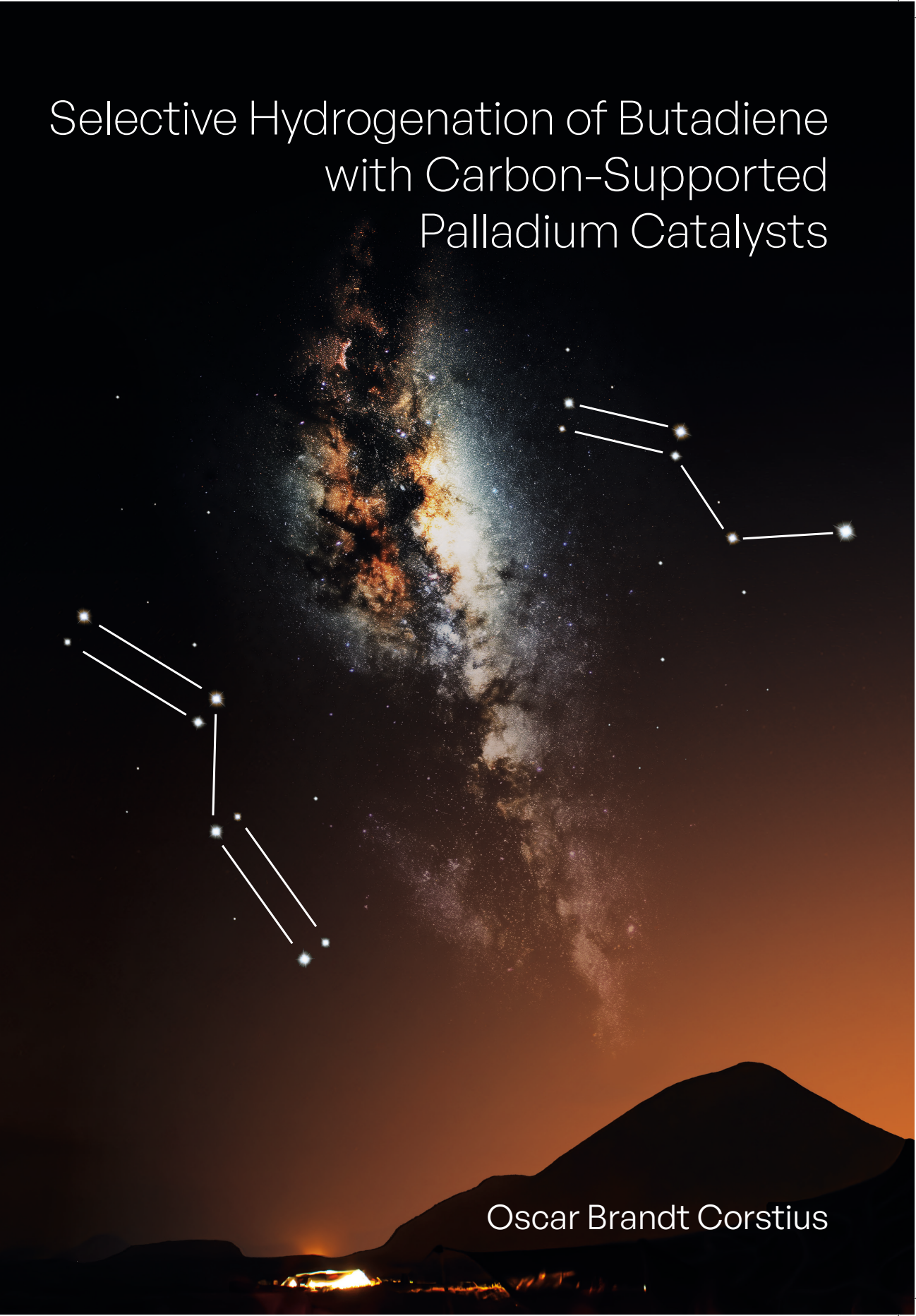

Oscar Brandt Corstius

Selective Hydrogenation of Butadiene with Carbon-Supported Palladium Catalysts

Oscar Brandt Corstius

PhD Thesis, Utrecht University
Author: Oscar Brandt Corstius
Title: Selective Hydrogenation of Butadiene with Carbon-Supported Palladium Catalysts
ISBN: 978-94-6483-900-5
DOI: 10.35540/2313
Cover design: Timo Wolf Kamp, persoonlijkproefschrift.nl
Printed by: Ridderprint, ridderprint.nl

Selective Hydrogenation of Butadiene with Carbon-Supported Palladium Catalysts

Selectieve Hydrogenatie van Butadieen met Koolstofgedragen Palladium Katalysatoren

(met een samenvatting in het Nederlands)

Proefschrift

ter verkrijging van de graad van doctor aan de
Universiteit Utrecht
op gezag van de
rector magnificus, prof. dr. H.R.B.M. Kummeling,
ingevolge het besluit van het college voor promoties
in het openbaar te verdedigen op

maandag 1 juli 2024 des middags te 4:15 uur

door

Oscar Ewoud Brandt Corstius

geboren op 1 juli 1996
te Amsterdam

Promotor:
Prof. dr. P.E. de Jongh

Copromotor:
Dr. J.E.S. van der Hoeven

Beoordelingscommissie:
Dr. M.F. Haase
Prof. dr. W.K. Kegel
Prof. dr. ir. L. Lefferts
Dr. M. Moret
Dr. C. Zlotea

This PhD thesis was financially supported by BP plc.

Table of Contents

Chapter 1

Introduction

1.1 Catalysis

Catalysis plays an indispensable role in our current and future everyday lives, the environment and the worldwide economy. Although catalytic processes have been used by humankind for centuries in, for example, sugar fermentation, the concept "catalysis" was first described by Berzelius in 1835 as: "Several compounds have the property to decompose and recombine the elements of which the compound itself remains indifferent".[1] This refers to the key property of a catalyst, which is to break apart molecules, and build different molecules out of the resulting atoms, without the catalyst itself being consumed. Since then, the field of catalysis has gradually grown in importance within chemistry and engineering, with close to 14% of the Nobel Prizes in Chemistry (and close to 20% of the laureates) awarded to catalyst-related findings.[2,3]

Catalysts are chemical accelerators: they increase the rate of chemical reactions, resulting in faster reactant decomposition and/or product formation and steer the selectivity within complex reactant mixtures towards specific products.[4] Catalysts are used in detergents, for the production of drugs and in everyday items (polymers such as plastics and cushion foam), in the generation of energy carriers such as liquid fuels, hydrogen and ammonia and in environmental applications such as exhaust catalysis. For instance, since the 1970s, legislation for sulphur dioxide and nitrogen-oxide emission (compounds leading to so-called "acid-rain") has spurred catalyst development for vehicle exhaust systems that were essential to mitigate emissions.[5] Today, every combustion engine-driven car is equipped with a catalytic converter to reduce harmful exhaust emissions. Hydrogen-powered vehicles also rely on the use of suitable electrolysis and fuel cell (electro)catalysts. More recently, catalytic processes are being developed to convert captured CO_2 into valuable chemicals in an effort to contribute to CO_2 circularity.[6–8]

It is estimated that 40% of the global gross domestic product (GDP, $104 trillion in 2023[9]) is directly related to catalysis or catalytic processes.[10] The major contribution is in the large-scale production of fuels and chemicals since 90% of chemical transformations are performed with the aid of a catalyst.[11] Heterogeneous catalysis, defined as a process where the reactant material and the catalyst are in different phases, is the backbone of the chemical industry. Typically, heterogeneous catalysts are solids such as extrudates containing supported metal nanoparticles, whereas the reactants and products are gas-phase or liquid-phase, which enables facile catalyst separation from the products.

1.2 Selective hydrogenation

1.2.1 Applications

One example of a (catalysed) chemical conversion is the hydrogenation of unsaturated molecules. Here, molecular hydrogen (H_2) is added to compounds which have one or more unsaturated bonds (*e.g.,* C=C bonds), which increases their saturation with H-atoms. Several hydrogenation processes, such as ammonia (NH_3) synthesis, CO hydrogenation, paraffin production and hydroconversion are carried out on a global scale for the production of fertilisers, chemical building blocks and fuels. Hence, it is not surprising that it is estimated that a quarter of all chemical transformations require at least one hydrogenation step.[12]

Selective hydrogenation means that a specific functional group or reactant is targeted while others are left untouched.[12,13] Examples of relevant selective hydrogenation processes are the semi-hydrogenation of alkynes or alkadienes to alkenes, the partial hydrogenation of α,β-unsaturated ketones or aldehydes to unsaturated alcohols and the selective hydrogenation of substituted nitro-arenes (Figure 1.1). These reactions are relevant for the industrial production of fine chemicals[14], food additives, flavours, fragrances and pharmaceuticals[15].

A large-scale application of selective hydrogenation is the semi-hydrogenation of polyunsaturated hydrocarbons (*e.g.,* alkynes or alkadienes) for the purification of alkenes, such as ethylene, propylene and butenes.[16] These alkenes (light olefins) are chemical building blocks for the production of polymers (plastics) with applications varying from low-cost plastic wraps ("cling film", low-density polyethylene) to flexible construction piping (poly(1-butene)).

Typically, alkenes are produced by steam cracking of an oil fraction such as the naphtha fraction (C5-C12). Under the harsh conditions in the steam cracker (>800 °C)[17,18], polyunsaturated molecules are generated in addition to the desired alkenes. These alkyne or alkadiene impurities, typically present in concentrations below 1 vol%, must be removed from the alkene feedstock to prevent deactivation of the polymerisation catalyst in the downstream process. Moreover, molecules with more than one

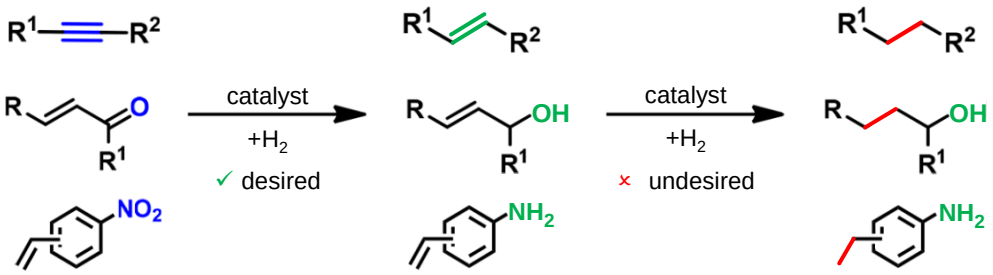

Figure 1.1. Examples of selective hydrogenation. Top to bottom: selective hydrogenation of alkynes, α,β-unsaturated ketones and nitro-arenes. Adapted from reference 12.

unsaturated carbon-carbon bond can induce branching of the polymer product, which can be detrimental to the quality of the specific polymer product and application. Therefore, a selective hydrogenation step of the alkene-rich feedstock is essential for the polymerisation industry, which produced over 400 megatons of polymer products in 2022.[19]

In selective hydrogenation or semi-hydrogenation, the reactant molecules are hydrogenated to only form alkenes. The undesired complete hydrogenation is referred to as over-hydrogenation. In this purification process, the conversion of polyunsaturates should be very high so that a minimum amount of the impurities remains in the alkene feed. Examples are the removal of acetylene from ethylene, propyne/propadiene from propylene, and butyne/butadiene from butene, as well as butadiene removal from acetylene-rich feeds.[16] Importantly, the process should be very selective since unselective hydrogenation of the alkene products or feed will lead to loss of alkenes. Hence, a challenging balancing act is required during operation: reaching near-complete conversion without over-hydrogenation.

1.2.2 Industrial considerations

The removal of polyunsaturated hydrocarbons by selective hydrogenation is performed either by so-called “front-end” or “tail-end” operation, which refers to the position of the selective hydrogenation reactor with respect to the de-methaniser unit.[16,20,21] The two industrial routes are schematically depicted in Figure 1.2.[22,23] In both cases, an alkene-rich feed is produced from cracking a carbon-containing source. After the steam cracker, a mixture of hydrocarbons (HCs), CO and H_2 is obtained. The mixture is fed either directly into the selective hydrogenation reactor (front-end) or first in a de-methaniser unit (tail-end). In the de-methaniser, the lightest molecules (CH_4, CO, H_2) are removed from the mixture by distillation. Therefore, in front-end conditions, the polyolefin-olefin mixture contains a large excess of H_2 and high CO concentration (Table 1.1). In tail-end operation, lighter elements are removed, and the H_2 and CO concentrations are controlled by external feeding to the selective hydrogenation reactor. This facilitates the operation at a low H_2:C_xH_y ratio, typically close to unity, which limits over-hydrogenation.

Both front-end and tail-end operations have advantages and disadvantages. Front-end conditions favour a high activity due to the high hydrogen-to-hydrocarbon ratio, but prevention of over-hydrogenation and thermal runaway is more challenging. In tail-end operation, the amount of hydrogen fed into the reactor is lower (Table 1.1) and can be externally controlled, leading to less over-hydrogenation. However, more oligomers and coke deposits are formed during tail-end operation, resulting in lower stability of the catalyst. In short, tail-end operation can be better controlled but is slower and requires more frequent regeneration of the catalyst, increasing the energy intensity of

Table 1.1. Typical gas composition and operation conditions for selective hydrogenation.

Parameter	Unit	Tail-end	Front-end	Utrecht
Polyunsaturated hydrocarbon (HC)	mol%	2.0	0.2	0.3
Excess alkene	mol%	71	37	30
Hydrogen	mol%	2.4	22	20
Alkanes	mol%	25	40	-
CO	ppm	40	2 800	-
H_2/polyunsaturated HC ratio	[-]	1.5	110	67
Pressure	bar	20	35	1.0
Temperature	°C	60	70	20-250
Space velocity	$m^3\ m_{cat}^{-3}\ h^{-1}$	3 000	2 000	20 000

the process.[24] Hence, the front-end route is advantageous concerning lower energy consumption, less catalyst and longer catalyst lifetime.[25,26] From an academic point of view, the challenge of retaining good selectivity in hydrogen excess is interesting to study. Therefore, the research described in this thesis concerns selective hydrogenation under typical front-end concentrations, with 20% hydrogen and a 100-fold alkene excess (Table 1.1). For simplification of the reaction mixture, no CO is introduced into the reactor, which will affect the activity and the selectivity of the catalysis. Another noteworthy distinction in reaction conditions lies in the pressure. Under industrial conditions, the high pressure results in a partial condensation of the reactants and

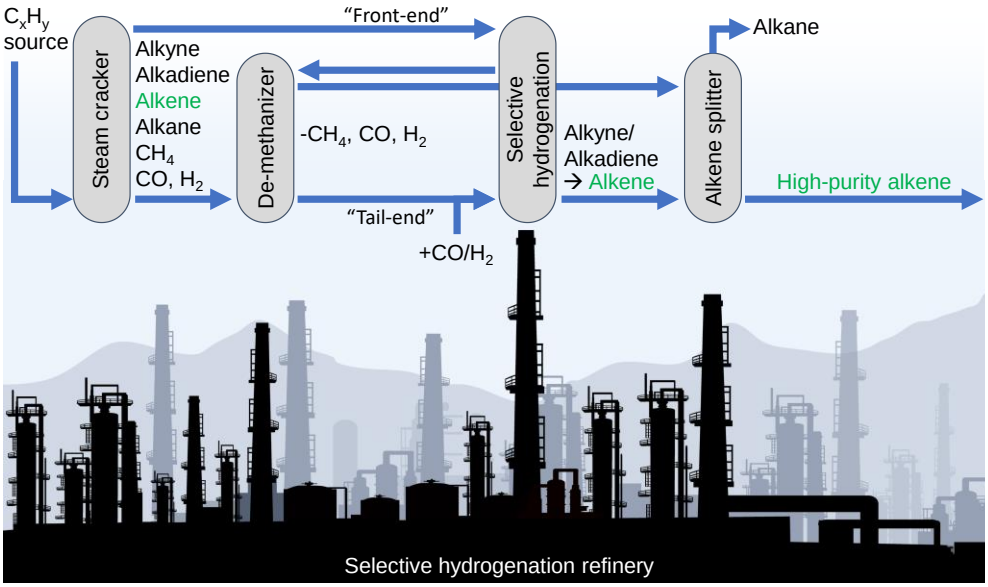

Figure 1.2. Schematic overview of reaction steps used in a typical selective hydrogenation refinery. Two routes are depicted for the production of high-purity alkenes, by either front-end or tail-end operation.

products in the micropores of the catalysts. In contrast, our laboratory testing conditions maintain entirely gaseous reactants at atmospheric pressure.

1.3 Butadiene hydrogenation

This thesis focuses on one specific step in the refinery processes, which is the removal of 1,3-butadiene (butadiene hereafter) impurities. Butadiene is a reactant of specific interest since it is the main impurity in butenes feedstocks (C_4-hydrocarbons). Also, in C_2-rich hydrocarbon feeds (acetylene/ethylene mixture), butadiene is an undesired impurity since it can react with acetylene to form coke deposits, which decrease the activity and stability of the catalysts.[16,27–29] Interestingly, semi-hydrogenation of butadiene leads to different butene isomers, namely 1-butene, trans-2-butene and cis-2-butene. Therefore, not only reactant selectivity (alkadiene *vs* alkenes) but also product isomer selectivity is of relevance. Hydrogenation of butadiene is both industrially important, as well as a suitable model reaction to investigate catalyst performance regarding both activity and selectivity.[30] For polymer (plastic) production, 1-butene is highly favoured since it is the only butene-isomer that can produce a high molecular weight polymer. Moreover, high-purity 1-butene has value as an additive in the growing market of linear low-density polyethylene (LLDPE), which contains 4 to 10 wt% 1-butene.[16,31,32]

1.3.1 Thermodynamics

Butadiene removal from an excess of propylene has been the subject of academic publications over the past decade.[33–38] The different chain lengths of the polyunsaturated impurity (butadiene) and desired alkenes (propylene) facilitate the distinction between direct over-hydrogenation (n-butane) and alkane (propane) formation side reactions. Figure 1.3 depicts the possible reaction paths from butadiene and propylene and the reaction enthalpies and entropies. Under typical hydrogenation conditions, all hydrogenation steps are spontaneous ($\Delta G<0$) and exothermic ($\Delta H<0$), with a slight entropy loss ($T\Delta S<0$).[39] From Figure 1.3, it is evident that butane and propane are more stable than butene and propene. Therefore, butadiene hydrogenation has to be favoured, but butene hydrogenation has to be kinetically limited by the use of an appropriate catalyst to achieve high selectivity. Removing 0.3% butadiene from a 100-fold excess of propylene (typical front-end concentrations, Table 1.1) is like catalytically removing a needle from a haystack, while thermodynamically, the exothermic hydrogenation is like trying to burn selectively a match that is located in a haystack, without setting the whole “propylene haystack” on fire (thermal runaway).

The semi-hydrogenation of butadiene can yield three butene isomers: 1-butene, trans-2-butene and cis-2-butene. The Gibbs free energies of formation of these isomers from butadiene are similar (ΔG=-79 to -86 kJ/mol at 25 °C).[39,40] Trans-2-butene is the

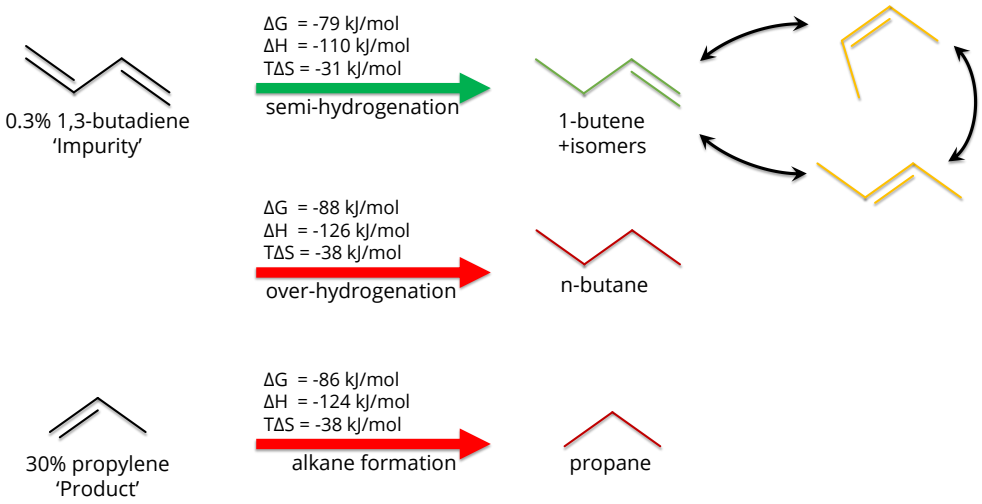

Figure 1.3. Reactant and products during the selective hydrogenation of butadiene from an excess of propylene. Values above the arrows indicate the change in Gibbs free energy (ΔG), the heat of reaction (ΔH) and the entropic change (ΔS) for hydrogenation of each reactant, obtained at 298 K and 1 bar from HSC Chemistry 9 software.[39]

most stable isomer (lowest ΔG) and has a thermodynamically expected fraction above 50% up to 200 °C (Figure 1.4A), followed by cis-2-butene, whereas 1-butene is the least stable isomer (roughly below 10%). Interestingly, 1-butene has the highest entropy (less negative ΔS), increasing its stability with increasing temperature. The ratio of the 2-butene isomers is temperature dependent (Figure 1.4B) and varies from *ca.* 1.7 *trans:cis* 2-butene ratio at 25 °C to 1.4 at 200 °C.

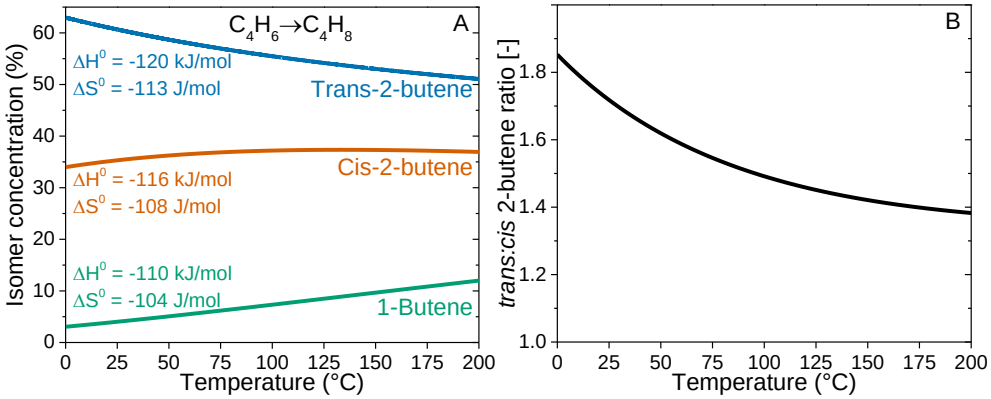

Figure 1.4. Thermodynamic equilibria of butene-isomers. Composition calculated with HSC Chemistry 9 at 1 bar.[39] (A) Values of ΔH and ΔS for the butadiene semi-hydrogenation towards the three butene-isomers at 25 °C are listed, showing the butene isomer composition as a function of the temperature. (B) The 2-butene *trans:cis* ratio as a function of the temperature.

1.3.2 Hydrogenation mechanism

Hydrogenation of unsaturated hydrocarbons over metal surfaces generally occurs via the so-called "Horiuti–Polanyi" mechanism.[41] Molecular hydrogen is dissociatively adsorbed onto the metal surface. The unsaturated hydrocarbon is adsorbed onto the metal surface, and hydrogen atoms are added to the C=C bond in a successive manner. In Figure 1.5, this is visualised for the shortest alkene, ethylene.[42] The fundamental steps include the adsorption of ethylene, successive H-insertion and desorption of ethane. In this example, the addition of deuterium (red atoms) is depicted to differentiate between the pristine hydrogen atoms of ethylene (green atoms) and the atoms added by saturation of the hydrocarbon.

The number of possible reactions increases for longer hydrocarbons, such as depicted for butadiene in Figure 1.6.[22] At room temperature, gaseous butadiene can be present in two conformations: the most stable S-*trans*-1,3-butadiene form (*Anti*, 95%) and the S-*cis*-1,3-butadiene form (*Syn,* 5%).[43,44] The hydrogenation pathway of butadiene over metal surfaces was investigated in the 1960s by Wells and co-workers, who identified two main routes for hydrogenation.[45–49] Because of the high concentration in the gas phase, predominantly the *trans*-configuration of butadiene will be present on the metal surface, resulting in Route I as the dominant pathway for hydrogenation. Following the Horiuti-Polanyi mechanism, the hydrocarbon is hydrogenated by sequential addition of two H-atoms (steps 1 and 2). The first H-addition to the adsorbed butadiene molecule is to either of the C=C bonds in the symmetrical adsorbed butadiene molecule (step 1).

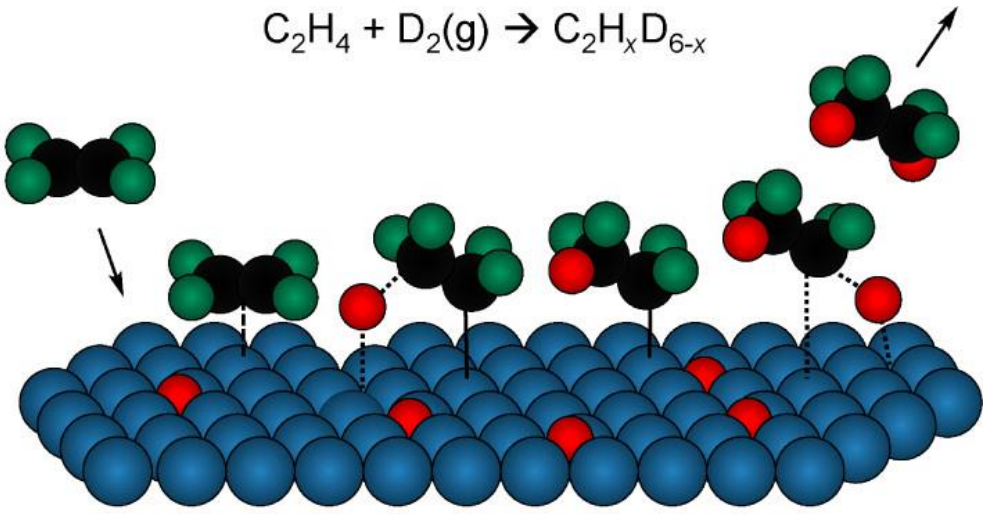

Figure 1.5. Schematic hydrogenation (deuteriation) of ethylene over metal surface. Metal atoms are blue, carbon atoms are black, hydrogen atoms are green, and deuterium atoms are red. Reprinted with permission from reference 42. Copyright 2013 American Chemical Society.

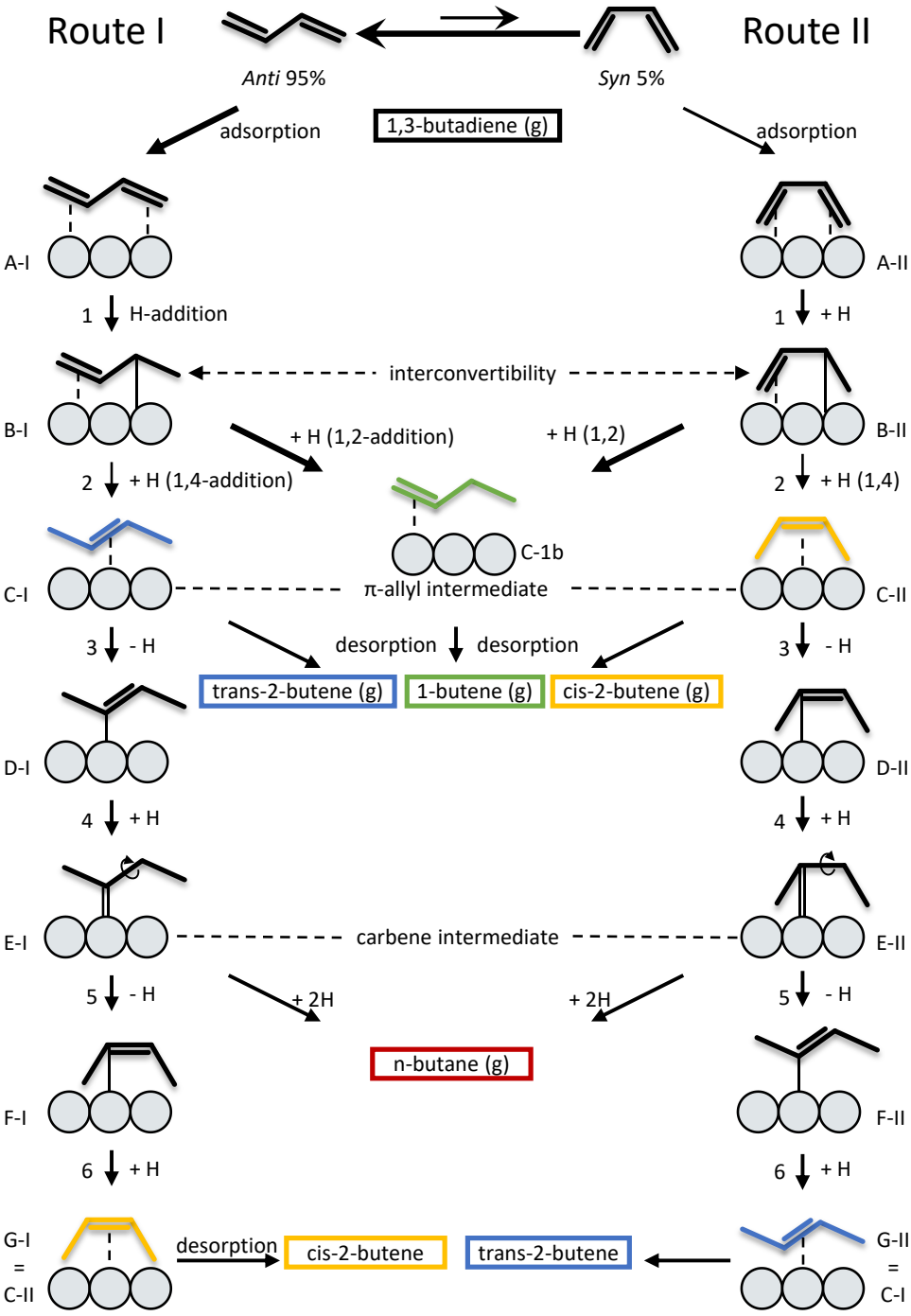

Figure 1.6. Pathway for hydrogenation of butadiene towards different products. H-atoms are omitted from the line structures for clarity. Single dashed, solid and double solid lines represent π-, σ-bond and carbene-bond to the metal atoms (grey circles), respectively.

The second H-addition, in part, determines the selectivity of the reaction. If 1,2-addition is preferred, 1-butyl intermediate (C-1b) will be formed, which yields gaseous 1-butene as a product when desorbed from the metal surface. 1,4-addition will generate 2-butyl intermediates (C-I and C-II) and 2-butene products. The ratio of 1-butenes to 2-butenes, as well as the *trans:cis* ratio in the 2-butene products, is dictated by the ratio of the π-alkyl intermediates. Wells *et al.* concluded that the product selectivity of a metal can be explained as follows: if the metal (such as is the case for Pt and Rh) allows interconversion between B-I and B-II species (indicated by the dashed arrow), a *trans:cis* 2-butene ratio close to thermodynamic equilibrium (Figure 1.4B) is found.[48] The absence of interconversion (*e.g.,* on Pd) is associated with high *trans:cis* ratios, close to the a*nti:syn* ratio of gaseous butadiene.

Later, Boitiaux *et al.* proposed a novel interpretation of the mechanism.[50–53] They postulated that interconversion is, in fact, slow on all metals. Rather, the formation of a carbene intermediate (E-I or E-II in Figure 1.6) is a precursor for lower *trans:cis* ratios and more butane formation.[53] The carbene intermediate allows skeletal isomerisation (step 5) of adsorbed 2-butenes. Moreover, this carbene is susceptible to further hydrogenation, yielding n-butane as a product. Hence, over metals where the carbenes are formed (Pt and Rh), the product selectivity for butadiene hydrogenation will shift towards more n-butane formation and lower trans-2-butene concentration. This correlation was substantiated by experimental results for Ru, Rh, Pd, Os, Ir and Pt catalysts.[53]

1.4 Carbon-supported Pd nanoparticle catalysts

1.4.1 Pd in selective hydrogenation reactions

High surface-area metals, such as Raney nickel[54], Pd- and Pt-black and the Pd-based Lindlar catalyst[55], are widely used for (selective) hydrogenation reactions in industrial applications. For the hydrogenation of 1,3-butadiene, metal powder catalysts of platinum-group-metals (PGMs: Ru, Rh, Pd, Os, Ir, Pt)[45,46,48], base-metal (Fe, Co, Ni)[47] and coinage metals (Cu, Ag, Au)[47,56,57] have been investigated. The PGM catalysts show higher activities than the base and coinage metal catalysts and require lower temperatures for hydrogenation, for example, 200 °C for Fe and 0 °C for Pd.[45,47] Of the PGMs, Pd is the most active for butadiene hydrogenation, while at the same time, it shows the highest selectivity to olefins.[45] Other metals such as Pt and Rh show lower selectivities, with the formation of n-butane even at low conversions.[58] This substantiates the mechanism postulated by Boitiaux (Figure 1.6), for which Pt and Rh yield low *trans:cis* 2-butene ratios and initial n-butane formation, whereas Pd does not form carbene intermediates and hence shows no initial n-butane formation and high (>10) *trans:cis* ratios.

Supported nanoparticle catalysts of many of these metals have also been tested in the selective hydrogenation of butadiene traces from an excess of propylene, in line with typical industrial conditions.[34–37,59–63] The coinage metals show good selectivities towards butene. The surface averaged activity, expressed as turnover frequency (TOF) at 120-125 °C was 0.2×10^{-3}, 4×10^{-3} and 6×10^{-3} $mol_{butadiene}\ mol_{metal,surface}^{-1}\ s^{-1}$ for Ag, Au and Cu, respectively.[37,63] Lucci *et al.* demonstrated that a combination of Cu with Pt in the dilute regime (1:140 Pt:Cu ratio) showed good selectivity and stability for selective butadiene hydrogenation, although relatively high temperatures were required (160 °C).[34]

In this thesis, we focus on Pd-based (both monometallic and bimetallic) metal nanoparticles. Monometallic Pd is highly active, with a TOF of 1-10 s^{-1} at 40-47 °C, while retaining nearly 100% butene selectivity up to almost complete butadiene removal (*e.g.,* 90% conversion).[35,64] Its unique combination of activity and selectivity for the hydrogenation of polyunsaturated hydrocarbons makes Pd the most investigated and industrially applied metal candidate for selectivity hydrogenation reactions.[12,16,20,57,65] The high activity of Pd can also be problematic for retaining the selectivity. Especially near complete butadiene conversion (*e.g.,* >90% conversion), achieving high semi-hydrogenation selectivity is challenging, as alkane formation is reported.[20] In an effort to combine the activity of Pd with the selectivity of coinage metals, bimetallic PdAu, PdAg and PdCu are investigated.

During selective hydrogenation reactions, *i.e.,* in the presence of H_2 and hydrocarbons, monometallic Pd can potentially form both Pd hydrides (PdH_x) and Pd carbides (PdC_y).[23,65] Both phases are known to affect the catalytic performance of Pd.[23,66] The formation of β–PdH_x increases the activity but also leads to lower selectivity, whereas surface-H leads to more selective semi-hydrogenation.[66] Under ambient reaction conditions (298 K, 0.2 bar H_2), macrocrystalline Pd forms β-PdH_x up to a H content of x=0.6, which is stable up to ~60 °C.[67,68] Pd-carbide formation increases the selectivity by inhibiting the formation of bulk hydrides.[23,66] PdC_y (up to y=0.13) can form upon exposure to unsaturated hydrocarbons, especially for smaller alkynes (*e.g.*, acetylene) and to a lesser extent, for alkenes or larger molecules (*e.g.,* butadiene).[69,70] The surface carbides decompose in the H_2 atmosphere at 100 °C, while the bulk carbides remain stable under selective hydrogenation conditions.[71] Dilution of Pd in another metal limits the formation of β–PdH_x, which increases the selectivity.[20]

1.4.2 Hydrocarbon adsorption

Hydrocarbon adsorption and desorption are essential steps in selective hydrogenation, and hence, the adsorption strength of the reactant and product molecules is of great importance. In the literature, using density functional theory (DFT), the adsorption modes of relevant hydrocarbon molecules for butadiene hydrogenation on Pd surfaces were calculated and they are depicted in Figure 1.7. On Pd(111)[72], trans-butadiene

adsorbs most strongly with 1,2,3,4-tetra-σ binding on a Pd-tetramer, where each of the four carbon atoms is bound to a different Pd atom. Adsorption of cis-butadiene is slightly less exothermic (-1.60 eV *vs* -1.72 eV) and coordinates to three Pd atoms. Interestingly, the cis-butadiene geometry allows for the coordination of both C=C bonds to the same Pd surface atom, which is more likely on sites with lower coordination, such as corners. For nanosized Au, such a geometric effect was demonstrated, where cis-2-butene was preferentially formed on corner and edge sites through Route II of Figure 1.6.[73] In their optimal binding mode on Pd(111), both cis- and trans-butadiene are bound parallel with respect to the metal surface. When only one C=C bond of butadiene is coordinated to the surface, as depicted in Figure 1.7C, a considerably lower adsorption strength is found (-0.94 eV). The large difference in the tetra- and di-σ binding of trans-butadiene indicates that on extended Pd(111) planes, almost all butadiene molecules are bound flat on the surface.

Butenes (1-butene, trans-2-butene and cis-2-butenes) all adsorb in a similar manner and with a similar adsorption energy, as the olefins are di-σ bound to two adjacent Pd atoms with both carbon atoms of the C=C bond. DFT predicts that 1-butene is the most stable butene-isomer on a Pd(111) surface (-0.90 eV), followed by cis-2-butene (-0.77 eV) and trans-2-butenes (-0.72 eV), resulting in a higher product selectivity to 1-butene.[72] The di-σ configuration of the olefins is favoured over the di-π configuration (C=C bound to one Pd atom) by *ca.* -0.12 eV.[72] For propylene, similar reported adsorption strengths were found on Pd(111), between -0.73 and -0.75 eV.[38,74] In contrast, the saturated alkanes (propane and butane) bind very weakly, with an enthalpy close to zero (-0.02 to -0.07 eV).[74–76]

The large difference in adsorption energy between butadiene and the alkenes allows a high selectivity to butene products during butadiene hydrogenation, as the strongly adsorbing butadiene effectively blocks propylene from adsorbing onto the surface. Moreover, butadiene replaces the butene products as soon as they are formed on the surface, decreasing the butene residence time on the metal surface and resulting in little over-hydrogenation to butane. The formation of alkanes will occur only when the butadiene concentration near the Pd surface is low.

Figure 1.7A-F depicts geometries calculated on Pd(111), which has the lowest surface energy surface of Pd and, hence, the highest facet abundance for Pd nanoparticles.[77] However, nanoparticles expose various facets, also depending on size.[78–80] Moreover, the surface of smaller nanoparticles will contain more sites with lower coordination (*e.g.,* edge- and corner-sites) and less extended terraces. Because of the lower coordination of the Pd atom in these sites, the interaction with the reactants is different on a stepped surface, such as Pd(211).

For the alkenes, the adsorption strength on Pd(211) was calculated slightly higher than on Pd(111) (-1.01, -0.88 and -0.95 eV for 1-butene, trans-2-butene and propylene).[74,75]

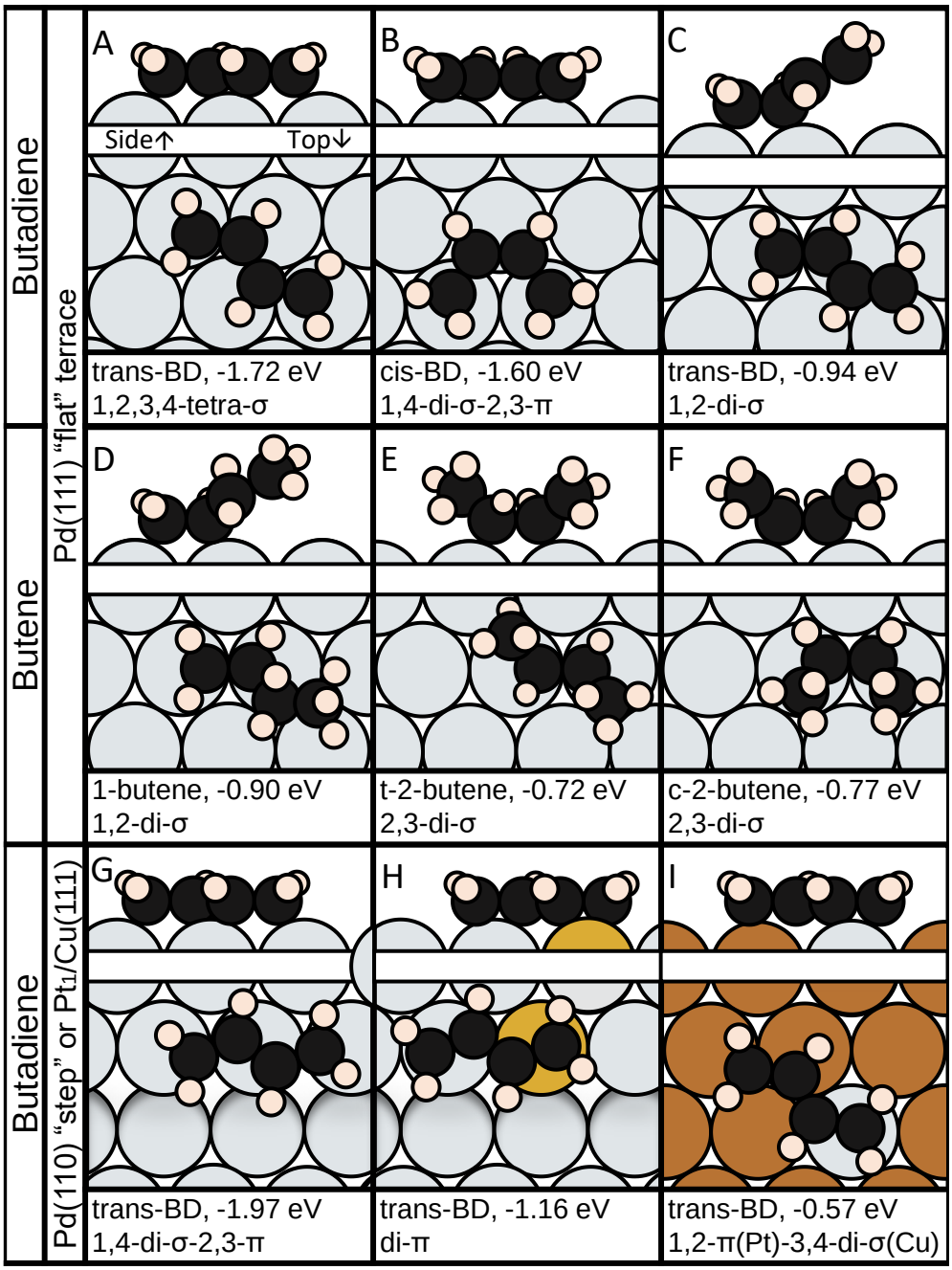

Figure 1.7. Hydrocarbon binding geometries on Pd. Adsorption modes of (A-C) butadiene ("BD") and (D-F) butene-isomers on Pd(111).[72] (G-I) Adsorption of butadiene on "stepped" (G) Pd(110), (H) $Au_1Pd(110)$ and (I) $Pt_1Cu(111)$ surface.[28,75,83] Depicted geometries show the most stable biding mode (except for C, see main text). Corresponding adsorption enthalpy is given in eV. Black, light-orange, grey, gold and copper colours represent C, H, Pd, Au and Cu atoms.

For trans-butadiene, an adsorption enthalpy of -1.94 eV was calculated on the Pd(211), similar in energy and mode as Pd(110) (1.97 eV, Figure 1.7G), and indicating stronger interaction than on Pd(111) (-1.72 eV).[28,81] On these corrugated surfaces, trans-butadiene binds to three adjacent (linear) Pd atoms, different than on a flat Pd(111) tetramer (Figure 1.7A).

The increased adsorption strength of the hydrocarbons on Pd(211) edge sites, compared to Pd(111), suggests a particle-size dependence where smaller nanoparticles with more edge-sites bind the reactants more strongly than larger nanoparticles with extended terraces. However, these calculations consider a single molecule on an infinite plane, whereas in reality, Pd ensembles are finite in size. For butadiene, smaller Pd ensembles do not facilitate the most stable configuration, where the hydrocarbon is bound to 3 or 4 Pd atoms. Hence, part of the butadiene will bind to only one or two Pd atom(s), significantly lowering adsorption energy. For example, for the di-σ binding onto lower coordinated geometries, such as corners or small edges, the adsorption enthalpy of butadiene (-0.94 eV, Figure 1.7C) is closer to that of the butenes (-0.88 to -1.01 eV) and propylene (-0.95 eV) on Pd(211).[74] Hence, on small nanoparticles, butadiene adsorption is more competitive with butenes and propylene compared to on large particles with extended surfaces.

The adsorption of reactants strongly depends on the specific metal, as described in detail for Pd in the paragraph above. On some other metals, hydrocarbons bind more weakly, such as for butadiene on Au(111) (-0.42 eV) or Cu(111) (-0.34 eV).[38,82] When one Pd atom in Pd(110) was replaced with a Au atom, a significant decrease in adsorption energy was calculated, from -1.96 eV for Pd(110) to -1.16 eV for Au_1/Pd(110) (Figure 1.7G-H). Reduction of the Pd concentration in bimetallic alloys down to the single atom limit further decreased the hydrocarbon adsorption enthalpy.

Unfortunately, no DFT calculations were found in the literature that describe the interaction of butadiene with isolated Pd atoms in coinage host metals. There are, however, reports on the butadiene hydrogenation over isolated Pt_1/Cu(111).[34,82,83] For an isolated Pt atom diluted in a Cu(111) host, adsorption enthalpies of -0.57 eV were found for butadiene (Figure 1.7I).[83] Because only one C=C bond is coordinated to the Pt atom, similar adsorption energies were found for 1-butene, trans-2-butene and cis-2-butene over Pt_1/Cu(111) (-0.51, -0.28 and -0.39 eV, respectively). Note that these interactions are 1.1 eV weaker than on Pt(111) for butadiene and *ca.* 0.5 eV for the butenes.[72] Similar values were obtained for the interaction of butadiene with isolated Pd on a bare carbon (graphene) support, which showed -0.57 eV for butadiene and -0.48 eV for 1-butene.[84]

These trends were also observed for alkyne adsorption, as isolated Pd atoms resulted in adsorption energies that were much weaker than monometallic Pd and closer to the interaction of the coinage hosts.[83,85–91] Interestingly, the hydrocarbon adsorption depended on the Pd ensemble size, as dimer and trimers showed higher adsorption strength compared to isolated Pd.[82,87] For example, Pt_2/Cu(111) showed an adsorption

enthalpy for butadiene of -0.78 eV, where both C=C bonds can coordinate to a Pt site. For the butenes, with only one C=C bond, similar adsorption enthalpies as on Pt-monomers were calculated (-0.49, -0.25 and -0.32 eV for 1-butene, trans-2-butene and cis-2-butene). However, the Pt-dimers showed weaker adsorption than when coordinated to two Pt atoms in Pt(111). This shows hydrocarbon adsorption depends on geometric effects such as ensemble size. Alloying Pd induces electronic effects associated with a shift of the d-band centre away from the Fermi level, which also contributes to reduced adsorption energy.[92]

1.4.3 Hydrogen activation

In addition to hydrocarbon adsorption, the activation of molecular hydrogen (H_2) is essential. The hydrogen adsorption energies show similar trends as for the hydrocarbon adsorption energies: Pd binds H_2 more exothermically than the coinage metals (+0.47, -0.09 and -0.79 eV on Au, Cu and Pd(111) surfaces respectively), but weaker than hydrocarbons, discussed in the previous section.[93] For Pd-alloys, the hydrogen adsorption is always weaker than on monometallic Pd and increases in strength with Pd ensemble size.[87,94,95] Also, the activation energy of hydrogen dissociation is of importance for the hydrogenation activity.[90,91] The activation barrier for dissociative adsorption of H_2 on monometallic Pd is negligible.[33,96] Isolated Pd in Au(111) or Cu(111) shows slightly higher activation energies of 0.20 and 0.02 eV, which is considerably lower than on monometallic Au(111) or Cu(111) (1.04 and

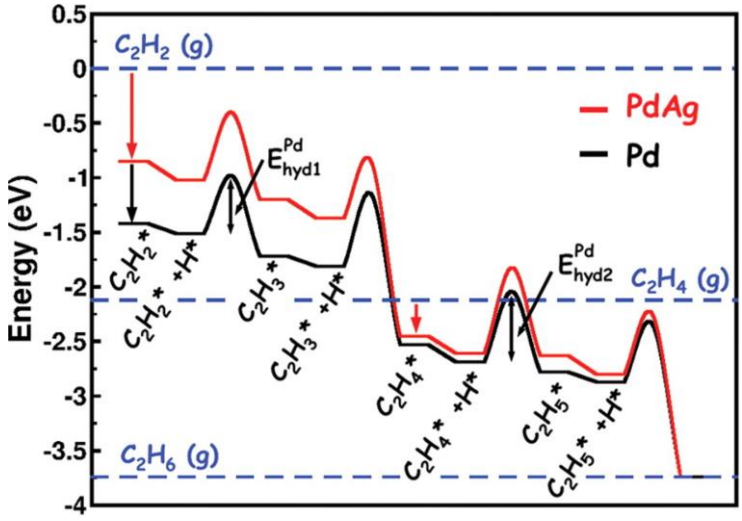

Figure 1.8. Energy landscape for the hydrogenation of acetylene. Black and red lines represent Pd(111) and PdAg(111) metal surfaces, respectively. Dotted lines indicate the relative energy of gaseous molecules. Adsorption energies are depicted by the downward arrows, while double sides arrows highlight the activation energy for hydrogenation. Reprinted from reference 100 with permission from AAAS.

0.5 eV, respectively).[33,96,97] Although the activation energy is greatly reduced compared to Au(111), the (selective) hydrogenation reactions over Pd_1Au monomers are typically found to be rate-limited by the high activation barrier for hydrogen dissociation, which results in a low surface concentration of hydrogen.[33,89–91,93–99] For Pd-trimers, a higher activity for dissociation was obtained.[87,94,95] Hence, during selective hydrogenation reactions, the catalytic activity and selectivity depend on the adsorption and activation of both reactants (polyunsaturated hydrocarbon and molecular hydrogen), which is influenced by the nature and geometry of the active site.

Lastly, we describe the H-insertion into the unsaturated adsorbed hydrocarbon moiety on the metal surface. Studt *et al.* illustrated how this affected the activity and selectivity of acetylene (C_2H_2) hydrogenation over monometallic Pd and bimetallic PdAg.[100] Figure 1.8 visualises the energy landscape for the hydrogenation of acetylene over Pd(111) and PdAg(111). Acetylene is adsorbed onto the metal surface and sequentially hydrogenated (so-called "Horiuti-Polanyi mechanism", Figure 1.5). The adsorption energy of acetylene, indicated by the first downward arrow, is more exothermic on Pd than on PdAg. The higher catalytic turnover rate of Pd is associated with a lower activation energy for H-insertion (E_{hyd1}) and the more exothermic acetylene adsorption. H-insertion onto adsorbed ethylene (C_2H_4* in the figure) also shows a lower activation energy (E_{hyd2}) on Pd than on PdAg. Therefore, over-hydrogenation to ethane-precursors is faster over Pd. Moreover, the activation energy for over-hydrogenation on PdAg is substantially higher than the ethylene adsorption energy (indicated by the horizontal dashed lines). Therefore, the molecules desorb rather than hydrogenate, resulting in a high ethylene yield and little ethane formation on PdAg.

Note that in Figure 1.8, the energies of the adsorbed H-atoms are added to the adsorbed hydrocarbon without an activation barrier. As discussed before, hydrogen activation should also be considered in the complete hydrogenation pathway. Moreover, in dilute Pd-alloys, hydrocarbons adsorption and hydrogen activation occur on spatially separated active sites. To facilitate the hydrogenation of the unsaturated hydrocarbon, diffusion of atomic hydrogen to the active site where the hydrocarbon is adsorbed is required ("spillover"), which is associated with an additional energy cost.[94] When spillover is slow, as on Au, this decreases the reaction rate, whereas, on Cu, efficient spillover creates a beneficial interplay between Pd and Cu sites.[33,97]

1.4.4 Carbon as support material

Metal nanoparticles of a few nanometres (nm) are typically deposited onto a catalyst support material. This increases the dispersion of the metal compared to metal powder or wire catalysts. The support acts as a physical anchoring site for the nanoparticles, increasing both the dispersion and the stability by preventing nanoparticle agglomeration and growth during catalytic operation.[101] In this thesis, we use carbon as a support material because of its exceptionally high thermal heat conductivity

(>420 W m^{-1} K^{-1})[102], much higher than, for example, mesoporous silica (<0.1 W m^{-1} K^{-1})[103,104], which limits the generation of local temperature hot-spots of the exothermic hydrogenation reactions.

Carbon materials are of interest as catalyst supports, because of their relatively weak metal-support interaction.[105,106] For selective hydrogenation under front-end conditions, Benavidez *et al.* demonstrated that Pd nanoparticles of similar size (0.7 to 0.8 nm) were more selective when supported on carbon than when supported on Al_2O_3.[107] They found that a higher Pd-oxide content (15%) in the as-reduced alumina-supported Pd, which was absent in the carbon-supported catalyst, had a negative electronic effect on the selectivity of the catalyst. Lewis-acidic supports, such as TiO_2, are detrimental for reactions with polyunsaturated hydrocarbons since the conversion of olefins to carbonaceous deposits (oligomerisation or fouling) readily occurs on the Lewis-acid sites of the support. This fouling results in poor stability and rapid deactivation of Au- and Cu-catalysts that were supported on TiO_2.[36,62]

This work uses graphitic nanoplatelets (GNP) as a carbon support, consisting of graphene layers stacked into graphitic flakes of 10-20 nm thickness and 0.5-1.0 micron width. It was shown that this carbon material is effective in (selective) oxidation and hydrogenation reactions.[37,108–110] This GNP has a high surface (500 m^2/g) and an accessible surface without channel-like pores, which is beneficial for the deposition of nanoparticles during synthesis and facilitates diffusion of reactants and products during catalysis. This graphitic carbon does not show strong Lewis acidity, although slight Brønsted acidity from the carboxylic and phenolic surface groups is present (4.6 atom% O, 0.19 groups nm^{-2}).[110] Interestingly, the nanoplatelet structure has been reported to intercalate hydrogen, which can be beneficial in activity for hydrogenation reactions.[111]

1.5 Scope of this thesis

In the next chapters, some key parameters for the catalytic performance of carbon-supported Pd nanoparticles (Pd/C) are discussed. The focus is on understanding structure-performance relationships in the selective hydrogenation of a butadiene/propylene gas mixture over Pd-based catalysts. The effect of the catalyst structure, such as size, shape and composition are addressed, as well as the influence of the reaction conditions. A schematic overview of the experimental chapters (Chapters 2 to 4) is provided in Figure 1.9.

In Chapter 2, the effect of **nanoparticle size** of monometallic Pd particles is discussed. From a series of differently sized catalysts (between 2 and 20 nm in Pd diameter), the catalytic activity and selectivity were correlated to the structure of the exposed surface sites. Smaller nanoparticles, with many corner-, step- and edge-sites, showed a different catalytic activity from larger nanoparticles, for which flat and extended terrace sites are

dominant. This size-dependent activity trend was different for butadiene and propylene reactants, which resulted in a size-dependent selectivity of the reaction.

In Chapter 3, we reflect on the effects of **mass transfer limitations**. A series of catalysts was prepared with similar particle size but varying weight loadings between 0.02 and 2.5 wt%, and therefore varying Pd surface site density (0.01 to 2.6 m^2_{Pd}/g_{cat}). These catalysts were pelletised and sieved into different size fractions to achieve catalyst grains between, on average, 20 to 200 µm. The impact of external and internal heat and mass transfer limitations on the catalyst activity and selectivity was evaluated. In particular, we found a strong effect of butadiene concentration gradients within the catalyst grains induced by internal mass transfer limitations. This chapter helps to recognise and prevent diffusion limitations, which can skew results in a way that can be wrongly ascribed to the properties of the catalyst rather than to the reaction conditions.

In Chapter 4, the combination of active Pd and selective Cu are investigated in **bimetallic Pd_xCu_{100-x}** catalysts. By a colloidal synthesis approach, monodisperse particles were prepared with Pd content varying from 0 to 13% while keeping size and shape constant. The interaction of Pd and Cu within individual nanoparticles was investigated by extensive characterisation, both in the as-synthesised materials and during catalytic operation. The local electronic configuration and the geometric ensemble size of the Pd atoms were correlated to the catalytic performance of the bimetallic nanoparticles. The results showed that the surface- and mass-normalised

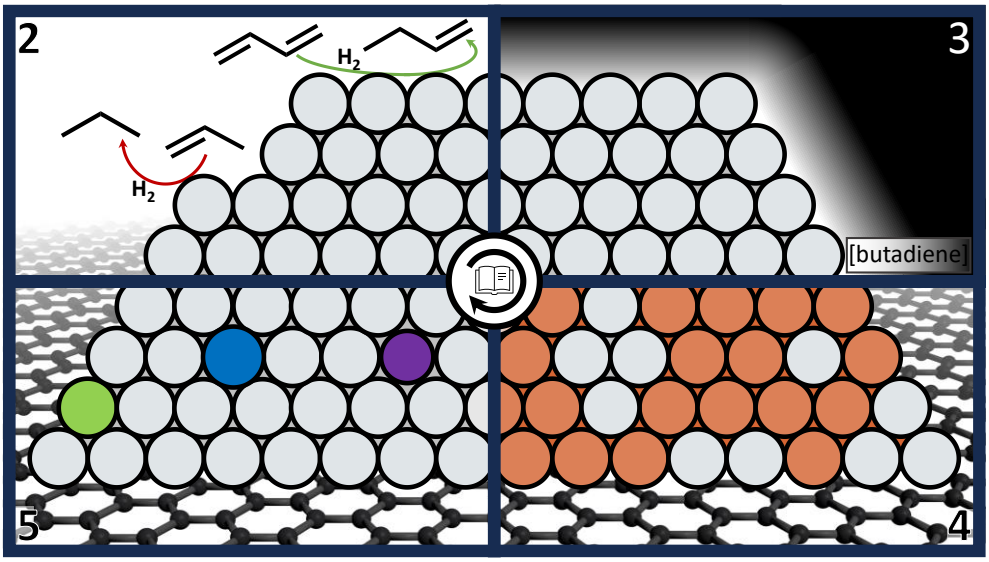

Figure 1.9. Overview of experimental chapters. Effect of (2) particle size, (3) mass transfer limitations, (4) bimetallic Pd_xCu_{100x} composition and (5) dopants on the selective hydrogenation of butadiene in a large excess of propylene over carbon-supported Pd nanoparticle catalysts.

activity of Pd were dependent on the Pd concentration. Also, the selectivity of the reaction was affected by variations in the Cu:Pd ratio, especially near complete butadiene conversion. These insights contribute to the understanding of bimetallic catalysts for selective hydrogenation reactions, controlling the activity-selectivity balance through the Pd concentration.

In Chapter 5, the effect of **additives** on Pd/C catalysts is discussed. To mitigate effects due to Pd dilution, a low (1:10) dopant-to-Pd ratio was used. The mixing of various metal(oxide) dopants (K, Mn, Cu, Zn or Ag) and the Pd metal within the nanoparticles was investigated. During the selective butadiene hydrogenation, large differences in activity and selectivity were found for some dopants. By further isomerisation tests of 1-butene as the reactant, the trends in isomer selectivity during selective hydrogenation were explained. Altogether, this chapter indicates how adding a minority of a secondary element impacts the performance of Pd-rich catalyst for selective (di)olefin hydrogenation and isomerisation.

Chapter 6 provides a brief overview of the previously described chapters. In this **summary**, the most important results on Pd-based catalysts for selective hydrogenation of butadiene are compared, and the key descriptors that determine the performance of the catalytic reaction are highlighted. These insight contribute to the ration design of Pd-based catalysts for selective hydrogenation reactions. Also, an **outlook** is provided with ideas for future work. Lastly, a lay **summary in Dutch** is provided in Chapter 7.

1.6 References

1. Berzelius, J. J. Sur un force jusqu'ici peu remarquée qui est probablement active dans la formation des composes organiques. *Jahres-Bericht* **14**, 237 (1835).
2. NobelPrize.org. All Nobel Prizes in Chemistry. https://www.nobelprize.org/prizes/lists/all-nobel-prizes-in-chemistry.
3. Thayer, A. M. Nobel Prizes Recognized Notable Developments In Catalysis. *Chem. Eng. News* **91**, (2013).
4. Laidler, K. J. A glossary of terms used in chemical kinetics, including reaction dynamics (IUPAC recommendations 1996). *Pure Appl. Chem.* **68**, 149-192 (1996).
5. Acres, G. J. K. & Harrison, B. The development of catalysts for emission control from motor vehicles: early research at Johnson Matthey. *Top. Catal.* **28**, 3-11 (2004).
6. Zhu, X. *et al.* Recent advances in direct air capture by adsorption. *Chem. Soc. Rev.* **51**, 6574-6651 (2022).
7. Aresta, M., Dibenedetto, A. & Angelini, A. Catalysis for the valorization of exhaust carbon: From CO_2 to chemicals, materials, and fuels. technological use of CO_2. *Chem. Rev.* **114** 1709-1742 (2014).
8. Modak, A., Bhanja, P., Dutta, S., Chowdhury, B. & Bhaumik, A. Catalytic reduction of CO_2 into fuels and fine chemicals. *Green Chem.* **22**, 4002-4033 (2020).
9. International Monetary Fund. GDP, current prices. *World Economic Outlook* https://www.imf.org/external/datamapper/ngdpd@weo/oemdc/advec/weoworld (*October 2023*).
10. Hutchings, G. *et al.* Modern Developments in Catalysis. vol. 2 (World Scientific, 2023).
11. Ma, Z. & Zaera, F. Heterogeneous Catalysis by Metals. in *Encyclopedia of Inorganic and Bioinorganic Chemistry* (Wiley, 2014). doi:10.1002/9781119951438.eibc0079.pub2.
12. Zhang, L., Zhou, M., Wang, A. & Zhang, T. Selective Hydrogenation over Supported Metal Catalysts: From Nanoparticles to Single Atoms. *Chem. Rev.* **120**, 683-733 (2020).
13. Louis, C. & Delannoy, L. Selective hydrogenation of polyunsaturated hydrocarbons and unsaturated aldehydes over bimetallic catalysts. *Adv. Catal.* **64**, 1-88 (2019).
14. Blaser, H.-U. *et al.* Selective Hydrogenation for Fine Chemicals: Recent Trends and New Developments. *Adv. Synth. Catal.* **345**, 103-151 (2003).
15. Chen, B. *et al.* New developments in hydrogenation catalysis particularly in synthesis of fine and intermediate chemicals. *Appl. Catal. A Gen.* **280**, 17-46 (2005).
16. Derrien, M. L. Chapter 18: Selective Hydrogenation Applied to the Refining of Petrochemical Raw Materials Produced by Steam Cracking. in *Studies in Surface Science and Catalysis* **27** 613-666 (1986).
17. Cai, H., Krzywicki, A. & Oballa, M. C. Coke formation in steam crackers for ethylene production. *Chem. Eng. Process.* **41**, 199-214 (2002).
18. White, W. C. Butadiene production process overview. *Chem. Biol. Interact.* **166**, 10-14 (2007).
19. Plastics - the fast Facts 2023. *Plastics Europe* https://plasticseurope.org/nl/resources/market-data/ (2023).
20. McCue, A. J. & Anderson, J. A. Recent advances in selective acetylene hydrogenation using palladium containing catalysts. *Front. Chem. Sci. Eng.* **9**, 142-153 (2015).
21. Takht Ravanchi, M., Sahebdelfar, S. & Komeili, S. Acetylene selective hydrogenation: a technical review on catalytic aspects. *Rev. Chem. Eng.* **34**, 215-237 (2018).
22. Molnár, Á., Sárkány, A. & Varga, M. Hydrogenation of carbon-carbon multiple bonds: chemo-, regio- and stereo-selectivity. *J. Mol. Catal. A Chem.* **173**, 185-221 (2001).
23. Borodziński, A. & Bond, G. C. Selective Hydrogenation of Ethyne in Ethene-Rich Streams on Palladium Catalysts. Part 1. Effect of Changes to the Catalyst During Reaction. *Catal. Rev.* **48**, 91-144 (2006).
24. Ren, T., Patel, M. & Blok, K. Olefins from conventional and heavy feedstocks: Energy use in steam cracking and alternative processes. *Energy* **31**, 425-451 (2006).

25. Anastas, P. T. & Zimmerman, J. B. Peer Reviewed: Design Through the 12 Principles of Green Engineering. *Environ. Sci. Technol.* **37**, 94A-101A (2003).
26. Anastas, P. & Eghbali, N. Green Chemistry: Principles and Practice. *Chem. Soc. Rev.* **39**, 301-312 (2010).
27. Asplund, S. Coke formation and its effect on internal mass transfer and selectivity in Pd-catalysed acetylene hydrogenation. *J. Catal.* **158**, 267-278 (1996).
28. Yang, B., Burch, R., Hardacre, C., Hu, P. & Hughes, P. Mechanistic Study of 1,3-Butadiene Formation in Acetylene Hydrogenation over the Pd-Based Catalysts Using Density Functional Calculations. *J. Phys. Chem. C* **118**, 1560-1567 (2014).
29. Ahn, I. Y., Lee, J. H., Kum, S. S. & Moon, S. H. Formation of C4 species in the deactivation of a Pd/SiO_2 catalyst during the selective hydrogenation of acetylene. *Catal. Today* **123**, 151-157 (2007).
30. Sanjay, P., Gupta, K., Ahmad, E. & Processes, R. Catalysis for Clean Energy and Environmental Sustainability. Catalysis for Clean Energy and Environmental Sustainability vol. 2 (Springer International Publishing, 2021).
31. Bender, M. An Overview of Industrial Processes for the Production of Olefins - C4 Hydrocarbons. *ChemBioEng Rev.* **1**, 136-147 (2014).
32. Geilen, F. M. A., Stochniol, G., Peitz, S. & Schulte-Koerne, E. Butenes. in *Ullmann's Encyclopedia of Industrial Chemistry* (Wiley, 2014). doi:10.1002/14356007.a04_483.pub3.
33. Kyriakou, G. *et al.* Isolated Metal Atom Geometries as a Strategy for Selective Heterogeneous Hydrogenations. *Science* **335**, 1209-1212 (2012).
34. Lucci, F. R. *et al.* Selective hydrogenation of 1,3-butadiene on platinum-copper alloys at the single-atom limit. *Nat. Commun.* **6**, 8550 (2015).
35. Yan, H. *et al.* Single-Atom Pd_1/Graphene Catalyst Achieved by Atomic Layer Deposition: Remarkable Performance in Selective Hydrogenation of 1,3-Butadiene. *J. Am. Chem. Soc.* **137**, 10484-10487 (2015).
36. Masoud, N. *et al.* Superior Stability of Au/SiO_2 Compared to Au/TiO_2 Catalysts for the Selective Hydrogenation of Butadiene. *ACS Catal.* **7**, 5594-5603 (2017).
37. Totarella, G. *et al.* Supported Cu Nanoparticles as Selective and Stable Catalysts for the Gas Phase Hydrogenation of 1,3-Butadiene in Alkene-Rich Feeds. *J. Phys. Chem. C* **125**, 366-375 (2021).
38. van der Hoeven, J. E. S. *et al.* Unlocking synergy in bimetallic catalysts by core-shell design. *Nat. Mater.* **20**, 1216-1220 (2021).
39. A. Roine. HSC Chemistry 9. Software available at www.metso.com/hsc. Metso, Pori (2023).
40. Maccoll, A. & Ross, R. A. The Hydrogen Bromide Catalyzed Isomerization of n-Butenes. I. Equilibrium Values. *J. Am. Chem. Soc.* **87**, 1169-1170 (1965).
41. Horiuti, I. & Polanyi, M. Exchange reactions of hydrogen on metallic catalysts. *Trans. Faraday Soc.* **30**, 1164-1172 (1934).
42. Mattson, B. *et al.* Heterogeneous catalysis: The horiuti-polanyi mechanism and alkene hydrogenation. *J. Chem. Educ.* **90**, 613-619 (2013).
43. Smith, W. B. & Massingill, J. L. Two chemical determinations of the population of conformations in 1,3-butadiene. *J. Am. Chem. Soc.* **83**, 4301-4302 (1961).
44. Saltiel, J., Sears, D. F. & Turek, A. M. UV spectrum of the high energy conformer of 1,3-butadiene in the gas phase. *J. Phys. Chem. A* **105**, 7569-7578 (2001).
45. Bond, G. C., Webb, G., Wells, P. B. & Winterbottom, J. M. The hydrogenation of alkadienes. Part I. The hydrogenation of buta-1,3-diene catalysed by the Noble Group VIII metals. *J. Chem. Soc.* 3218 (1965) doi:10.1039/jr9650003218.
46. Wells, P. B. & Bates, A. J. The hydrogenation of alkadienes, Part II. The hydrogenation of buta-1,3-diene catalysed by rhodium, palladium, iridium, and platinum wires. *J. Chem. Soc. A Inorganic, Phys. Theor.* (1968) doi:10.1039/J19680003064.
47. Phillipson, J. J., Wells, P. B. & Wilson, G. R. The hydrogenation of alkadienes. Part III. The hydrogenation of buta-1,3-diene catalysed by iron, cobalt, nickel, and copper. *J. Chem. Soc. A Inorganic, Phys. Theor.* 1351 (1969) doi:10.1039/j19690001351.

48. Bates, A. J., Leszczynski, Z. K., Phillipson, J. J., Wells, P. B. & Wilson, G. R. The hydrogenation of akladienes. Part IV. The reaction of buta-1,3-diene with deuterium catalysed by rhodium, palladium, and platinum. *J. Chem. Soc. A Inorganic, Phys. Theor.* 2435-2441 (1970) doi:10.1039/j19700002435.
49. Wells, P. B. & Wilson, G. R. The hydrogenation of alkadienes. Part V. the hydrogenation of trans- and of cis-penta-1,3-diene catalysed by cobalt, nickel, copper, palladium, and platinum. *J. Chem. Soc. A Inorganic, Phys. Theor. Chem.* (1970) doi:10.1039/J19700002442.
50. Boitiaux, J. P., Cosyns, J. & Vasudevan, S. Hydrogenation of highly unsaturated hydrocarbons over highly dispersed palladium catalyst. Part I: behaviour of small metal particles. *Appl. Catal.* **6**, 41-51 (1983).
51. Boitiaux, J. P., Cosyns, J. & Vasudevan, S. Hydrogenation of highly unsaturated hydrocarbons over highly dispersed Pd catalyst. Part II: Ligand effect of piperidine. *Appl. Catal.* **15**, 317-326 (1985).
52. Boitiaux, J. P., Cosyns, J. & Robert, E. Hydrogenation of unsaturated hydrocarbons in liquid phase on palladium, platinum and rhodium catalysts. III. Quantitative Selectivity Ranking of Platinum, Palladium and Rhodium in the Hydrogenation of 1-Butene, 1,3-Butadiene and 1-Butyne Using a Single Reaction Scheme. *Appl. Catal.* **35**, 193-209 (1987).
53. Boitiaux, J. P., Cosyns, J. & Robert, E. Additive effects in the selective hydrogenation of unsaturated hydrocarbons on platinum and rhodium catalysts. II. Influence of various compounds containing phosphorus, oxygen, sulphur and chlorine on the catalytic performance of platinum catalyst. *Appl. Catal.* **49**, 235-246 (1989).
54. Raney, M. Method of producing finely-divided nickel. U.S. Patent 1,628,190-A (1927).
55. Lindlar, H. Ein neuer Katalysator für selektive Hydrierungen. *Helv. Chim. Acta* **35**, 446-450 (1952).
56. Sárkány, A. & Révay, Z. Some features of acetylene and 1,3-butadiene hydrogenation on Ag/SiO_2 and Ag/TiO_2 catalysts. *Appl. Catal. A Gen.* **243**, 347-355 (2003).
57. Bond, G. C. Hydrogenation of Alkadienes and Poly-Enes. in *Metal-Catalysed Reactions of Hydrocarbons* 357-394 (Springer US, 2006). doi:10.1007/0-387-26111-7_8.
58. Michalak, W. D., Krier, J. M., Komvopoulos, K. & Somorjai, G. A. Structure Sensitivity in Pt Nanoparticle Catalysts for Hydrogenation of 1,3-Butadiene: In Situ Study of Reaction Intermediates Using SFG Vibrational Spectroscopy. *J. Phys. Chem. C* **117**, 1809-1817 (2013).
59. Hugon, A., Delannoy, L. & Louis, C. Supported gold catalysts for selective hydrogenation of 1,3-butadiene in the presence of an excess of alkenes. *Gold Bull.* **41**, 127-138 (2008).
60. Wang, Z. *et al.* A selective and stable Fe/TiO_2 catalyst for selective hydrogenation of butadiene in alkene-rich stream. *Chem. Commun.* **57**, 7031-7034 (2021).
61. Hou, R., Yu, W., Porosoff, M. D., Chen, J. G. & Wang, T. Selective hydrogenation of 1,3-butadiene on PdNi bimetallic catalyst: From model surfaces to supported catalysts. *J. Catal.* **316**, 1-10 (2014).
62. Wang, Z., Wang, G., Louis, C. & Delannoy, L. Novel non-noble bimetallic $Cu-Zn/TiO_2$ catalysts for selective hydrogenation of butadiene. *J. Catal.* **347**, 185-196 (2017).
63. Masoud, N. *et al.* Silica-Supported Au-Ag Catalysts for the Selective Hydrogenation of Butadiene. *ChemCatChem* **9**, 2418-2425 (2017).
64. Garcia Cervantes, G. Compared properties of Pd on thermo-conductor supports (SiC, Si_3N_4) and Pd on oxide supports (Al_2O_3, SiO_2) for the 1,3-butadiene hydrogenation reaction. *J. Catal.* **214**, 26-32 (2003).
65. Borodziński, A. & Bond, G. C. Selective Hydrogenation of Ethyne in Ethene-Rich Streams on Palladium Catalysts, Part 2: Steady-State Kinetics and Effects of Palladium Particle size, Carbon Monoxide, and Promoters. *Catal. Rev.* **50**, 379-469 (2008).
66. Teschner, D. *et al.* The Roles of Subsurface Carbon and Hydrogen in Palladium-Catalyzed Alkyne Hydrogenation. *Science* **320**, 86-89 (2008).
67. Dekura, S., Kobayashi, H., Kusada, K. & Kitagawa, H. Hydrogen in Palladium and Storage Properties of Related Nanomaterials: size, Shape, Alloying, and Metal-Organic Framework Coating Effects. *ChemPhysChem* **20**, 1158-1176 (2019).

68. Nag, N. K. A study on the formation of palladium hydride in a carbon-supported palladium catalyst. *J. Phys. Chem. B* **105**, 5945-5949 (2001).
69. Teschner, D. *et al.* Understanding palladium hydrogenation catalysts: When the nature of the reactive molecule controls the nature of the catalyst active phase. *Angew. Chemie - Int. Ed.* **47**, 9274-9278 (2008).
70. Tew, M. W., Janousch, M., Huthwelker, T. & van Bokhoven, J. A. The roles of carbide and hydride in oxide-supported palladium nanoparticles for alkyne hydrogenation. *J. Catal.* **283**, 45-54 (2011).
71. Bugaev, A. L. *et al.* Palladium Carbide and Hydride Formation in the Bulk and at the Surface of Palladium Nanoparticles. *J. Phys. Chem. C* **122**, 12029-12037 (2018).
72. Valcárcel, A., Clotet, A., Ricart, J. M., Delbecq, F. & Sautet, P. Comparative DFT study of the adsorption of 1,3-butadiene, 1-butene and 2-cis/trans-butenes on the Pt(111) and Pd(111) surfaces. *Surf. Sci.* **549**, 121-133 (2004).
73. Yang, X.-F., Wang, A.-Q., Wang, Y.-L., Zhang, T. & Li, J. Unusual Selectivity of Gold Catalysts for Hydrogenation of 1,3-Butadiene toward cis -2-Butene: A Joint Experimental and Theoretical Investigation. *J. Phys. Chem. C* **114**, 3131-3139 (2010).
74. Araujo-Lopez, E., Joos, L., Vandegehuchte, B. D., Sharapa, D. I. & Studt, F. Theoretical Investigations of (Oxidative) Dehydrogenation of Propane to Propylene over Palladium Surfaces. *J. Phys. Chem. C* **124**, 3171-3176 (2020).
75. Genest, A., Silvestre-Albero, J., Li, W. Q., Rösch, N. & Rupprechter, G. The origin of the particle-size-dependent selectivity in 1-butene isomerization and hydrogenation on Pd/Al_2O_3 catalysts. *Nat. Commun. 2021 121* **12**, 1-8 (2021).
76. Yan, Y. Q. *et al.* Electrochemistry-assisted selective butadiene hydrogenation with water. *Nat. Commun.* **14**, 2106 (2023).
77. Kabalan, L., Kowalec, I., Catlow, C. R. A. & Logsdail, A. J. A computational study of the properties of low- and high-index Pd, Cu and Zn surfaces. *Phys. Chem. Chem. Phys.* **23**, 14649-14661 (2021).
78. Yang, F. *et al.* size Dependence of Vapor Phase Hydrodeoxygenation of m-Cresol on Ni/SiO_2 Catalysts. *ACS Catal.* **8**, 1672-1682 (2018).
79. Sterk, E. B. *et al.* Structure Sensitivity of CO_2 Conversion over Nickel Metal Nanoparticles Explained by Micro-Kinetics Simulations. *JACS Au* **2**, 2714-2730 (2022).
80. Barberis, L. *et al.* Competition between reverse water gas shift reaction and methanol synthesis from CO_2: influence of copper particle size. *Nanoscale* **14**, 13551-13560 (2022).
81. Fu, Q., Yang, J. & Luo, Y. First-principles calculations of adsorption and dehydrogenation of trans-2-butene molecule on Pd(110) surface. *J. Chem. Phys.* **131**, 154703 (2009).
82. Yang, K. & Yang, B. Identification of the Active and Selective Sites over a Single Pt Atom-Alloyed Cu Catalyst for the Hydrogenation of 1,3-Butadiene: A Combined DFT and Microkinetic Modeling Study. *J. Phys. Chem. C* **122**, 10883-10891 (2018).
83. Lv, C. Q., Liu, J. H., Guo, Y. & Wang, G. C. Selective hydrogenation of 1,3-butadiene over single $Pt_1/Cu(1\ 1\ 1)$ model catalysts: A DFT study. *Appl. Surf. Sci.* **466**, 946-955 (2019).
84. Yan, Z. *et al.* Theoretical study the catalytic performance and mechanism of novel designed single atom catalysts $M_1/2DMs$ for 1,3-butadiene hydrogenation. *Appl. Surf. Sci.* **617**, 156585 (2023).
85. Jiang, L. *et al.* Facet engineering accelerates spillover hydrogenation on highly diluted metal nanocatalysts. *Nat. Nanotechnol.* **15**, (2020).
86. Liu, J. *et al.* Integrated Catalysis-Surface Science-Theory Approach to Understand Selectivity in the Hydrogenation of 1-Hexyne to 1-Hexene on PdAu Single-Atom Alloy Catalysts. *ACS Catal.* **9**, 8757-8765 (2019).
87. Foucher, A. C. *et al.* Influence of Pd Concentration in Au-Pd Nanoparticles for the Hydrogenation of Alkynes. *ACS Appl. Nano Mater.* **6**, 22927-22938 (2023).
88. Pei, G. X. *et al.* Performance of Cu-Alloyed Pd Single-Atom Catalyst for Semihydrogenation of Acetylene under Simulated Front-End Conditions. *ACS Catal.* **7**, 1491-1500 (2017).

89. Luneau, M. *et al.* Achieving High Selectivity for Alkyne Hydrogenation at High Conversions with Compositionally Optimized PdAu Nanoparticle Catalysts in Raspberry Colloid-Templated SiO_2. *ACS Catal.* **10**, 441-450 (2020).
90. van der Hoeven, J. E. S. *et al.* Unraveling 1-Hexene Hydrogenation over Dilute Pd-in-Au Alloys. *J. Phys. Chem. C* **126**, 15710-15723 (2022).
91. Ngan, H. T. *et al.* Hydrogen Dissociation Controls 1-Hexyne Selective Hydrogenation on Dilute Pd-in-Au Catalysts. *ACS Catal.* **12**, 13321-13333 (2022).
92. Sheth, P. A., Neurock, M. & Smith, C. M. First-Principles Analysis of the Effects of Alloying Pd with Ag for the Catalytic Hydrogenation of Acetylene−Ethylene Mixtures. *J. Phys. Chem. B* **109**, 12449-12466 (2005).
93. Darby, M. T., Stamatakis, M., Michaelides, A. & Sykes, E. C. H. Lonely Atoms with Special Gifts: Breaking Linear Scaling Relationships in Heterogeneous Catalysis with Single-Atom Alloys. *J. Phys. Chem. Lett.* **9**, 5636-5646 (2018).
94. Van Der Hoeven, J. E. S. *et al.* Entropic Control of HD Exchange Rates over Dilute Pd-in-Au Alloy Nanoparticle Catalysts. *ACS Catal.* **11**, 6971-6981 (2021).
95. Marcella, N. *et al.* Decoding reactive structures in dilute alloy catalysts. *Nat. Commun. 2022 131* **13**, 1-9 (2022).
96. Lucci, F. R. *et al.* Controlling Hydrogen Activation, Spillover, and Desorption with Pd-Au Single-Atom Alloys. *J. Phys. Chem. Lett.* **7**, 480-485 (2016).
97. Tierney, H. L., Baber, A. E., Kitchin, J. R. & Sykes, E. C. H. Hydrogen dissociation and spillover on individual isolated palladium atoms. *Phys. Rev. Lett.* **103**, 246102 (2009).
98. Brandt Corstius, O. E., van der Hoeven, J. E. S., Sunley, G. J. & de Jongh, P. E. Influence of particle size in Pd-catalysed selective hydrogenation of 1,3-butadiene. *J. Catal.* **427**, 115103 (2023).
99. Furlong, B. K., Hightower, J. W., Chan, T. Y. L., Sarkany, A. & Guczi, L. 1,3-Butadiene selective hydrogenation over Pd/alumina and CuPd/alumina catalysts. *Appl. Catal. A Gen.* **117**, 41-51 (1994).
100. Studt, F. *et al.* Identification of Non-Precious Metal Alloy Catalysts for Selective Hydrogenation of Acetylene. *Science* **320**, 1320-1322 (2008).
101. De Jong, K. P. Synthesis of supported catalysts. *Curr. Opin. Solid State Mater. Sci.* **4**, (1999).
102. Smith, A. W. Low-Temperature Thermal Conductivity of a Canadian Natural Graphite. *Phys. Rev.* **95**, 1095-1096 (1954).
103. Butts, D. M. *et al.* Engineering mesoporous silica for superior optical and thermal properties. *MRS Energy Sustain.* **7**, 39 (2020).
104. Bippus, L., Jaber, M., Lebeau, B., Schleich, D. & Scudeller, Y. Thermal conductivity of heat treated mesoporous silica particles. *Microporous Mesoporous Mater.* **190**, (2014).
105. De Jong, K. P. & Geus, J. W. Carbon Nanofibers: Catalytic Synthesis and Applications. *Catal. Rev. - Sci. Eng.* **42**, (2000).
106. Gerber, I. C. & Serp, P. A Theory/Experience Description of Support Effects in Carbon-Supported Catalysts. *Chem. Rev.* **120**, 1250-1349 (2020).
107. Benavidez, A. D. *et al.* Improved selectivity of carbon-supported palladium catalysts for the hydrogenation of acetylene in excess ethylene. *Appl. Catal. A Gen.* **482**, 108-115 (2014).
108. Donoeva, B., Masoud, N. & De Jongh, P. E. Carbon Support Surface Effects in the Gold-Catalyzed Oxidation of 5-Hydroxymethylfurfural. *ACS Catal.* **7**, 4581-4591 (2017).
109. Mattarozzi, F. *et al.* Surface-Modified Carbon Materials for CO_2 Electroreduction. *Eur. J. Inorg. Chem.* **26**, e202300152 (2023).
110. Visser, N. L. *et al.* Influence of carbon support surface modification on the performance of nickel catalysts in carbon dioxide hydrogenation. *Catal. Today* **418**, 114071 (2023).
111. Dobrezberger, K. *et al.* Hydrogenation on Palladium Nanoparticles Supported by Graphene Nanoplatelets. *J. Phys. Chem. C* 124, 23674-23682 (2020)

Chapter 2

Particle size effects

This chapter is based on: Brandt Corstius, O.E., van der Hoeven, J.E.S., Sunley, G.J. & de Jongh, P.E. Influence of particle size in Pd-catalysed selective hydrogenation of 1,3-butadiene. *Journal of Catalysis*, 427, 115103 (2023). DOI:10.1016/j.jcat.2023.115103

Abstract

Supported Pd nanoparticles are widely used as catalysts for the selective hydrogenation of alkynes and diolefins. They have a high activity, but limiting over-hydrogenation to alkanes remains challenging. We varied the nanoparticle size of a Pd on carbon catalyst from 2 to 17 nm and studied its effect on the catalytic activity and selectivity in the selective hydrogenation of 1,3-butadiene in the presence of an excess of propylene. The butadiene hydrogenation activity per metal surface atom increased slightly with Pd particle size, from 17 s^{-1} to 34 s^{-1} at 25 °C for 2 nm to 17 nm particles. Contrarily, the propylene hydrogenation activity decreased with particle size: from 2.6 s^{-1} to 0.4 s^{-1} from 2 to 17 nm particles. Overall, a higher product selectivity was obtained with increasing particle size over the full butadiene conversion range. Altogether, this paper provides valuable insight into the rational design of monometallic Pd-catalyst for selective hydrogenation.

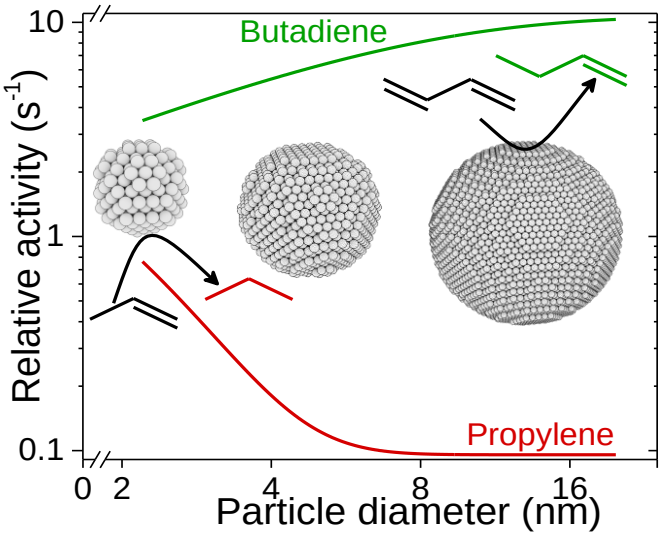

2.1 Introduction

Typical industrial catalysts for selective hydrogenation are supported palladium nanoparticles (Pd NPs).[1,2] Palladium is preferred due to its high activity at low temperatures. Of the platinum group metals, Pd is also the most selective metal for alkyne/alkadiene hydrogenation.[3] However, pure Pd still produces side products, particularly at high polyunsaturated hydrocarbon conversion levels. Therefore, secondary metals such as silver are added to decrease the ensemble size of Pd by dilution in a second metal.[4] In a different approach to reduce alkane formation, unselective sites are intentionally deactivated by the introduction of surface modifiers such as lead acetate or quinoline.[5] This increases the selectivity but inevitably comes at the expense of activity. For example, in the commercial Lindlar-catalyst[6] (Pb- and quinoline-modified 5 wt% Pd/$CaCO_3$), it has been estimated that only 0.02 wt% of the Pd is active during operation.[5,7] Detailed understanding of the catalytic performance of monometallic Pd NPs is key to steering towards atom-efficient use of scarce metals for sustainable selective hydrogenation catalysts. Moreover, industrial catalysts such as the Lindlar-catalyst are structurally complex, making it challenging to derive structure-performance relationships of the different components.

One important structure-performance relationship is the size-(in)sensitivity of a reaction, which is reported as the dependency of the surface-normalised activity on the size of the metal particles. This is especially important for metal particles ranging from 1 to 20 nm, where atoms with low coordination numbers (corners, edges and steps) dominate the surface of the smallest NPs, while on larger NPs, more coordinated terraces are the most abundant surface sites.[8–10] Since activity per (surface) atom is an averaged value over all available sites, this can be highly dependent on the metal particle size. For example, it is often reported that hydrogenation of simple alkene structures, such as ethylene and propylene, is structure-insensitive,[11] that is, the intrinsic hydrogenation activity is independent of particle size. Regarding more complex polyunsaturated olefins, Pt-catalysed 1,3-butadiene hydrogenation showed no particle size effect on activity or selectivity.[12] Contrarily, Boitiaux *et al.* showed that for butyne and butadiene, the turnover frequency (TOF) of Pd decreased for particles smaller than 4 nm, while activity to butene hydrogenation was constant for different metal dispersions.[13] Explanations for the increase in TOF over larger particles involve both electronic[14–16] and geometric effects[17–20]. For example, Silvestre-Albero *et al.* showed on well-defined Pd/Al_2O_3/NiAl(110) crystals that an increasing TOF with size was found when activity was normalised to the number of surface atoms.[17] However, when normalised to atoms in the Pd(111) plane of their model structure, the TOF was independent of particle size. More recently, other well-defined model systems, such as single-atom catalysts, have been studied for selective hydrogenation reactions.[21–27] Surface science studies on these well-defined model systems provide a powerful tool to investigate structure-performance relationships, albeit restricted to low pressures and sub-ambient temperatures. These conditions can be very different from the industrial

conditions. Bridging the gap between fundamental research and industrially relevant conditions is not straight-forward.

Support materials for heterogeneous catalysts are typically metal-oxides due to their high thermal and chemical stability.[28] Carbon supports have a weaker interaction with supported metal nanoparticles and are often used for Pd-catalysed selective hydrogenation reactions.[2] The interaction between support and nanoparticle can also influence the selectivity. For example, the selective hydrogenation of a 1:70 acetylene:ethylene mixture over Pd NPs of similar size (*ca.* 1 nm) was more selective when supported on carbon than when supported on Al_2O_3 or MgO.[15] Utilising carbon as a support also provides good heat conductivity, which limits local temperature hot-spots that can occur in exothermic hydrogenation reactions. Regarding carbon-supported particle size effects, Tardy *et al.* reported that Pd particles from 1.4 to 3.5 nm showed an increase in TOF with particle diameter.[29] The low activity of smaller NPs was ascribed to rapid deactivation by carbon coverage, in line with findings of Boitiaux *et al.*[13] However, these tests were performed in batch-operation and without excess alkene, making it challenging to translate these conclusions to more realistic operating conditions. Moreover, Pd size-dependency studies on selective hydrogenation were mainly focused on catalytic activity towards the alkyne or alkadiene rather than the selectivity of the reaction.

In this chapter, we describe the size-dependent activity and selectivity of Pd on carbon (Pd/C) catalysts for a range of nanoparticle sizes varying from 2 to 17 nm. The selective hydrogenation of 0.3 vol% butadiene was investigated in the presence of a 100-fold excess of propylene and 20 vol% hydrogen during continuous operation, in line with typical industrial front-end concentrations.[1,20,30,31] The activity and selectivity of the catalysts towards all reactants and products were taken into account and determined with respect to the average Pd NP size.

2.2 Experimental details

2.2.1 Chemicals and gasses

For the catalyst synthesis, the following chemicals were used without further purification: Aqueous solutions of 10 wt% tetraaminepalladium(II)nitrate (99.99%, Sigma Aldrich) and 65 vol% HNO_3 (AnalaR NORMAPUR analytical reagent, VWR Chemicals). Impregnation solutions were prepared by dilution of the Pd-precursor in purified water (mQ with a resistivity of 18.2 MΩ · cm at 25 °C, Direct-Q® 3 UV). Graphene NanoPlatelets (GNP) were used as a carbon catalyst support (xGNP®C-500, 500 m^2/g, 1-20 nm average thickness, 0.5-1.0 µm average width, XG Sciences).

For the catalyst preparation and the catalytic testing, the following gasses were used: 1,3-butadiene (>99.5% purity, Air Liquide Benelux, 0.21% cis-2-butene impurity), Propylene (>99.5% purity, The Linde Group, 0.04% propane impurity), Hydrogen

(>99.9990% purity), Helium (>99.9990% purity), Nitrogen (>99.9990% purity), 1-butene (>99.0% purity, Linde).

2.2.2 Catalyst preparation

A series of Pd/C catalysts with different sizes was prepared by incipient wetness impregnation of aqueous palladium(II)tetraamine nitrate precursor on dried GNP, followed by drying and reduction at different temperatures. It was shown before that this carbon material is effective in (selective) oxidation and hydrogenation reactions.[32-35] In short, carbon support was dried for 30 minutes at 150 °C under a dynamic vacuum (< 3 mbar). The pore volume was determined at 0.81 mL/g as determined by N_2-physisorption. 0.732 g of 10 wt% tetraaminepalladium(II)nitrate precursor solution (1.052 g/mL) was weighed into a syringe and dropwise added to 1.000 g of dried carbon under a small static vacuum. The impregnated support was gently stirred for at least 2 hours to homogenise and dried overnight under a dynamic vacuum at room temperature. The dried solids were heat treated with a ramp of 0.5 °C/min to 200 °C with 1-hour isothermal hold in 100 mL/min N_2 to decompose the nitrate and amine precursors. In a second heating step the precatalyst was reduced in 100 mL/min of 20% H_2/N_2. Metallic Pd NPs with different sizes were grown from the same batch of precatalyst (dried and heat treated) by varying the final reduction temperature between 160 and 600 °C.

Larger Pd particles were prepared in an alternative approach without the need for reduction temperatures above 600 °C. Pd nanoparticles were prepared by growing them in the precursor solution. Here, 4.663 g of a 10 wt% aqueous solution of tetraaminepalladium(II)nitrate was acidified with 0.0456 g of 65 vol% HNO_3 (final pH≈1), after which the acidified solution was diluted to 5 mL with mQ water. The solution was diluted another 40 times with 0.1 M HNO_3 and left undisturbed in a closed vial for 7 days in the dark at room temperature. 2.00 g GNP was incipiently wetted with 1.79 g of this liquid. After impregnation, this catalyst was homogenised, dried and heated under N_2, as described in the previous paragraph, without a final reduction step.

2.2.3 Characterisation

The shape, size and spatial distribution of the supported nanoparticles were analysed by Transmission Electron Microscopy (TEM). Bright-field micrographs were obtained on a Talos 120C (Thermo Scientific) transmission electron microscope operated at 120 kV. The powder sample was applied to the TEM grids by spreading the dry catalyst powder onto the Holey Carbon Film-covered Cu grids of 300 micron mesh (Agar Scientific). Size analysis was performed by manually measuring particle diameters in the micrographs using the ImageJ software. The number-averaged particle diameter is defined as:

$$d_{\mathrm{TEM}} \pm \sigma_{\mathrm{TEM}} = \frac{1}{N}\sum_{i=1}^{N} d_i \pm \sqrt{\frac{1}{N-1}\sum_{i=1}^{N}(d_i - d_{\mathrm{TEM}})^2} \qquad \text{Eq. 2.1}$$

where d_i is the measured diameter determined by TEM and σ_{TEM} is the spread of measured particles defined as the standard deviation. From the individual measurements, a mean volume-area diameter (d_{VA} or Sauter-diameter)[36] was calculated, assuming spherical particle shape, as follows: [37]

$$d_{\mathrm{VA}} \pm \sigma_{\mathrm{VA}} = \frac{\sum_{i=1}^{N} d_i^3}{\sum_{i=1}^{N} d_i^2} \pm \sqrt{\frac{1}{N-1}\sum_{i=1}^{N}(d_i - d_{\mathrm{VA}})^2} \qquad \text{Eq. 2.2}$$

Phase analysis and crystallite size determination were performed by X-ray Diffraction (XRD) on a Bruker D2 Phaser, equipped with a cobalt (K_α, 1.78897 Å) radiation source. Diffractograms were obtained by measuring 0.2 g of material in a 2.5 mm PMMA Bruker powder specimen holder with a diffraction angle from 20 to 70° 2θ and a 1-2 second step-size of 0.05° under 15 rpm rotation. Pd crystallite sizes (d_{XRD}) were determined from the width of the Pd(111) diffraction signal using the Scherrer equation:[38]

$$d_{\mathrm{XRD}} = \frac{k\,\lambda}{\beta\,cos\theta} \qquad \text{Eq. 2.3}$$

where k is a dimensionless shape factor (0.93)[39], λ is the incident X-ray wavelength (Co-K_α, 0.179×10^{-9} meter), β is the integral breadth of the peak, related to the full width at half maximum (1.06×FWHM) for a Gaussian peak shape[40], and θ is the position of the diffraction peak (23.3° for Pd(111)) with angles of β and θ in radians.

2.2.4 Catalytic testing

The performance of the catalysts was tested in a custom-built gas-phase hydrogenation set-up to study the selective hydrogenation of butadiene in a 100-fold excess of propylene, as previously described by Masoud *et al.*[41] Herein, we used 50 mL/min flow of a reaction gas consisting of 0.3%, 30% and 20% by volume for butadiene, propylene and H_2, respectively, and He as balance, in line with typical industrial concentrations under front-end conditions.[30] A thermocouple was pressed into a glass notch directly after the catalytic bed to measure the temperature of the catalytic bed as accurately as possible without interacting with the reactant gasses. The Pd/C catalyst powders were diluted in dried carbon support and pressed into a pellet (74 MPa), which was then gently crushed over a set of sieves to obtain sieve fractions of 38-75 µm. The reactor bed was further diluted with *ca.* 0.30 g SiC of 212-400 µm. Prior to the introduction of the reaction gas, the reactor was flushed with 50 mL/min N_2 for 15 minutes to remove traces of air and water. Isomerisation experiments were performed with 50 mL/min flow of 0.3% 1-butene, 5% H_2 and He as balance.

Product distributions were analysed by an on-line gas chromatograph sampling every 15 minutes and equipped with an FID detector (Thermo Scientific TRACE 1300, hydrocarbons detected: C_1 to C_5). Chromatogram peak areas of products and reactants

were compared to a known calibration gas mixture consisting of 1,3-butadiene, 1-butene, trans-2-butene, cis-2-butene, n-butane, hydrogen, helium, propylene and propane (The Linde Group). Prior to each catalytic test, the mixed reaction gas composition was analysed to certify its composition before passing it over the catalyst in the reactor.

The concentrations of products and reactants were monitored during operation from which conversion (X_i) was defined as:

$$X_{\text{1,3-butadiene}} = \frac{C_{\text{1-butene}} + C_{\text{trans-2-butene}} + C_{\text{cis-2-butene}} + C_{\text{n-butane}}}{C_{\text{1-butene}} + C_{\text{trans-2-butene}} + C_{\text{cis-2-butene}} + C_{\text{n-butane}} + C_{\text{1,3-butadiene}}} \quad \text{Eq. 2.4}$$

for butadiene conversion and

$$X_{\text{propylene}} = \frac{C_{\text{propane}}}{C_{\text{propane}} + C_{\text{propylene}}} \quad \text{Eq. 2.5}$$

for conversion of propylene, where C_i is the concentration in ppm of the individual hydrocarbons.

The selectivity (S_i) of the reactions is defined as:

$$S_{\text{butenes}} = \frac{C_{\text{1-butene}} + C_{\text{trans-2-butene}} + C_{\text{cis-2-butene}}}{C_{\text{1-butene}} + C_{\text{trans-2-butene}} + C_{\text{cis-2-butene}} + C_{\text{n-butane}} + C_{\text{propane}}} \quad \text{Eq. 2.6}$$

for the total selectivity towards alkene products (butenes) and

$$S_{\text{C4,isomer}} = \frac{C_{\text{C4Hx}}}{C_{\text{1-butene}} + C_{\text{trans-2-butene}} + C_{\text{cis-2-butene}} + C_{\text{n-butane}}} \quad \text{Eq. 2.7}$$

for the C_4-isomer selectivity, where C_{C4Hx} is the concentration of either of the C_4-products.

The yield (Q) of 1-butene is defined as:

$$Q_{\text{1-butene}} = X_{\text{1,3-butadiene}} \times S_{\text{butenes}} \times S_{\text{1-butene}} \quad \text{Eq. 2.8}$$

Turnover frequencies (TOFs) were calculated as the number of reactant molecules being converted per Pd surface atom per second, obtained at stable conversion levels (typically 3 hours on stream). To determine the TOF, the flow and composition of the reaction gas, the conversion, the product concentrations in the chromatogram, the amount of catalyst, the Pd weight loading and the metal dispersion were used as follows:

$$TOF(\text{s}^{-1}) = \frac{\frac{p}{RT} \times F \times C_i^0 \times X_i}{\frac{m_{\text{Pd}}}{M} \times D} \quad \text{Eq. 2.9}$$

where p is the pressure in the reactor (1.013 bar), R is the ideal gas constant (83.145 mL bar K^{-1} mol^{-1}), T is the gas inlet temperature (295 K), F is the reaction gas flow (0.833 mL/s), C_i^0 is the inlet reactant concentration (0.3% for butadiene, 30% for propylene) and X_i is the conversion of the individual reactant (see above). The numerator depicts the number of molecules (in moles) converted every second. The

denominator normalises the activity to the number of Pd surface atoms, where m_{Pd} is the mass of Pd in the reactor (g), M is the molar mass (106.42 g/mol) and D is the dispersion of the Pd NPs, which is defined as:

$$D(\%) = \frac{6(v_{\mathrm{Pd}}/a_{\mathrm{Pd}})}{d_{\mathrm{VA}}} \times 100\% \qquad \text{Eq. 2.10}$$

where v_{Pd} is the volume of a Pd atom (14.70 Å^3), a_{Pd} is the area of a Pd atom (7.93 Å^2, based on bulk Pd metal properties) and d_{VA} is mean volume-area diameter as determined from TEM.[37] The equation simplifies to $D = 1.112/d_{\mathrm{VA}}$ for Pd NPs with d_{VA} in nanometers, assuming spherical particles and fcc structure.

Kinetic studies were performed by changing the temperature (up to 100 °C) or partial gas pressures (0.15-0.60%, 15-60% and 10-40% by volume for butadiene, propylene and H_2, respectively) while keeping the total flow constant at 50 mL/min. The changes in partial pressures were realised by varying one of the reactants at a time and counteracting He as a balance. Reaction orders were obtained by a linear fit of the relation between log(TOF) and log(partial pressure) for the different reactants (hydrogen, butadiene and propylene).

2.3 Results and discussion

2.3.1 Preparation of the palladium on carbon catalysts

The carbon-supported Pd-catalysts, heated to different reduction temperatures, were imaged by Transmission Electron Microscopy (TEM). The micrographs in Figure 2.1A-E show the as-prepared catalysts, having been prepared using different synthesis parameters to tune the particle size. Manual measurements of the particles' diameter resulted in average particle sizes of 2.4±1.0 (A, blue), 3.4±1.0 (B, yellow), 4.4±1.1 (C, grey), 9.4±2.7 (D, orange) and 17±8.6 nm (E, light blue). The inset of each subfigure shows a spherical representation of a Pd crystallite of corresponding diameter, assuming an fcc structure, single crystalline particles and an atomic Pd radius of 138 pm.[37] This visualises the expected exposed surface of Pd. The smallest NPs show a rough Pd surface, rich in corner and edge sites, whereas larger NPs show a larger fraction of extended terrace sites.

The Pd particles were likely metallic, as no reducible species were observed by temperature programmed reduction below 250 °C. All carbon-supported Pd-catalysts are referred to as "*X*_Pd/C" throughout this chapter, where *X* is the number averaged particle diameter in nanometres. The spread of the particle sizes within the catalysts was analysed from the corresponding size histograms (Figure 2.1F). For example, for the 2_Pd/C catalyst, roughly 40% of the measured particles had a diameter smaller than 2.0 nm and more than 75% below 3.0 nm. In contrast, for 4_Pd/C, more than 90% of the measured particles were above 3.0 nm. Similarly, for 9_Pd/C, at least 90% of the diameters were larger than 6.0 nm, a size range in which almost no particles were

detected for the catalysts reduced at lower temperatures. This degree of polydispersity resulted in only limited overlap of particle sizes between different catalysts, which allowed the establishment of a size-performance relationship for these Pd/C catalysts.

The particle sizes of the Pd/C catalysts shown in Figure 2.1A-E were confirmed by the X-ray Diffraction (XRD) in Figure 2.1G. All materials showed a broad feature between 48 and 55° 2θ attributed to the overlap of (100) and (101) reflections of the graphitic support. The Pd-containing catalysts exhibited an additional diffraction peak of metallic Pd(111) at 46.7° and a shoulder indicative of Pd(200) at 54.2° 2θ, more noticeable after subtraction of the carbon diffraction. The width of the Pd(111) peak clearly decreased with increasing particle size. The weak intensity and broad peaks for the 2_Pd/C and 3_Pd/C catalysts can be ascribed to a lower crystallinity of the 2 and 3 nm NPs compared to the 4 and 9 nm particles. For 17_Pd/C, a Pd(111) peak was observed, but it was very weak due to the low weight loading of this catalyst (about 40 times lower than for the other catalysts).

The full-width at half-maximum (FWHM) of the Pd(111) peak was analysed to derive the crystallite sizes listed in Table 2.1. For 3_Pd/C, peak analysis could not be performed due to the low crystallinity. The reduction temperature for this catalyst (160 °C) initiated particle formation (Figure 2.1B) but potentially was not sufficient for restructuring into ordered crystallites. The crystallite sizes from XRD are in good agreement with the values and trend obtained from TEM. The only noticeable exception

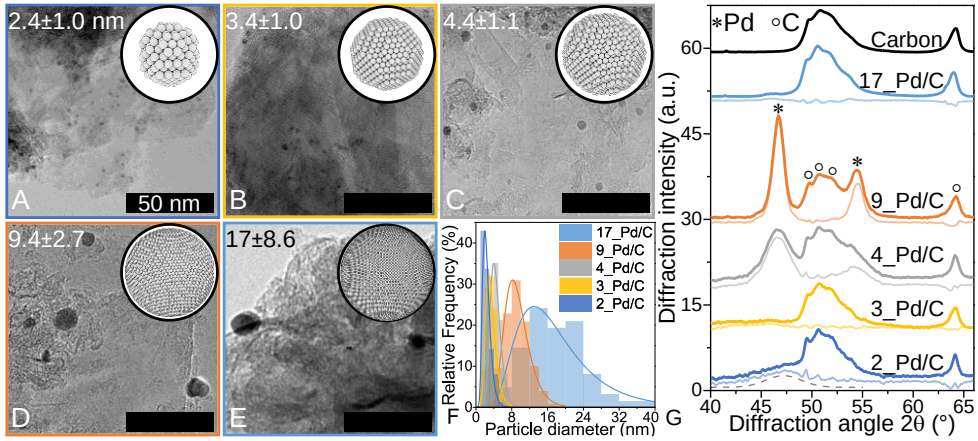

Figure 2.1. Structural characterisation of as-synthesised Pd/C catalyst with different NP sizes. (A-E) Bright-field TEM micrographs of carbon-supported nanoparticles of, on average, 2 nm (A, blue), 3 nm (B, yellow), 4 nm (C, grey), 9 nm (D, orange) and 17 nm (E, light blue), with as inset a schematic representation of a spherical Pd particle with the measured average diameter. (F) Size histograms of the Pd nanoparticles measured by TEM. The solid lines are a lognormal distribution fitted to the data. (E) Powder X-ray diffractograms of untreated carbon support and Pd/C catalysts. The upper lines show the intensity normalised to the C(004) peak at 64° 2θ, and the lower lines show the intensity after subtracting the carbon diffractogram. Dashed line is added to guide the eye for the broad Pd(111) peak at 46.7° 2θ in 2_Pd/C.

Table 2.1. Overview of the catalysts used in this chapter.

Catalyst	Diameter d_{TEM} (nm)[a]	Dispersion (%)[b]	Crystallite size d_{XRD}(nm)[c]	Pd wt%[e]	Reduction temperature (°C)
2_Pd/C	2.4 ± 1.0	34.7%	2.1	2.54[f]	300
3_Pd/C	3.4 ± 1.0	28.1%	n.d	2.54[f]	160[g]
4_Pd/C	4.4 ± 1.1	22.5%	4.1	2.54[f]	500
9_Pd/C	9.4 ± 2.7	10.3%	9.3	2.53	600
17_Pd/C	17 ± 8.6	4.6%	8.0[d]	0.07	n.a.

[a] Number averaged particle diameter from TEM measurements. [b] From $D=1.112/d_{VA}$, where $d_{VA}=\sum_{i=1}^{N} d_{TEM,i}^{3}/\sum_{i=1}^{N} d_{TEM,i}^{2}$. [c] Derived from the Scherrer equation on the Pd(111) peak.[39] [d] Less accurate fit due to low weight loading. [e] Determined by the metal amount present in the impregnation solution. [f] Grown from the same batch of precatalyst. [g] Reduced with 1.0 °C/min ramp, compared to 0.5 °C/min for the other Pd/C catalysts.

is the 17_Pd/C catalyst, where d_{XRD} is significantly smaller than d_{TEM}. This could be explained by polycrystallinity in these large particles of 17 nm (found by TEM), which on average consist of multiple agglomerates of roughly 8 nm crystallite domains (found by XRD). We found no indication of such agglomeration from TEM, as spherical particles were found without indication of any crystallite grain boundaries. However, the low intensity of the Pd(111) diffraction due to the low weight loading (Figure 2.1G) limits the accuracy of the FWHM fitting and could underestimate the derived crystallite size.

2.3.2 Impact of Pd particle size on butadiene and propylene conversion

The catalysts were tested for selective hydrogenation of butadiene in 100-fold excess of propylene. The reactors were loaded with different amounts of total Pd mass to ensure a similar Pd surface area in each catalytic test (0.3-0.4 cm^2 Pd per test; see Table 2.2). After an initial activation period, all catalysts showed stable conversion levels between 10 and 25% conversion of butadiene at 25 °C (Figure 2.2A). Low butadiene conversion levels were chosen to stay in the kinetically limited regime and study the butadiene and propene performance of the catalysts. Mass-transfer limitations were minimised (Weisz modulus < 0.03 and Carberry number < 0.001 at 25 °C for all catalysts; more details in Chapter 3). For all catalysts, the conversion of propylene (open symbols) was more than 2 orders of magnitude lower than the conversion of butadiene (closed symbols), demonstrating the preferential conversion of butadiene over propylene by all Pd/C catalysts. For example, 4_Pd/C showed 9.5% butadiene conversion at 25 °C, whereas only 0.006% of propylene was converted. The difference between butadiene and propylene conversion levels further increased for larger NPs: 17_Pd/C showed 18% butadiene conversion concomitant with 0.002% propylene conversion at 25 °C.

Turnover frequencies (TOFs) at 25 °C for both butadiene and propylene were determined from the steady-state conversion levels of Figure 2.2A (after 1.5-3 hours)

Table 2.2. Additional catalytic experimental details.

Catalyst	m_{cat} (mg)	Dilution[a]	m_{Pd} (µg)	Pd surface area, (cm^2)[b]	TOS (h)	T_{max} (°C)	$d_{TEM,used}$ (nm)[c]
2_Pd/C	2.83	306	0.23	0.36	28	50	2.1 ± 0.7
3_Pd/C	1.06	121	0.22	0.28	n.d.	n.d.	n.d.
4_Pd/C	0.97	65	0.38	0.38	82	50	4.4 ± 1.4
9_Pd/C	2.70	100	0.68	0.31	n.d.	n.d.	n.d.
17_Pd/C	1.85	-	1.37	0.28	66	75	16 ± 10.3

[a] Diluted in bare graphitic carbon support prior to pelletising and sieving. [b] $A_{Pd}=S_{sp}\times m_{Pd}$ and $S_{sp}=4.5\times10^6\times D$ ($cm^2\ g^{-1}$), where D is the metal dispersion.[37] [c] Number averaged particle diameter from TEM measurements.

and catalytic experimental details in Table 2.2, taking into account the differences in Pd mass loading, metal dispersion and reactant concentrations. The Pd nanoparticles did not grow during catalysis ($d_{TEM,used}$, Table 2.2), hence d_{VA} of the as-synthesised catalysts was used for the calculation of the TOF. Figure 2.2B summarises the TOFs for butadiene (closed symbols) and propylene hydrogenation (open symbols) for all Pd/C catalysts. The butadiene TOF of the catalysts slightly increased with particle size, from 17 to 34 $mol_{butadiene}\ mol_{Pd,surface}^{-1}\ s^{-1}$ for catalysts with 2 to 17 nm particles, respectively. The propylene TOF depended more strongly on the particle size and decreased from 2.6 $mol_{propylene}\ mol_{Pd,surface}^{-1}\ s^{-1}$ for 2_Pd/C catalyst to 0.65 s^{-1} for 4_Pd/C and below 0.5 s^{-1} for the 9 nm and 17 nm particles.

The 1-2 orders of magnitude higher TOF of butadiene compared to propylene can, in part, be explained by the difference in adsorption energy of the hydrocarbons. Density functional theory (DFT) calculations showed that on Pd(111), Pd(100) and Pd(110)

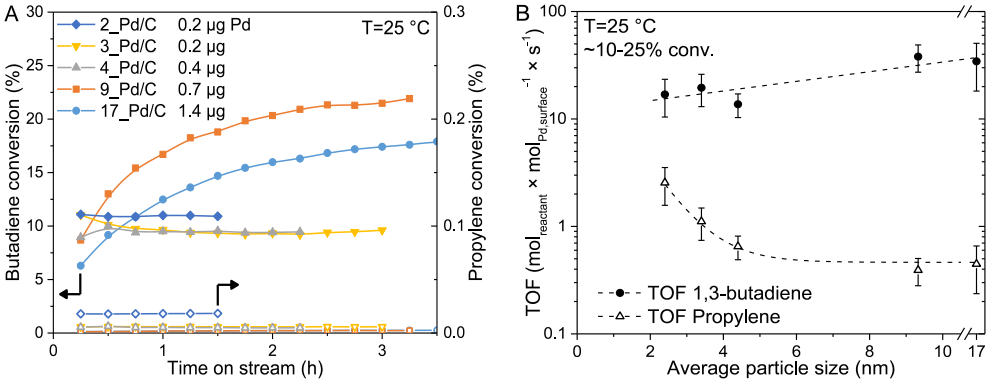

Figure 2.2. Activity of Pd/C catalysts as function of NP size. (A) Conversion of butadiene (closed symbols) and propylene (open symbols) at 25 °C. Catalysts loaded to different amounts, indicated by the Pd mass in the legend (see Table 2.2). (B) Turnover frequencies (TOFs) towards butadiene (closed circles) and propylene (open triangles) as a function of average particle diameter. Dashed lines to guide the eye. Conditions: 50 mL/min, 1 atm, 22.000 h^{-1} GHSV, 0.3% butadiene, 30% propylene, 20% hydrogen and He balance.

facets the adsorption energy of butadiene was much higher (-1.4 eV to -1.8 eV) compared to that of both propylene and butene (both roughly -0.8 to -1.0 eV).[42] Similar results were found on Pd(111) for butadiene compared to 1-butene, trans-2-butene and cis-2-butene (-1.72 eV versus -0.90, -0.72 and -0.77 eV, respectively).[43] We also studied the influence of competitive adsorption during the hydrogenation of butadiene or propylene in the absence of the other hydrocarbon. In short, the hydrogenation activity of butadiene was not affected by the presence of propylene, whereas the propylene hydrogenation activity decreased by 1-2 orders of magnitude when 0.3% butadiene was co-fed into the reaction mixture. With an equimolar mixture of 1% butadiene and 1% propylene, 2-3 orders of magnitude preferential activity towards butadiene compared to propylene was observed.

The TOF values are comparable to those reported in the literature for butadiene conversion over Pd/C (*ca.* 20 s^{-1} for 2.8 nm at room temperature)[29] and Pd/SiO_2 (*ca.* 17 s^{-1} for 4.1 nm at 20 °C)[44]. For propylene hydrogenation over commercial monometallic Pd/SiO_2, a TOF of roughly 10 s^{-1} was reported[45], in line with the TOFs in our experiments in the absence of butadiene (11.4 and 9.3 s^{-1} for 4_Pd/C and 17_Pd/C). The increasing butadiene hydrogenation activity per Pd surface atom with increasing particle size in Figure 2.2B is in line with results reported by Borodziński, who observed a little over two-fold increase in TOF for acetylene in excess of ethylene when increasing particle size from 4.2 to 16 nm.[19] The increase was ascribed to larger fraction of exposed Pd(100) and Pd(111) terraces. The insets of Figure 2.1A-E show that a substantial increase in the exposed fraction of terraces for larger nanoparticles is expected in the investigated size range. A similar explanation was reported for the size-dependent butadiene hydrogenation over Pd/Al_2O_3/NiAl(110) (in the absence of an alkene excess).[17] Figure 2.2B confirms that such correlation also holds for butadiene in large excess of propylene. From our work, we conclude that the catalytic intrinsic activity of

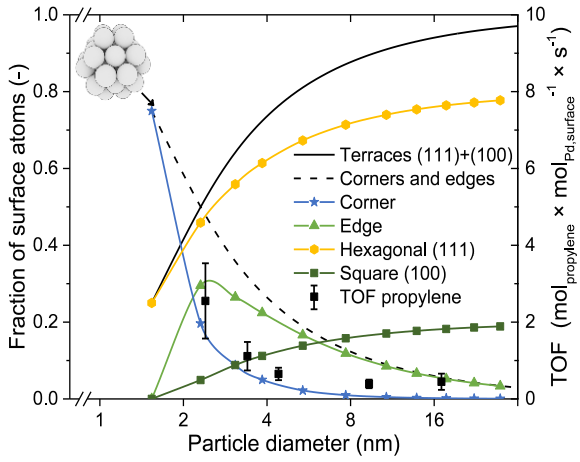

Figure 2.3. Surface atom speciation. Fraction of corners, edges and planes for truncated octahedron particle shape, which is most similar to the Wulff-constructed shape of Pd.[46] Inset represents the smallest possible nanoparticle of this shape with an edge length of two atoms.

Pd NPs towards butadiene hydrogenation in large excess of propylene and hydrogen increases with particle size.

The decrease in propylene TOF with increasing NP size (Figure 2.2B) under these reaction conditions was not reported before, also not for other small olefinic molecules such as ethylene and butene.[11,13] The strong decrease in propylene TOF for particles up to 5 nm may be due to a decrease in the fraction of undercoordinated edge/corner sites with increasing particle size, as qualitatively seen from the insets in Figure 2.1A-E. Calculation of the fraction of edge/corner sites of various particle shapes shows a strong decrease in the 1-5 nm range, after which this fraction is more constant (Figure 2.3).[9,10,46] The observed trend in propylene TOF matches the decrease in the fraction of edge/corner surface sites. Therefore, we propose that geometric effects explain the particle size effects, where the corner and edge sites contribute most to the conversion of propylene. This is supported by DFT calculations, which showed that butadiene binds very strongly onto Pd(111), Pd(100) and Pd(110) planes[42] as well as on Pd(211) step sites[47]. In all cases, the most stable configuration of the butadiene molecule was parallel to the metal surface and bound to 3 or 4 adjacent Pd atoms. For example, on Pd(111), the 1,2,3,4-tetra-σ bound configuration has a much higher adsorption energy (-1.72 eV) compared to the di-σ configuration (-0.94 eV) bound to two Pd surface atoms.[43] This indicates that on terrace sites, high selectivity is obtained due to the preferential binding of butadiene over propylene and butene, whereas on lower coordinated geometries (*e.g.,* corners), the adsorption energy of butadiene is closer to that of the alkenes (*e.g.,* for propylene -0.73 and -0.95 eV on Pd(111) and Pd(211)).[48]

As discussed in section 1.4.1, the formation of Pd-carbide or Pd-hydride phases can affect the catalytic performance during selective hydrogenation.[31,49–51] Under the reaction conditions (298 K, 0.2 bar H_2), macrocrystalline Pd forms stable β-PdH_x with x=0.6, which decreases down to x=0.46 and 0.42 for 7.0 nm and 2.6 nm particles.[52] Therefore, the ratio of surface-to-bulk hydrogen increases for smaller Pd particles.[53] The formation of carbide is found irrespective of particle size.[51,54] Thus, decreasing the particle size of Pd NPs mitigates bulk Pd-hydride formation, which is associated with lower selectivity, but increases surface-to-bulk H ratio and Pd-carbide formation. If this would be a dominant effect, the selectivity would be higher for smaller Pd particles, while the opposite was found. Hence, the hydride and carbide formation effects do not explain the reported results.

2.3.3 Reaction orders and apparent activation energies

Further investigation into the competitive adsorption and kinetics was performed by the study of reaction orders and apparent activation energies. Figure 2.4A shows the reaction order in hydrogen to be a near first-order dependence. This is in line with reports from selective alkadiene and alkyne hydrogenation studies.[24,55,56] There is a

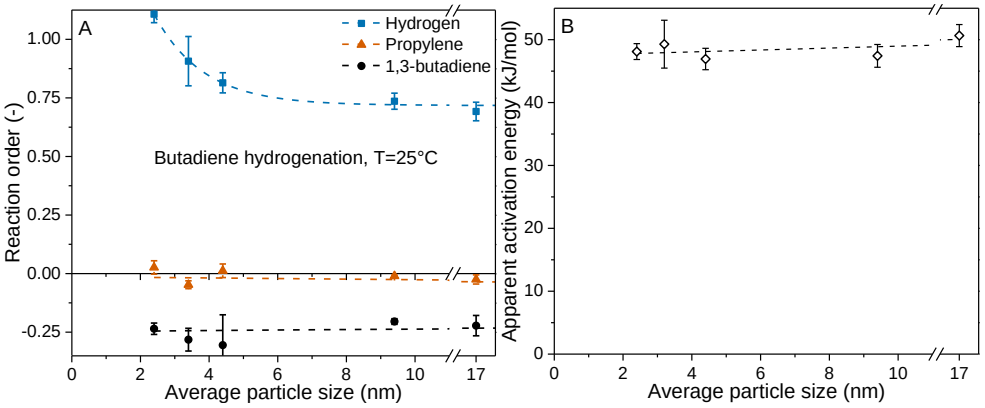

Figure 2.4. Kinetic measurements for butadiene hydrogenation. (A) Reaction orders determined at steady state activity at 25 °C for (10-20% initial conversion) butadiene hydrogenation as a function of average particle size. Dashed lines as guide for to eye. Orders are calculated from a linear fit of log(TOF) vs log(p/p^0) plots, varying the partial pressure of the reactants hydrogen (blue squares), propylene (orange triangles) or butadiene (black circles) one at a time, counteracted by He as balance. Partial pressures varied from 0.5 to 2.0 times the normal reaction gas composition (0.3% butadiene, 30% propylene, 20% hydrogen). (B) Apparent activation energies for butadiene hydrogenation determined from linear fit of log(TOF)-T^{-1} between 25 and 40 °C, obtained below 40% conversion.

slight particle size dependence for the reaction order in hydrogen, which decreases from +1.1 for 2_Pd/C to +0.7 for 17_Pd/C. This suggests hydrogen is more limiting for the reaction rate over smaller NPs. Regarding the hydrocarbon reactants, the reaction orders are about -0.25 and 0 for butadiene and propylene respectively. The apparent orders are size-independent. The insensitivity (zero-order) to the propylene concentration indicates that propylene does not compete for the same active sites as butadiene under the given reaction conditions. The negative reaction order (-0.25) in butadiene means that less butadiene is converted when the inlet concentration of butadiene is increased. This counter-intuitive response is explained by the fact that under these reaction conditions, strongly bound butadiene effectively inhibits H_2 adsorption. From the H_2-order, it was found that this is the most critical factor in determining the reaction rate, as is observed in other Pd-based selective hydrogenation studies.[17,24]

Figure 2.4B shows that the apparent activation energies of butadiene were insensitive to particle size and roughly 50 kJ/mol, a value in line with the literature.[57] Similar activation energies substantiate the difference in activity (Figure 2.2B) is ascribed to a difference in a number of active sites (*e.g.*, terrace sites) and not due to the difference in apparent activation energy. Moreover, this indicates that severe mass transfer limitations do not occur in the temperature range (25-40 °C) used for the Arrhenius fit of the activity data, as in a diffusion-limited regime, the apparent activation energy would shift to lower values.

2.3.4 Effect of particle size on the product selectivity

The product selectivity of the catalyst was influenced by the average particle size. Figure 2.5A (black closed squares) shows the total alkenes selectivity of the reaction for each Pd/C catalyst at 25 °C. The selectivity towards the butene isomers increased with increasing particle size and was 82% for 2_Pd/C (*i.e.,* 18% selectivity to n-butane and propane) and 98% for 9_Pd/C. More specifically, regarding the C4-selectivity, 2_Pd/C converts 4.7% of butadiene to n-butane, whereas the amount of n-butane decreased to 0.3% for 17_Pd/C. This indicates a particle size dependence in both total selectivity (alkenes *vs* alkanes formation) and over-hydrogenation (n-butane formation), where larger NPs are more selective.

The selectivity to the different butene-isomers (open symbols) shows that for all Pd/C catalysts, 1-butene was the major product, followed by trans-2-butene and cis-2-butene. Although the high fraction of 1-butene is in contrast with the thermodynamic equilibrium of butenes (Figure 1.4A),[58] it can be explained by the so-called "Horiuti-Polanyi mechanism".[59] In this mechanism, molecular hydrogen is adsorbed dissociatively on the metal surface first. Then, the alkadiene is adsorbed and two hydrides are added successively to the unsaturated molecule. Sequential 1,2-addition to the terminal C=C bond of 1,3-butadiene forms an adsorbed 1-butene intermediate. Gaseous 1-butene is formed when desorption is faster than isomerisation or further hydrogenation, explaining the high 1-butene levels in Figure 2.5A. For all catalysts, trans-2-butene is approximately 10 times more abundant than cis-2-butene. Although trans-2-butene is the favoured conformational isomer, the *trans:cis* ratio is higher than thermodynamically expected (1.7 at 25 °C, Figure 1.4B). Both the high

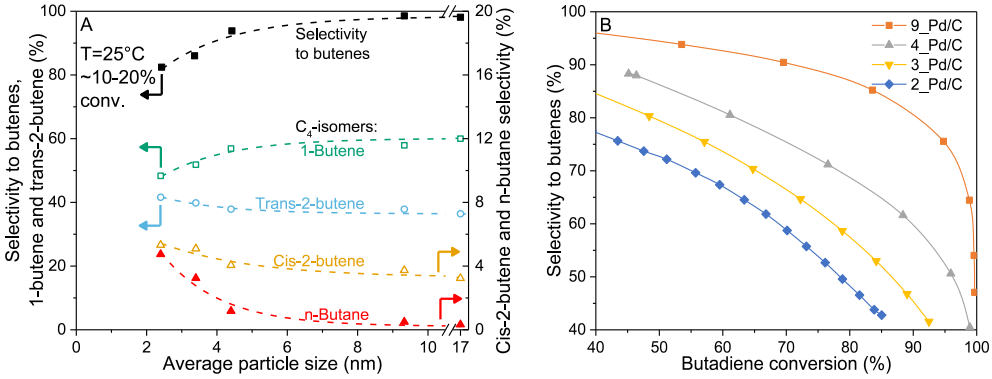

Figure 2.5. Particle size dependent selectivity. (A) Butene selectivity (closed squares) defined as the percentage of butenes relative to the sum of butenes, n-butane and propane. Product distribution of the C4-isomers (open symbols) defined as the percentage of 1-butene (green squares), trans-2-butene (blue circles), cis-2-butene (yellow triangles) and n-butane (red closed triangles) in the C4-product stream. Data obtained at steady state conversion (10-25%) at 25 °C. (B) Butene selectivity as function of temperature for 9_Pd/C (orange squares), 4_Pd/C (grey triangles), 3_Pd/C (yellow downward triangles) and 2_Pd/C (blue diamonds). The conversion is varied by a temperature variation of up to 100 °C.

1-butene levels and *trans:cis* ratio indicate the reaction is determined by kinetics rather than thermodynamic equilibria.

Interestingly, a particle size dependence was also observed in the isomer compositions. For example, 1-butene levels increased from 50% to 60% from 2_Pd/C to larger NPs. Simultaneously, the composition levels for trans-2-butene decreased from 44% to 37%. Cis-2-butene levels decreased in a similar fashion, but with a slightly steeper decline, from 5.6% to 3.2%. Therefore, the gain in 1-butene yield for the larger nanoparticle catalysts comes at the expense of 2-butenes, indicating a lower isomerisation activity. Isomerisation tests of 0.3% 1-butene in 5% H_2/He confirm there is a relatively higher isomerisation activity compared to hydrogenation activity, which increased over smaller NPs, and the obtained *trans:cis* ratio is around 1.0 for all catalysts, which is lower than obtained from butadiene hydrogenation (*trans:cis* of 8-12, Figure 2.5A). This indicates that the 2-butene isomers are formed mainly through direct hydrogenation of adsorbed butadiene and only to a limited extent by readsorption of 1-butene followed by isomerisation. Furthermore, for butadiene hydrogenation, a higher reaction order in hydrogen was observed on smaller nanoparticles (Figure 2.4). This higher order indicates that the availability of hydrogen on the surface becomes more limiting, which explains the increased isomerisation.

The increase in *trans:cis* ratio with particle size may be understood from the different binding geometry of the 2-butene intermediates. For the cis geometry, two π-allylic bonds to the same Pd binding site are required, analogous to an inorganic bidentate ligand complexes.[3,60] Such coordination is more likely on active sites with lower coordination numbers, such as corners. This geometric effect was demonstrated earlier for Au, where cis-2-butene was preferentially formed on corner and edge sites.[61] In contrast, on flat terraces, C_4-intermediates likely bind on two (or more) surface atoms, which results in more trans-2-butene. This could partly explain the larger amount of cis-2-butene formed over smaller Pd particles.

Figure 2.5B depicts the selectivity over the Pd/C catalysts at higher conversion levels, which was achieved by gradually raising the operation temperature. All catalysts show a decreasing selectivity with increasing conversion, mostly due to more propane formation. Over-hydrogenation to n-butane also increases with conversion but to a lesser extent (below 5% at the highest reported conversions). Nanoparticles of 9 nm exhibit a selectivity to butenes of roughly 85% at 85% conversion, whereas for 2_Pd/C, the selectivity is close to 40% at similar conversion levels. This illustrates the higher selectivity towards butenes of larger particles at higher conversion levels.

The 1-butene yield as a function over butadiene conversion was determined to probe the selectivity of butadiene semi-hydrogenation, as opposed to over-hydrogenation or isomerisation. For all catalysts, an optimum in 1-butene yield is observed (Figure 2.6A), which for larger nanoparticles had a higher value and was obtained at higher butadiene conversion. The catalyst 9_Pd/C was very selective towards 1-butene up to 95% butadiene conversion without significant selectivity loss due to isomerisation and over-

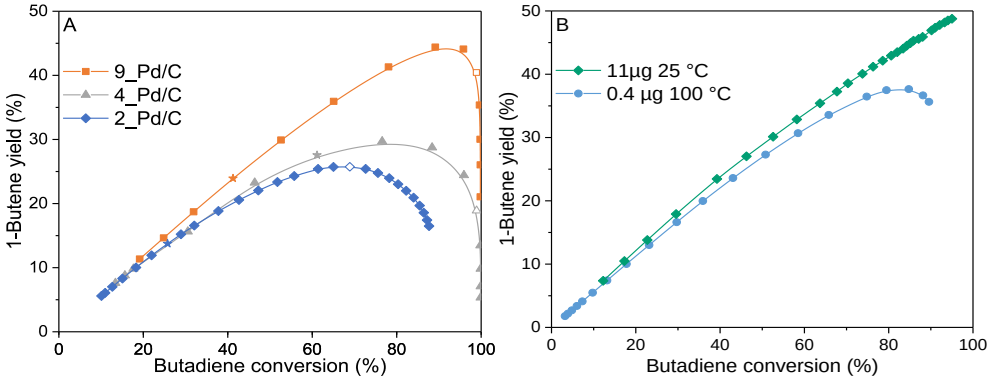

Figure 2.6. 1-Butene yield. (A) 1-Butene yield as function of the corresponding butadiene conversion of differently sized Pd NPs. (B) 1-Butene yield of 17_Pd/C as function of corresponding butadiene conversion for test at high temperature and low loading, and low temperature and high loading.

hydrogenation side reactions. Interestingly, despite the lower dispersion of the 9 nm NPs compared to the 4 nm particles, they showed similar activity per gram of Pd due to the higher TOF of 9_Pd/C. These results demonstrate that 2 nm particles (albeit with high gravimetric activity) do not satisfy the requirement for selective hydrogenation reactions to operate near full conversion[1,20,30,31], and larger NPs of *ca.* 10 nm are needed to retain good selectivity.

Finally, the impact of temperature and metal loading was investigated by comparing two catalytic tests: one ran at 25 °C with 11 µg of Pd, and one at 100°C with 0.4 µg (Figure 2.6B). The 17_Pd/C catalyst at lower temperature and higher loading showed a butene selectivity above 85%, of which almost 50% to 1-butene, up to 95% butadiene conversion and was stable up to 100 hours on stream. On the contrary, at higher temperatures and lower metal loading, the catalyst showed a butene selectivity below 80%, a maximum obtained 1-butene yield of 38% and deactivated after 24 hours on stream. Therefore, depending on the desired application, different catalyst designs as well as catalytic conditions can be chosen for optimal performance. For example, one might prefer to have small nanoparticles operated at higher temperatures, considering maximum activity per gram of metal. However, when the goal is obtaining and retaining a high selectivity close to complete conversion for prolonged operation times in selective hydrogenation reactions, larger Pd nanoparticles at lower temperatures are more desired.

2.4 Conclusions

A series of 2 to 17 nm carbon-supported Pd nanoparticle catalysts were prepared and tested in the selective hydrogenation of butadiene in the presence of a 100-fold excess of propylene. The butadiene hydrogenation activity per surface Pd atom slightly increased with nanoparticle size, from 17 s^{-1} to 34 s^{-1} at 25 °C for 2 nm to 17 nm particles, respectively. The propylene hydrogenation activity decreased with nanoparticle size from 2.6 to 0.65 and 0.4 s^{-1} for particles of 2 nm, 4 nm and 17 nm, respectively. Therefore, the selectivity towards alkene products is size-dependent, where larger particles exhibit a higher selectivity. These trends are explained by a decrease in corner and edge surface sites with increasing particle size. These undercoordinated sites are more prone to facilitate alkane formation in comparison to terrace surface sites, which favour butadiene hydrogenation. In addition to preferential hydrogenation (alkadiene *vs* alkene), less 1-butene isomerisation occurs on larger particles. This resulted in higher 1-butene yields for larger NPs, obtained at butadiene conversion levels closer to 100%. Lastly, for similar conversion levels, the selectivity and stability were better at 25 °C with higher Pd loading than with a lower Pd loading at 100 °C.

2.5 References

1. Derrien, M. L. Chapter 18: Selective Hydrogenation Applied to the Refining of Petrochemical Raw Materials Produced by Steam Cracking. in *Studies in Surface Science and Catalysis* vol. 27 613-666 (1986).
2. Chen, B. *et al.* New developments in hydrogenation catalysis particularly in synthesis of fine and intermediate chemicals. *Appl. Catal. A Gen.* **280**, 17-46 (2005).
3. Bond, G. C., Webb, G., Wells, P. B. & Winterbottom, J. M. The hydrogenation of alkadienes. Part I. The hydrogenation of buta-1,3-diene catalysed by the Noble Group VIII metals. *J. Chem. Soc.* 3218 (1965) doi:10.1039/jr9650003218.
4. Pei, G. X. *et al.* Ag Alloyed Pd Single-Atom Catalysts for Efficient Selective Hydrogenation of Acetylene to Ethylene in Excess Ethylene. *ACS Catal.* **5**, 3717-3725 (2015).
5. García-Mota, M. *et al.* A density functional theory study of the 'mythic' Lindlar hydrogenation catalyst. *Theor. Chem. Acc.* **128**, 663-673 (2011).
6. Lindlar, H. Ein neuer Katalysator für selektive Hydrierungen. *Helv. Chim. Acta* **35**, 446-450 (1952).
7. Vilé, G., Albani, D., Almora-Barrios, N., López, N. & Pérez-Ramírez, J. Advances in the Design of Nanostructured Catalysts for Selective Hydrogenation. *ChemCatChem* **8**, 21-33 (2016).
8. Van Santen, R. A. Complementary Structure Sensitive and Insensitive Catalytic Relationships. *Acc. Chem. Res.* **42**, 57-66 (2009).
9. Yang, F. *et al.* size Dependence of Vapor Phase Hydrodeoxygenation of m-Cresol on Ni/SiO_2 Catalysts. *ACS Catal.* **8**, 1672-1682 (2018).
10. Sterk, E. B. *et al.* Structure Sensitivity of CO_2 Conversion over Nickel Metal Nanoparticles Explained by Micro-Kinetics Simulations. *JACS Au* **2**, 2714-2730 (2022).
11. Cremer, P. S. & Somorjai, G. A. Surface science and catalysis of ethylene hydrogenation. *J. Chem. Soc. Faraday Trans.* **91**, 3671-3677 (1995).
12. Jackson, S. D. *et al.* Supported Metal Catalysts: Preparation, Characterization, and Function. *J. Catal.* **162**, 10-19 (1996).
13. Boitiaux, J. P., Cosyns, J. & Vasudevan, S. Hydrogenation of highly unsaturated hydrocarbons over highly dispersed palladium catalyst. Part I: behaviour of small metal particles. *Appl. Catal.* **6**, 41-51 (1983).
14. Ryndin, Y. A., Stenin, M. V., Boronin, A. I., Bukhtiyarov, V. I. & Zaikovskii, V. I. Effect of Pd/C dispersion on its catalytic properties in acetylene and vinylacetylene hydrogenation. *Appl. Catal.* **54**, 277-288 (1989).
15. Benavidez, A. D. *et al.* Improved selectivity of carbon-supported palladium catalysts for the hydrogenation of acetylene in excess ethylene. *Appl. Catal. A Gen.* **482**, 108-115 (2014).
16. Boitiaux, J. P., Cosyns, J. & Vasudevan, S. Hydrogenation of highly unsaturated hydrocarbons over highly dispersed Pd catalyst. Part II: Ligand effect of piperidine. *Appl. Catal.* **15**, 317-326 (1985).
17. Silvestre-Albero, J., Rupprechter, G. & Freund, H.-J. Atmospheric pressure studies of selective 1,3-butadiene hydrogenation on well-defined $Pd/Al_2O_3/NiAl(110)$ model catalysts: Effect of Pd particle size. *J. Catal.* **240**, 58-65 (2006).
18. Silvestre-Albero, J., Rupprechter, G. & Freund, H.-J. From Pd nanoparticles to single crystals: 1,3-butadiene hydrogenation on well-defined model catalysts. *Chem. Commun.* **1**, 80-82 (2006).
19. Borodziński, A. The effect of palladium particle size on the kinetics of hydrogenation of acetylene-ethylene mixtures over Pd/SiO_2 catalysts. *Catal. Letters* **71**, 169-175 (2001).
20. Borodziński, A. & Bond, G. C. Selective Hydrogenation of Ethyne in Ethene-Rich Streams on Palladium Catalysts, Part 2: Steady-State Kinetics and Effects of Palladium Particle size, Carbon Monoxide, and Promoters. *Catal. Rev.* **50**, 379-469 (2008).
21. Kyriakou, G. *et al.* Isolated Metal Atom Geometries as a Strategy for Selective Heterogeneous Hydrogenations. *Science* **335**, 1209-1212 (2012).

22. Lucci, F. R. *et al.* Selective hydrogenation of 1,3-butadiene on platinum-copper alloys at the single-atom limit. *Nat. Commun.* **6**, 8550 (2015).
23. Yan, H. *et al.* Single-Atom Pd_1/Graphene Catalyst Achieved by Atomic Layer Deposition: Remarkable Performance in Selective Hydrogenation of 1,3-Butadiene. *J. Am. Chem. Soc.* **137**, 10484-10487 (2015).
24. Yan, H. *et al.* Understanding the underlying mechanism of improved selectivity in Pd_1 single-atom catalyzed hydrogenation reaction. *J. Catal.* **366**, 70-79 (2018).
25. Huang, X. *et al.* Toward Understanding of the Support Effect on Pd_1 Single-Atom-Catalyzed Hydrogenation Reactions. *J. Phys. Chem. C* **123**, 7922-7930 (2019).
26. Giannakakis, G., Flytzani-Stephanopoulos, M. & Sykes, E. C. H. Single-Atom Alloys as a Reductionist Approach to the Rational Design of Heterogeneous Catalysts. *Acc. Chem. Res.* **52**, 237-247 (2019).
27. Hannagan, R. T., Giannakakis, G., Flytzani-Stephanopoulos, M. & Sykes, E. C. H. Single-Atom Alloy Catalysis. *Chem. Rev.* **120**, 12044-12088 (2020).
28. Zhang, L., Zhou, M., Wang, A. & Zhang, T. Selective Hydrogenation over Supported Metal Catalysts: From Nanoparticles to Single Atoms. *Chem. Rev.* **120**, 683-733 (2020).
29. Tardy, B. *et al.* Catalytic hydrogenation of 1,3-butadiene on Pd particles evaporated on carbonaceous supports: Particle size effect. *J. Catal.* **129**, 1-11 (1991).
30. McCue, A. J. & Anderson, J. A. Recent advances in selective acetylene hydrogenation using palladium containing catalysts. *Front. Chem. Sci. Eng.* **9**, 142-153 (2015).
31. Borodziński, A. & Bond, G. C. Selective Hydrogenation of Ethyne in Ethene-Rich Streams on Palladium Catalysts. Part 1. Effect of Changes to the Catalyst During Reaction. *Catal. Rev.* **48**, 91-144 (2006).
32. Donoeva, B., Masoud, N. & De Jongh, P. E. Carbon Support Surface Effects in the Gold-Catalyzed Oxidation of 5-Hydroxymethylfurfural. *ACS Catal.* **7**, 4581-4591 (2017).
33. Totarella, G. *et al.* Supported Cu Nanoparticles as Selective and Stable Catalysts for the Gas Phase Hydrogenation of 1,3-Butadiene in Alkene-Rich Feeds. *J. Phys. Chem. C* **125**, 366-375 (2021).
34. Mattarozzi, F. *et al.* Surface-Modified Carbon Materials for CO_2 Electroreduction. *Eur. J. Inorg. Chem.* **26**, e202300152 (2023).
35. Visser, N. L. *et al.* Influence of carbon support surface modification on the performance of nickel catalysts in carbon dioxide hydrogenation. *Catal. Today* **418**, 114071 (2023).
36. Sauter, J. Die Grössenbestimmung der im Gemischnebel von Verbrennungskraftmaschinen vorhandenen Brennstoffteilchen. (1926).
37. Bergeret, G. & Gallezot, P. Characterization of Solid Catalysts: Sections 3.1.1-3.1.3. in *Handbook of Heterogeneous Catalysis* vols 1-5 427-582 (Wiley-VCH Verlag GmbH, 2008).
38. Scherrer, P. Bestimmung der inneren Struktur und der Größe von Kolloidteilchen mittels Röntgenstrahlen. in *Kolloidchemie Ein Lehrbuch* 387-409 (Springer Berlin, 1912). doi:10.1007/978-3-662-33915-2_7.
39. Patterson, A. L. The Scherrer Formula for X-Ray Particle size Determination. *Phys. Rev.* **56**, 978-982 (1939).
40. Weidenthaler, C. Pitfalls in the characterization of nanoporous and nanosized materials. *Nanoscale* **3**, 792-810 (2011).
41. Masoud, N. *et al.* Silica-Supported Au-Ag Catalysts for the Selective Hydrogenation of Butadiene. *ChemCatChem* **9**, 2418-2425 (2017).
42. van der Hoeven, J. E. S. *et al.* Unlocking synergy in bimetallic catalysts by core-shell design. *Nat. Mater.* **20**, 1216-1220 (2021).
43. Valcárcel, A., Clotet, A., Ricart, J. M., Delbecq, F. & Sautet, P. Comparative DFT study of the adsorption of 1,3-butadiene, 1-butene and 2-cis/trans-butenes on the Pt(111) and Pd(111) surfaces. *Surf. Sci.* **549**, 121-133 (2004).
44. Garcia Cervantes, G. Compared properties of Pd on thermo-conductor supports (SiC, Si_3N_4) and Pd on oxide supports (Al_2O_3, SiO_2) for the 1,3-butadiene hydrogenation reaction. *J. Catal.* **214**, 26-32 (2003).

45. Rebelli, J., Detwiler, M., Ma, S., Williams, C. T. & Monnier, J. R. Synthesis and characterization of Au-Pd/SiO_2 bimetallic catalysts prepared by electroless deposition. *J. Catal.* **270**, 224-233 (2010).
46. Kabalan, L., Kowalec, I., Catlow, C. R. A. & Logsdail, A. J. A computational study of the properties of low- and high-index Pd, Cu and Zn surfaces. *Phys. Chem. Chem. Phys.* **23**, 14649-14661 (2021).
47. Yang, B., Burch, R., Hardacre, C., Hu, P. & Hughes, P. Mechanistic Study of 1,3-Butadiene Formation in Acetylene Hydrogenation over the Pd-Based Catalysts Using Density Functional Calculations. *J. Phys. Chem. C* **118**, 1560-1567 (2014).
48. Araujo-Lopez, E., Joos, L., Vandegehuchte, B. D., Sharapa, D. I. & Studt, F. Theoretical Investigations of (Oxidative) Dehydrogenation of Propane to Propylene over Palladium Surfaces. *J. Phys. Chem. C* **124**, 3171-3176 (2020).
49. Teschner, D. *et al.* The Roles of Subsurface Carbon and Hydrogen in Palladium-Catalyzed Alkyne Hydrogenation. *Science* **320**, 86-89 (2008).
50. Teschner, D. *et al.* Understanding palladium hydrogenation catalysts: When the nature of the reactive molecule controls the nature of the catalyst active phase. *Angew. Chemie - Int. Ed.* **47**, 9274-9278 (2008).
51. Tew, M. W., Janousch, M., Huthwelker, T. & van Bokhoven, J. A. The roles of carbide and hydride in oxide-supported palladium nanoparticles for alkyne hydrogenation. *J. Catal.* **283**, 45-54 (2011).
52. Dekura, S., Kobayashi, H., Kusada, K. & Kitagawa, H. Hydrogen in Palladium and Storage Properties of Related Nanomaterials: size, Shape, Alloying, and Metal-Organic Framework Coating Effects. *ChemPhysChem* **20**, 1158-1176 (2019).
53. Tew, M. W., Miller, J. T. & van Bokhoven, J. A. Particle size Effect of Hydride Formation and Surface Hydrogen Adsorption of Nanosized Palladium Catalysts: L_3 Edge *vs* K Edge X-ray Absorption Spectroscopy. *J. Phys. Chem. C* **113**, 15140-15147 (2009).
54. Tew, M. W., Nachtegaal, M., Janousch, M., Huthwelker, T. & Van Bokhoven, J. A. The irreversible formation of palladium carbide during hydrogenation of 1-pentyne over silica-supported palladium nanoparticles: *In situ* Pd K and L_3 edge XAS. *Phys. Chem. Chem. Phys.* **14**, 5761-5768 (2012).
55. Luneau, M. *et al.* Achieving High Selectivity for Alkyne Hydrogenation at High Conversions with Compositionally Optimized PdAu Nanoparticle Catalysts in Raspberry Colloid-Templated SiO_2. *ACS Catal.* **10**, 441-450 (2020).
56. Totarella, G., de Rijk, J. W., Delannoy, L. & de Jongh, P. E. Particle size Effects in the Selective Hydrogenation of Alkadienes over Supported Cu Nanoparticles. *ChemCatChem* **14**, e202200348 (2022).
57. Bond, G. C. Hydrogenation of Alkadienes and Poly-Enes. in *Metal-Catalysed Reactions of Hydrocarbons* 357-394 (Springer US, 2005). doi:10.1007/0-387-26111-7_8.
58. A. Roine. HSC Chemistry 9. Software available at www.metso.com/hsc. Metso, Pori (2023)
59. Horiuti, I. & Polanyi, M. Exchange reactions of hydrogen on metallic catalysts. *Trans. Faraday Soc.* **30**, 1164-1172 (1934).
60. Bates, A. J., Leszczynski, Z. K., Phillipson, J. J., Wells, P. B. & Wilson, G. R. The hydrogenation of akladienes. Part IV. The reaction of buta-1,3-diene with deuterium catalysed by rhodium, palladium, and platinum. *J. Chem. Soc. A Inorganic, Phys. Theor.* 2435-2441 (1970) doi:10.1039/j19700002435.
61. Yang, X.-F., Wang, A.-Q., Wang, Y.-L., Zhang, T. & Li, J. Unusual Selectivity of Gold Catalysts for Hydrogenation of 1,3-Butadiene toward cis -2-Butene: A Joint Experimental and Theoretical Investigation. *J. Phys. Chem. C* **114**, 3131-3139 (2010).

Chapter 3

Influence of mass transport

This chapter is based on: Brandt Corstius, O.E., Kikkert, M., Roberts, S.T., Doskocil, E.J., van der Hoeven, J.E.S. & de Jongh, P.E. Mass transport effects in gas-phase selective hydrogenation of 1,3-butadiene over supported Pd. *Reaction Chemistry & Engineering,* Advance Article, (2024). DOI:10.1039/d4re00039k

Abstract

As demonstrated in the previous chapter, retaining high selectivity at high conversion using a Pd catalyst is challenging during selective hydrogenation reactions. The resulting undesired alkane formation is often ascribed to intrinsic properties of the Pd metal. However, in this chapter, we show that heat and mass transport effects strongly impact the catalytic activity and selectivity of Pd nanoparticles on carbon (Pd/C) catalysts in the selective hydrogenation of butadiene. By systematically varying the Pd loading and catalyst grain size, we show that higher loadings and larger grains strongly decrease the butene selectivity. This is ascribed to an effect of internal diffusion limitations arising from butadiene depletion in the core of the catalyst grains and not by intrinsic properties of Pd. The comprehensive assessment of heat and mass transport phenomena is essential to reliably relate experimental observations to catalyst properties such as Pd particle size, support or promoter effects. It contributes to the understanding of catalysts for selective hydrogenation of butadiene and can be extended to other reactions and/or supported metal catalysts.

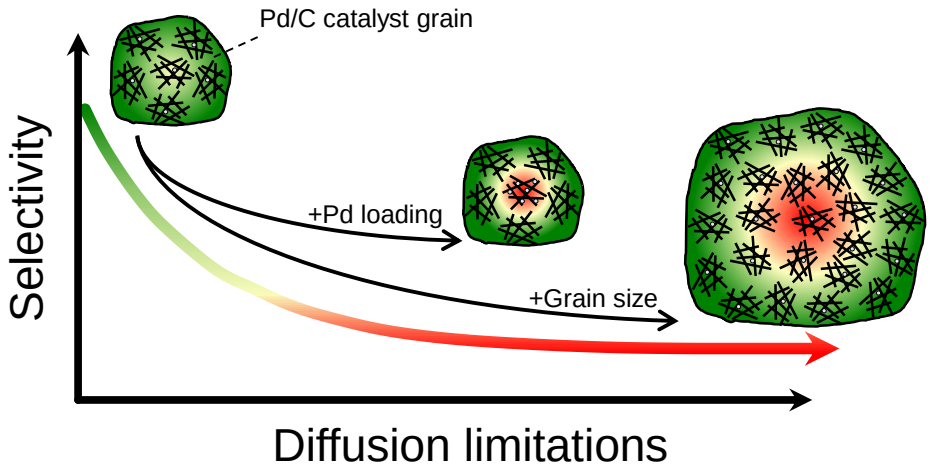

3.1 Introduction

Selective hydrogenation is of great interest both for academic research as well as for industrial applications ranging from the production of fine chemicals, pharmaceuticals, food additives and agrochemicals to the purification of polymer-grade purity olefins.[1-4] Typically, supported Pd-based catalysts are used for selective hydrogenation reactions because of their superior activity at moderate temperatures.[5–7] Their high activity, however, also induces challenges in retaining good selectivity, as Pd often leads to unwanted alkane production. The poor performance of monometallic Pd is ascribed to properties such as strong heat of adsorption of the reactant[8] and/or the formation of Pd-hydride[6]. Therefore, commercially available Pd-based catalysts for selective hydrogenation are typically modified with secondary metals such as Ag[9] or Pb[10] and/or molecular adsorbates[10,11]. Proposed explanations for the increased selectivity of modified Pd include geometric[12–14] and/or electronic[8,14–17] effects. Such modifications increase the selectivity but often come at the expense of the conversion. The surface- or mass-normalised activity roughly decreases by 1 to 2 orders of magnitude compared to monometallic Pd, which is undesirable considering the scarcity and costs of Pd metal.[12,16–19] This raises the question of how improved selectivity can be disentangled from the effects of reduced activity. Hence, a fundamental understanding of Pd-based catalyst intrinsic performance is valuable.

In addition to the chemical properties of a catalyst, a considerable influence on the catalytic performance is related to the physical and structural properties in combination with the reaction conditions. For example, heat generation in exothermic reactions can induce local temperature effects on or near the active metal nanoparticle surface if the overall heat conductivity of the system is not sufficient. Early attempts by Luss to model the heat generated by an exothermic reaction over platinum nanoparticles predicted a temperature increase with an upper bound as high as 200 to 500 °C.[20] Sharma *et al.* spectroscopically showed that the surface temperature of a 1% Pt/SiO_2 catalyst increased by 119 °C, from 98 to 217 °C, upon continuous exposure to a CO/O_2 mixture.[21] Similarly, a temperature difference of 130 °C between the metal nanoparticle and the reaction gas was found during steady-state oxidation of 2% CO over a Pt/Al_2O_3 monolith.[22] Geitenbeek *et al.* showed by luminescence thermometry that a sharp increase in temperature is induced during methanol-to-hydrocarbons (MTH) reactions.[23] Upon exposure of the reaction gas (18% methanol in He) over H-ZSM-5 zeolite catalyst, a temperature increase of 100 °C was observed, from 500 to 600 °C, which took up to 2 hours to stabilise to steady-state conversion. This illustrates that exothermic reactions can cause local heating effects that can be deliberately applied to induce higher catalytic activity[24] but should be avoided when determining the intrinsic structure-performance relationships of a catalyst.

In heterogeneous catalysis, the activity scales with the concentration of the reactants and the reaction order. Hence, the reactant concentration at the catalyst active site is highly relevant. In typical reactors (*e.g.,* plug flow), unless operating in differential

conversion mode, a significant concentration gradient over the catalytic bed exists due to the difference in reactant concentration at the beginning (inlet) and end of the catalytic bed (outlet). This concentration gradient increases with the increasing conversion. If a catalyst reaction rate surpasses the reactant diffusion rate, a concentration gradient is generated in the vicinity of the catalyst, which is referred to as mass transport or diffusion limitations.

With external mass transport limitations, the reaction rate is limited by the reactant supply from the bulk gas or liquid phase to the catalyst grains. Internal mass transport limitations describe the limitations of diffusion within a catalyst grain, as a gradient is induced from the surface to its interior. A framework for assessing the effect of these mass transport limitations has been developed by Thiele, Weisz and Prater.[25,26] For selective hydrogenation reactions, the presence of diffusion limitations can negatively influence not only the activity but also the selectivity.[27,28] This is aggravated by the presence of micropores[29], larger catalyst grain sizes[30], and/or coke build-up.[31–34] The Barreto group studied the kinetics of selective hydrogenation of butyne- and butadiene-butene mixtures in trickle bed reactors.[35,36] They demonstrated that the local concentration of polyunsaturated molecules sharply dropped inside the catalyst grains due to internal mass transfer limitations. These results gave valuable insights into some parameters determining selectivity during selective hydrogenation reactions. However, the literature has been focused on liquid-phase hydrogenation in batch operation, whereas academic selective hydrogenation of alkynes and alkadienes mostly occurs in the gas phase during continuous operation.[4] Liquid-phase and gas-phase hydrogenation differ from a kinetic viewpoint, as the effective diffusion of gasses is orders of magnitude faster than in the condensed phase.[37] Moreover, in liquid-phase hydrogenation reactions, the reaction kinetics depend on the solubility of molecular hydrogen, which complicates the comparison of literature with gas-solid heterogeneous catalysis.

Therefore, in this chapter, we describe the effects of heat and mass transport during the gas-phase selective hydrogenation of 1,3-butadiene. We demonstrate that diffusion limitations strongly affect the catalytic performance of Pd/C catalysts and explain how these effects are identified and avoided.

3.2 Experimental details

3.2.1 Catalyst preparation and characterisation

Carbon-supported Pd-catalysts (Pd/C) were prepared by incipient wetness impregnation of Pd-precursor onto graphene nanoplatelets (GNP) support, as described in section 2.2.2. The desired metal weight loading (2.5 wt%) of the Pd/C catalyst was achieved by dilution of the 10 wt% tetraamine palladium(II) nitrate with purified water, while the lower weight loadings (0.5 wt%, 0.1 wt% and 0.02 wt%) were

prepared by successive further dilution of the impregnation solution of the 2.5 wt% Pd/C catalyst with purified water. Pd nanoparticles were grown to the desired size (see Chapter 2) using a high-temperature reduction step at 500 °C in 10% H_2 (1 °C/min, 1-hour hold, 10 and 90 mL/min H_2 and N_2 flow).[19,38]

Bright-field TEM images were collected at 120 kV on Talos L120C (Thermo Scientific) electron microscope. Images of the post-catalysis samples were acquired by scanning TEM (STEM) on a Talos F200X (Thermo Scientific) electron microscope in dark field mode operated at 200 kV. Nanoparticle sizes were determined by manually measuring the diameters of 100-400 Pd particles in different regions of the sample using ImageJ software. The number-average diameters and volume area averaged diameters were determined by Eq. 2.1 and 2.2.

Accordingly, the available surface area of Pd (SA, m^2_{Pd}/g_{cat}) is calculated from the dispersion (D, Eq. 2.10) and Pd weight loading ($wt\%$) as

$$SA = wt\%\ N_{\mathrm{Av}}\ a_{\mathrm{Pd}}\ D/M_{\mathrm{Pd}} \qquad \text{Eq. 3.1}$$

where N_{Av} is Avogadro's constant (6.022×10^{23} mol^{-1}) and M_{Pd} is the molar mass of Pd (106.42 g/mol).

X-ray diffraction (XRD) measurements were performed as described in Section 2.2.3. Scans were continuously accumulated for at least 60 hours to improve the signal-to-noise ratio for determination of the crystallite size of the low wt% catalysts.[39]

3.2.2 Catalytic testing

The catalytic performance was assessed in a custom-built gas-phase hydrogenation set-up. Experimental details are provided in section 2.2.4. The as-prepared catalysts of 2.5%, 0.5% and 0.1% Pd/C (by weight) were diluted in bare carbon (GNP), so the final weight loading of all Pd/C-C mixtures was 0.02% Pd (Figure 3.1). Of the (diluted) catalysts, 1.0 g was pressed into a pellet (74 MPa), which was then gently crushed over a set of sieves to obtain sieve fractions of 1-37 µm, 38-74 µm, 75-149 µm and 150-211 µm. For each catalytic test, 2.50 mg of (diluted) catalyst was mixed with 0.30 g of SiC (212-400 µm), which resulted in a constant metal loading of 0.50 µg Pd in the reactor.

The conversion (X_i) and selectivity (S_i) during the catalytic test were determined by Eq.2.4-8. The selective butenes yield (Q) of the reaction was determined as the product of conversion and selectivity as:

$$Q_{\mathrm{butenes}} = X_{\text{1,3-butadiene}}\ S_{\mathrm{butenes}} \qquad \text{Eq. 3.2}$$

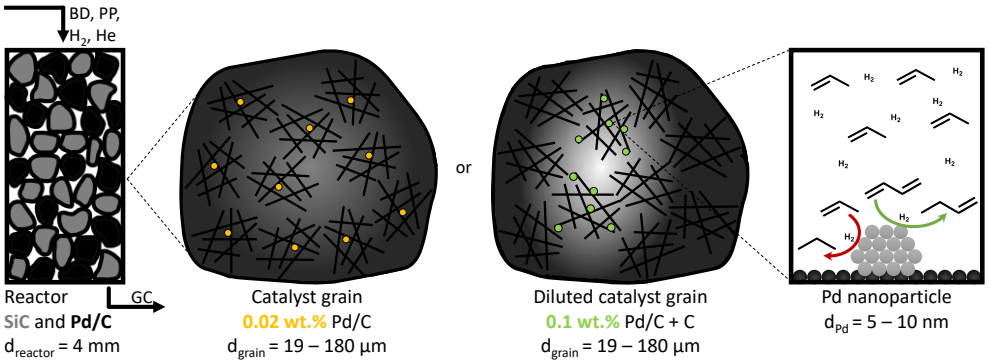

Figure 3.1. Schematic representation of selective hydrogenation reactor at different length scales. From left to right: 4.0 mm internal diameter fixed bed reactor with inlet gas mixture of 0.3% butadiene (BD), 30% propylene (PP), 20% hydrogen and 49.7% helium. Pd/C catalyst grains (black) are mixed with nonporous and inert SiC particles (grey). Reactant and product concentrations are analysed by on-line gas chromatography (GC). Middle: catalyst grains with non-diluted 0.02% Pd/C or 0.1% Pd/C diluted in GNP to achieve equal Pd weight loading in each reactor. The greyscale schematically indicates the reactant concentration in the grains during catalysis, as it is converted over the active Pd nanoparticles, but not over the inert carbon dilutant. Right: selective hydrogenation of butadiene over Pd nanoparticles, in an excess of hydrogen and propylene. Drawings not to scale.

3

3.2.3 Calculations of transport phenomena

Estimations of heat and mass transfer effects in catalytic fixed-bed reactions were calculated using the Eurokin web-tool[40] and the references therewithin. As criteria for mass and heat transport limitations, a deviation of more than 5% from the non-limited activity is considered as a transport-limited reaction.[25,26,40,41] A detailed description of the calculations is provided in the supporting information. The calculations are based on the diffusion and thermal properties of the gasses as obtained from the literature (Table S3.1). Temperature-dependent values are determined at the relevant reaction temperature during the catalysis. The density of the gas mixture is based on the ideal gas law, assuming constant pressure (1 atm). The properties of the reactor and the catalyst materials are listed in Table 3.1. The pellet density was calculated by measuring the thickness of a 13 mm catalyst pellet with known mass prior to sieving, pressed at 74 MPa. The porosity was calculated by adding a known amount of material to the catalytic reactor and measuring the height of a catalyst bed.

For the diffusion criteria, butadiene is taken as the limiting reactant (0.3 mol%) in the gas mixture. The calculated bulk diffusivity ($D_{BD,bulk}$, Eq. S3.1-Eq. S3.3) of butadiene in the mixture was between 1.5 and 2.5×10^{-6} m^2/s for 25 and 100 °C, respectively (Table S3.1). Taking in consideration Knudsen diffusion, the effective diffusivity ($D_{BD,eff}$, Eq. S3.4-Eq. S3.6) was between 3.5×10^{-7} and 3.9×10^{-7} m^2/s (see section 3.6 on page 71 for details), in line with other estimations on gas-phase diffusion in porous

Table 3.1. Properties of reactor and catalyst.

Pressure	1.013×10^{5}	Pa	**Pellet porosity (ε_p)**	0.82	m^3/m^3_{cat}
Molar inlet flow (F)	3.44×10^{-5}	mol/s	**Pellet density (ρ_p)**	657	kg/m^3_{cat}
Internal diameter	4.0×10^{-3}	m	**Catalyst density (ρ_{cat})**	1045	kg/m^3_{bed}
Bed porosity (ε)	0.37	m^3/m^3_{bed}	**Mass catalyst (m_{cat})**	2.5	$\times10^{-6}$ kg
Tortuosity (τ)	1.64	-	**Catalyst grain size (d_p)[a]**	19, 56, 112, 180	$\times10^{-6}$ m
Reaction-order (n)	-0.25[19]	-	**Catalyst surface area**	500	$\times10^{3}$ m^2/kg

[a] Average grain size from 1-37, 38-74, 75-149 and 150-211 µm sieve fractions.

solids.[37] In this calculation, cylindrical pores were assumed for the support, for which the pore diameter was estimated from the catalyst density and the surface area of the carbon (Table 3.1). This geometrical assumption overestimated the microporosity of the carbon, which has a relatively open catalyst structure (*vide infra*, section 3.3.1). For the carbon support, porosity arises from the stacking of graphitic plate-like sheets and not from channel-like micropores. Hence, the provided values for $D_{BD,eff}$ should be considered as a lower limit for butadiene diffusion rates.

External and internal heat transfer phenomena were calculated based on the rate and exothermicity of the reactions and the thermal properties of the gas mixture (Table S3.1) or the solid catalyst. The heat of the reaction was determined from the hydrogenation reaction enthalpy of each reactant (butadiene, butene, propylene). In the butadiene hydrogenation reaction, the different butene products have slightly different reaction enthalpies (-110, -120 and -116 kJ/mol for 1-butene, trans-2-butene and cis-2-butene, respectively). An average value of -113.8 kJ/mol is obtained for the typical product distribution of Pd-catalysed butadiene hydrogenation (60% 1-butene, 37% trans-2-butene and 3% cis-2-butene).[19,42] For the hydrogenation of propylene, -124 kJ/mol is used, and -125 kJ/mol for the over-hydrogenation of 1-butene to n-butane. External temperature gradients were calculated as the temperature difference over the gas film surrounding the catalyst grain (Eq. S3.9-13). The difference between the average temperature of the catalyst grain and the external surface temperature of the grain was calculated as the internal temperature gradient (Eq. S3.14). The temperature differences were compared to the dimensionless activation energy of butadiene hydrogenation to check the activity criterion (<5% deviation) as a result of heat transfer limitations.

External and internal mass transfer limitations were assessed by comparison of the effective diffusion of butadiene and the observed consumption rate of butadiene molecules. The volumetric reaction rate of the catalyst grains, $R_{\text{vol.}}^{\text{Obs}}$ (mol m^{-3} s^{-1}), is defined as:

$$R_{\text{vol.}}^{\text{Obs}} = R_{\text{mass}}^{\text{Obs}}\,\rho_{\text{cat}} = \frac{F\,x_i\,X_i\,\rho_{\text{cat}}}{m_{\text{cat}}} \qquad \text{Eq. 3.3}$$

where $R_{\text{mass}}^{\text{Obs}}$ is the observed gravimetric reaction rate (mol kg^{-1} s^{-1}), ρ_{cat} is the density of the catalyst grains (1045 kg m^{-3}), F is the reaction gas flow (3.44×10^{-5} mol s^{-1}), x_i is the reactant inlet fraction (0.003 for butadiene, 0.3 for propylene), X_i is the conversion of the individual reactant and m_{cat} is the loaded mass of catalyst (2.5×10^{-6} kg). External diffusion limitations were assessed based on the Carberry number, which describes the difference between the bulk gas-phase concentration (C_{BD}^{0}, 0.3 mol%) and the concentration at the external surface of a catalyst grain ($C_{\text{BD}}^{\text{surf}}$, see Eq. S3.16). Internal diffusion limitations were calculated by the Weisz-Prater criterion.[26] The Weisz-modulus (Φ) was defined as:

$$\Phi = \left(\frac{n+1}{2}\right)\frac{R_{\text{vol.}}^{\text{Obs}}\,(d_{\text{p}}/6)^2}{D_{\text{BD,eff}}\,C_{\text{BD}}^{\text{surf}}} \qquad \text{Eq. 3.4}$$

where $C_{\text{BD}}^{\text{surf}}$was be determined from the Carberry number (Eq. S3.16). To fulfil the Weisz-Prater criterion (deviation less than 5% due to diffusion limitation in small pores), the Weisz-modulus should be less than 0.08.[43] Analogous to the Weisz-Prater modulus (Φ) is the Thiele modulus (φ)[25] which is defined as:

$$\varphi = \frac{d_{\text{p}}}{6}\sqrt{\left(\frac{n+1}{2}\right)\frac{R_{\text{vol.}}^{\text{Obs}}}{D_{\text{BD,eff}}}\,{C_{\text{BD}}^{\text{surf}}}^{n-1}}. \qquad \text{Eq. 3.5}$$

The Thiele- and Weisz-moduli are related by $\Phi = \eta_{\text{int}}\varphi^2$, where $\eta_{int}$is the effectiveness factor, which is a measure for the catalyst utilisation between 0 and 100%. The effectiveness factor is defined as the ratio between the observed average reaction rate and the rate of reaction at the catalyst surface (in the absence of any diffusion limitations).[44,45] It provides an average fraction of the catalyst material which is used in the catalysis to its full potential. Without any limitations, η_{int}=1, which decreases as a result of increasing mass transport limitations, when part of the catalyst interior will contribute less to the total reactions. For a first-order reaction η_{int} is derived from the Thiele modulus as:

$$\eta_{\text{int}} = \frac{1}{\varphi}\left(\frac{1}{\tanh(3\varphi)} - \frac{1}{3\varphi}\right) \qquad \text{Eq. 3.6}$$

Since the catalyst reaction rate depends on the reactant concentration, we define the internal effectiveness factor to be related to the concentration profile inside a catalyst grain. Here, the mathematical integration of the concentration profile as function of penetration depth, $f(d,x)$, over the entire grain represents the value of η_{int}. Assuming spherical grains, this means:

$$\int_0^{d_p/2} 4\pi \left(d - d_p/2\right)^2 \times f(d,x)\mathrm{d}d \;=\; \eta_{int} \times \int_0^{d_p/2} 4\pi \left(d - d_p/2\right)^2 \mathrm{d}d \qquad \text{Eq. 3.7}$$

where d is the penetration depth inside the catalyst grain, $d_p/2$ is the centre of the grain at half the diameter and $f(d,x)$ is the concentration profile as a function of the penetration depth. For $f(d,x)$ multiple functions can be assumed, such as an exponential decrease

$$f(d,x) = e^{-dx} \qquad \text{Eq. 3.8}$$

which is valid for a reaction with positive reaction order (n), a linear concentration-depth profile

$$f(d,x) = 1 - dx \qquad \text{Eq. 3.9}$$

which describes a zero-order reaction, or a concentration profile which is expected for n <0 such as

$$f(d,x) = 1 - e^{dx} \qquad \text{Eq. 3.10}$$

where the values for x can be determined if η_{int} is known, using a numerical solver and Eq. 3.7.

3.3 Results and discussion

3.3.1 Structural properties of supported Pd catalysts

Pd-catalysts of different weight loadings were prepared by incipient wetness impregnation followed by a reduction treatment at 500 °C to induce Pd particle growth.[19,38] Figure 3.2A shows the Transmission Electron Microscopy (TEM) image of a typical Pd/C catalyst grain of roughly 1 micron. Figure 3.2B-E depict higher magnification images of the supported Pd nanoparticles of four selected catalysts. The images show Pd particles of similar size dispersed over the carbon support. The number of visible particles per image decreased with decreasing weight loading, showing just a single Pd particle in the TEM image with the lowest Pd loading (Figure 3.2E, 0.02 wt%). Average Pd particle sizes between 4.4 and 9.6 nm in diameter were found for the different catalysts, resulting in a specific Pd surface area between 0.01 and 2.6 m^2/g (Table 3.2). An increasing trend in size was observed with decreasing weight loading, contrary to expected loading-size correlations, where higher metal loadings typically result in more agglomeration and, thus, larger particles.[46–49] The observed trend in particle size might be attributed to slight instability of the diluted Pd-precursor, as the catalysts were prepared from high to low weight loading in successive order (see section 3.2). Nevertheless, the nanoparticles in the different catalysts were of a suitable size (> 4 nm), so minimal effects due to size-dependent catalytic performance are present.[19] For the catalytic results, the catalysts will be referred to according to their

Table 3.2. Palladium nanoparticles properties.

Catalyst	Pd wt%[a]	d_{TEM} (nm)	d_{VA} (nm)	Dispersion	SA (m^2_{Pd}/g_{cat})	d_{XRD} (nm)
2.6_Pd/C	2.51	4.4±1.1	4.9±1.2	22.6%	2.55	3.8
0.4_Pd/C	0.49	5.3±1.2	5.8±1.3	19.3%	0.42	4.3
0.06_Pd/C	0.10	6.6±2.0	7.8±2.5	14.2%	0.064	5.8
0.01_Pd/C	0.019	9.6±2.1	10.4±2.3	10.6%	0.0091	n.d.[b]

[a] Determined from precursor amount in incipient wetness impregnation. [b] Not determined due too low weight loading.

specific Pd surface area (SA) as *X*_Pd/C, where *X* is the exposed surface of the Pd nanoparticles, in $m^2_{Pd}/g_{catalyst}$.

X-ray diffraction (XRD, Figure 3.2F) showed diffraction peaks of graphite (support) and metallic palladium nanoparticles and no indication of other crystalline phases, such as Pd-oxide, between 20 and 70° 2θ. Figure 3.2F shows the Pd(111) diffraction at 46.6° 2θ, which increased in intensity for higher Pd weight loading. The carbon-subtracted spectra in the inset of the figure give the isolated Pd(111) peak. The crystallite size of

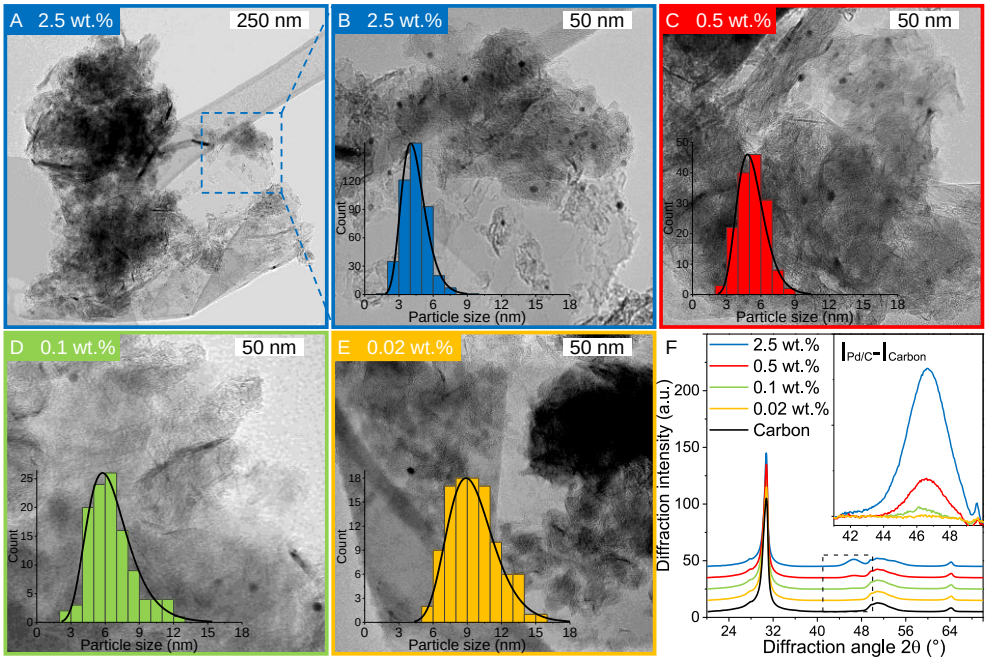

Figure 3.2. Catalyst characterisation. (A-E) Transmission electron microscopy (TEM) images of Pd/C catalysts with weight loading of (AB) 2.5 wt% at low (A) and high (B) magnification, (C) 0.5 wt% (D) 0.1 wt% and (E) 0.02 wt%. Insets show size histograms of the individually measured diameters from TEM and lognormal fit to the distribution. (F) X-ray diffractogram of the Pd/C catalysts. The inset shows the carbon-subtracted intensity, highlighting the Pd(111) diffraction.

Pd particles was determined from the full width at half maximum (FWHM) of the carbon-subtracted Pd(111) diffraction peak, according to the Scherrer equation.[39,50,51] Average crystallite sizes between 3.8 and 5.8 nm were found for the catalyst between 2.5 and 0.1 wt% Pd, respectively (Table 3.2). For the 0.02 wt% catalyst, the diffraction signal was too weak to observe any Pd diffraction. The trends in crystallite size from XRD corroborate the particle sizes obtained by TEM (Table 3.2), suggesting that the Pd particles are single crystalline.

3.3.2 Conversion and catalyst activity

Figure 3.3A depicts the conversion of butadiene as a function of temperature for 0.01_Pd/C and 2.6_Pd/C for the smallest (19 µm) and largest (180 µm) average grain size. The conversion increased with temperature and showed an S-shaped curve. This shape reflects an initial exponential increase followed by saturation when approaching complete conversion.

Surprisingly, the observed activity at 25 °C differed for the different catalyst grain sizes within the same catalyst sample (comparing triangles to circles), even though an identical amount of Pd metal was loaded in each reactor (0.50 µg Pd). For example, the activity of the 180 µm grains was 1.4-1.5 times higher than the 19 µm grains at 25 °C. A local heating effect can explain this phenomenon. With the larger grains, the same amount of catalyst is concentrated in fewer grains. For example, decreasing the radius of one spherical grain by a factor of 2 results in 2^3=8 times smaller grains with a combined volume equal to the single larger grain. Therefore, with a larger grain size,

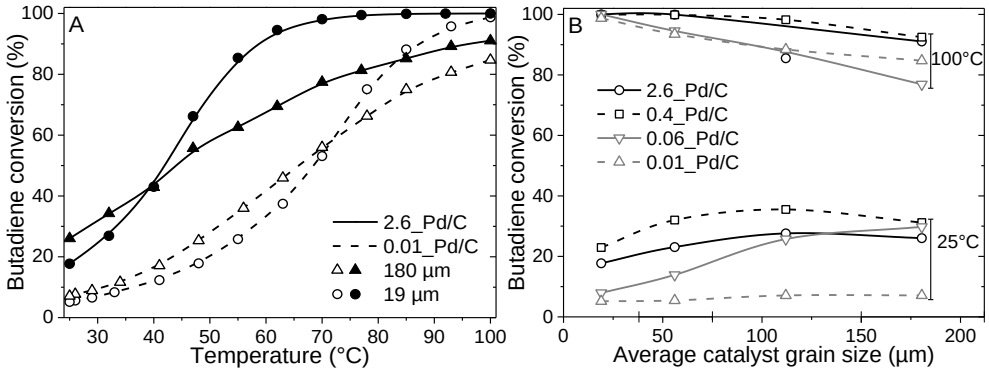

Figure 3.3. Catalytic activity. (A) Butadiene conversion as function of temperature for 2.6_Pd/C (solid line, filled symbols) and 0.01_Pd/C (dashed line, open symbols) catalysts with an average grain size of 19 µm (circles) or 180 µm (triangles). Conversion was stabilised for 1.5 hours at 25 °C before heating to 100 °C with 0.5 °C/min. (B) Comparison of conversion of all catalyst-grain size combination at 25 °C and 100 °C. Reaction conditions: 0.50 µg Pd, 50 mL/min reaction gas mixture of 0.3% butadiene, 30% propylene, 20% H_2 and He balance.

the generated heat from the exothermic hydrogenation reactions was retained in fewer particles in a smaller fraction of the catalyst bed. The generated heat within the vicinity of the catalyst grains resulted in a higher local temperature, which induced higher apparent activity. The 1.4-1.5 times increase corresponds to a temperature increase of 5-6 °C assuming Arrhenius behaviour and 50 kJ/mol activation energy, which is less than 9.1 °C adiabatic temperature increase estimated at 100% butadiene conversion (Eq. S3.8).[5,19]

Figure 3.3A also shows that at 25 °C, the activity for 2.6_Pd/C was roughly 3.5 times higher than for 0.01_Pd/C with an equal amount of metal loaded in the reactor. The activity ratio between these two catalysts (3.5) was larger than their corresponding metal dispersion ratio (2.1, Table 3.2). Therefore, the particle size difference cannot explain the activity increase of 2.6_Pd/C. The trends in higher activity with higher Pd loading were ascribed to more local heating of the catalysts with higher Pd loading. In the undiluted 0.01_Pd/C (Figure 3.1), the distribution of Pd is uniform over the catalyst grain. In contrast, for 0.06_Pd/C, the specific Pd area is 7 times more concentrated and more heterogeneously distributed throughout the catalyst grain since it is mixed in a 1:4 ratio with bare carbon (Figure 3.1). Such local concentration effects also contributed to local heating in the 0.4_Pd/C and 2.6_ Pd/C catalysts, with 25 and 125 times more concentrated Pd in parts of the catalyst grain.

From the initial exponential increase with temperature, the apparent activation energies (E_{act}) were derived between 25 and 47 °C. The Arrhenius plots (Figure S3.1) yield E_{act} of 45.9±0.4 and 43.4±0.3 kJ/mol for 2.6_Pd/C and 0.01_Pd/C with 19 μm grain size, respectively, in line with previous studies on Pd-catalysed butadiene hydrogenation.[5,19] For the 0.01_Pd/C catalyst with 180 μm grains, a similar E_{act} (43.3±0.7 kJ/mol) was found, whereas for 2.6_Pd/C, the obtained value is only 25.8±2 kJ/mol. The lower apparent activation energies for higher loadings and larger grains suggested the occurrence of mass transport limitations already below 47 °C and 40% conversion.

At higher conversion, the 19 μm grains were more active than the 180 μm grains and an inverted trend was observed compared to at 25 °C (Figure 3.3AB). The decrease in activity for the larger grains originated from mass transfer limitations becoming more prominent, as evidenced by the decreasing slope in the Arrhenius plot (Figure S3.1). Because of the increasing activity of Pd/C at elevated temperatures, the diffusion rate of butadiene became limiting. Hence, a part of the volume of the catalyst grains was deficient in butadiene concentration, resulting in a lower average activity. As a result, none of the tested catalysts with 180 μm grains showed 100% conversion at 100 °C, whereas for the smaller grains, complete conversion was obtained (Figure 3.3B).

In short, reactors with equal Pd mass loading showed variable catalytic activity, which cannot be explained by an effect of particle size.[19] Local heating effects induced higher activity over Pd/C catalysts with higher Pd loading and/or larger grain size, especially at low conversion. At higher conversion, the activity trend as a function of grain size

was inverted due to increasing mass transfer limitations. Here, smaller grains outperformed the larger grains, as depicted by the cross-over point of the catalysts in Figure 3.3A. Local concentration gradients, as a result of diffusion limitations, have a large influence on obtaining active catalysts.[24] However, this only describes the activity of the catalyst, whereas selectivity is of essential importance, especially in selective hydrogenation applications.

3.3.3 Selectivity to butenes

Figure 3.4A shows the selectivity to butenes as of function over butadiene conversion of 2.6_Pd/C and 0.01_Pd/C catalysts for the smallest (19 µm) and largest (180 µm) tested average grain size. The 19 µm grains showed a selectivity close to 100% at low (*e.g.,* <25%) butadiene conversion levels. The high butene selectivity is explained by the strong adsorption of butadiene, in comparison to butenes or propylene (adsorption energy of -1.7 eV for butadiene, between -0.7 and -0.9 eV for propylene and butenes on Pd(111)).[52,53] Therefore, as a result of strong competitive adsorption, the Pd nanoparticle surface is covered by butadiene, which effectively blocks propylene adsorption and limits the residence time of the butene that is formed. Only at higher butadiene conversion levels (*e.g.,* >85%), the selectivity decreased due to a decreasing concentration of butadiene at the nanoparticle surface.

The 0.01_Pd/C catalyst with larger grains (180 µm) also showed a high selectivity at low conversion levels (*e.g.,* >90% selectivity below 50% conversion), whereas for 2.6_Pd/C, the selectivity was below 80% at 26% conversion. For the butane selectivity, similar trends were observed as a function of Pd loading and grain size (Figure S3.1B). The low selectivity of 2.6_Pd/C catalyst with 180 µm grain size is ascribed to internal mass transfer limitations, as will be discussed in more detail in section 3.3.4. The

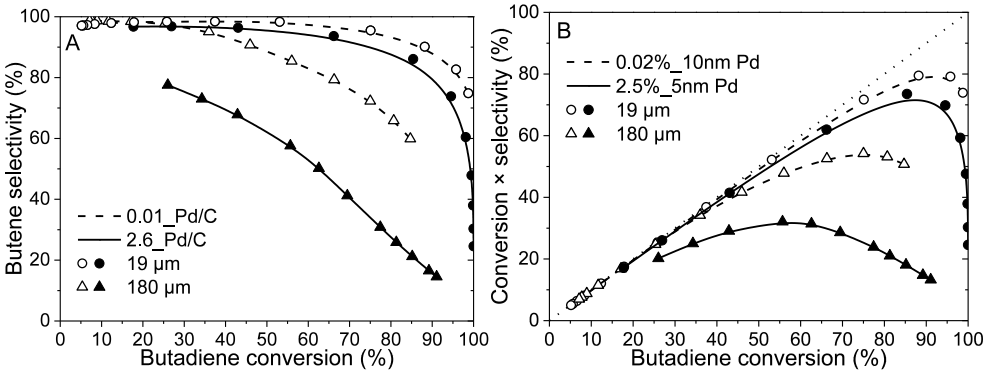

Figure 3.4. Butene selectivity. (A) Selectivity as function of butadiene conversion of 2.6_Pd/C (solid line, filled symbols) and 0.01_Pd/C (dashed line, open symbols) catalysts with an average grain size of 19 µm (circles) or 180 µm (triangles). (B) Butenes yield during the selective hydrogenation of butadiene.

combination of a high loading and large grains induced an intraparticle butadiene concentration gradient, which decreases from the edge of the grain toward the interior. As a result, near the edge of the grain, butadiene was converted selectively, whereas further inside the grain, butane and propane formation occured due to the lower butadiene concentration and, hence, higher coverage with alkenes. For the combination of the tested highest Pd loading and grain size, this selectivity was already limited at low temperatures (25 °C, 26% conversion), where smaller grain and lower loading retained their selectivity up to higher conversion. For example, the 19 µm grains retained a selectivity above 90% up to 75% conversion.

Figure 3.4B depicts the butene yield as a function of butadiene conversion, where yield was calculated by multiplication of conversion and selectivity (Eq. 3.2). At low conversions, the yield increased linearly, following the diagonally (*i.e.,* 100% selectivity) dotted lines because the total reaction selectivity was constant and near 100% (Figure 3.4A). The yield slowly deviated from the diagonal line upon increasing conversion as selectivity declined. Eventually, the total yield even decreased with increasing conversion. Thus, the interplay between increasing butadiene conversion and decreasing butene selectivity induced an optimum butene concentration in the gas mixture. This optimum was close to 80% butene yield (95% conversion) for the 0.01_Pd/C with 19 µm grains, whereas lower values for the optimum yield and conversion were found for the larger grains (Figure 3.4B). For example, over the 2.6_Pd/C catalyst with 180 µm grains, a maximum yield of only 32% was obtained at 58% conversion.

Thus, the selectivity of the reaction strongly depended on the Pd loading and catalyst grain size, especially at higher conversion levels. All tested catalysts showed a decrease in selectivity with increasing conversion. The smallest tested grains (19 µm) showed good butene selectivity up to ~100% butadiene conversion, in line with the requirements for selective hydrogenation.[3–5] On the contrary, the largest tested catalyst grains (180 µm) showed a steep decrease in selectivity already at moderate conversion levels (<50%). The strong dependence of the selectivity on catalyst grain size showed that internal mass transfer limitations can greatly influence catalyst selectivity.

3.3.4 The influence of heat and mass transport

To better understand the experimental observations in sections 3.3.2 and 3.3.3, potential heat and mass transport limitations were assessed. First, the catalyst of which the performance was most affected by transport limitations (180 µm grain size, 2.6_Pd/C) was studied in more detail. An overview of all the heat and mass transport calculations is presented in Table S3.2. In short, heat transport limitations were negligible, as the estimated temperature gradients (external and internal) were less than 0.7 °C (Eq. S3.9 & Eq. S3.14). This low value is related to the high thermal

conductivity of the reaction mixture (50% He and 20% H_2, >150 mW/(mK)[54]) and the solid catalyst material (Pd and C, >70 and >400 W/(mK), respectively).[55,56]

External mass transfer limitations, resulting in a butadiene concentration gradient from the bulk gas phase to the outer surface of the catalyst grain, had little to no influence on catalysis. Even at 100 °C, a Carberry number of 0.03 (Table S3.2) was calculated, well below the 0.2 criterion for a 5% activity deviation (Eq. S3.15). However, internal mass transfer limitations were present already at 25 °C, as a Weisz-modulus (Φ) of 0.09 was calculated, just above the Weisz-Prater criterion of 0.08 (Eq. 3.4). At higher temperatures, the increased activity led to more diffusion limitations of the reactants (Φ=0.3), resulting in an effectiveness factor of 87% at 100 °C.

Since internal diffusion limitations were the main contributor to transport limitations, they were examined in more detail. Figure 3.5A shows the calculated Weisz-modulus of 0.01_Pd/C and 2.6_Pd/C catalysts, with either 19 µm or 180 µm average grain size. The 19 µm grains showed a small Weisz-modulus (Φ<0.005 at 100 °C) and internal mass transfer limitations can be neglected. More severe limitations were observed over the larger grains, with Φ=0.02 or 0.09 at 25 °C for 2.6_Pd/C or 0.01_Pd/C, respectively. With increasing temperature, the Weisz-moduli increased to values above 0.3 at 100 °C, indicating strong internal diffusion limitations. Figure 3.5B provides an overview of the derived Weisz-moduli of tested Pd loadings and grain sizes, at the lowest (25 °C) and highest (100 °C) tested temperature. For the 180 µm grains at 25 °C, only the 0.01_Pd/C catalyst showed a sufficiently low Weisz-modulus below the Weisz-Prater criterion (Φ<0.08, dashed horizontal line). At 100 °C, catalysts with 56 µm or smaller grains were needed to satisfy this criterion. The calculated values of Φ for the catalysts in Figure 3.5A clearly indicates the importance of internal mass transfer limitations for both the experimentally observed activity (Figure 3.3A) and selectivity (Figure 3.4A),

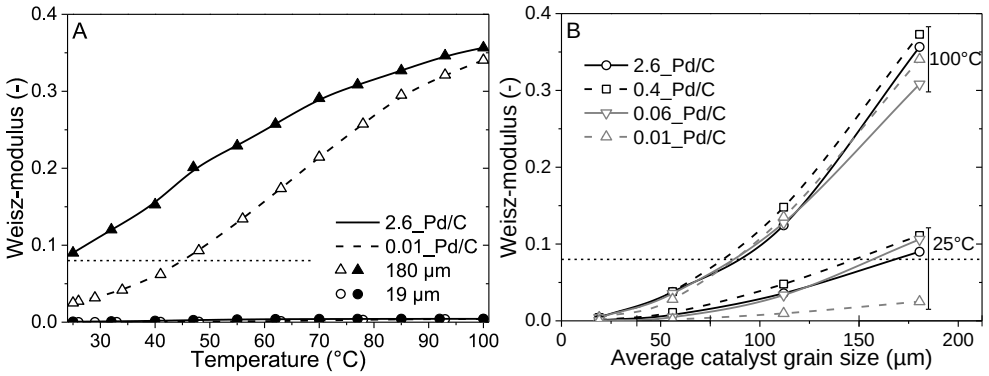

Figure 3.5. Internal diffusion limitations. (A) Weisz-modulus of 2.6_Pd/C (solid line, filled symbols) and 0.01_Pd/C (dashed line, open symbols) catalysts with average catalyst grain size of 19 µm (circles) or 180 µm (triangles). (B) Overview of the Weisz-moduli for the tested combinations of Pd loading and grain size at lowest (25 °C) and highest (100 °C) tested temperature. Dashed horizontal lines indicate Weisz-Prater criterion (Φ=0.08).

which both decrease with increasing Weisz-modulus, hence larger grains induce diffusion limitations.

The internal effectiveness factor, η_{int}, can be used to estimate the butadiene concentration gradient within the catalyst grain (Eq. 3.7). Figure 3.6 shows the calculated butadiene concentration in a spherical 180 µm grain of the 0.01_Pd/C catalyst. The values for η_{int} were taken at the lowest (25 °C) and highest (100 °C) catalysis testing temperatures, and the Pd loading was assumed to be uniformly distributed throughout a spherical grain. At 25 °C, an effectiveness factor of 98% was obtained, resulting in a relatively flat concentration profile (black lines in Figure 3.6). This means the average butadiene concentration in the grain equalled 98% of the concentration at the surface of the grain (d=0, Eq. 3.7). At 100 °C, the bulk concentration was slightly lower, following the ideal gas law. Moreover, a lower effectiveness factor of 84% was obtained. Accordingly, a steeper decrease of the butadiene concentration gradient was calculated (red lines in Figure 3.6A).

For a linear concentration gradient (assuming zero-order reaction, n=0), the butadiene concentration in the middle of the grain was calculated to be less than 37% of the surface concentration. When a negative reaction order (n<0) is assumed (as observed for strongly adsorbing butadiene[5,19]), the reaction rate increases with decreasing reactant concentration, resulting in a faster-declining gradient towards the middle of the catalyst grain.[57] As a result, in this example, part of the grain (31% of the diameter, 3.0% of the volume) is entirely free of butadiene, which enables alkane formation in the interior. The estimated concentration profile of a spherical particle is visualised in Figure 3.6B. Although near the external surface of the grain, hydrogenation is selective due to the high concentration of butadiene[58], the unselective alkane formation in the

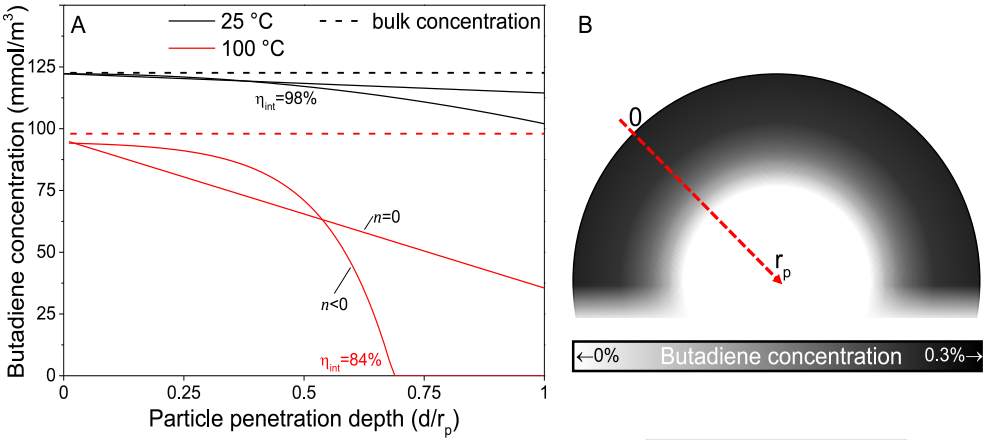

Figure 3.6. Intraparticle concentration profile. (A) Estimated butadiene concentration as function of penetration depth into an exemplary catalyst grain. Calculated by Eq. 3.9 ($\boldsymbol{n}$=0) or Eq. 3.10 ($\boldsymbol{n}$<0). Bulk concentration calculated from the ideal gas law at 1 atm. Surface concentration estimated from Carberry number for 180 µm grains (Eq. S3.16). (B) The grayscale illustrates the concentration inside a spherical catalyst grain at 100 °C with η_{int}=84% (n<0).

interior of the grain will strongly decrease the overall selectivity. Note that this concentration profile in Figure 3.6A is a one-dimensional representation of the grain and for a spherical shape, half of the volume is located in the outer 21% radial distance. Moreover, this analysis assumed uniformly distributed Pd throughout the catalyst grain, which in practice is only valid for the undiluted 0.01_Pd/C catalyst. For the higher weight loadings, the Pd/C catalyst was mixed with inert carbon (see Figure 3.1), resulting in locally higher Pd concentration and steeper local butadiene concentration gradients.

From the experimental data in sections 3.3.2 and 3.3.3 and the calculations in this section, it is evident that internal mass transfer limitations strongly affect the performance in selective butadiene hydrogenation. Figure 3.7 depicts the dependence of the butene selectivity (taken at 85% butadiene conversion) as a function of the calculated Weisz-modulus for different Pd loading and grain size combinations. All catalysts showed a steep decrease in selectivity with increasing Φ, already at Φ<0.05, well below the generally accepted criterion of Φ<0.08[25,26,40,41], indicating that the selectivity was more strongly affected than the activity by internal diffusion limitations. The 0.01_Pd/C showed higher selectivity than the catalyst with higher Pd loading, even at similar estimated diffusion limitations. This is ascribed to the preparation of the catalyst grains, where the catalysts 0.1%, 0.5% and 2.5% Pd/C were diluted with inert carbon powder (5, 25 and 125 times, respectively) to obtain a final weight loading of 0.02 wt% Pd (Figure 3.1). Therefore, within these catalyst grains, there is a heterogeneity of Pd-rich and purely inert (carbon) regions at the scale of the support sheets (0.5-1.0 μm, Figure 3.2A). The calculations of the Weisz-modulus do not take into account these local Pd concentrations. As a result, the Pd-rich regions of the grain will have a steeper butadiene concentration gradient at the same conversion and internal

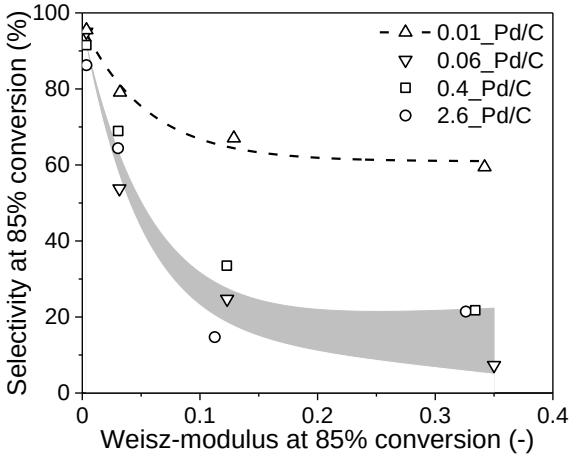

Figure 3.7. Weisz-modulus as selectivity descriptor. Comparison of the experimentally measured selectivity (taken at 85% conversion) and the calculated Weisz-modulus of the tested catalysts. Lines as a guide for the eye.

Table 3.3. Maximum catalyst grain size (d_p) for other metal catalysts from the literature.

Catalyst	Nanoparticle size (nm)	wt%	TOF (s^{-1})	T (°C)	n	d_p (μm)[a]
Pd/C[19,This work]	5.0	0.1%	20	25	-0.25	53
Cu/C[59]	7.3	6.3%	6×10^{-3}	125	0.25	268
Cu/SiO$_2$[59]	7.3	5.7%	5×10^{-3}	125	0.25	309
Ag/SiO$_2$[60]	2.9	1.8%	0.2×10^{-3}	120	0.75[61]	1 807
Au/SiO$_2$[60]	2.6	3.7%	4×10^{-3}	120	0.2[62]	437

[a] Calculated so that $\Phi<0.03$. Catalyst properties, intrinsic activity (TOF) and reaction order in butadiene (n) taken from the literature. Calculations based on selective butadiene hydrogenation (20% conversion, 0.3 mol% inlet).

effectiveness factor, which is associated with lower selectivities, especially at high conversion levels.

Lastly, these insights into the selectivity trends were used to provide some guidelines for catalyst design for the selective hydrogenation of butadiene and similar reactions and can be extended to metal catalysts other than Pd. If a metal turnover frequency (TOF) is measured or estimated, the volumetric reaction rate of the catalyst ($R_{vol.}^{est}$) can be calculated from Eq. S3.7. Analogous to section 3.2.3, the Weisz-modulus can be calculated (Eq. 3.4) and compared to the effective diffusion rate required for good selectivity. Figure 3.7 indicates that a Weisz-modulus smaller than 0.03 is necessary for retaining high selectivity above 70% at 85% butadiene conversion. Table 3.3 provides an overview of various metal catalysts for the selective hydrogenation of butadiene in large excess of propylene that are reported in the literature.[19,59–62] For Pd/C, a maximum grain size of *ca.* 50 μm is required, in line with the experimental results from Figure 3.7. The coinage metals (Cu, Ag, Au) show orders of magnitude lower intrinsic metal activity (TOF), even at the higher reaction temperature. Therefore, the critical grain sizes for internal diffusion limitations are 5 to 34 times larger than for Pd catalysts, even at higher weight loading and smaller nanoparticle sizes.

Our findings emphasise the need to assess internal mass transfer limitations during selective hydrogenation of trace amounts (*e.g.,* 0.3%) of butadiene over highly active Pd and show the importance of carefully evaluating if experimental trends are not partially due to heat or mass transfer effects. The same supported Pd nanoparticles showed a broad range of catalytic performance, which could wrongfully be ascribed to intrinsic catalyst properties rather than to diffusion limitations. Therefore, for academic research, the occurrence of any of these effects should be carefully discarded before ascribing trends to various catalyst properties such as metal nanoparticle size, weight loading and/or promoters. Diffusion-related effects also rely on catalyst geometry, accessibility, meso- and/or microporosity, grain size and/or gas-solid interaction with the support. The impact of a variation of the thermal properties should also be carefully assessed, for example, when comparing conductive to insulating catalyst supports or

when varying inert dilute gasses such as Ar and He, which have a tenfold difference in thermal conductivity.[63]

More generally, this manuscript its experimental observations and calculations can be extended to any heterogeneous catalysis system. One can estimate the associated transport phenomena by adapting some of the properties of Table 3.3 for the desired application, as typical industrial catalysts operate at very different reaction conditions than those discussed for selective hydrogenation. For example, in Cu-catalysed hydrogenation of CO/CO_2 to methanol, metal weight loadings up to 60 wt% Cu and temperatures around 230 °C are used, greatly increasing the catalysts volumetric activity.[64] The effective diffusion, however, is also much higher due to 20% CO/CO_2 reactant feed and 50-100 atm operation pressure. However, reactants might condense inside the catalyst pores, which greatly lowers diffusion rates. In short, the mass transport limitations strongly influence the catalytic performance, especially for the combination of highly active metals, such as Pd, and trace amounts of reactants. Metals with lower activity, such as Cu, are less affected by this, especially when the inlet reactant concentrations are higher.

3.4 Conclusions

The influence of heat and mass transport limitations was investigated for the gas-phase selective hydrogenation of butadiene in a large excess of propylene with Pd/C catalysts. At low temperatures and conversions, higher Pd loading and larger catalyst grains led to enhanced activity due to local heating by the exothermic reactions. However, at high conversions, the activity of larger grains was lowered due to mass transfer limitations. The selectivity towards butenes strongly depended on internal diffusion limitations and strongly decreased with increasing Pd loading and catalyst grain size. The combination of catalytic results and calculations highlighted the importance of diffusion-induced concentration gradients inside catalyst grains. The impact on selectivity was much more severe than the impact on activity according to the Weisz-Prater criterion. Our insights provide guidelines for the understanding of the influence of catalyst structure for Pd-catalysed hydrogenation reactions and can be extended to other catalysts and reactions to better understand catalytic materials and design reliable catalytic testing conditions.

3.5 References

1. Blaser, H.-U. *et al.* Selective Hydrogenation for Fine Chemicals: Recent Trends and New Developments. *Adv. Synth. Catal.* **345**, 103-151 (2003).
2. Chen, B. *et al.* New developments in hydrogenation catalysis particularly in synthesis of fine and intermediate chemicals. *Appl. Catal. A Gen.* **280**, 17-46 (2005).
3. Derrien, M. L. Chapter 18: Selective Hydrogenation Applied to the Refining of Petrochemical Raw Materials Produced by Steam Cracking. in *Studies in Surface Science and Catalysis* vol. 27 613-666 (1986).
4. Zhang, L., Zhou, M., Wang, A. & Zhang, T. Selective Hydrogenation over Supported Metal Catalysts: From Nanoparticles to Single Atoms. *Chem. Rev.* **120**, 683-733 (2020).
5. Bond, G. C. Hydrogenation of Alkadienes and Poly-Enes. in *Metal-Catalysed Reactions of Hydrocarbons* 357-394 (Springer US, 2005). doi:10.1007/0-387-26111-7_8.
6. Borodziński, A. & Bond, G. C. Selective Hydrogenation of Ethyne in Ethene-Rich Streams on Palladium Catalysts. Part 1. Effect of Changes to the Catalyst During Reaction. *Catal. Rev.* **48**, 91-144 (2006).
7. Borodziński, A. & Bond, G. C. Selective Hydrogenation of Ethyne in Ethene-Rich Streams on Palladium Catalysts, Part 2: Steady-State Kinetics and Effects of Palladium Particle size, Carbon Monoxide, and Promoters. *Catal. Rev.* **50**, 379-469 (2008).
8. Studt, F. *et al.* Identification of Non-Precious Metal Alloy Catalysts for Selective Hydrogenation of Acetylene. *Science* **320**, 1320-1322 (2008).
9. Johnson, M. M., Walker, D. W. & Nowack, G. P. Selective Hydrogenation Catalyst. U.S. Patent 4,404,124-A (1983).
10. Lindlar, H. Ein neuer Katalysator für selektive Hydrierungen. *Helv. Chim. Acta* **35**, 446-450 (1952).
11. Witte, P. T. *et al.* BASF NanoSelect™ technology: Innovative supported Pd- and Pt-based catalysts for selective hydrogenation reactions. *Top. Catal.* **55**, 505-511 (2012).
12. Yan, H. *et al.* Single-Atom Pd_1/Graphene Catalyst Achieved by Atomic Layer Deposition: Remarkable Performance in Selective Hydrogenation of 1,3-Butadiene. *J. Am. Chem. Soc.* **137**, 10484-10487 (2015).
13. Yan, H. *et al.* Understanding the underlying mechanism of improved selectivity in Pd_1 single-atom catalyzed hydrogenation reaction. *J. Catal.* **366**, 70-79 (2018).
14. Ibrahim, H., Weckman, T., Murzin, D. & Karoliina, H. Understanding Selective Hydrogenation of Phenylacetylene on PdAg Single Atom Alloy: DFT Insights on Molecule size and Surface Ensemble Effects. ChemRxiv https://chemrxiv.org/engage/chemrxiv/article-details/659533e4e9ebbb4db95303d2 (2024) doi:10.26434/chemrxiv-2024-7mq3w.
15. Kyriakou, G. *et al.* Isolated Metal Atom Geometries as a Strategy for Selective Heterogeneous Hydrogenations. *Science* **335**, 1209-1212 (2012).
16. Boucher, M. B. *et al.* Single atom alloy surface analogs in $Pd_{0.18}Cu_{15}$ nanoparticles for selective hydrogenation reactions. *Phys. Chem. Chem. Phys.* **15**, 12187-12196 (2013).
17. Hannagan, R. T., Giannakakis, G., Flytzani-Stephanopoulos, M. & Sykes, E. C. H. Single-Atom Alloy Catalysis. *Chem. Rev.* **120**, 12044-12088 (2020).
18. Aich, P. *et al.* Single-Atom Alloy Pd-Ag Catalyst for Selective Hydrogenation of Acrolein. *J. Phys. Chem. C* **119**, 18140-18148 (2015).
19. Brandt Corstius, O. E., van der Hoeven, J. E. S., Sunley, G. J. & de Jongh, P. E. Influence of particle size in Pd-catalysed selective hydrogenation of 1,3-butadiene. *J. Catal.* **427**, 115103 (2023).
20. Luss, D. Temperature rise of catalytic supported crystallites. *Chem. Eng. J.* **1**, 311-317 (1970).
21. Sharma, S., Boecker, D., Maclay, G. J. & Gonzalez, R. D. The simultaneous measurement of support, metal, and gas phase temperatures using an *in situ* IR spectroscopic technique. *J. Catal.* **110**, 103-116 (1988).

22. Theis, J. & Gulari, E. Estimating the temperatures of the precious metal sites on a lean NOx trap during oxidation reactions. *Appl. Catal. B Environ.* **75**, 39-51 (2007).
23. Geitenbeek, R. G. *et al.* In Situ Luminescence Thermometry To Locally Measure Temperature Gradients during Catalytic Reactions. *ACS Catal.* **8**, 2397-2401 (2018).
24. Arnby, K., Törncrona, A., Andersson, B. & Skoglundh, M. Investigation of Pt/γ-Al_2O_3 catalysts with locally high Pt concentrations for oxidation of CO at low temperatures. *J. Catal.* **221**, 252-261 (2004).
25. Thiele, E. W. Relation between Catalytic Activity and size of Particle. *Ind. Eng. Chem.* **31**, 916-920 (1939).
26. Weisz, P. B. & Prater, C. D. Interpretation of Measurements in Experimental Catalysis. *Adv. Catal.* **6**, 143-196 (1954).
27. Zhu, J. *et al.* Influence of internal diffusion on selective hydrogenation of 4-carboxybenzaldehyde over palladium catalysts supported on carbon nanofiber coated monolith. *Appl. Catal. A Gen.* **498**, 222-229 (2015).
28. Harju, H., Pipitone, G. & Lefferts, L. Influence of the Catalyst Particle size on the Aqueous Phase Reforming of n-Butanol Over Rh/ZrO_2. *Front. Chem.* **8**, 17 (2020).
29. Zhu, J., Li, M., Lu, M. & Zhu, J. Effect of structural properties on catalytic performance in citral selective hydrogenation over carbon-titania composite supported Pd catalyst. *Catal. Sci. Technol.* **3**, 737-744 (2013).
30. Nijhuis, T. A., Van Koten, G., Kapteijn, F. & Moulijn, J. A. Separation of kinetics and mass-transport effects for a fast reaction: The selective hydrogenation of functionalized alkynes. *Catal. Today* **79-80**, 315-321 (2003).
31. Asplund, S. Coke formation and its effect on internal mass transfer and selectivity in Pd-catalysed acetylene hydrogenation. *J. Catal.* **158**, 267-278 (1996).
32. Sarkany, A. Semi-hydrogenation of 1,3-butadiene over Pd—Ag/α-Al_2O_3 poisoned by hydrocarbonaceous deposits. *Appl. Catal. A Gen.* **165**, 87-101 (1997).
33. Sarkany, A. Hydrocarbonaceous deposit assisted n-butane formation in hydrogenation of 1,3-butadiene over Pd catalysts. *Appl. Catal. A Gen.* **175**, 245-253 (1998).
34. Sarkany, A. Effect of Hydrocarbonaceous Deposits on Competitive Hydrogenation of 1,3-Butadiene and Propene over Pd Catalyst. *J. Catal.* **180**, 149-152 (1998).
35. Bressa, S. P., Alves, J. A., Martínez, O. M. & Barreto, G. F. Selective hydrogenation of 1-butene rich cuts: The impact of the intraparticle diffusion limitations on the selectivity. *Chem. Eng. Technol.* **26**, 783-789 (2003).
36. Alves, J. A., García Colli, G., Martínez, O. M. & Barreto, G. F. Modeling and simulation of trickle bed reactors for the purification of 1-butene. *Int. J. Chem. React. Eng.* **21**, 1073-1090 (2023).
37. Ratnakar, R. R. & Dindoruk, B. The Role of Diffusivity in Oil and Gas Industries: Fundamentals, Measurement, and Correlative Techniques. *Processes* **10**, 1194 (2022).
38. Wagemans, R. W. P. Magnesium for Hydrogen Storage: from Micrometer to Nanometer. (PhD Thesis, Chapter 6: Particle size Effects in the Palladium-Carbon-Hydrogen System, Utrecht University, ISBN:90-393-4321-7, 2006).
39. Scherrer, P. Bestimmung der inneren Struktur und der Größe von Kolloidteilchen mittels Röntgenstrahlen. in *Kolloidchemie Ein Lehrbuch* 387-409 (Springer Berlin, 1912). doi:10.1007/978-3-662-33915-2_7.
40. EUROKIN spreadsheet on requirements for measurement of intrinsic kinetics in the gas-solid fixed-bed reactor. *EUROKIN_fixedbed_html* http://www.eurokin.org/wp-content/uploads/webtool/EUROKIN_fixed-bed_html.htm (2012).
41. Perry, R. H. & Green, D. W. Perry's Chemical Engineers' Handbook. Perry's Chemical Engineers' Handbook (McGraw-Hill Education, 2008).
42. Bond, G. C., Webb, G., Wells, P. B. & Winterbottom, J. M. The hydrogenation of alkadienes. Part I. The hydrogenation of buta-1,3-diene catalysed by the Noble Group VIII metals. *J. Chem. Soc.* 3218 (1965) doi:10.1039/jr9650003218.
43. Anderson, J. R. & Pratt, K. C. Introduction to characterization and testing of catalysts. 457 (1985).

44. Li, S. Chemical Reaction and Transport Phenomena in Heterogeneous System. in *Chemical Reaction Engineering* 265-310 (Elsevier, 2017). doi:10.1016/B978-0-12-410416-7.00006-9.
45. Fogler, H. S. Essentials of Chemical Reaction Engineering, 2nd Edition. Pearson Prentice Hall (Pearson Prentice Hall, 2017).
46. Beerthuis, R. *et al.* Particle size effects in copper-catalyzed hydrogenation of ethyl acetate. *J. Catal.* **388**, 30-37 (2020).
47. Totarella, G., de Rijk, J. W., Delannoy, L. & de Jongh, P. E. Particle size Effects in the Selective Hydrogenation of Alkadienes over Supported Cu Nanoparticles. *ChemCatChem* **14**, e202200348 (2022).
48. Visser, N. L. *et al.* Particle size Effects of Carbon Supported Nickel Nanoparticles for High Pressure CO_2 Methanation. *ChemCatChem* **14**, 1-11 (2022).
49. Barberis, L. *et al.* Competition between reverse water gas shift reaction and methanol synthesis from CO_2: influence of copper particle size. *Nanoscale* **14**, 13551-13560 (2022).
50. Patterson, A. L. The Scherrer Formula for X-Ray Particle size Determination. *Phys. Rev.* **56**, 978-982 (1939).
51. Weidenthaler, C. Pitfalls in the characterization of nanoporous and nanosized materials. *Nanoscale* **3**, 792-810 (2011).
52. Valcárcel, A., Clotet, A., Ricart, J. M., Delbecq, F. & Sautet, P. Comparative DFT study of the adsorption of 1,3-butadiene, 1-butene and 2-cis/trans-butenes on the Pt(111) and Pd(111) surfaces. *Surf. Sci.* **549**, 121-133 (2004).
53. van der Hoeven, J. E. S. *et al.* Unlocking synergy in bimetallic catalysts by core-shell design. *Nat. Mater.* **20**, 1216-1220 (2021).
54. Mukhopadhyay, P. & Barua, A. K. Thermal conductivity of hydrogen-helium gas mixtures. *Br. J. Appl. Phys.* **18**, 635-640 (1967).
55. Smith, A. W. Low-Temperature Thermal Conductivity of a Canadian Natural Graphite. *Phys. Rev.* **95**, 1095-1096 (1954).
56. Laubitz, M. J. & Matsumura, T. High-Temperature Transport Properties of Palladium. *Can. J. Phys.* **50**, 196-205 (1972).
57. Zhao, L. J. & Sun, Q. Calculations of effectiveness factors and the criteria of mass transfer effect for hightemperature methanation (HTM) catalyst. *Int. J. Low-Carbon Technol.* **10**, 288-293 (2013).
58. Johnson, B. A. & Ott, S. Diagnosing surface versus bulk reactivity for molecular catalysis within metal-organic frameworks using a quantitative kinetic model. *Chem. Sci.* **11**, 7468-7478 (2020).
59. Totarella, G. *et al.* Supported Cu Nanoparticles as Selective and Stable Catalysts for the Gas Phase Hydrogenation of 1,3-Butadiene in Alkene-Rich Feeds. *J. Phys. Chem. C* **125**, 366-375 (2021).
60. Masoud, N. *et al.* Silica-Supported Au-Ag Catalysts for the Selective Hydrogenation of Butadiene. *ChemCatChem* **9**, 2418-2425 (2017).
61. Sárkány, A. & Révay, Z. Some features of acetylene and 1,3-butadiene hydrogenation on Ag/SiO_2 and Ag/TiO_2 catalysts. *Appl. Catal. A Gen.* **243**, 347-355 (2003).
62. Hugon, A., Delannoy, L. & Louis, C. Influence of the reactant concentration in selective hydrogenation of 1,3-butadiene over supported gold catalysts under alkene rich conditions: A consideration of reaction mechanism. *Gold Bull.* **42**, 310-320 (2009).
63. Thornton, E. & Baker, W. A. D. Viscosity and thermal conductivity of binary gas mixtures: Argon-neon, argon-helium, and neon-helium. *Proc. Phys. Soc.* **80**, 1171-1175 (1962).
64. Waugh, K. C. Methanol Synthesis. *Catal. Letters* **142**, 1153-1166 (2012).
65. Lambert, A. J. D. *et al.* Transport properties of gaseous hydrocarbons. *Proc. R. Soc. London. Ser. A. Math. Phys. Sci.* **231**, 280-290 (1955).
66. Sakoda, N. *et al.* Viscosity measurements of hydrogen at high temperatures up to 573 K by a curved vibrating wire method. *J. Chem. Thermodyn.* **89**, 22-26 (2015).

67. Senftleben, H. Newly Measured Values of the Thermal Conductivity and Specific Heat at Various Temperatures for a Series of Gases. *Z. angew. Phys* **17**, 86-87 (1964).
68. Compton, D. A. C., George, W. O. & Maddams, W. F. Conformations of conjugated hydrocarbons. Part 1. A spectroscopic and thermodynamic study of buta-1,3-diene and 2-methylbuta-1,3-diene (isoprene). *J. Chem. Soc. Perkin Trans. 2* 1666-1671 (1976) doi:10.1039/p29760001666.
69. Bier, K., Ernst, G., Kunze, J. & Maurer, G. Thermodynamic properties of propylene from calorimetric measurements. *J. Chem. Thermodyn.* **6**, 1039-1052 (1974).
70. Chase, M. W. NIST-JANAF thermochemical tables. *J. Phys. Chem. Ref. Data* **9**, 1-1951 (1998).
71. Assael, M. J., Koutian, A., Huber, M. L. & Perkins, R. A. Reference Correlations of the Thermal Conductivity of Ethene and Propene. *J. Phys. Chem. Ref. Data* **45**, 1-22 (2016).
72. Fuller, E. N., Schettler, P. D. & Giddings, J. C. New Method for Prediction of Binary Gas-Phase Diffusion Coefficients. *Ind. Eng. Chem.* **58**, 18-27 (1966).
73. Punčochář, M. & Drahoš, J. The tortuosity concept in fixed and fluidized bed. *Chem. Eng. Sci.* **48**, 2173-2175 (1993).
74. Bergeret, G. & Gallezot, P. Characterization of Solid Catalysts: Sections 3.1.1-3.1.3. in *Handbook of Heterogeneous Catalysis* vols 1-5 427-582 (Wiley-VCH Verlag GmbH, 2008).
75. Mears, D. E. Diagnostic criteria for heat transport limitations in fixed bed reactors. *J. Catal.* **20**, 127-131 (1971).
76. Wakao, N., Kaguei, S. & Funazkri, T. Effect of fluid dispersion coefficients on particle-to-fluid heat transfer coefficients in packed beds. *Chem. Eng. Sci.* **34**, 325-336 (1979).

3.6 Supplementary information

3.6.1 Heat and mass transport phenomena

Gas diffusion

For the transport properties of the reaction gas (Table S3.1, references 54 and 65–71), the value of the mixture is determined as the sum of the four components as:

$$P_{mix} = \sum (x_\mathrm{i}\, P_\mathrm{i}) \qquad \text{Eq. S3.1}$$

where P_i is the property of interest and x_i is the molar fraction of each reactant. For simplicity, the initial molar fractions are used throughout the calculations. Even at the highest observed catalytic activity (100% butadiene and 5% propylene conversion at 100 °C) the average value of the transport properties of the mixture only varied by less than 0.8% because of the large excess of H_2 and He.

Diffusion volumes (v_i) of each reactant were estimated for C_4H_6, C_3H_6, He and H_2.[40] The diffusion of butadiene (BD) in the individual gasses ($D_{BD,i}$) was calculated from Fuller, Schettler and Giddings[72] as:

$$D_{BD,i} = \frac{3.2 \times 10^{-8}\, T^{1.75} \sqrt{\frac{1}{m_\mathrm{BD}} + \frac{1}{m_\mathrm{i}}}}{p\, ({v_\mathrm{BD}}^{1/3} + {v_\mathrm{i}}^{1/3})^2} \qquad \text{Eq. S3.2}$$

where T is the temperature (K), m_i is the molar mass (kg/mol) and p is the pressure (101325 Pa).

Table S3.1. Properties of reaction gasses.

	Molar fraction	Molar mass	Diffusion volume	$D_{BD,i}$[a]	Viscosity	Thermal conduc-tivity	Heat capacity
Reactant	**vol%**	**$\times 10^{-3}$ kg/mol**	**$\times 10^{-5}$ m^3/mol**	**$\times 10^{-6}$ m^2/s**	**$\times 10^{-6}$ Pa s**	**$\times 10^{-3}$ W/(mK)**	**J/(molK)**
Butadiene	0.3	54.09	7.79	n.a.[a]	8.7-10.5	15.0-24.3	79.9-97.7
Propylene	30	42.08	6.14	6.5-9.6	9.0-10.7	17.0-25.6	63.8-78.8
Hydrogen	20	2.016	0.707	4.0-5.9	8.9-10.4	179-210	28.7-28.9
Helium	49.7	4.003	0.288	3.4-5.1	19.7-23.1	154-180	18.5-17.2
Mixture	100	15.18	n.a.	1.5-2.5[b]	14.3-16.8	118-139	34.3-37.4

[a] Defined as the diffusivity of butadiene in the other gas. [b] Determined by the Wilke-equation (Eq. S3.3.). Temperature-dependent values are listed between the minimum and maximum temperature of the catalytic test, 25-100 °C.

3

The total diffusivity of butadiene in the reaction mixture is calculated with Wilke-equation[41] as:

$$D_{\mathrm{BD,mix}} = (1 - x_{\mathrm{BD}}) \times \left(\sum_{\mathrm{i} \neq \mathrm{BD}} \frac{x_{\mathrm{i}}}{D_{\mathrm{BD,i}}}\right)^{-1} \qquad \text{Eq. S3.3}$$

which results in a bulk diffusivity of 1.52—2.45×10^{-6} m^2/s for butadiene between 25—100 °C.

For diffusion inside the catalyst grains, in the presence of narrow pores, limitation due to gas-solid interactions should be taken into account in addition to gas-gas interactions. The Knudsen diffusion (D_{K}) is calculated as

$$D_{\mathrm{K}} = \frac{2 r_{\mathrm{pore}}}{3} \sqrt{\frac{8\,\mathrm{R}\,T}{\pi\, m_{\mathrm{BD}}}} \qquad \text{Eq. S3.4}$$

where R is the ideal gas constant (8.3145 $m^3\ Pa\ K^{-1}\ mol^{-1}$) and r is the estimated pore radius:

$$r_{\mathrm{pore}} = \frac{2\varepsilon_{\mathrm{cat}}}{\rho_{\mathrm{cat}} S} \qquad \text{Eq. S3.5}$$

where $\varepsilon_{\mathrm{cat}}$ is the catalyst porosity (0.82 m^3/m$^3_{\mathrm{cat}}$), ρ_{cat} is the catalyst density (657 kg/m$^3_{\mathrm{cat}}$) and S is the surface area of the catalyst (500×10^3 m^2/kg). This results in an estimated pore radius of 3.1×10^{-9} m (3.1 nm) and D_{K} between 7.1—8.0×10^{-7} m^2/s. From the combined resistivity of Knudsen diffusion and bulk diffusivity of butadiene, the effective diffusivity of butadiene ($D_{\mathrm{BD,eff}}$) is calculated as:

$$D_{\mathrm{BD,eff}} = \frac{\varepsilon}{\tau}\left(\frac{1}{D_{\mathrm{BD,mix}}} + \frac{1}{D_{\mathrm{K}}}\right)^{-1} \qquad \text{Eq. S3.6}$$

where τ is the catalyst tortuosity, which can be estimated from $\tau = 1/\sqrt{\varepsilon}$.[73] This results in an $D_{\mathrm{BD,eff}}$ of 3.5—3.9×10^{-7} m^2/s between 25—100 °C.

Activity

The volumetric reaction rate can be estimated for any catalytic system, for example by taking known turnover frequency (TOF) from the literature as:

$$R_{\mathrm{vol.}}^{\mathrm{est.}} = \frac{TOF\ D\ m_{\mathrm{metal}}\ \rho_{\mathrm{cat}}}{M_{\mathrm{metal}}\ m_{\mathrm{cat}}} \qquad \text{Eq. S3.7}$$

where TOF is the intrinsic surface-averaged activity (molecules surface-atom^{-1} s^{-1}), D is the catalyst dispersion[74] and M_{metal} is the molar mass of the metal.

Heat transfer

The adiabatic temperature rise (ΔT_{ad}) in the reactor due to exothermic reactions can be calculated as:

$$\Delta T_{\mathrm{ad}} = \frac{\sum_{\mathrm{i=BD,PP,n\text{-}but}}(x_{\mathrm{i}}\ X_{\mathrm{i}}\ |\ \Delta_{\mathrm{r}}H_{\mathrm{i}}|)}{C_{\mathrm{p,gas}}} \qquad \text{Eq. S3.8}$$

where $\Delta_{\mathrm{r}}H_{\mathrm{i}}$ is the hydrogenation reaction enthalpy of each reactant (see section 3.2.3 in the main text). $C_{\mathrm{p,gas}}$ is the heat capacity of the gas mixture (Table S3.1) which we assume constant even at full butadiene conversion since the molar fraction of is very low (0.3%) and conversion of propylene was always below 5%. For full butadiene semi-hydrogenation, this results in a temperature increase of the reaction gas of 9.1 °C, which increases up to 60 °C when 5% propylene conversion and 10% butane formation are considered.

External heat transfer limitations are calculated by the temperature difference over the gas film that surround the catalyst grain.[75]

$$\Delta T_{\mathrm{film}} = \frac{\sum_{\mathrm{i=BD,PP,n\text{-}but}}(R_{\mathrm{vol.,i}}^{\mathrm{Obs}}\ |\ \Delta_{\mathrm{r}}H_{\mathrm{i}}|)}{\alpha_{\mathrm{p}}\ a_{\mathrm{V}}} \qquad \text{Eq. S3.9}$$

where in $R_{\mathrm{vol.,i}}^{\mathrm{Obs}} \times |\Delta_{\mathrm{r}}H_{\mathrm{i}}|$ the produced heat by hydrogenation of butadiene, propylene and butene. α_{p} is the transfer coefficient (W/(m^{2}K)), which is defined as:

$$\alpha_{\mathrm{p}} = \frac{Nu\ \lambda_{\mathrm{gas}}}{d_{\mathrm{p}}} \qquad \text{Eq. S3.10}$$

where λ_{gas} is the thermal conductivity of the gas (Table S3.1) and Nu is the Nusselt number, defined as:

$$Nu = 2 + 1.1Re^{0.6}Pr^{1/3} \qquad \text{Eq. S3.11}$$

Where Prandtl number, Pr, is defined as:

$$Pr = \frac{C_{\mathrm{p,gas}}\ \mu}{\lambda_{\mathrm{gas}}} \qquad \text{Eq. S3.12}$$

To exclude external heat transfer effects to alter the catalytic activity by more than 5%, ΔT_{film} should be less than $0.05\gamma_b/T$, where T is temperature and γ_b is the dimensionless activation energy:

$$\gamma_{\text{b}} = \frac{E_{\text{act}}}{\text{R}\,T} \qquad \text{Eq. S3.13}$$

with E_{act} in J/mol, which for E_{act} of 50×10^3 J/mol results in ΔT_{film}<0.74 K at 25 °C and <1.2 K at 100°C.

Internal heat transport limitations are calculated as the difference between catalyst grain edge and the average grain temperature as:

$$\Delta T_{\text{int,av}} = \frac{{d_{\text{p}}}^2 \sum_{\text{i=BD,PP,n-but}}(R^{\text{Obs}}_{\text{vol,i}} \mid \Delta_{\text{r}}H_{\text{i}}\mid)}{60\,\lambda_{\text{cat}}} \qquad \text{Eq. S3.14}$$

where λ_{cat} is the heat conductivity of the catalyst grain, which because of the high heat transfer properties of graphite[55], we assume to be limited by Pd (72.1-73.5 W/(mK) for 25-100 °C)[56]. Analogous to external heat transport, deviations less than 5% of the catalytic activity when ΔT_{int}<$0.05\gamma_{\text{b}}/T$.

3

External mass transfer limitations

To understand the effect of external diffusion limitations by the Carberry number, Ca, is calculated which describes the difference between butadiene concentration at the catalyst grain exterior surface compared to the bulk gas-phase concentration. In other words, Ca=0.75 if the surface concentration is 25% of the reactor inlet concentration.

$$Ca = \frac{R^{\text{Obs}}_{\text{vol.}}}{k_{\text{g}}\,a_{\text{V}}\,C^0_{\text{BD}}} = \frac{C^0_{\text{BD}} - C^{\text{surf}}_{\text{BD}}}{C^0_{\text{BD}}} < \frac{0.05}{|n|} \qquad \text{Eq. S3.15}$$

where, $R^{\text{Obs}}_{\text{vol.}}$ is the volumetric reaction rate of the catalyst (mol ${\text{m}_{\text{cat}}}^{-3}$ s^{-1}), k_{g} is external mass transfer coefficient (m^3 m^{-2} s^{-1}), a_V is the external surface area of the catalyst grain ($6/d_{\text{p}}$ for spherical shape, where d_{p} is the average catalyst grain size in meters), C^{i}_{BD} is the concentration of butadiene in the bulk (C^0_{BD}= 0.3 mol% = 0.123 mol ${\text{m}_{\text{gas}}}^{-3}$ at 25°C) and at the external surface of the grain ($C^{\text{surf}}_{\text{BD}}$) which can be rewritten to determine surface concentration as:

$$C^{\text{surf}}_{\text{BD}} = C^0_{\text{BD}}(1 - Ca) = \eta_{\text{ext}}\,C^0_{\text{BD}} \qquad \text{Eq. S3.16}$$

where η_{ext} is the effectiveness factor of external diffusion.

The external mass transfer coefficient, k_g, is calculated as

$$k_{\text{g}} = D_{\text{BD,mix}}\,a_{\text{V}}\,Sh \qquad \text{Eq. S3.17}$$

where $D_{\text{BD,mix}}$ is molecular diffusivity of butadiene in the gas mixture (see Eq. S3.3) and Sherwood number, Sh is defined as:[76]

$$Sh = 2 + 1.1Re^{0.6}Sc^{1/3} \qquad \text{Eq. S3.18}$$

where the Reynolds number, Re, is defined as:

$$Re = \frac{d_{\mathrm{p}}\,\rho_{\mathrm{gas}}\,u}{\mu} \qquad \text{Eq. S3.19}$$

with ρ_{gas} the gas density (0.62-0.50 kg m^{-3}), u the superficial gas velocity (0.067-0.084 m s^{-1}) and μ the gas mixture viscosity (Table S3.1).
The Schmidt number, Sc, is defined as:

$$Sc = \frac{\mu}{\rho_{\mathrm{gas}}\,D_{\mathrm{BD,mix}}} \qquad \text{Eq. S3.20}$$

This results in a value of Carberry number between 0 and 1. For a criterion of less than 5% resistance of activity due to external diffusion limitations, Ca should be less than $0.05/|n|$, where n is the reaction order (-0.25 for butadiene).[19]

Table S3.2. Calculated heat and mass transport. Catalytic data taken from 180 µm 2.6_Pd/C.

Property	unit	low T	high T		Property	unit	low T	high T
T_{set}	°C	25	100		T_{set}	°C	25	100
$X_{\mathrm{C_4H_6}}$	%	26	91		$\Delta T_{\mathrm{int,bulk}}$	°C	0.022	0.35
$X_{\mathrm{C_3H_6}}$	%	0.07	5		ΔT_{ad}	°C	3.4	59
$S_{\mathrm{C_4H_{10}}}$	%	0.5	10		Ca	-	0.011	0.031
$R^{\mathrm{Obs}}_{\mathrm{vol.}}$	mol/m^{3}s	14.1	253		η_{ext}	%	98.9	96.9
ΔT_{film}	°C	0.03	0.44		Φ	-	0.09	0.3
$\Delta T_{\mathrm{int,av}}$	°C	0.012	0.23		η_{int}	%	95.0	87.0

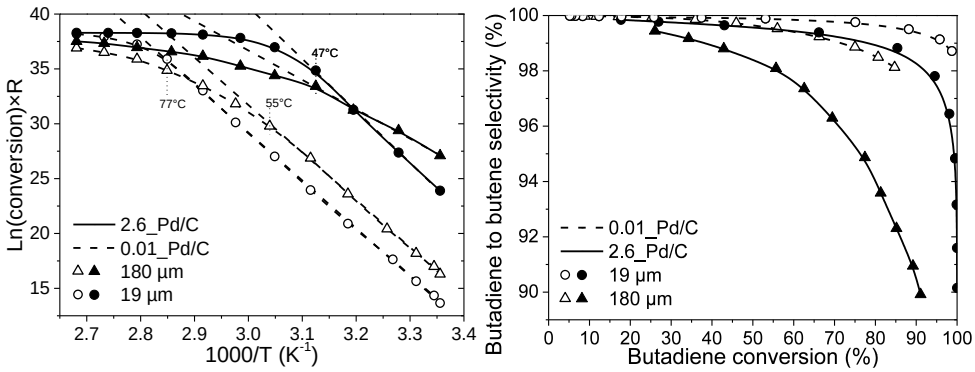

Figure S3.1. (Left) Arrhenius plot of catalysts depicted in Figure 3.2A of the main text. Dashed lines indicated the fitted data used for the determination of apparent activation energy. (Right) Selectivity to butenes, considering only the C_4H_x molecules, as a function of butadiene conversion.

Chapter 4

Bimetallic PdCu particles

This chapter is based on: Brandt Corstius, O.E., Nolten, H.L., Tierney, G.F., Xu, Z., Doskocil, E.J., van der Hoeven, J.E.S. & de Jongh, P.E. Tuneable bimetallic Pd_xCu_{100-x} catalysts for selective butadiene hydrogenation. *Catalysis Today,* under review, (2024).

Abstract

To improve the selectivity of Pd, especially at high conversion levels, it can be diluted with a more selective metal such as Cu, Ag or Au. We report a detailed study on the effect of the Pd:Cu ratio on the catalytic performance of carbon-supported Cu-rich catalysts for the selective hydrogenation of butadiene in an excess of propylene. Monodisperse bimetallic Pd_xCu_{100-x} nanoparticles of 7-8 nm diameter with tuneable Pd content of 0.6 to 13% were prepared colloidally. Catalytic turnover frequencies for butadiene hydrogenation increased with Pd-fraction up to 1.0 s^{-1} for Pd_7Cu_{93} and $Pd_{13}Cu_{87}$. The butene selectivity, measured at 90% conversion, was roughly 80% for the catalysts with a Pd fraction above 3% and slightly increased with lower Pd concentrations. *Operando* X-ray absorption spectroscopy identified an electron density transfer from Cu to Pd in the bimetallic catalysts and a slight preferential clustering of Pd. The trend in catalytic activity was ascribed to an increased Pd ensemble size, indicated by higher Pd-Pd coordination numbers. For bimetallic Pd_xCu_{100-x}/C catalysts, a Pd content of 3-7% retains a high selectivity of 78% at 90% conversion while improving the activity by 3-4 orders of magnitude compared to pure Cu catalysts. This chapter provides insights into controlling the activity-selectivity balance through metal nanoparticle compositions.

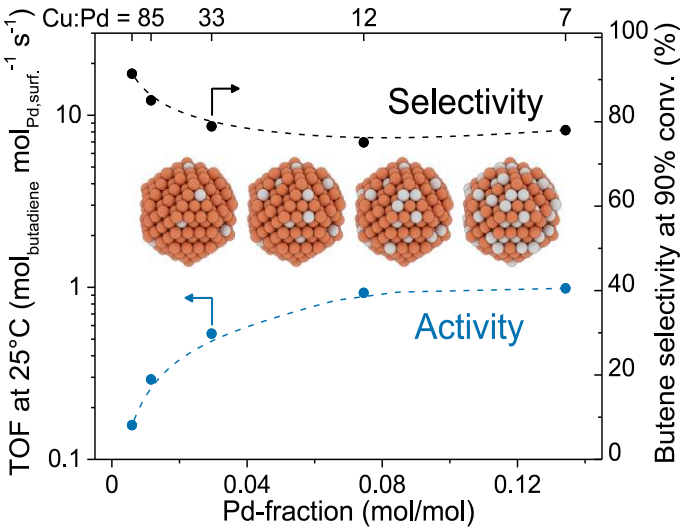

4.1 Introduction

As an alternative to Pd-based catalysts for selective hydrogenation reactions, coinage metals such as Cu[1-3], Ag[4] and Au[4-6] have been identified as hydrogenation catalysts with high selectivity, albeit at considerably lower activity. In an effort to combine the activity of Pd and the selectivity of the coinage metals, bimetallic systems such as PdCu, PdAg and PdAu have been investigated for selective hydrogenation reactions.[7-16] The dilution of Pd in a second metal often improves its selectivity, but compromises its activity compared to monometallic Pd.

The influence of diluting Pd with a secondary metal on the catalytic performance can be explained by both geometric and electronic effects. For very dilute Pd, active sites consist of isolated Pd atoms or small clusters, which interact differently with the reactants than extended Pd surfaces, such as those present in pure Pd. For example, isolated atoms show lower adsorption energies for hydrocarbons[13-21] and hydrogen[7,22-25], as well as a higher energy barrier for hydrogen dissociation[7,15,22,24-27], compared to the more active monometallic Pd. These effects are ensemble size dependent, resulting in higher activity over surface Pd dimers or trimers compared to isolated Pd atoms.[16,23,27,28] In addition, the hydrogenation of polyunsaturated molecules over dilute bimetallic Pd catalysts can require the cooperation of two spatially separated active sites, where hydrogen is dissociatively adsorbed on one site and thereafter spills over to an adjacent site where the hydrocarbon is adsorbed.[22]

The electronic effects of alloying Pd with Ag lead to lower adsorption energies of both acetylene and ethylene on PdAg compared to on Pd surfaces, as calculated by density function theory (DFT).[29] The reduced acetylene binding strength reduces the catalysts' activity, whereas lowered ethylene adsorption favours desorption rather than over-hydrogenation, resulting in a higher selectivity. DFT on isolated Pd surface sites in Au, Ag, and Cu surfaces indicated the largest electron transfer to Pd from the Cu host, which is associated with higher selectivity.[21] Several reports show the potency of bimetallic PdCu catalysts for selective hydrogenation reactions.[9,30-35] Yet, a systematic study investigating the performance of PdCu catalysts over a large range of Pd-Cu compositions while keeping other structural parameters such as the particle size and shape constant, is still missing.

We studied the effect of the Cu-to-Pd ratio in supported bimetallic nanoparticles on the selective hydrogenation of butadiene by tuning the Pd-fraction from 0.6% to 13% (167:1 and 7:1 Cu:Pd). The catalysts were tested in the selective hydrogenation of butadiene in the presence of excess propylene. We found that both the activity and selectivity of the catalysts depended on the Pd:Cu ratio and correlated this to the structural characteristics of these systems using *operando* X-ray absorption spectroscopy.

4.2 Experimental details

4.2.1 Catalyst preparation

The following chemicals were used without further purification: Cu(I)acetate (97%, Sigma-Aldrich, stored in Ar-glovebox), Pd(II)acetate (Pd 45.9-48.4%, Alfa Aesar), trioctylamine (TOA, >92.5%, Sigma-Aldrich, synthesis grade), tetradecylphosphonic acid (TDPA, 98%, Sigma-Aldrich), 2-propanol (isopropanol, 99.5%, anhydrous, Sigma-Aldrich), hexane (>95%, Sigma-Aldrich) and HNO_3 (aq, 65%, VWR chemicals). As carbon support, graphene nanoplatelets (xGnP® C-500 HP, ca. 500 m^2/g, XG Sciences) were used after functionalisation (*vide infra*).

Bimetallic PdCu and monometallic Cu colloidal particles were prepared by adapting a previously described method for Cu nanoparticles.[36,37] In short, 10 mL of TOA was heated under continuous stirring and N_2 flow to 130 °C, held for 60 minutes in a three-neck flask equipped with a water-cooled condenser, and cooled to room temperature. Next, 123 mg of Cu(I)acetate, a variable amount of Pd(II)acetate and 139 mg of TDPA were added, keeping the TOA mixture under a blanket of N_2. The flask was purged three times using vacuum/N_2 and rapidly (30-40 °C/min) heated to 180 °C, held for 30 minutes, and further heated to 270 °C. After 30 minutes at this temperature, the mixture was let to cool down to room temperature in 10-15 minutes. The suspension was diluted with 25 mL hexane and precipitated by addition of 150 mL isopropanol. The bimetallic PdCu particles were separated from the solvent by centrifugation (8000 rpm, 30 minutes) and redispersed in *ca.* 10 mL hexane. The colloidal suspensions were stored at 5 °C for 1 to 3 days (until deposition on the catalyst support).

An oxidation treatment was performed to increase the concentration of surface groups of the carbon supports. A detailed description of the procedure and the characterisation of the oxidised and untreated carbon is given by Visser *et al.*[38] In short, 400 mL 65% HNO_3 (aq) was carefully added to 10 g bare carbon in a 1 L round bottom flask equipped with a water-cooled condenser and at the top connected to two, in series connected, gas bubblers filled with water. The mixture was heated to 80 °C under vigorous stirring. After 2 hours, room temperature deionised water was added to a total volume of 1 L. The mixture was let to cool further to room temperature without stirring for an hour. The supernatant was decanted and the residue was washed with deionised water until a neutral pH was reached. The wet powder was dried overnight at 120 °C in static air.

PdCu/C catalysts were prepared by adding roughly 5 mL of the colloidal suspension to 1.0 gram of functionalised graphitic carbon support, whereafter the hexane was evaporated at 55 °C overnight. The dry powders were heated to 250 °C with 1 °C/min under 100 mL/min 20% O_2/N_2 flow and held at that temperature for 2 hours to remove the ligands and residual solvent. One catalyst was prepared without Pd(II)acetate and served as a Cu reference catalyst (Cu_{100}). After calcination, the PdCu/C and Cu/C samples were stored in their oxidised form under air.

Pd reference catalysts (Pd_{100}) were prepared by incipient wetness impregnation (see Chapters 2 and 3) of the functionalised carbon (0.8 mL/g as determined by N_2-physisorption) using a diluted (0.01-0.05 mol/L) Pd-tetraamine nitrate aqueous precursor solution. The concentration was chosen to obtain a Pd weight-loading similar to the Pd in PdCu/C catalysts (0.1-0.5 wt%, *vide infra*). The samples were heat treated (2 hours, 250 °C, N_2) to remove nitrate and amine precursors and reduced (1 hour, 500 °C, H_2) to induce particle growth of the carbon-supported Pd nanoparticles to the desired sizes.[39]

4.2.2 Characterisation

The PdCu and Cu colloidal nanoparticles suspended in hexane were drop cast onto holey carbon-coated grids (300 mesh, Au) and let to dry under ambient conditions, while the PdCu/C catalyst powders were dry-deposited onto the carbon-coated grids (300 mesh, Cu). The shape, size and dispersion of the metal nanoparticles were analysed using (scanning) transmission electron microscopy ((S)TEM) with a Talos F200X (Thermo Fisher Scientific) microscope operated at 200 kV. Elemental mapping and quantification of Cu and Pd were performed by energy dispersive X-ray spectroscopy (EDX) in STEM mode on both large-area images as well as individual nanoparticles. From the TEM images, the diameters of individual nanoparticles (d_i) were measured and the results were analysed using Eq. 2.1 and 2.2.

Inductively coupled plasma optical emissions spectroscopy (ICP-OES) was performed with a PerkinElmer Optima 8300 and a PerkinElmer S10 autosampler. Roughly 20 mg of the PdCu/C or Cu/C catalysts was dissolved in 3 mL aqua regia (3:1 HNO_3:HCl) for 3 hours. Afterwards, the solutions were diluted with 5% HNO_3 to ca. 0.5 mg/L of estimated Cu and/or Pd concentration. A calibration curve for the emission lines of known concentrations of Cu (225 nm) and Pd (340 nm) between 0 and 1.0 mg/L was measured, from which the Cu and Pd metal loadings in PdCu/C catalysts were calculated.

Thermogravimetric analysis (TGA) combined with mass spectrometry (MS) and infrared (IR) spectroscopy were performed to follow the ligand removal during the heat treatment (see above). TGA-MS was performed on Perkin Elmer Pyris 1 TGA instrument while heating from 30 to 800 °C with a 10 °C/min ramp under 20% O_2/Ar atmosphere. IR measurements were performed on powder samples with a Perkin Elmer 2000 FT-IR in attenuated total reflection (ATR) mode. Spectra were collected from 600 to 4000 cm^{-1}.

X-ray diffraction (XRD) was performed as described in section 2.2.3. Crystallite sizes were estimated from the full width at half maximum (FWHM) of the highest intensity CuO (41.5° 2θ) or Cu_2O (42.6° 2θ) oxide diffraction peaks.[40]

The lattice parameter (d_{hkl}) was determined from Bragg's law as

$$d_{\mathrm{hkl}} = \frac{\lambda}{2sin\,(\theta)} \qquad \text{Eq. 4.1}$$

Temperature programmed reduction (TPR) was performed with a Micromeritics AutoChem 2920. Typically, 40 mg of sample (>75 µm) was dried under Ar flow at 120 °C for 15 minutes and let to cool to room temperature, after which the gas flow was switched to 5% H_2/Ar. The H_2 consumption during reduction was followed with a TCD detector from room temperature to 800 °C with a 10 °C/min ramp. The onset of the reduction peak was determined as the intersection between the baseline and the slope of the peak at the maximum derivative.

In situ and *operando* X-ray absorption spectroscopy (XAS) measurements were performed at the Pd K-edge (23.50 keV) in fluorescence mode (photodiode detector) and the Cu K-edge (8.979 keV) in transmission mode at the ROCK beamline at SOLEIL (Gif-sur-Yvette, France).[41] At ROCK, continuous fast switching (~30 s) between both edges was possible using two Quick-XAS monochromators equipped with a Si(111) channel-cut crystal, which oscillated at 2 Hz. In this set-up, spectra of both elements were acquired in alternating fashion for 30 seconds at Cu and 120 seconds at Pd K-edge, with limited time lost between switching of the monochromators. The beam spot size was 100-200 µm^2. Approximately 7 mg of pelletised 38-75 µm sieve fraction catalyst material was loaded into a 5 mm bed packed between quartz wool into a 2.1 mm outer diameter quartz capillary with 50 µm wall thickness. The capillary was loaded onto a home-built gas-phase reactor placed at 45° with respect to the X-ray beam direction equipped with two graphite heating blocks. The temperature of the sample was monitored by a thermocouple placed in the quartz wool inside the reactor directly after the catalytic bed. The sample holder was flushed with 20 mL/min hydrogen (AlphaGaz 2, 99.9999%), reduced at 250 °C (3 °C/min) for 1 hour and let to cool to 30 °C in hydrogen while continuously acquiring spectra. Afterwards, pre-mixed reaction gasses were introduced over the catalyst at 30 °C, consisting of a 50 mL/min 50:30:20 vol% mixture of 0.6% butadiene/He (AirLiquide), propylene (>99.5%) and hydrogen, respectively, at atmospheric pressure. The concentration of the gasses was monitored by an on-line mass spectrometer. Reference spectra of Pd and Cu foils were acquired in transmission mode simultaneously to the measurement of the catalyst. PdO, CuO and Cu_2O pellets were acquired *ex situ*.

Analysis was performed with the Demeter software package, using the Athena and Artemis applications.[42] The spectra were energy calibrated to the peak maxima for the first derivative of the absorption spectra set at 23.50 keV for Pd K-edge and 8.979 keV for Cu K-edge. The extended X-ray absorption fine structure (EXAFS) was extracted from the normalised spectra in Athena by Forward Fourier transform of the *k*-space with R=1.0 cutoff, *k*-weight of 2 or 3 in the range 3.0<k<14 Å^{-1}. Linear combination fitting (LCF) was performed in Athena using the range from -20 to +50 eV from the inflection point. The best fit was determined by a fit of least squares of the metal foil

and metal oxide reference spectra. From the LCF, the reduction temperature was determined, which was defined as the temperature where half of the spectrum was fitted to the metal foil. The EXAFS fitting was performed in Artemis for 1.4<R<3.0 Å radial distance (R). An amplitude reduction factor (S_0^2) of 0.68 for Pd-foil was fitted, using a cif file of fcc Pd (mp-2 reference[43], average Pd-Pd distance 2.77 Å). The quality of the EXAFS fits was assessed by the R-factor (R_f), which quantifies the misfit of the data and the determined model.

4.2.3 Catalytic testing

Catalytic testing was performed on the set-up described in Chapter 2. After loading the catalyst, the reactors were flushed for 15 minutes with 50 mL/min N_2 before switching to 20 mL/min H_2. The PdCu/C and Cu/C catalysts were fully reduced *in situ* by heating to 250 °C in H_2 with 3.8 °C/min and 1-hour isothermal hold before cooling to 25 °C in H_2 in 30 minutes before introducing the reaction gas.

Turnover frequencies (TOFs) per metal surface atom were calculated with Eq 2.9, assuming a homogeneous distribution of Pd and Cu in the nanoparticles. For the inclusion of Cu into the calculations, 63.546 g/mol molar mass, 11.83 Å^3 atomic volume and 6.85 Å^2 atomic surface area were taken for Cu. The estimation of the dispersion (Eq. 2.10) simplifies to $D_{\mathrm{Pd}} = \frac{1.112}{d_{\mathrm{VA}}}$ for monometallic Pd nanoparticles and $D_{\mathrm{Cu}} = \frac{1.036}{d_{\mathrm{VA}}}$ for Cu with d_{VA} in nanometers, assuming spherical particles and an fcc structure. For the bimetallic PdCu nanoparticles, the dispersion is estimated as a linear combination between Cu and Pd as:

$$D_{\mathrm{PdCu}} = \frac{1.112 \times \theta_{\mathrm{Pd}} + 1.036 \times (1 - \theta_{\mathrm{Pd}})}{d_{\mathrm{VA}}} \qquad \text{Eq. 4.2}$$

where θ_{Pd} is the molar Pd-fraction (Pd/(Cu+Pd), between 0 and 1) of Pd, as determined by ICP-OES.

4.3 Results

4.3.1 Structure of the PdCu/C catalysts

The as-prepared PdCu colloids (Figure 4.1A) were, on average, 6.5 ± 0.9 nm in diameter, as determined by transmission electron microscopy (TEM). Elemental mapping using energy dispersive X-ray spectroscopy (EDX) of the Cu and Pd in sample Pd_3Cu_{97} (Figure 4.1B) visualised the homogeneous co-existence of both metals in each individual colloid and did not indicate separated metal domains. The bulk Cu:Pd ratio of these colloids was 26, as determined over a large area of colloids (550×550 nm^2). This is close to the value found by ICP-OES (33, see Table 4.1). Quantification of a

Table 4.1. Overview of as-synthesised PdCu/C catalysts.

Sample	Pd wt%[a]	Cu wt%[a]	Cu:Pd[a]	Pd/(Cu+Pd) (mol/mol)[a]	Particle diameter (nm)[c]	Crystallite size (nm)[d]
Cu_{100}	-	3.52	n.a.	0	6.2 ± 1.3	6.7
$Pd_{0.6}Cu_{99.4}$	0.03	3.10	167	0.006	7.5 ± 4.3	7.9
$Pd_{1.2}Cu_{98.8}$	0.05	2.29	85	0.012	7.9 ± 1.3	6.6
Pd_3Cu_{97}	0.21	4.11	33	0.030	7.4 ± 1.4	6.5
Pd_7Cu_{93}	0.18	1.33	12	0.074	7.0 ± 1.3	5.6
$Pd_{13}Cu_{87}$	0.50	1.94	6.5	0.134	7.4 ± 1.0	5.0
Pd_{100}(0.1%)	0.1[b]	-	n.a.	1	5.0 ± 1.6	n.d.
Pd_{100}(0.5%)	0.5[b]	-	n.a.	1	5.3 ± 1.2	4.3

[a] Determined by ICP-OES. [b] Determined by precursor concentration during impregnation. [c] Number-averaged diameter from TEM. [d] Calculated from Scherrer equation on CuO or Cu_2O diffraction peak.[40]

representative subset of 10 individual nanoparticles depicted in Figure 4.1B showed similar Cu:Pd ratios in all particles and the composition of the two metals was uniform throughout the sample with a standard deviation of 22%.

After deposition onto the carbon, 7.4 ± 1.4 nm particles (Figure 4.1C) were homogeneously distributed over the entire carbon support particles. Similar sizes in Figure 4.1C and Figure 4.1A evidence that limited particle growth had occurred during colloid deposition and heat treatment at 250 °C for 2 hours in 20% O_2/N_2. Table 4.1 shows an overview of the metal loading, composition and particle size of the different catalysts in the series. It shows total loadings of 1.3-4.1 wt% Cu and 0.03-0.50 wt% Pd on carbon, resulting in Pd-fractions varied between 0.6% and 13.4% for the bimetallic catalysts, which are referred to as "Pd_xCu_{100-x}" throughout this manuscript, where *x* is the percentage of Pd in PdCu, as measured by ICP-OES. The analysis of the TEM images

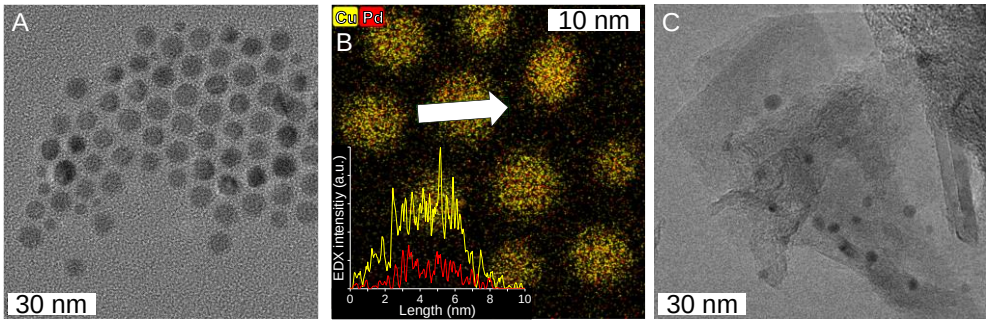

Figure 4.1. Electron microscopy of the free-standing and carbon-supported PdCu colloids. (A) Bright-field transmission electron microscopy (BF-TEM) micrograph and (B) scanning TEM energy dispersive X-ray (STEM-EDX) map of the Pd_3Cu_{97} colloids. The inset shows a linescan over the diameter of the particle as indicated by the white arrow. (C) BF-TEM micrograph of metal nanoparticles of this sample after deposition on the carbon support.

of all PdCu/C catalysts after oxidative heat treatment shows similar particle diameters and polydispersities independent of the Pd content.

To verify at which temperature the organic TOA and TDPA were removed by oxidative heat treatment, thermogravimetric analysis was used (TGA, Figure 4.2A). In 20% O_2/N_2, the weight loss of the PdCu/C catalysts between 200 and 400 °C was ascribed to the removal of organics from the particles. Attenuated total reflection infrared spectroscopy (ATR-IR, Figure 4.2B) did not exhibit C-H vibrations associated with TOA and TDPA after 2 hours at 250 °C, evidencing complete removal of the organics by this mild oxidative treatment.[44] X-ray diffraction (XRD) measurements on PdCu/C calcined at a higher temperature (350 °C) indicated decomposition of the carbon support accompanied by growth of particles, observed by a loss of C diffraction intensity and narrowing of CuO diffraction peak, respectively. Hence, the mild oxidative treatment (calcination) for 2 hours at 250 °C in 20% O_2/N_2 provided sufficient removal of residual organic solvent and/or capping ligands that originated from the nanoparticles but did not induce significant carbon decomposition or metal particle growth.

The X-ray diffractograms (Figure 4.3A) showed diffraction peaks ascribed to CuO ((002) and (111) at 41.5° and 45.3° 2θ) and/or Cu_2O ((111) at 42.6° 2θ) for all Cu-rich catalysts after calcination in 20% O_2/N_2. No diffraction due to crystalline PdO or Pd was observed for the PdCu catalysts (highest diffraction intensity expected for PdO(101) at 39.5° or Pd(111) at 46.9° 2θ), which proved that no significant amount of Pd (oxide) crystallites was present. From the full width at half maximum (FWHM) of the Cu-oxide

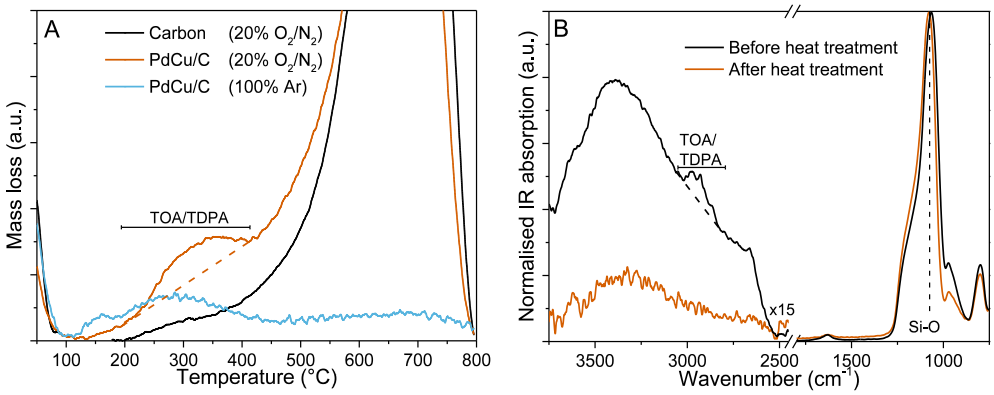

Figure 4.2. Ligand removal heat treatment. (A) Mass loss of PdCu/C (orange) and carbon support (black) under 20% O_2/N_2 (orange) and PdCu/C under Ar (blue) atmosphere. Samples heated with 10 °C/min ramp. (B) IR spectra of PdCu/SiO_2 catalyst before and after heat treatment (2h, 250 °C, 20% O_2/N_2) normalised to Si-O peak. Deposition onto SiO_2 instead of carbon was necessary to minimise C-H vibration absorption of the support. The additional peak between 3020 and 2820 cm^{-1} in the black curve (before heat treatment) indicate the presence of organic ligand and is in line with reference IR spectra of trioctylamine (TOA, SpectraBase® compound ID BoJQr2Kggzj) and tetradecylphosphonic acid (TDPA, SpectraBase® compound ID 5hGnvRTmUTG).[44]

diffraction peaks, crystallite sizes were determined between 5.0 and 7.9 nm, in line with observations by TEM (Table 4.1).

Additional compositional information of the bimetallic materials was derived from the diffraction peak position in the X-ray diffractograms in Figure 4.3A, where a peak shift to lower angles was observed with increasing Pd-fraction. By incorporation of larger Pd atoms (0.138 nm atomic radius, 0.203 nm Pd-O bond distance compared to 0.128 nm Cu metal radius, 0.184 nm Cu-O bond distance) into the Cu-oxide lattice, the lattice parameter increased and the peak position shifted to lower angles. The derived lattice parameter of Cu_2O increased from 2.54 Å for $Pd_{1.2}Cu_{98.8}$ to 2.60 Å for $Pd_{13}Cu_{87}$; an expansion slightly larger than expected by Vegard's law (0.033 Å) for a 10% larger bond distance of Pd-O compared to Cu-O. This peak shift substantiates the results of elemental mapping (Figure 4.1B), that Cu and Pd are mixed on the atomic scale in the individual nanoparticles/crystallites.

Since Pd atoms act as active sites for H_2 dissociation, if Pd and copper oxide are well mixed, the presence of Pd and H-spillover onto the Cu-oxide are expected to result in lower reduction temperatures of the Cu-oxide.[7] The reduction profiles of all catalysts (Figure 4.3B) show a complete reduction to metallic Cu at temperatures below 250 °C. A trend in the peak maximum and peak onset is observed towards lower temperatures for higher Pd concentration, evidencing reduction promotion of the copper oxide by the Pd. Lastly, since all catalysts were fully reduced at 250 °C, this temperature was chosen as the reduction pre-treatment temperature for further characterisation and catalytic testing. After reduction, the bimetallic catalysts were more resistant to re-oxidation in air compared to the monometallic Cu/C catalyst, as found by XRD. After two weeks in air, the diffraction peak area of oxide:metal was 37:63 for $Pd_{0.6}Cu_{99.4}$, whereas almost complete oxidation (84:16) was observed over Cu/C.

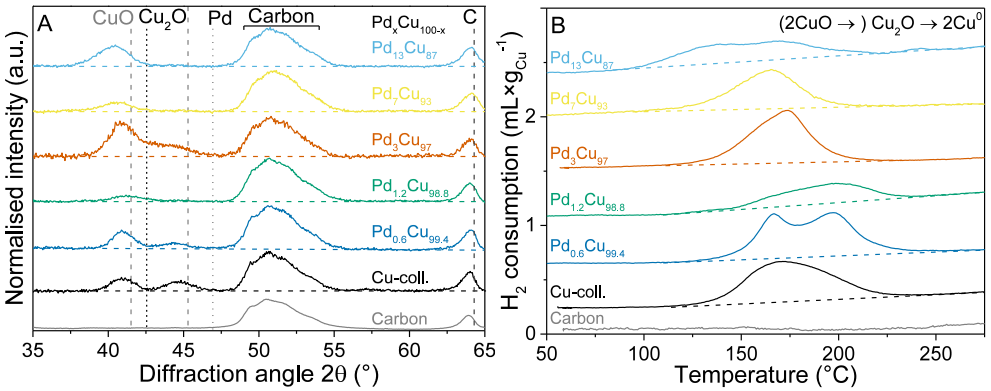

Figure 4.3. Characterisation of PdCu/C catalysts by XRD and TPR. (A) Powder X-ray diffractograms normalised to C(004) peak at 64° 2θ. Peak positions of refences indicated by vertical dotted and dashed lines. (B) Temperature programmed reduction profiles of PdCu/C catalysts normalised to Cu mass.

4.3.2 Catalytic activity

The activity of the catalysts after reduction was tested in the selective hydrogenation of 0.3 vol% butadiene in 100-fold excess of propylene and 20 vol% hydrogen (Figure 4.4). Panel A shows the conversion as a function of the temperature of the bimetallic catalysts and monometallic references. The monometallic Cu on carbon catalyst only showed considerable butadiene activity above 110 °C, in line with results reported in the literature for Cu/C and Cu/SiO_2 catalysts of similar size.[1] For the Cu_{100} catalyst, the surface normalised activity, expressed in turnover frequency (TOF), was 6.4×10^{-3} $mol_{butadiene}$ $mol_{Cu,surface}$ s^{-1} at 130 °C. This value is similar to that reported earlier in literature for 7 nm Cu/C nanoparticles (6×10^{-3} s^{-1} at 125 °C)[1] under identical reaction conditions but prepared by incipient wetness impregnation and reduction of a Cu-nitrate precursor. The similar activity of these Cu/C catalysts suggests there is no influence of possible traces of residual ligands for the present series of colloidally prepared catalysts.

The conversion for all bimetallic catalysts showed a similar temperature dependence (Figure 4.4A). From the Arrhenius plot (Figure 4.4B), apparent activation energies were between 52 and 93 kJ/mol (Table 4.2, butadiene conversion below 40%). The apparent activation energies for the bimetallic PdCu samples were similar and all between 57 and 65 kJ/mol, which is substantially lower than for monometallic Cu/C (93 kJ/mol, Figure 4.4B) and closer to that of monometallic Pd (52 kJ/mol). This indicates that the exposed Pd atoms/clusters are likely the active sites for butadiene

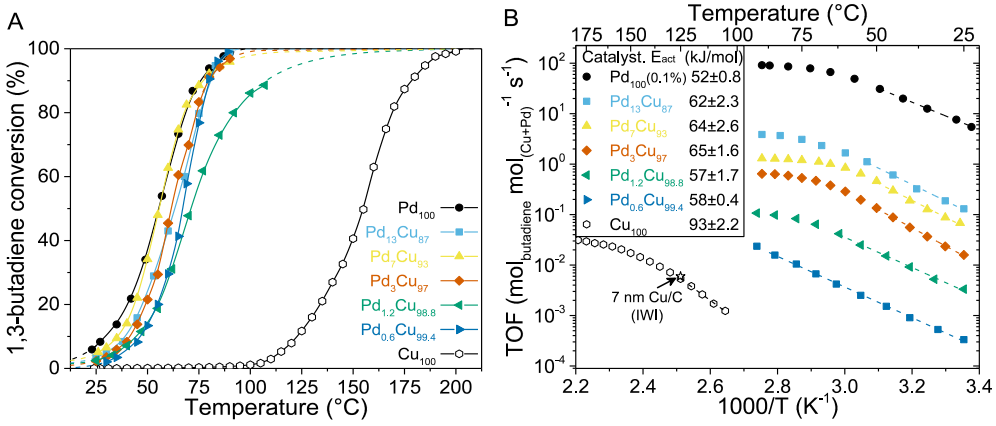

Figure 4.4. Catalytic activity. (A) Butadiene conversion as function of temperature. Reactors were loaded with varying amounts of catalyst (between 0.5 and 16 µg of Pd, Table 4.2) to achieve conversions <7.5% at 25 °C. (B) Arrhenius plots for butadiene hydrogenation in TOF per metal surface atoms (Cu+Pd). From the linear fit of the slope of Ln(TOF)-T^{-1} plots, the activation energies were determined, below 40% butadiene conversion. Star and arrow represent data from the literature for 7 nm Cu/C prepared by conventional incipient wetness impregnation.[1] Reaction conditions: 50 mL/min 0.3% butadiene, 30% propylene, 20% H_2, He balance.

Table 4.2. Details of the catalytic tests.

Catalyst	µg Pd[a]	µg Cu[a]	Dilution[b]	E_{act} (kJ/mol)[c]	TOF at 25 °C per metal ($\times 10^{-3}$ s^{-1})	TOF at 25 °C per mol Pd (s^{-1})
Cu_{100}	-	1600	-	93 ± 2.2	n.d.	n.a.
$Pd_{0.6}Cu_{99.4}$	15.5	1600	-	58 ± 0.4	0.62 ± 0.16	0.16 ± 0.04
$Pd_{1.2}Cu_{98.8}$	8.3	420	-	57 ± 1.7	4.6 ± 0.77	0.29 ± 0.05
Pd_3Cu_{97}	4.4	240	-	65 ± 1.6	16 ± 3.0	0.55 ± 0.10
Pd_7Cu_{93}	4.3	32	3.1	64 ± 2.6	110 ± 20	0.93 ± 0.17
$Pd_{13}Cu_{87}$	3	12	12.7	62 ± 2.3	210 ± 30	0.99 ± 0.13
Pd_{100}(0.1%)	0.5	-	25.3	52 ± 0.8	6610 ± 2114	6.6 ± 2.1

[a] Amount of Pd and/or Cu in each reactor for the catalysis shown in Figure 4.4A. [b] Dilution of each catalyst was prepared in oxidised carbon prior to pelletising and sieving. [c] Apparent activation energy derived from linear fit of ln(TOF)-T^{-1} plot between 25 and 50 °C (Figure 4.4B).

hydrogenation in the PdCu/C catalysts. Cu might undergo surface oxidation by oxygen traces in the reaction gas, especially at lower temperatures where CuO is thermodynamically favoured.[1] To rule out any effects related to partial oxidation, we tested the bimetallic PdCu/C during heating and cooling to 90 °C and under isothermal reaction conditions at 40 °C but found no indication of instability or deactivation.

To compare the intrinsic activities, the TOFs were calculated, which takes into account the amount of catalyst loaded and the nanoparticle size. For the bimetallic PdCu/C catalyst, a random distribution of Pd and Cu over the bimetallic nanoparticles was assumed; hence, the surface ratio is assumed to be the same as the overall metal ratio. For the monometallic references, the surface-normalised activity per metal atom (Table 4.2) of Pd was 5-7 orders of magnitude higher activity compared to Cu (Figure 4.5A). In the bimetallic PdCu/C catalyst, the activity increased strongly with increasing Pd fraction, from 0.6 to 210 $mmol_{butadiene}$ $mol_{Pd+Cu,surface}^{-1}$ s^{-1} for $Pd_{0.6}Cu_{99.4}$ and $Pd_{13}Cu_{87}$. Hence, we assumed the exposed Pd atoms to be the only contributor to the

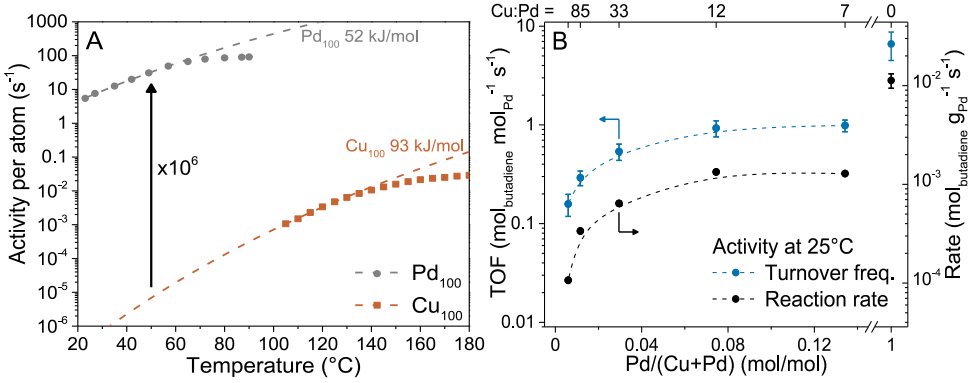

Figure 4.5. Activity overview. (A) Direct comparison of monometallic Pd- and Cu-references. (B) Surface-normalised Pd turnover frequencies (TOFs) of Pd and PdCu catalysts at 25 °C as function of Pd-fraction.

total activity and the activity of Cu to be negligible, which is especially true at temperatures below 110 °C. Normalised to the exposed Pd atoms, the TOF in the PdCu/C catalysts (Figure 4.5B, blue symbols) shows values between 0.16 and 1.0 $mol_{butadiene}$ $mol_{Pd,surface}^{-1}$ s^{-1}, which are lower than monometallic Pd/C (6.6 s^{-1}). The TOF increased from 0.16 s^{-1} for 0.6 mol% Pd up to 1.0 s^{-1} at 7 mol% Pd, after which it stabilised and remained similar even when the doubling the Pd content (*i.e.,* TOF is approximately 1.0 s^{-1} for both Pd_7Cu_{93} and $Pd_{13}Cu_{87}$). Because of the similar particle sizes of the colloidally prepared nanoparticles (Table 4.1), a near-identical trend is observed in the reaction rate per gram of Pd (Figure 4.5B, black symbols). The reaction rate increased roughly ten-fold from 0.11×10^{-3} $mol_{butadiene}$ g_{Pd}^{-1} s^{-1} for $Pd_{0.6}Cu_{99.4}$ to 1.3×10^{-3} mol g^{-1} s^{-1} for Pd_7Cu_{93} and $Pd_{13}Cu_{87}$. The 5 nm monometallic Pd nanoparticles showed an order of magnitude higher activity at 11×10^{-3} mol g^{-1} s^{-1}.

4.3.3 Selectivity

During the hydrogenation of butadiene, the selectivity towards the butene products (1-butene, trans-2-butene and cis-2-butene) was monitored as a function of conversion (Figure 4.6A). Herein, both butane and propane formation are taken as the unselective products during selective hydrogenation. All catalysts showed a butene selectivity close to 100% at low butadiene conversions, which slightly decreased with increasing conversion and showed a steeper decrease when approaching complete conversion. Monometallic Cu and Cu-rich (≥98.8% Cu) catalysts retained good selectivity up to high conversion, whereas the bimetallic PdCu catalysts with lower Cu-fraction and the monometallic Pd reference showed similar selectivity-activity relationship. For a better comparison with $Pd_{13}Cu_{87}$, a monometallic Pd/C catalyst was tested with similar Pd weight loading (0.5 wt%, Table 4.1), which showed worse selectivity compared to $Pd_{13}Cu_{87}$. The selectivity trend was ascribed to an increasing amount of internal mass

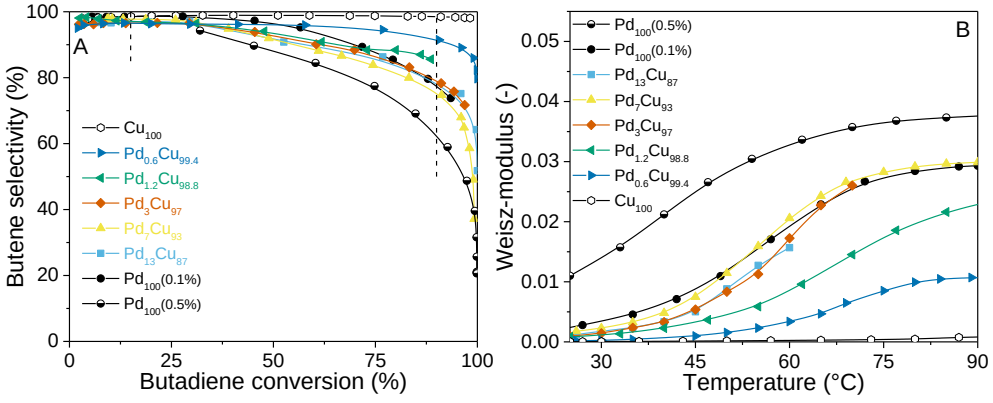

Figure 4.6 Butene selectivity. (A) Selectivity as a function of conversion. (B) Weisz-modulus (see Chapter 3) calculated for all catalysts, indicating the trend in selectivity can be ascribed to the amount of internal diffusion limitations.

transfer limitations (see Chapter 3), as evidenced by the higher Weisz-modulus for the less selective catalysts (Figure 4.6B).

To investigate the intrinsic performance of the catalysts with minimal influence of mass transfer limitations, selectivities at low butadiene conversions (15%) are reported as filled circles in Figure 4.7A. At these low conversion levels, the selectivity of the monometallic and bimetallic catalysts hardly differed from each other; the butene selectivities were between 96.5% and 98.5% (*i.e.,* 1.5-3.5% combined butane and propane levels). To assess the catalysts' performance more closely to their industrial operation conditions, we report the butene selectivities at high conversion levels (90%) as open circles in Figure 4.7A. All catalysts show a reasonably good selectivity, above 75% towards butene products at 90% butadiene conversion. A decreasing trend in butene selectivity was observed with increasing Pd-fraction from 91.4% for $Pd_{0.6}Cu_{99.4}$ to 85% for $Pd_{1.2}Cu_{98.8}$ and roughly 78% for Pd_3Cu_{97} and higher Pd-content. $Pd_{13}Cu_{87}$ showed a higher butene selectivity (78%) than the 0.5 wt% Pd/C reference (62%, square in Figure 4.7A).

In addition to the butene selectivity (alkene *vs* alkane products), the selectivity towards individual C_4-products was investigated at high conversion levels (90%, Figure 4.7B). During butadiene hydrogenation, all catalysts predominantly produced 1-butene, followed by trans-2-butene and showed the lowest isomer selectivity towards cis-2-butene. For Pd/C and PdCu/C, the relative ratios were identical and roughly 60%, 35% and 5% for 1-butene, trans-2-butenes and cis-2-butenes characteristic of Pd-catalysed butadiene hydrogenation.[39,45,46]. For monometallic Cu, a different C_4-isomer distribution was observed (73%, 17% and 10% respectively), in line with reports on Cu-catalysed butadiene hydrogenation.[1,2] The formation of n-butane was very limited for all catalysts (<2%). Therefore, even at 90% butadiene conversion, most of the unselective alkane products came from the hydrogenation of the 100-fold excess of

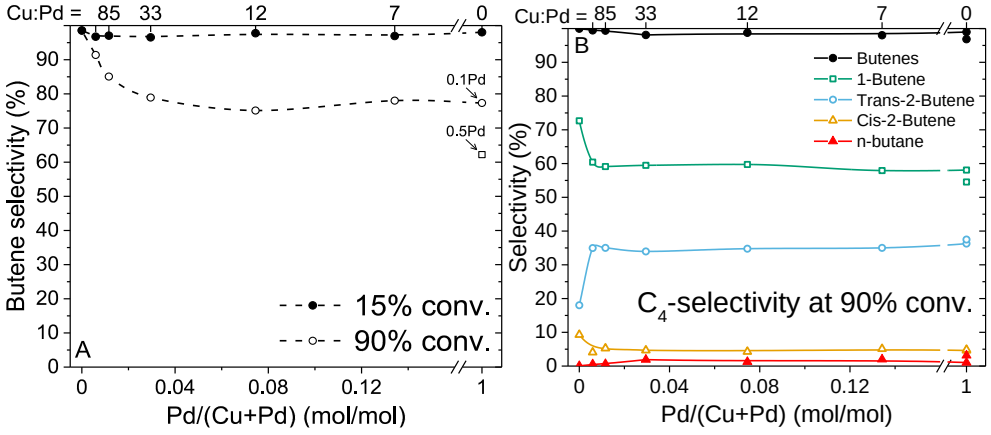

Figure 4.7. Selectivity of bimetallic PdCu and monometallic Cu and Pd catalysts. (A) Butenes selectivity at low (15%) and high (90%) butadiene conversion levels. (B) Butene-isomer and butane selectivity obtained close to full butadiene conversion (90%).

propylene and not from the over-hydrogenation of butene. For example, the 78% butene selectivity of $Pd_{13}Cu_{87}$ (Figure 4.7A) involved only 2% butane formation (Figure 4.7B) and ten times more propane formation.

4.3.4 X-ray absorption spectroscopy

***In situ* reduction**

The Pd_3Cu_{97}, Pd_7Cu_{93} and $Pd_{13}Cu_{87}$ catalysts were investigated by X-ray absorption spectroscopy (XAS) under relevant conditions for reduction and catalysis. For $Pd_{0.6}Cu_{99.4}$ and $Pd_{1.2}Cu_{98.8}$, the Pd-loading (Table 4.1) was too low to acquire spectra of sufficient quality. XAS spectra were acquired while alternating between the Cu K-edge (8.979 keV) and the Pd K-edge (23.50 keV). The X-ray absorption near edge structure (XANES) normalised spectra at the Cu K-edge (Figure 4.8A) of Pd_7Cu_{93} showed that at 30 °C in pure H_2, the Cu-speciation was mostly Cu^{2+} as the spectral features resembled the CuO reference. During the ramped heating to 250 °C, the Cu^{2+} was reduced to Cu^{+} and eventually Cu^0, depicted by a shift of the edge jump to lower energies and a reduced white line intensity peak after the edge-jump. At the Pd K-edge (Figure 4.8B), a reduction of Pd^{2+} to Pd^0 was observed, with slightly more noisy spectra due to the lower weight loading of Pd in the catalyst.

Similar spectral changes in both edges are observed for Pd_3Cu_{97} and $Pd_{13}Cu_{87}$. The reduction of Pd appears to occur at lower temperatures compared to Cu, as shown by the colour of the lines just before reaching the final oxidation state (green *vs* yellow/orange lines for Pd and Cu, respectively). From linear combination fitting of the XANES, the reduction temperature of the elements was determined for the catalysts. With increasing Pd concentration in the catalysts, the reduction temperature decreased and was 136, 122 and 123 °C for Cu-species and 117, 93 and 94 °C for Pd-species for Pd_3Cu_{97}, Pd_7Cu_{93} and $Pd_{13}Cu_{87}$ catalysts, respectively (±3-6 °C due to temperature ramp during acquisition). This trend is in line with TPR measurements (Figure 4.3B), although the values obtained by XAS are slightly lower, ascribed to lower temperature ramp (3 *vs* 10 °C/min), higher hydrogen concentration (100% *vs* 5%) and lower catalyst mass (7 *vs* 50 mg) during XAS measurements.

From the normalised XANES spectra, extended X-ray absorption fine structure (EXAFS) analysis was performed. Similar to the changes in XANES, the radial scatting paths from EXAFS for the PdCu catalyst showed a transition from Cu^{2+} (Figure 4.8C) and Pd^{2+} (Figure 4.8D) species towards Cu^0 and Pd^0 during reduction. Interestingly, the reduced Pd atoms showed a scattering at a slightly lower radial distance than Pd-Pd of the Pd foil reference, which indicated the large contribution of Pd-Cu scattering in the bimetallic catalyst and evidenced the alloying during the pretreatment.

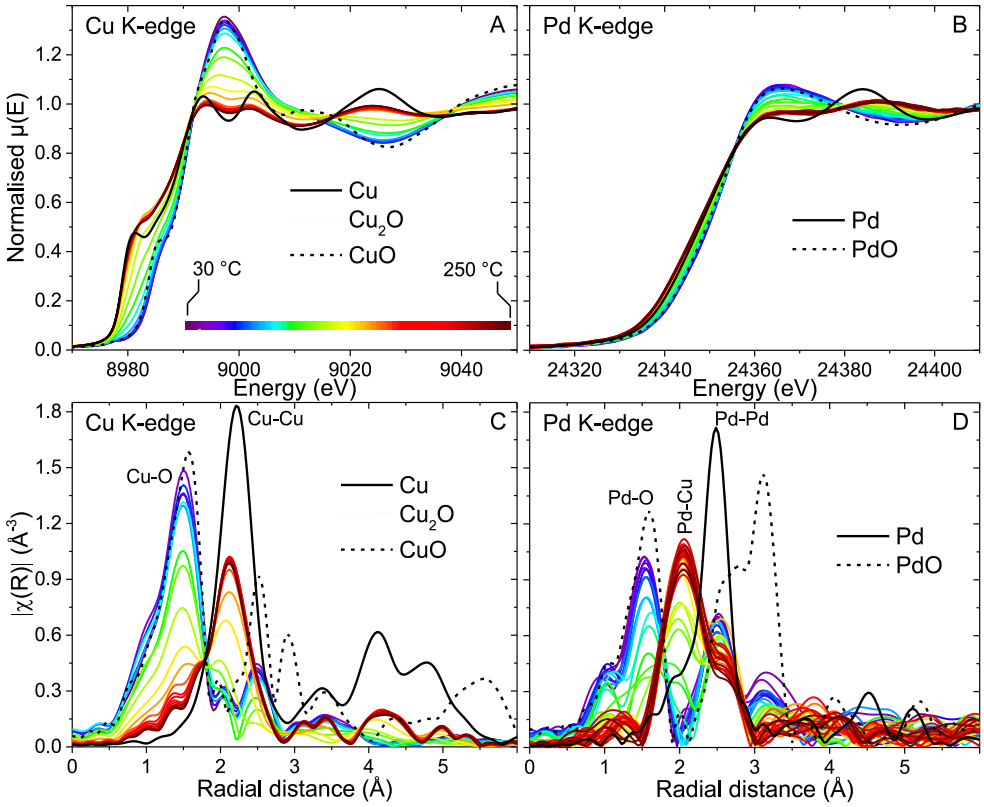

Figure 4.8. *In situ* XAS measurement of Pd_7Cu_{93} during reduction. Spectra acquired by alternating at the Cu K-edge (AC) and Pd K-edge (BD). (AB) XANES spectra and (CD) derived EXAFS scattering paths during ramped heating (3 °C/min) under H_2 flow. For the Cu and Pd metal foil references, the EXAFS intensity is halved for visualisation purposes.

***Operando* measurements**

After cooling to 30 °C in H_2, a longer scan of 15 minutes at the Pd K-edge and 5 minutes at the Cu-K edge was performed. Afterwards, the reaction gas was introduced at 30 °C. Hereafter, we focus on the speciation of Pd because, regarding activity and selectivity, this is the dominant element in the bimetallic catalysts. Figure 4.9A shows the XANES spectra at the Pd K-edge of Pd_3Cu_{97}, Pd_7Cu_{93} and $Pd_{13}Cu_{87}$ under selective hydrogenation reaction conditions, as well as the *ex situ* PdO and Pd-foil references. The spectra were acquired during the first 20 minutes of the *operando* synchrotron measurement. The spectra of the three PdCu/C catalysts in Figure 4.9A overlap, indicative of a similar oxidation state. The position of the edge jump (taken as the first maximum of the absorption derivative) was at lower energies than for the Pd-foil reference. This indicates that Pd in PdCu was more electron-rich than Pd in the Pd-foil, which can be attributed to electron density transfer from Cu to Pd in the reduced bimetallic particles.[21] Figure 4.9B shows the EXAFS radial scattering paths for Pd_3Cu_{97}, Pd_7Cu_{93}, $Pd_{13}Cu_{87}$ and Pd(O)-references. The PdCu/C catalysts showed a large

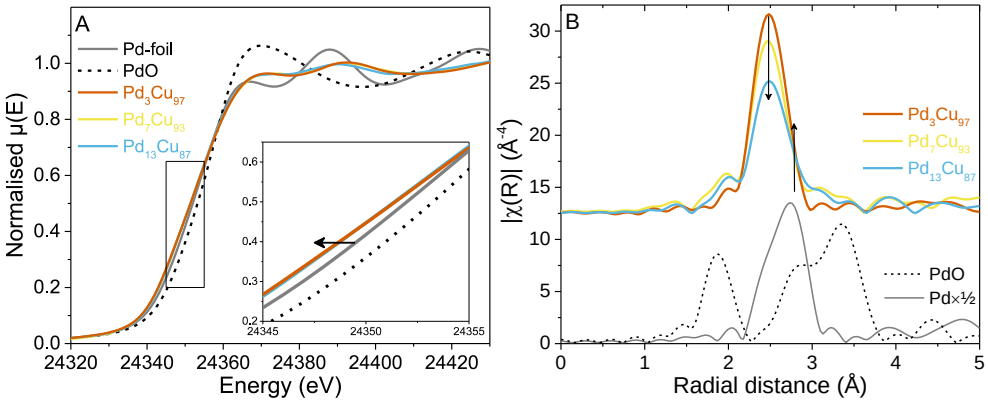

Figure 4.9. *Operando* X-ray absorption spectroscopy. (A) Normalised Pd K-edge absorption spectra of the PdCu/C catalysts at 30 °C under reaction gas and PdO and Pd-references. (B) Corresponding phase-corrected k^3-weigthed Fourier transforms of PdCu/C, PdO and Pd spectra. Reaction conditions: 50 mL/min 0.3%:30%:20%:49.7% C_4H_6:C_3H_6:H_2:He.

contribution from a scattering path at 2.5 Å, ascribed to the scattering of Pd atoms with neighbouring Cu-atoms. This scattering path decreased in intensity with increasing Pd content, *i.e.,* decreasing Cu:Pd ratio. Furthermore, a shoulder is present for all bimetallic catalysts at 2.7 Å, which indicates the presence of Pd-Pd scattering, which slightly increases for high Pd content.

The catalysts showed activity during *operando* XAS, which was very similar to the laboratory catalytic tests (comparing Figure 4.4A and Figure 4.10). At 30 °C, the three catalysts showed 5-10% butadiene conversion, as determined by on-line MS. During heating of the reactor, the butadiene conversion reached almost 100% at 80-90 °C and showed limited amount of n-butane formation. Little change in activity and selectivity

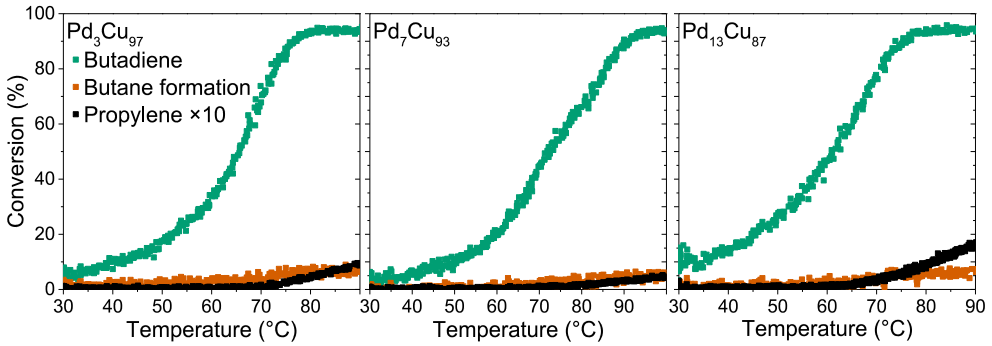

Figure 4.10. *Operando* activity. Butadiene conversion (green symbols) monitored by on-line MS during the catalytic test at ROCK for the Pd_3Cu_{97} (left), Pd_7Cu_{93} (middle) and $Pd_{13}Cu_{87}$ (right) catalysts. Red/orange symbols indicate the butadiene to butane selectivity and black symbols show the propylene conversion, for which the values are amplified tenfold for visualisation purposes.

Table 4.3. Fitted EXAFS parameters. PdCu/C catalysts fitted with both Pd-Cu and Pd-Pd scatter paths under reaction gas atmosphere at 25 °C after *in situ* reduction (H_2, 1h, 250 °C). Fitting window of 3.0<k<14 $Å^{-1}$ and 1.4<R<3.0 Å.

Sample	Scatter path	CN	Radial distance (Å)	$2\sigma^2 \times 10^{-3}$ ($Å^{-2}$)	ΔE_0 (eV)	R_f (%)
Pd_3Cu_{97}	Pd-Cu	9.1 ± 0.1	2.578 ± 0.003	6.2 ± 0.1	-4.4 ± 0.2	0.14
	Pd-Pd	2.9 ± 0.3	2.696 ± 0.01	0.9 ± 0.1		
Pd_7Cu_{93}	Pd-Cu	7.9 ± 0.7	2.580 ± 0.001	6.1 ± 0.9	-0.9 ± 0.6	2.4
	Pd-Pd	3.5 ± 0.7	2.704 ± 0.007	0.9 ± 0.2		
$Pd_{13}Cu_{87}$	Pd-Cu	7.3 ± 0.5	2.582 ± 0.005	8.2 ± 0.5	-2.2 ± 0.7	2.9
	Pd-Pd	3.9 ± 0.8	2.710 ± 0.009	0.8 ± 0.3		
Pd-foil	Pd-Pd	11.9 ± 0.6	2.739 ± 0.003	5.1 ± 0.3 (S_o^2=0.68)	-2.6 ± 0.4	0.95
Cu_3Pd	Pd-Cu	12	2.627	Reference structure, n.a.		
Cu-foil	Cu-Cu	12	2.542			

were observed during controlled cooling of the reactor back to 30 °C. For the three catalysts, similar scattering paths (Figure 4.11) were obtained at 30 °C in H_2 after reduction, in the reaction gas at the start of the reaction and after a heating/cooling cycle to 90 °C. Therefore, we decided to further investigate the Pd-speciation only at the start of the reaction, in line with the data presented in Table 4.2 and Figure 4.5B. The *operando* EXAFS spectra at the start of the reaction were fitted and the obtained fitting parameters are presented in Table 4.3. The CNs of Pd-Cu were 9.1 ± 0.1, 7.9 ± 0.7 and 7.3 ± 0.5 for Pd_3Cu_{97}, Pd_7Cu_{93} and $Pd_{13}Cu_{87}$, respectively, indicating Pd is mainly coordinated with Cu. The CN of Pd-Cu slightly decreased with increasing Pd content. Simultaneously, the fitted CNs of Pd-Pd increased with increasing Pd-fraction and were 2.9 ± 0.4, 3.3 ± 0.8 and 3.9 ± 0.5 for Pd_3Cu_{97}, Pd_7Cu_{93}, and $Pd_{13}Cu_{87}$. Based on the Cu:Pd ratios of these catalysts (between 7 and 33) and the fitted CNs, Pd showed a slight

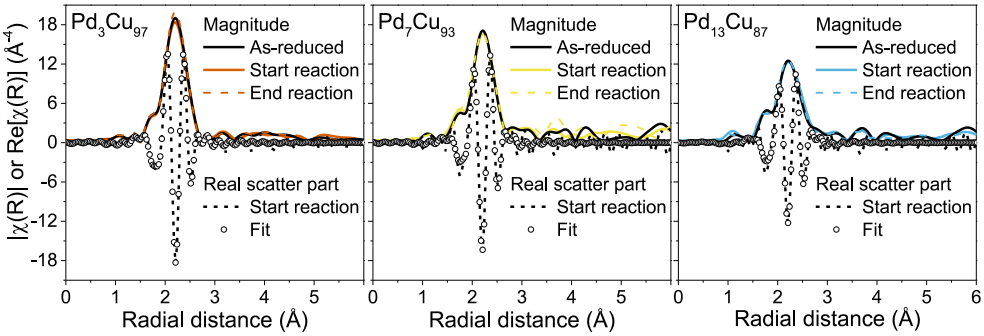

Figure 4.11. *Operando* EXAFS fits. Radial scattering magnitude (solid and coloured lines), real scatter path (black dashed lines) and its corresponding EXAFS fit (open symbols) of the spectra at the start of the reaction. Non phase-corrected data is shown. The feature at ~1.7 Å is not reminiscent of Pd-O scattering, as there is no match in the fitting of the real scattering path. Hence only Pd-Pd and Pd-Cu scatter paths have been considered.

preference to coordinate to Pd under these conditions. The total CN (sum of Pd-Pd and Pd-Cu) of the three catalysts was similar: 12.0 ± 0.4, 11.4 ± 1.4 and 11.2 ± 1.3 (Table 4.3), and in line with a particle size >5 nm as found by TEM (Table 4.1).[47,48]

4.4 Discussion

The butadiene hydrogenation catalytic results indicate that the Pd atoms or clusters exposed at the surface are likely responsible for activity in the bimetallic catalysts, as evidenced by the similar selectivities (Figure 4.7) and apparent activation energies (Figure 4.5) of PdCu/C and Pd/C. The Pd-normalised activity of all bimetallic PdCu catalysts was lower than for monometallic Pd, which can be explained by geometric and electronic effects. At low Pd content, isolated Pd atoms or small clusters (<4 atoms) do not accommodate a strong tetra-σ binding of butadiene molecules to the surface, as it would on monometallic Pd, decreasing the activity over bimetallic catalysts.[49] It was recently demonstrated that for acetylene hydrogenation over Pd-Zn catalysts, Pd_3Zn surface sites dominated the total activity, whereas Pd_1Zn sites were found to be nearly inactive and monometallic Pd was an order of magnitude more active than the pure Pd_3Zn surface phase.[50] Such a fraction-dependent activity aligns with our findings for butadiene hydrogenation over PdCu/C catalysts (Figure 4.5B), where increasing activity with higher Pd-fraction is ascribed to a larger Pd ensemble size ($CN_{Pd\text{-}Pd}$, Table 4.3).

The electron density transfer from Cu to Pd, as observed by XANES in Figure 4.9A, may have induced a weaker interaction of $Pd^{\delta-}$ with hydrocarbons and hydrogen, resulting in lower activity. This electronic effect is supported by density functional theory (DFT) calculations: a decrease in the adsorption energy of butadiene was observed from Pd to PdCu to Cu with values of -1.6 eV for Pd(111), -1.2 eV for PdCu(111)[51] and -0.34 eV for Cu(111)[28], where the latter showed the lowest catalytic activity (Figure 4.5). Similarly, dilute Pd in $Pd_{0.18}Cu_{15}/Al_2O_3$ alloy catalyst was reported to be less active than the monometallic $Pd_{0.18}/Al_2O_3$ reference for the hydrogenation of styrene.[8] Lastly, the lower activity of PdCu could be ascribed to a more rate limiting hydrogen activation, as on isolated Pd surface sites, the dissociation of molecular hydrogen and the H-spillover to the adsorbed hydrocarbon site are slower than on pure Pd.[15]

The high selectivity of the catalysts can be explained by the large difference in the adsorption energy of butene or propylene (-0.82 and -0.75 eV, respectively)[14] and butadiene (between -1.6 and -1.7 eV)[49,51], as calculated for Pd(111). Therefore, the strongly binding butadiene effectively blocks propylene from adsorbing onto the surface, resulting in high butene selectivities (Figure 4.7A). Similarly, butadiene replaces the butene products as soon as they are formed, decreasing the butene residence time on the Pd surface, resulting in little over-hydrogenation to butane (Figure 4.7B). Only at very low butadiene concentrations, close to complete conversion (Figure 4.6A), or due to the occurrence of internal mass transfer limitations[52]

(Figure 4.6B), a significant number of alkenes start to be hydrogenated associated with lower selectivity.

The butene isomer distribution (Figure 4.7B) formed over Pd and PdCu showed a high selectivity to 1-butene (*ca.* 60%), different from the thermodynamic equilibrium where 2-butenes are favoured.[53] Kinetically, 1-butene is formed by sequential 1,2-addition of two hydrogen atoms to one of the terminal C=C bonds of adsorbed butadiene. Formation of 2-butenes can be direct by 1,4-addition or by skeletal rearrangement of (re)adsorbed 1-butene species and showed a *trans:cis* ratio of ~10 over Pd. From DFT, 1-butene is predicted as the most stable butene-isomer on Pd(111) (adsorption energy of -0.90 eV, compared to between -0.72 and -0.77 eV for trans- and cis-2-butene), resulting in the high selectivity to 1-butene.[49] The Cu-catalysed isomer distribution is substantially different: 73% of 1-butene is formed, and the remaining 2-butenes have a *trans:cis* ratio close to the thermodynamic ratio of 1.7.[53] The high 1-butene selectivity over Cu cannot be fully explained by the stability of the intermediates, since similar adsorption energies are found for 1-butene, trans-2-butene and cis-2-butene (-0.12, -0.08 and -0.11 eV).[28] However, the higher reaction order in hydrogen (+1.7, Figure S4.1) showed a strongly H-limited reaction step in the butadiene hydrogenation over Cu, indicating that less isomerisation will occur.[15] Together with facile desorption associated with the low butene adsorption energy on Cu, this explains the high 1-butene selectivity

4.5 Conclusions

The influence of the Pd-to-Cu ratio was investigated for Cu-rich catalysts in the selective hydrogenation of butadiene. The Pd mass- and surface-normalised activity in bimetallic PdCu catalysts was lower than that of monometallic Pd but gradually increased with Pd content. *Operando* X-ray absorption spectroscopy shows a slight preferential clustering of the Pd in the bimetallic nanoparticles, as well as electron density transfer from Cu to Pd. These changes in the active site in terms of the Pd ensemble site and its electronic properties, and hence adsorption energies, explain why the behaviour is very different from that of pure Pd. The Pd-containing catalysts showed similar isomer and high butene selectivities up to near-complete butadiene conversion. Monometallic Cu and Cu-rich (Cu:Pd≥85) catalysts showed slightly superior butene selectivity at high conversions, albeit at much lower activities. This chapter highlights the importance of tuning the Pd-concentration in Cu-rich bimetallic catalysts to combine favourable activities with high selectivities while minimising the Pd content.

4.6 Acknowledgements

We acknowledge SOLEIL for provision of synchrotron radiation facilities, and we would like to thank Anthony Beauvois and Valérie Briois for assistance in using the ROCK beamline (proposal ID 20221222). The work at ROCK was supported by a public grant overseen by the French National Research Agency (ANR) as part of the "Investissements d'Avenir" program (ANR-10-EQPX-45). We thank Kristiaan Helfferich for the assistance in the preparation and execution of the experiments at ROCK.

4.7 References

1. Totarella, G. *et al.* Supported Cu Nanoparticles as Selective and Stable Catalysts for the Gas Phase Hydrogenation of 1,3-Butadiene in Alkene-Rich Feeds. *J. Phys. Chem. C* **125**, 366-375 (2021).
2. Totarella, G., de Rijk, J. W., Delannoy, L. & de Jongh, P. E. Particle size Effects in the Selective Hydrogenation of Alkadienes over Supported Cu Nanoparticles. *ChemCatChem* **14**, e202200348 (2022).
3. Beerthuis, R., Sunley, John, G., De Jong, K. & De Jongh, P. Selective Hydrogenation of Polyunsaturates. WO2019/233961 (2019).
4. Masoud, N. *et al.* Silica-Supported Au-Ag Catalysts for the Selective Hydrogenation of Butadiene. *ChemCatChem* **9**, 2418-2425 (2017).
5. Masoud, N. *et al.* Superior Stability of Au/SiO_2 Compared to Au/TiO_2 Catalysts for the Selective Hydrogenation of Butadiene. *ACS Catal.* **7**, 5594-5603 (2017).
6. Hugon, A., Delannoy, L. & Louis, C. Supported gold catalysts for selective hydrogenation of 1,3-butadiene in the presence of an excess of alkenes. *Gold Bull.* **41**, 127-138 (2008).
7. Kyriakou, G. *et al.* Isolated Metal Atom Geometries as a Strategy for Selective Heterogeneous Hydrogenations. *Science* **335**, 1209-1212 (2012).
8. Boucher, M. B. *et al.* Single atom alloy surface analogs in $Pd_{0.18}Cu_{15}$ nanoparticles for selective hydrogenation reactions. *Phys. Chem. Chem. Phys.* **15**, 12187-12196 (2013).
9. McCue, A. J., McRitchie, C. J., Shepherd, A. M. & Anderson, J. A. Cu/Al_2O_3 catalysts modified with Pd for selective acetylene hydrogenation. *J. Catal.* **319**, 127-135 (2014).
10. Pei, G. X. *et al.* Ag Alloyed Pd Single-Atom Catalysts for Efficient Selective Hydrogenation of Acetylene to Ethylene in Excess Ethylene. *ACS Catal.* **5**, 3717-3725 (2015).
11. Aich, P. *et al.* Single-Atom Alloy Pd-Ag Catalyst for Selective Hydrogenation of Acrolein. *J. Phys. Chem. C* **119**, 18140-18148 (2015).
12. Hugon, A., Delannoy, L., Krafft, J. M. & Louis, C. Selective hydrogenation of 1,3-butadiene in the presence of an excess of alkenes over supported bimetallic gold-palladium catalysts. *J. Phys. Chem. C* **114**, 10823-10835 (2010).
13. Luneau, M. *et al.* Achieving High Selectivity for Alkyne Hydrogenation at High Conversions with Compositionally Optimized PdAu Nanoparticle Catalysts in Raspberry Colloid-Templated SiO_2. *ACS Catal.* **10**, 441-450 (2020).
14. van der Hoeven, J. E. S. *et al.* Unlocking synergy in bimetallic catalysts by core-shell design. *Nat. Mater.* **20**, 1216-1220 (2021).
15. van der Hoeven, J. E. S. *et al.* Unraveling 1-Hexene Hydrogenation over Dilute Pd-in-Au Alloys. *J. Phys. Chem. C* **126**, 15710-15723 (2022).
16. Foucher, A. C. *et al.* Influence of Pd Concentration in Au-Pd Nanoparticles for the Hydrogenation of Alkynes. *ACS Appl. Nano Mater.* **6**, 22927-22938 (2023).
17. Yan, Z. *et al.* Theoretical study the catalytic performance and mechanism of novel designed single atom catalysts $M_1/2DMs$ for 1,3-butadiene hydrogenation. *Appl. Surf. Sci.* **617**, 156585 (2023).
18. Jiang, L. *et al.* Facet engineering accelerates spillover hydrogenation on highly diluted metal nanocatalysts. *Nat. Nanotechnol.* **15**, (2020).
19. Lv, C. Q., Liu, J. H., Guo, Y. & Wang, G. C. Selective hydrogenation of 1,3-butadiene over single $Pt_1/Cu(1\ 1\ 1)$ model catalysts: A DFT study. *Appl. Surf. Sci.* **466**, 946-955 (2019).
20. Liu, J. *et al.* Integrated Catalysis-Surface Science-Theory Approach to Understand Selectivity in the Hydrogenation of 1-Hexyne to 1-Hexene on PdAu Single-Atom Alloy Catalysts. *ACS Catal.* **9**, 8757-8765 (2019).
21. Pei, G. X. *et al.* Performance of Cu-Alloyed Pd Single-Atom Catalyst for Semihydrogenation of Acetylene under Simulated Front-End Conditions. *ACS Catal.* **7**, 1491-1500 (2017).
22. Tierney, H. L., Baber, A. E., Kitchin, J. R. & Sykes, E. C. H. Hydrogen dissociation and spillover on individual isolated palladium atoms. *Phys. Rev. Lett.* **103**, 246102 (2009).
23. Van Der Hoeven, J. E. S. *et al.* Entropic Control of HD Exchange Rates over Dilute Pd-in-Au

Alloy Nanoparticle Catalysts. *ACS Catal.* **11**, 6971-6981 (2021).
24. Darby, M. T., Stamatakis, M., Michaelides, A. & Sykes, E. C. H. Lonely Atoms with Special Gifts: Breaking Linear Scaling Relationships in Heterogeneous Catalysis with Single-Atom Alloys. *J. Phys. Chem. Lett.* **9**, 5636-5646 (2018).
25. Lucci, F. R. *et al.* Controlling Hydrogen Activation, Spillover, and Desorption with Pd-Au Single-Atom Alloys. *J. Phys. Chem. Lett.* **7**, 480-485 (2016).
26. Ngan, H. T. *et al.* Hydrogen Dissociation Controls 1-Hexyne Selective Hydrogenation on Dilute Pd-in-Au Catalysts. *ACS Catal.* **12**, 13321-13333 (2022).
27. Marcella, N. *et al.* Decoding reactive structures in dilute alloy catalysts. *Nat. Commun.* **13**, 832 (2022).
28. Yang, K. & Yang, B. Identification of the Active and Selective Sites over a Single Pt Atom-Alloyed Cu Catalyst for the Hydrogenation of 1,3-Butadiene: A Combined DFT and Microkinetic Modeling Study. *J. Phys. Chem. C* **122**, 10883-10891 (2018).
29. Studt, F. *et al.* Identification of Non-Precious Metal Alloy Catalysts for Selective Hydrogenation of Acetylene. *Science* **320**, 1320-1322 (2008).
30. Pei, G. X., Liu, X. Y., Chai, M. Q., Wang, A. & Zhang, T. Isolation of Pd atoms by Cu for semi-hydrogenation of acetylene: Effects of Cu loading. *Chinese J. Catal.* **38**, 1540-1548 (2017).
31. Furlong, B. K., Hightower, J. W., Chan, T. Y. L., Sarkany, A. & Guczi, L. 1,3-Butadiene selective hydrogenation over Pd/alumina and CuPd/alumina catalysts. *Appl. Catal. A Gen.* **117**, 41-51 (1994).
32. McCue, A. J., Gibson, A. & Anderson, J. A. Palladium assisted copper/alumina catalysts for the selective hydrogenation of propyne, propadiene and propene mixed feeds. *Chem. Eng. J.* **285**, 384-391 (2016).
33. Yuan, D., Cai, L., Xie, T., Liao, H. & Hu, W. Selective hydrogenation of acetylene on Cu-Pd intermetallic compounds and Pd atoms substituted Cu(111) surfaces. *Phys. Chem. Chem. Phys* **23**, 8653-8660 (2021).
34. Gao, Q. *et al.* Atomic Layers of B2 CuPd on Cu Nanocubes as Catalysts for Selective Hydrogenation. *J. Am. Chem. Soc.* **145**, 19961-19968 (2023).
35. Fedorov, P. P., Shubin, Y. V. & Chernova, E. V. Copper-Palladium Phase Diagram. *Russ. J. Inorg. Chem.* **66**, 891-893 (2021).
36. Hung, L.-I., Tsung, C.-K., Huang, W. & Yang, P. Room-Temperature Formation of Hollow Cu_2O Nanoparticles. *Adv. Mater.* **22**, 1910-1914 (2010).
37. Manthiram, K., Beberwyck, B. J. & Alivisatos, A. P. Enhanced Electrochemical Methanation of Carbon Dioxide with a Dispersible Nanoscale Copper Catalyst. *J. Am. Chem. Soc.* **136**, 13319-13325 (2014).
38. Visser, N. L. *et al.* Influence of carbon support surface modification on the performance of nickel catalysts in carbon dioxide hydrogenation. *Catal. Today* **418**, 114071 (2023).
39. Brandt Corstius, O. E., van der Hoeven, J. E. S., Sunley, G. J. & de Jongh, P. E. Influence of particle size in Pd-catalysed selective hydrogenation of 1,3-butadiene. *J. Catal.* **427**, 115103 (2023).
40. Scherrer, P. Bestimmung der inneren Struktur und der Größe von Kolloidteilchen mittels Röntgenstrahlen. in *Kolloidchemie Ein Lehrbuch* 387-409 (Springer Berlin, 1912). doi:10.1007/978-3-662-33915-2_7.
41. La Fontaine, C., Belin, S., Barthe, L., Roudenko, O. & Briois, V. ROCK: A Beamline Tailored for Catalysis and Energy-Related Materials from ms Time Resolution to µm Spatial Resolution. *Synchrotron Radiat. News* **33**, 20-25 (2020).
42. Ravel, B. & Newville, M. ATHENA, ARTEMIS, HEPHAESTUS: Data analysis for X-ray absorption spectroscopy using IFEFFIT. in *Journal of Synchrotron Radiation* vol. 12 (2005).
43. Huck, P., Jain, A., Gunter, D., Winston, D. & Persson, K. A Community Contribution Framework for Sharing Materials Data with Materials Project. in *2015 IEEE 11th International Conference on e-Science* 535-541 (IEEE, 2015). doi:10.1109/ eScience.2015.75.

44. SpectraBase®. https://spectrabase.com/spectrum.
45. Bond, G. C., Webb, G., Wells, P. B. & Winterbottom, J. M. The hydrogenation of alkadienes. Part I. The hydrogenation of buta-1,3-diene catalysed by the Noble Group VIII metals. *J. Chem. Soc.* 3218 (1965) doi:10.1039/jr9650003218.
46. Bates, A. J., Leszczynski, Z. K., Phillipson, J. J., Wells, P. B. & Wilson, G. R. The hydrogenation of akladienes. Part IV. The reaction of buta-1,3-diene with deuterium catalysed by rhodium, palladium, and platinum. *J. Chem. Soc. A Inorganic, Phys. Theor.* 2435 (1970) doi:10.1039/j19700002435.
47. Jentys, A. Estimation of mean size and shape of small metal particles by EXAFS. *Phys. Chem. Chem. Phys.* **1**, 4059-4063 (1999).
48. Bergeret, G. & Gallezot, P. Characterization of Solid Catalysts: Sections 3.1.1-3.1.3. in *Handbook of Heterogeneous Catalysis* vols 1-5 427-582 (Wiley-VCH Verlag GmbH, 2008).
49. Valcárcel, A., Clotet, A., Ricart, J. M., Delbecq, F. & Sautet, P. Comparative DFT study of the adsorption of 1,3-butadiene, 1-butene and 2-cis/trans-butenes on the Pt(111) and Pd(111) surfaces. *Surf. Sci.* **549**, 121-133 (2004).
50. Dasgupta, A. *et al.* Atomic control of active-site ensembles in ordered alloys to enhance hydrogenation selectivity. *Nat. Chem.* **14**, 523-529 (2022).
51. Huang, Y. & Chen, Z. X. Alloying effect on the C-C coupling reactions in acetylene hydrogenation by palladium-coinage metal alloys, a DFT study and microkinetic modeling. *Appl. Surf. Sci.* **575**, 151513 (2022).
52. Brandt Corstius, O. E. *et al.* Mass transport effects in gas-phase selective hydrogenation of 1,3-butadiene over supported Pd. *React. Chem. Eng.* 10, (2024). doi:10.1039/d4re00039k.
53. Maccoll, A. & Ross, R. A. The Hydrogen Bromide Catalyzed Isomerization of n-Butenes. I. Equilibrium Values. *J. Am. Chem. Soc.* **87**, 1169-1170 (1965).

4

4.8 Supplementary information

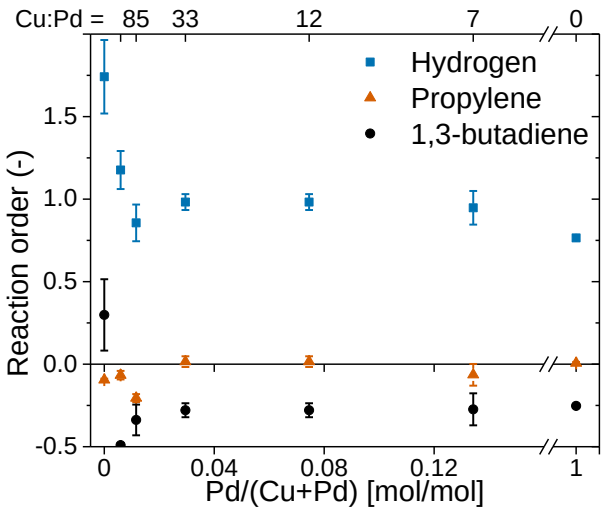

Figure S4.1. Reaction orders. Determined at steady state butadiene conversion (10-20%). Orders are calculated from a linear fit of log(activity) *vs* log(p/p^0) plots, varying the partial pressure of the reactants hydrogen (blue squares), propylene (orange triangles) or butadiene (black circles) one at a time, counteracted by He as balance. Experimental details are provided in Figure 2.4A.

Chapter 5

Dopant effects

This chapter is based on: Studying the promotional effects of different metals on Pd catalysts for the selective hydrogenation of 1,3-butadiene, MSc thesis by S.M.J. Wilms (2023).

Abstract

To retain high selectivities in hydrogenation reactions, Pd is often alloyed with less active, more selective metals such as Cu, Ag or Au. However, these metals are typically in large excess compared to Pd, resulting in the superimposed effects of electronic and geometric contributions. In this chapter, we investigate Pd catalysts to which only 10 mol% of dopants (K, Mn, Cu, Zn, Ag) were added. During the selective hydrogenation of butadiene, an increased activity was found for K-Pd/C, whereas Zn- and Ag-addition strongly decreased the activity, ascribed to a shift in the d-band centre. The butene selectivity was highest for undoped Pd/C. Interestingly, the C_4-distribution showed a higher 1-butene fraction for Cu-, Zn- and Ag-doped catalysts. 1-Butene isomerisation tests demonstrated that these three catalysts had a lower activity for 1-butene hydrogenation and isomerisation. Altogether, this chapter shows how the addition of a minority additive impacts the performance of Pd/C catalyst for selective (di)olefin hydrogenation and thereby contributes to the understanding of Pd-based catalysts as effective hydrogenation or isomerisation catalysts.

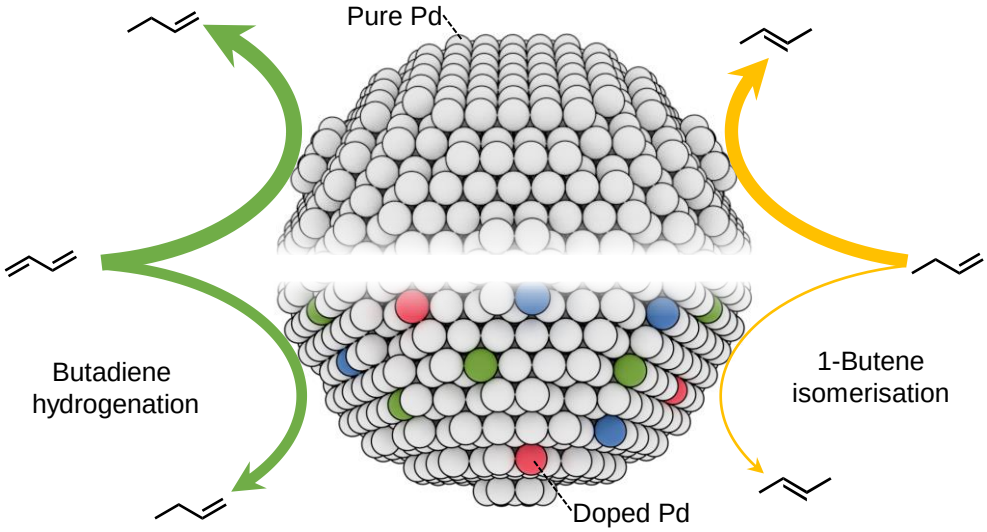

5.1 Introduction

Building on the Chapters 2, 3 and 4, we have gained understanding on how activity and selectivity of Pd-based catalysts are connected, and investigated how addition of a secondary metal such as Cu influences performance. Next to PdCu[1–4], bimetallic Pd-alloys such as PdNi[5–8], PdZn[9–12], PdAg[13–17], and PdAu[18–23] have been investigated for the selective hydrogenation of alkadienes and alkynes. The selectivity of these catalysts towards semi-hydrogenation products is typically enhanced by alloying the Pd with a second metal. However, compared to the monometallic Pd reference catalysts, the activity is often lower.[1,5,9,13,18] The difference in catalytic performance of the bimetallic catalysts is ascribed to electronic effects[24,25], geometric effects[9,20,26] or a combination of the two[1,2].

The addition of the second metal induces an electron density transfer to or from the Pd, which alters the interaction of the Pd surface atoms with the reactants, intermediates and products and thereby changes the yield of products of the reaction. Studt *et al.* indicated important descriptors for selectivity and activity for acetylene hydrogenation by density functional theory (DFT) calculations. Mixing of Pd with Ag shifted the d-band centre down with respect to the Fermi level, which weakened the ethylene adsorption (higher selectivity) but also reduced the activity by lowered acetylene adsorption strength, compared to monometallic Pd.[24] For butadiene hydrogenation over various metals, an electronic effect is described by Wells *et al.*, where the 1-butene selectivity increases with increasing Pauling electronegativity.[27] The more filled d-band led to more 1,2-addition compared to 1,4-addition, due to progressive destabilisation of the π-allyl intermediate (C-I and C-II in Figure 1.6), which increased the 1-butene yield.

Geometric effects related to the Pd ensemble size also influence the catalytic performance. By reducing the ensemble size of Pd down to the single-atom limit in what is sometimes called single-atom catalysts, which contain at the surface Pd atoms entirely surrounded by other non-Pd metal atoms, the binding modes with the reactant inevitably change.[23,26,28,29] For example, on these catalysts, butadiene is coordinated with one C=C bond to the Pd atom, whereas on extended Pd surfaces, the most stable configuration is coordinated to four different atoms with both C=C bonds flat the surface.[26,29] Moreover, remarkably different catalytic behaviour has been observed over dilute Pd-in-Au catalysts for monomers, dimers and trimers (Pd_1Au, Pd_2Au and Pd_3Au, respectively) in the activation of hydrogen[30,31] and the interaction with alkynes[20]. The effect of ensemble size was also demonstrated for PdZn systems by Dasgupta *et al.,* who prepared catalyst surfaces with well-defined PdZn monomers, trimers and a mixture of both. They showed that the Pd_3Zn sites dominated the activity of the surface, whereas Pd_1Zn sites were found almost inactive for selective hydrogenation.[9] Strikingly, Pd_3Zn still showed an order of magnitude lower activity than monometallic Pd.

In all the abovementioned studies, the focus has been on systems where Pd is the minority metal (*i.e.,* Pd<<M), often in the single-atom limit.[32,33] Hence, in addition to electronic effects (charge transfer between two metals), there are large contributions

Table 5.1 Dopant effects on Pd-catalysed hydrogenation of acetylene and relevant properties for mixing and electronic interactions.

Dopant	K	Mn	Cu	Zn	Ag
Activity to acetylene	+	+	-	-	-
Selectivity to ethylene	+	+	+	+	+
Fraction miscible with in Pd fcc	n.a.	0-12%	0-25%	0-18%	0-100%
Expected species during reaction	oxide	oxide	metallic	oxide/metal	metallic
Pauling EN metal (Pd=2.20)[49]	0.82	1.55	1.90	1.65	1.93
References	40,48	43,47	3,45	39,46	14,44

from geometric effects associated with Pd ensemble size. Furthermore, advanced characterisation is necessary to establish whether the surface composition is the same as the overall composition, as interaction with gases might selectively draw metals to the surface. This complicates establishing a clear structure-performance relationship induced by the second metal or additive. Moreover, the reported selectivity enhancements are often concomitant with a significant decrease in activity (and vice versa), which makes it difficult to disentangle the improved selectivity from the reduced activity in these bimetallic Pd-catalysts. Therefore, a systematic study that disentangles electronic from geometric effects in selective hydrogenation reactions over Pd-catalysts is missing. In this Chapter, we focus on the effects of adding various metals or metal oxides on the performance of Pd-catalysts in low (10 mol%) dopant concentration to investigate electronic effects while minimising the Pd ensemble size.

Literature proposes a number of candidates as additives for Pd-based catalysts for selective hydrogenation.[34–38] In this paragraph, a few of these candidates are highlighted; an overview of the discussed dopants is provided in Table 5.1. Limited reports for butadiene hydrogenation were found, hence we describe the dopant effects in acetylene hydrogenation and comment on the general trends we expect for butadiene as a reactant. In addition to PdAg[14] (as discussed before), PdZn[39] and PdCu[3] are reported to lead to a higher ethylene selectivity, with lower acetylene conversion, compared to Pd. The influence of the additive on the catalysis was ascribed to an electron density transfer to Pd, resulting in further filling of the d-orbital and a weaker interaction with the hydrocarbons. Similar electronic effects were ascribed in K-doped Pd/Al_2O_3 catalysts.[40] Regarding activity, higher conversions were found over the catalysts doped with elements at the left side of the period table, which was ascribed to faster desorption of ethylene. In contrast, the addition of coinage metals led to lower activities. Recently, Mn was identified as an interesting promoter for several Cu-catalysed hydrogenation reactions, such as methanol synthesis and ester hydrogenation.[41,42] For acetylene hydrogenation, there is one report where $Mn\text{-}Pd/Al_2O_3$ showed higher conversion and selectivity than Pd/Al_2O_3.[43] Although a complete explanation for the effect of Mn-addition remained unclear, it presents an intriguing promoter to study. Since the discussed trends are ascribed to the interaction

strength of Pd with acetylene or ethylene, similar trends might be expected for butadiene and butene reactants.

Interaction and/or miscibility between the dopant and Pd is of importance. Ag and Pd are fully miscible over the entire alloy fraction, independent of temperature.[44] For Cu-[45], Zn-[46] and Mn-addition[47], multiple discrete phases can be formed, depending on the M:Pd stoichiometry. At 90 at% Pd, however, all these systems are predicted to obtain a Pd fcc phase, where the dopant is substituted in the host lattice. For Pd-K, mixed phases are observed only above 5×10^3 bar and are not expected to form under ambient conditions.[48] However, these phase diagrams assumed that only metallic compounds are present. Under ambient conditions, especially K and Mn, as well as Zn, will form oxides. For Cu and Ag, the more noble metals, a metallic dopant species is expected under relevant synthesis and reaction conditions, which mixes with the metallic Pd. When mixed, the Pd and metallic dopant have an electronic interaction, which depends on their relative electronegativity (EN). The Pauling EN decreases from right to left in the periodic table as: Pd (2.20) > Ag (1.93) ~ Cu (1.90) > Zn (1.65) > Mn (1.55) > K (0.82).[49] However, as mentioned before, the more electropositive elements such as K, Mn and Zn can be present in their oxidic form, and this EN value is not accurate. The values of the metallic elements values indicate that the species are less electronegative than Pd. Therefore, electron transfer is expected to Pd, increasing its d-orbital filling.

In this chapter, we focus on the effects of several metals, with electronic properties varying from s-metals to transition metals on the right of the d-metal block, on the Pd-catalysed selective hydrogenation of butadiene while excluding geometric effects by keeping a low dopant-to-Pd ratio (M:Pd=0.1). We show that the addition of minority K, Mn, Cu, Zn or Ag to Pd/C nanoparticle catalysts strongly affected the catalytic performance of the selective semi-hydrogenation of butadiene traces from an excess of propylene. Through 1-butene isomerisation tests, we provide additional mechanistic insight into the observed selectivity trends among the promoted Pd catalysts.

5.2 Experimental details

5.2.1 Preparation of the Pd/C catalyst

Carbon-supported Pd catalysts were prepared by incipient wetness impregnation (IWI) methods (see Chapter 2). The samples were reduced at either 500 or 600 °C (0.5-1.0 °C/min) for 2 hours. The lower reduction temperature resulted in the growth of smaller Pd nanoparticles of *ca.* 5 nm, denoted as Pd_s/C throughout this chapter, whereas the larger nanoparticles (*ca.* 9 nm) are denoted as Pd/C.

Table 5.2. Catalysts synthesis parameters.

Sample	Support	Pd wt%[a]	M wt%[a]	M:Pd (molar)	T_{heat} (°C)	T_{red} (°C)
Pd_S /C	GNP	1.88	-	-	250	500
Pd/oxC	oxGNP	2.54	-	-	250	500
Pd/C	GNP	2.53	-	-	250	600
K-Pd/C	Pd/C	2.53	0.10	0.11	-	-
Mn-Pd/C	Pd_S/C	1.88	0.12	0.12	250	560
Cu-Pd/C	Pd/C	2.53	0.17	0.11	500	450
Zn-Pd/C	Pd_S/C	1.88	0.14	0.12	350	600
Ag-Pd/C	Pd/oxC	2.54	0.28	0.11	400	590

[a] Based on the precursor amount added in incipient wetness impregnation.

5.2.2 Synthesis of M-Pd/C catalysts

For the doping of Pd/C catalysts the following precursors were used: KNO_3 (ACS reagent, ≥99.0%), $Mn(NO_3)_2{\cdot}4H_2O$ (analysis grade, Acros Organics), $Cu(NO_3)_2{\cdot}3H_2O$ (99%, Acros Organics), $Zn(NO_3)_2{\cdot}6H_2O$ (98% reagent grade, Sigma Aldrich), $AgNO_3$ (Laboratory reagent grade, Fisher Scientific).

The doped M-Pd/C materials were prepared by sequential impregnation on the reduced Pd/C or Pd_s/C catalysts. Notably, similar surface areas (BET, m^2/g_{carbon}) and pore volumes (single point at p/p^0=0.995, cm^3/g_{carbon} at STP) were found by physisorption for the untreated carbon support (522 m^2/g, 0.756 cm^3/g), and the Pd/C (511 m^2/g, 0.684 cm^3/g) catalyst after drying, heat treatment and reduction. Similar to the IWI of Pd/C materials, the support was dried before the impregnation of the metal nitrate precursors. The concentration of metal nitrate precursors was chosen for the M:Pd to result in a 0.1 molar ratio. The impregnated solids were dried overnight under a dynamic vacuum and heat treated under nitrogen flow to 250-500 °C (T_{heat}, Table 5.2). Finally, the catalysts were reduced at 450-600 °C (T_{red}, Table 5.2) with 0.5-1.0 °C/min, 2 hours isothermal hold.

No additional heat treatments were performed for K-promoted Pd catalysts because the reported conditions for nitrate decomposition were too harsh (>700 °C)[50,51] and were expected to cause severe nanoparticle agglomeration and support gasification. For Ag-promoted catalyst, the carbon support was oxidised prior to Pd-impregnation by the method of Visser *et al.*[52] to prevent the Ag nanoparticles from growing too much.[53] Furthermore, all synthesis steps which involved handling of Ag-precursors were performed with glassware and reactors shielded from light. Lastly, references of K/C, Cu/C, Zn/C and Ag/C were prepared without Pd by following the same steps as M-Pd/C catalysts above, but with impregnation of the dopant directly onto the carbon support instead of onto Pd on carbon catalyst.

5.2.3 Characterisation

Bright-field TEM image acquisition and STEM-EDX elemental mapping of the as-synthesised M-Pd/C catalysts were performed as described in Chapter 4. Nanoparticle sizes were determined by manually measuring at least 200 nanoparticles at different regions of the sample and analysing the dataset with Eq. 2.1 and Eq 2.2. Pd crystallite sizes and lattice parameters are determined from XRD by Eq. 2.3 and Eq. 4.1.

Nitrogen physisorption was performed on the carbon support and as-synthesised Pd/C catalyst to determine the porosity properties of the materials. BET surface area and single point pore volume (at p/p^0=0.995) were determined on a Micromeritics TriStar II Plus. Prior to N_2-dosing, the samples were dried at 150 °C in N_2 for 10 minutes.

5.2.4 Catalytic testing

The catalytic performance was tested as described in Chapter 2. For each catalytic test, 2-3 mg of diluted catalyst was mixed with 0.3 g of SiC (212-400 μm), which resulted in a constant metal loading of 0.6-0.7 μg Pd in the reactor. Conversion and selectivity calculated by Eq. 2.4 to Eq. 2.7.

For the calculation of the metal TOF, Eq. 2.9 is used. Here, several assumptions were made based on the nanoparticle size, shape and composition. For all particles, we assumed a spherical shape and fcc structure consistent with our TEM results.[54] We assume homogeneous mixing of the Pd with the dopant within the nanoparticles, where the surface composition is the same as the bulk (M:Pd=0.1). Since the exact location of the dopant atoms is uncertain, we simplified the dispersion of the nanoparticle to be solely dependent on the atomic parameters of Pd (Eq. 2.9), and we did not consider the average atomic volume and area variations induced by the incorporation of the second metal. Overall, this will not change the dispersion significantly since the second metal is present in a 10 mol% concentration only.

5.3 Results and discussion

5.3.1 Synthesis of supported nanoparticles

The shape, size and distribution of the metal nanoparticles in the as-synthesised M-Pd/C catalysts were analysed by transmission electron microscopy (TEM, Figure 5.1). The micrograph of the monometallic Pd/C catalyst (reduced at 600 °C) in Figure 5.1A shows Pd nanoparticles on the carbon support with a volume-area mean diameter (d_{VA}) of 10.9 ± 3.1 nm (Figure 5.1D, Table 5.2), resulting in a metal dispersion of 10.3% (at% of Pd at the surface). For the doped Pd-catalysts, particle sizes close to the value of Pd/C were obtained. For example, in the synthesis of Zn-Pd/C (Figure 5.1K)

and Ag-Pd/C (Figure 5.1L), the particles grew to d_{VA} values of 8.6 and 9.8 nm, respectively, even though they were impregnated onto Pd/C catalyst with smaller nanoparticles (4.3 and 4.5 nm, Table 5.2). For Mn-Pd/C, reduced at 560 °C, slightly smaller nanoparticles were obtained (Figure 5.1F, d_{VA}=6.4 nm), in line with the expected size for monometallic Pd/C reduced at that temperature.[55]

The distribution of the dopant atoms within individual Pd nanoparticles was investigated by scanning TEM energy dispersive X-ray spectroscopy (STEM-EDX) mapping. Figure 5.2A depicts the spatial overlap of Zn- and Pd-species in the Zn-Pd/C catalyst. The linescan intensity over one individual supported particle (Figure 5.2B)

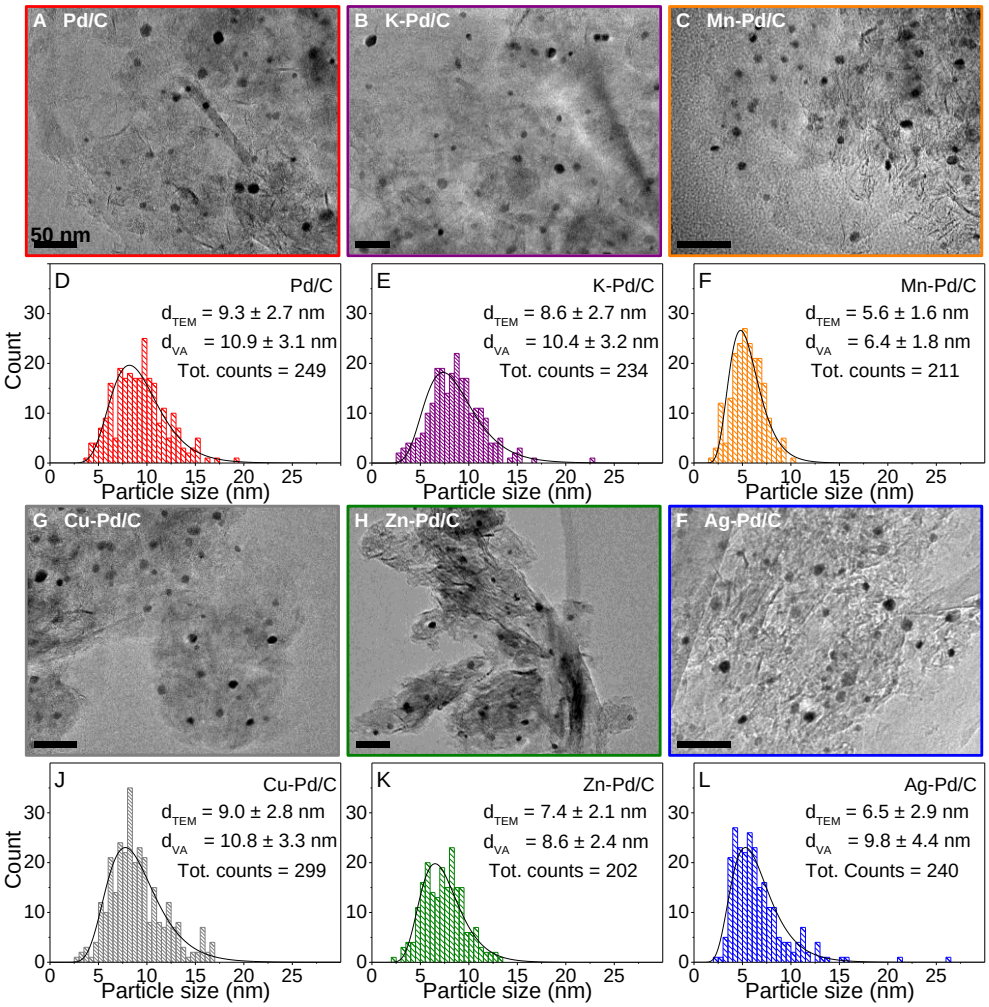

Figure 5.1. Electron microscopy of supported (doped) Pd nanoparticle catalysts. (A-C,G-F) Bright field TEM micrographs of as-synthesised doped and undoped Pd catalysts (50 nm scale bars). (D-F,J-L) The corresponding histograms of the particle diameters. Solid lines are a lognormal fit to the distributions.

Table 5.3. Catalysts characterisation overview.

Sample	d_{TEM} (nm)[a]	d_{VA} (nm)[b]	Dispersion[c]	d_{XRD} (nm)[d]	$d_{(111)}$ (Å)[e]	$\Delta d_{(111)}$ (Å)
Pd/C	9.3 ± 2.7	10.9 ± 3.1	10.3%	7.9 ± 0.1	2.275	-
K-Pd/C	8.6 ± 2.7	10.4 ± 3.2	10.7%	7.2 ± 0.1	2.279	0.004
Mn-Pd/C	5.6 ± 1.6	6.4 ± 1.8	17.3%	6.4 ± 0.1	2.272	-0.003
Cu-Pd/C	9.0 ± 2.8	10.8 ± 3.3	10.3%	7.7 ± 0.1	2.262	-0.013
Zn-Pd/C	7.4 ± 2.1	8.6 ± 2.4	13.0%	7.3 ± 0.1	2.264	-0.011
Ag-Pd/C	6.5 ± 2.9	9.8 ± 4.4	11.3%	6.8 ± 0.1	2.275	0.000

[a] Number-averaged diameter from TEM. [b] Mean volume-area diameter: $\sum_{i=1}^{N} d_i^3 / \sum_{i=1}^{N} d_i^2$. [c] Dispersion(%)=1.112/d_{VA}. [d] Average crystallite size from full-width at half maximum (FWHM) of Pd(111) peak in Figure 5.3B. FWHM obtained by Gaussian peak fit from 44.3 to 48.6° 2θ. [e] Derived from Eq. 4.1, where peak position is obtained from the Gaussian fit.

shows the uniform distribution of both metals. The emission spectrum (Figure 5.2C) shows no detectable Zn- or Pd-species on the carbon support. Quantification over the area of an individual nanoparticle resulted in a Zn:Pd atomic ratio of 0.14, in line with the synthesis precursor ratio of 0.12 (Table 5.2).

The M-Pd nanoparticles were further characterised by X-ray diffraction (XRD). The diffractograms of the (M-)Pd/C samples (Figure 5.3A) contain diffraction lines for crystalline graphitic carbon and Pd domains, as evidenced by the C(002) at 30.3°, overlapping C(100)/C(101) between 48.4° and 53.0° and (004) at 63.8° 2θ, as well as Pd(111) and Pd(200) at 46.4° and 54.0° 2θ, respectively. Pd was the only observed crystalline metal(oxide) phase, as no diffraction from oxidised PdO nor from any of the dopants (either metallic or oxidic) was detected. The Pd crystallite size was determined from the peak width of the carbon-subtracted diffractogram (Figure 5.3B) by the Scherrer equation (Eq. 2.3) on the Pd(111) diffraction peak at 46-47° 2θ. The (M-)Pd crystallite sizes varied between 6.4 and 7.9 ± 0.1 nm, in line with the results obtained from TEM analysis (Table 5.2). Interestingly, a peak shift was observed towards higher

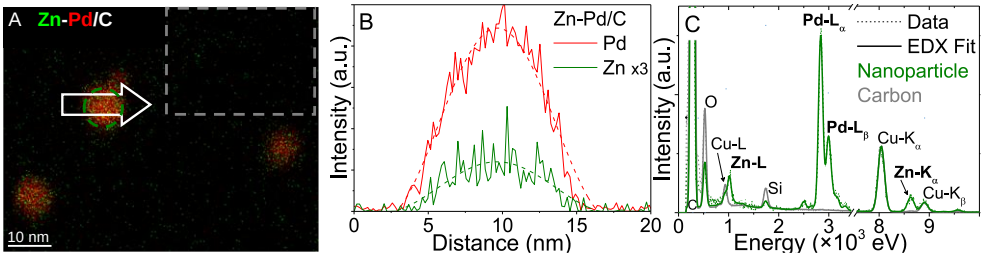

Figure 5.2. Elemental analysis of Zn-Pd/C catalysts. (A) STEM-EDX map for Zn- and Pd-species. (B) Linescan intensity for Zn-K and Pd-L emission over an individual nanoparticle as shown by the arrow in panel A. (C) EDX intensity for metal nanoparticle (green circle in panel A) and bare carbon support (grey square in panel A). Intensities in (C) were normalised to the Cu-K emission due to the Cu-mesh TEM grid.

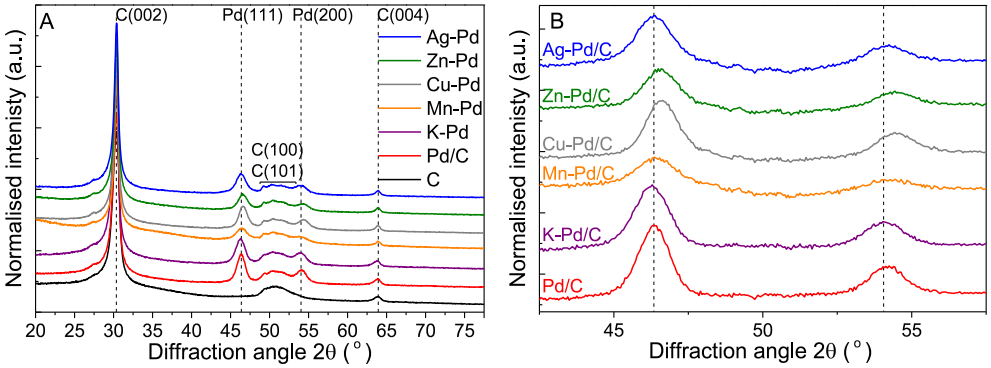

Figure 5.3. X-ray diffraction of M-Pd/C. (A) Diffractograms normalised to the C(002) diffraction peak at 30.3° 2θ of carbon support, Pd/C and M-Pd/C catalysts. (B) Carbon-subtracted intensity of (M-)Pd/C catalysts, indicating a slight shift in the Pd(111) and Pd(200) diffraction peaks.

diffraction angles for the Pd(111) and Pd(200) peaks in Zn- and Cu-Pd/C samples. This shift indicated that the average lattice distance decreased (Eq. 4.1). This can be explained by the incorporation of smaller transition metal atoms into the Pd-lattice, as expected based on the Cu-Pd and Zn-Pd phase diagram.[45,46] For Cu-Pd/C, an average Pd(111) lattice compression of 0.013 Å was derived from Figure 5.3B, which matches with the theoretical expected decrease of 0.015 Å based on Vegard's law, the molar ratios of Pd and Cu, and the metal radii of 137 and 128 pm for Pd and Cu, respectively. No significant shifts in lattice parameters were observed for Ag-Pd/C, Mn-Pd/C and K-Pd/C. For Mn-Pd/C and K-Pd/C, the limited change in lattice parameter is consistent with oxide formation, meaning that the second metal did not dissolve in the Pd host but was dispersed over the Pd/C catalyst.

5.3.2 Catalyst activity

The butadiene conversion as a function of temperature for M-Pd/C catalysts during heating is depicted in Figure 5.4A. Every catalytic test was performed with a similar amount (0.6-0.7 µg Pd) of Pd metal and butadiene conversions varied between 4.7% and 22% at 25 °C and increased with temperature to 95% conversion between 70 and 122 °C. Similar conversion levels were observed for the individual catalysts during the cooling of the reactor (Figure 5.4B), hence there was no indication of either activation or deactivation. The dopant reference catalysts without Pd showed negligible activity for butadiene or propylene hydrogenation (< 0.1% butadiene and < 0.0003% (~1 ppm) propylene at 100 °C). Therefore, the reported activity is ascribed to the (doped) Pd nanoparticles and not to the carbon support or isolated dopant metal sites.

The highest butadiene conversions at 25 °C (Figure 5.4A) were observed for K-Pd/C and Mn-Pd/C, with 22% and 21%, respectively, followed by 14% butadiene conversion for Pd/C and Cu-Pd/C, and 6.2% and 4.7% conversion for Ag-Pd/C and Zn-Pd/C, respectively. These results indicate that the initial activity of the doped catalysts is similar to or slightly higher than Pd/C for the K-, Mn- and Cu-doped materials. In contrast, a significant decrease in activity is observed by the Zn- and Ag-addition. At high conversion levels, Pd/C was the most active catalyst, surpassing the activity of Mn- and K-Pd/C. The surface-normalised activity (TOF, Figure 5.4C) showed a similar trend as the conversion (Figure 5.4A), with the most notable difference being that the activity of Mn-Pd/C is lower than that of the Pd/C catalyst. The high conversion of Mn-Pd/C is therefore explained by the smaller nanoparticles (Table 5.2, d_{VA}=6.4 nm) compared to Pd/C (11.9 nm), resulting in a higher active site density (m^2_{Pd}/g_{cat}) and higher reaction rate. The K-Pd/C catalyst was the only catalyst that was intrinsically more active than the monometallic Pd/C catalyst below 40 °C and showed a 60% higher TOF at 25 °C. Because no additional heat treatments were performed in the preparation of K-Pd/C,

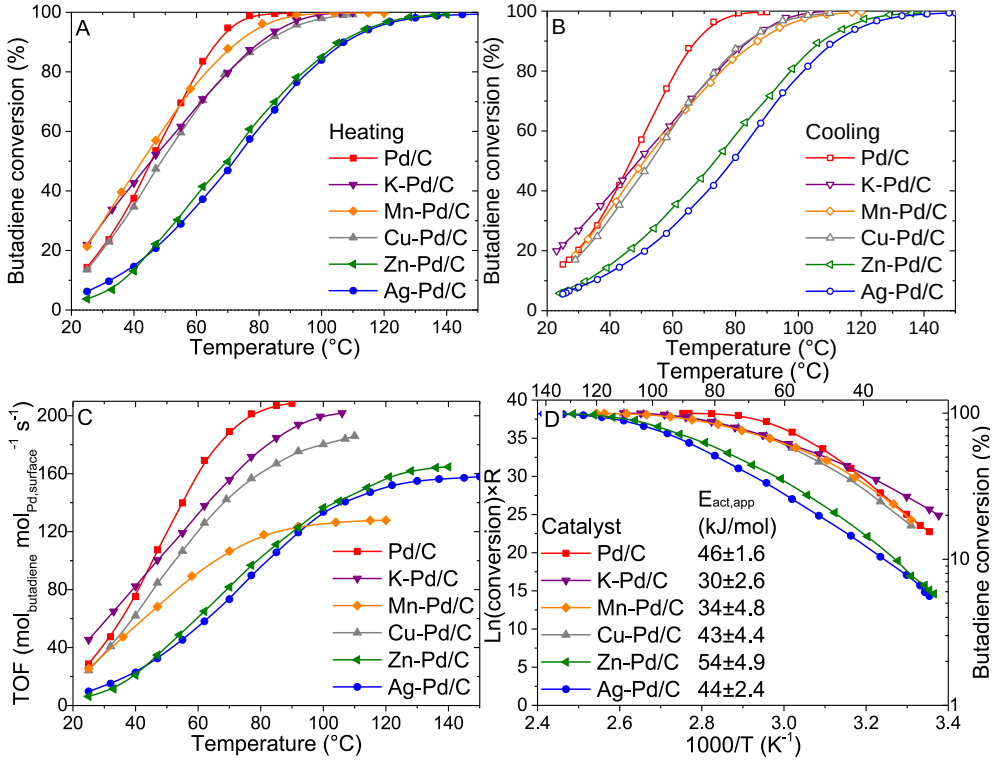

Figure 5.4. Catalytic activity. (A) Conversion of butadiene as a function of temperature for (M-)Pd/C catalysts during heating and (B) cooling of the reactor. (C) Calculated corresponding turnover frequencies (TOFs) for butadiene hydrogenation during heating. (D) Arrhenius plot of data in (C). Activation energies determined below 45 °C. Reaction conditions: 50 mL/min 0.3% butadiene, 30% propylene, 20% H_2, He balance, 1 atm, 0.5 °C/min ramp. All reactors contained 0.6-0.7 µg of Pd metal.

both K^+ and NO_3^- were dispersed over the Pd/C catalysts. The nitrate anion could have a strong electronic effect on Pd, which could explain the higher activity compared to Pd/C. Noteworthy, both Zn- and Ag-Pd/C showed a significantly lower TOF compared to Pd/C, by a factor of 4.0 and 2.6 at 25 °C for Zn and Ag, by the addition of only 10 mol% of the dopant.

The temperature-dependency of the activity showed an exponential increase for most catalysts at the lowest tested temperatures only, *e.g.,* below 45 °C. Between 25 and 45 °C, the maximum value for the apparent activation energy ($E_{act,app}$, Figure 5.4D) was found to be between 43 and 54 kJ/mol for Pd/C, Cu-Pd/C, Zn-Pd/C and Ag-Pd/C, in line with the values for Pd/C and PdCu/C catalysts in Chapter 4. For K-Pd/C and Mn-Pd/C, lower values were obtained; 30 and 34 kJ/mol, respectively. The lower values are a sign of mass transfer limitations induced by either a faster volumetric reaction rate or slower butadiene diffusion (see Chapter 3). For Mn-Pd/C, its smaller nanoparticle size resulted in a higher active site density and higher reaction rate. For K-Pd/C, with a similar nanoparticle size as Pd/C, a higher intrinsic activity was observed compared to Pd/C, as evidenced by the higher TOF in Figure 5.4C.

Summarising, our findings showed that at low conversion, K-Pd/C was slightly more active than Pd/C, while a significant decrease in activity was observed for the Ag- and Zn-containing catalysts. Similar results have been reported earlier for acetylene hydrogenation, where an increase in activity was found for K-promoted Pd/Al_2O_3[40], as well as a decrease by Ag- and Zn-addition[9,14]. Intriguingly, in literature for these dopants with opposite effects on the activity, a similar explanation was provided based on acetylene hydrogenation: electron transfer to Pd increased its electron density, which downshifted the d-band centre resulting in weaker interaction with the hydrocarbons. For the $K-Pd/Al_2O_3$ catalyst, the higher acetylene hydrogenation activity was ascribed to a weaker binding of ethylene, which favoured a facile desorption of the formed product.[40] Contrarily, for Zn- and Ag-Pd/C, a lower reactivity towards acetylene due to the downshifted d-band was provided as a reason for the reduced activity.[9,14] The improved activity of K-Pd/C might be in part explained by the residual NO_3^- anions on the catalyst. However, it is clear that more systematic and precise studies, involving spectroscopic and computational assessment of which dopant species are present under reaction conditions, and what their electronic influence is, are necessary to fully understand the observed effects.

5.3.3 Catalyst selectivity

The semi-hydrogenation selectivity to the butene isomers (sum of 1-butene, trans-2-butene and cis-2-butene) as a function of butadiene conversion is shown in Figure 5.5A. At low butadiene conversion levels (<35%), all catalysts exhibited a high selectivity of >90% towards the butene products (*i.e.,* <10% combined butane and propane formation). At higher conversion levels, the selectivity towards butene

isomers decreased, especially when approaching full butadiene conversion. The butene selectivity was highest for monometallic Pd/C and decreased upon addition of the dopants with Ag > Zn ~ Cu ~ Mn > K. Figure 5.5B depicts a detailed overview of the C_4-product distribution as a function of butadiene conversion for the different catalysts. For example, the selectivity towards the 1-butene isomer decreased as Ag > Zn > Cu > undoped Pd > Mn > K. Concomitant with the decreasing 1-butene trend, the formation of 2-butenes and n-butane increased as a result of 1-butene isomerisation to 2-butene and over-hydrogenation to n-butane. The trend in 1-butene selectivity is visualised in Figure 5.5C, which compares the 1-butene fraction of all catalysts at low (19-24%) and high (83-88%) butadiene conversion. At low conversions, a similar selectivity was obtained for all catalysts, between 55 and 60% 1-butene. At higher conversions, the difference in selectivity between the catalysts increased, as the Zn- and Ag-Pd/C showed a slight increase in selectivity, Pd/C and Cu-Pd/C showed a similar selectivity, and K-Pd/C and Mn-Pd/C exhibited a lower selectivity.

The selectivity to the sum of butenes as well as the 1-butene selectivity, decreased for K- and Mn-Pd/C catalysts at relatively low butadiene conversions (<50%). This low

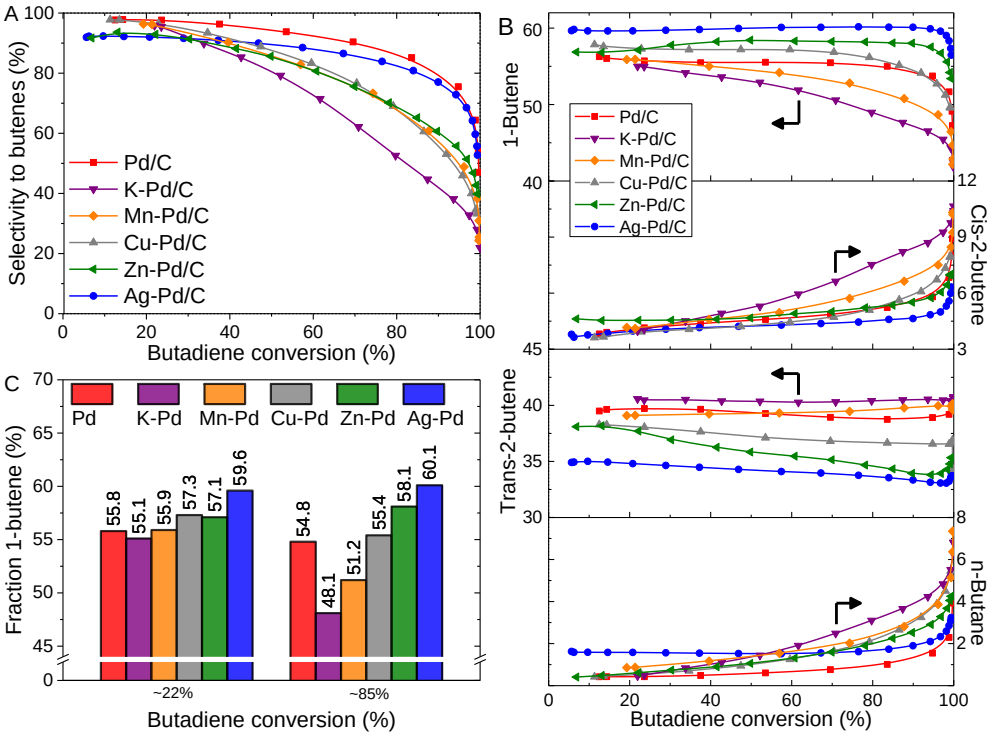

Figure 5.5. Butene selectivity for the unpromoted and promoted Pd nanoparticle catalysts. (A) Selectivity towards the butene isomers (1-butene, trans-2-butene and cis-2-butene) as a function of the butadiene conversion. (B) The distribution of C_4-products as a function of the butadiene conversion. (C) Fraction of 1-butene in the C_4-product stream at low conversion levels (19-24%) and high conversion levels (83-88%).

selectivity can be explained by internal diffusion limitations (Chapter 3), as were observed in section 5.3.2. On the contrary, over Zn-Pd/C and Ag-Pd/C, the 1-butene fraction slightly increased with increasing conversion and less isomerisation was observed compared to the monometallic Pd/C catalyst. Strikingly, all doped catalysts show more alkane formation than Pd/C, both in propane (Figure 5.5A) as well as butane (Figure 5.5B). Therefore, there is a clear difference in the product distribution of the doped and undoped catalysts. Over Pd/C, alkane formation is most suppressed and hence showed the highest butene selectivity. Over Zn-Pd/C and Ag-Pd/C, isomerisation was limited, and therefore the 1-butene yield was highest.

The dopant-induced change in performance might be explained by electronic effects, as a clear trend for the dopants and their position in the periodic table is observed. The lowest selectivity and highest activity was obtained by K-addition, whereas Zn- and Ag-Pd/C showed the lowest activity and high selectivity. These effects are likely electronic in nature, but cannot be fully explained solely by Pauling electronegativity (EN) (since $EN_{Cu} \sim EN_{Ag}$ and $< EN_{Pd}$ for all dopants) of the elements, and more extensive characterisation and systematic studies are required.

5.3.4 1-Butene isomerisation

The butadiene hydrogenation mechanism over doped and undoped Pd was further elucidated by isomerisation tests of 0.3% 1-butene in 5% hydrogen (helium balance). The 1-butene conversion (combined isomerisation and hydrogenation) for all catalysts is shown in Figure 5.6A. The TOF for 1-butene conversion is depicted in Figure 5.6B. The addition of K slightly increased the intrinsic activity, whereas addition of the coinage metals showed a decrease in activity in the order Cu > Zn > Ag. For Mn-Pd/C a near-identical intrinsic activity was found compared to Pd/C, calculated at 25 °C as roughly 15-16 $mol_{1\text{-butene}}\ mol_{Pd,surface}^{-1}\ s^{-1}$. Compared to the butadiene hydrogenation activity (Figure 5.4C), the TOF values for 1-butene conversion for all catalysts were between 1.4 to 7.5 times lower at 25 °C (Figure 5.6C). The ratio between the TOFs for hydrogenation of butadiene and of 1-butene follows the trend of Ag-Pd/C > Zn-Pd/C > Cu-Pd/C > undoped Pd/C > K-Pd/C ~ Mn-Pd/C. Here, K- and Mn-doped catalysts showed a $TOF_{butadiene}$:$TOF_{butenes}$ ratio near 1.0 at 60 °C, whereas for Ag-Pd/C, this was almost tenfold higher, strongly favouring activity for butadiene hydrogenation over 1-butene over the whole temperature range. Regarding the preferential hydrogenation of butadiene over 1-butene, the observed trend indicated that transition metal dopants with more higher 3d-orbital filling are more selective, and addition of Ag (4d-metal) yields the highest preferentiality. Further studies, including reaction order studies for the isomerisation would be interesting to elucidate the origin of the differences.

The C_4-distribution during 1-butene conversion is depicted in Figure 5.6D. At 30 °C low n-butane formation and isomerisation was found for all catalysts. At higher temperatures (80 °C), a trend in selectivity emerged. K- and Mn-doped catalysts

performed slightly worse than undoped Pd/C since more n-butane was formed with a similar amount of 2-butenes. The selectivity increased when Pd/C was doped with Cu, Zn or Ag, especially for the latter, which showed little n-butane formation and a very low amount of isomerisation products. The observed *trans:cis* ratio of 1.4-1.7 that is obtained with 1-butene isomerisation aligns with the thermodynamic butene equilibrium (see Figure 1.4B)[56,57], whereas for butadiene hydrogenation, a *trans:cis* ratio close to 10 was found. This significant difference points towards a different mechanism of 2-butene formation. During 1-butene isomerisation, formation of 2-butenes occurs by sequential H-addition, skeletal rearrangement and H-extraction, resulting in a *trans:cis* close to equilibrium.[18,57,58] In contrast, during butadiene hydrogenation, 2-butenes form through direct semi-hydrogenation of adsorbed butadiene in a high (~10) *trans:cis* ratio, characteristic for monometallic Pd catalysts.[59-61] Therefore, readsorption of 1-butene followed by isomerisation during butadiene hydrogenation (Figure 5.5C) is likely negligible, since that would have

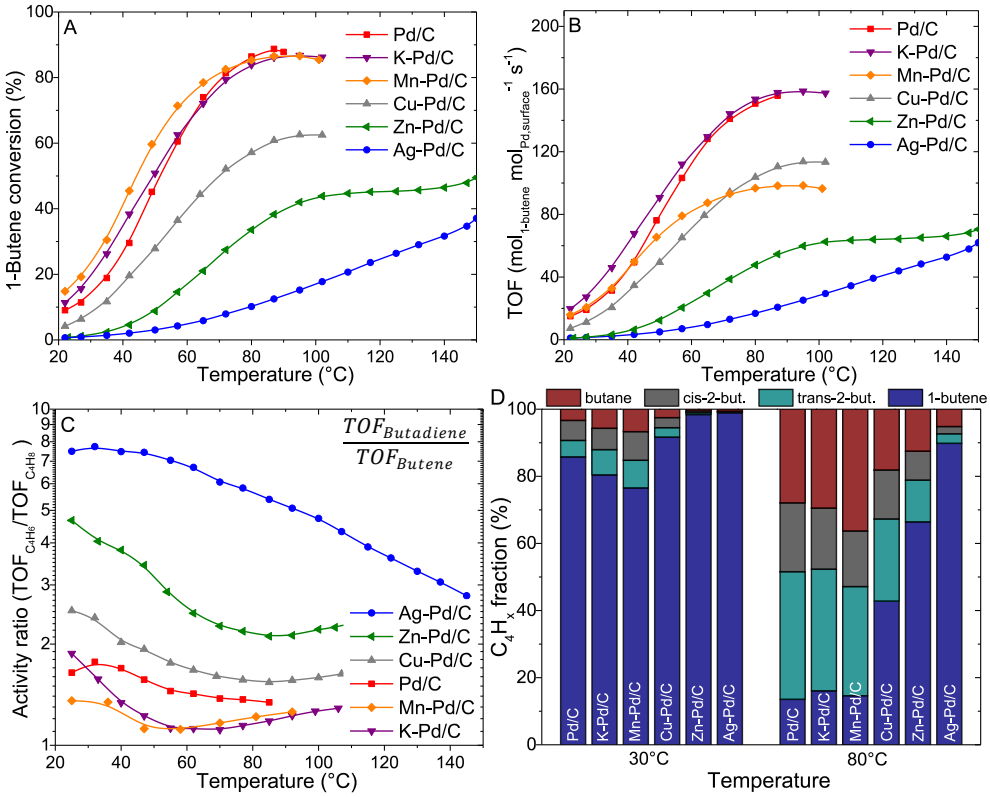

Figure 5.6. 1-Butene isomerisation. (A) Conversion of 1-butene over (M-)Pd/C catalyst as function of temperature. (B) TOF for 1-butene conversion. (C) Ratio between the TOFs of butadiene hydrogenation and 1-butene conversion as a function of temperature. (D) C_4-product distribution at low (30 °C) and high (80 °C) temperature during 1-butene conversion. Catalysts loading and temperature programs identical to the tests in Figure 5.4.

resulted in a *trans:cis* ratio closer to 1.7, as was observed during 1-butene hydrogenation (Figure 5.6D).

5.4 Conclusions

The effect of various additives (K, Mn, Cu, Zn, and Ag-based) on the performance of Pd-catalysts was investigated during the selective hydrogenation over butadiene. The addition of the dopants decreased the butadiene hydrogenation activity, especially at higher temperatures and conversion levels. The decrease in catalytic activity was particularly strong for Zn- and Ag-doped catalysts. This was likely due to electron density transfer to Pd, further occupying the d-band electronic states, which decreased the interaction with butadiene. Furthermore, the lowest amount of alkane formation (propane and n-butane) was observed over the undoped Pd-catalyst. Interestingly, higher 1-butene selectivities were found for the Cu-, Zn- and Ag-containing catalysts. Isomerisation tests of 1-butene showed that the addition of Cu, Zn or Ag species suppressed the 1-butene conversion relative to the butadiene conversion, which resulted in higher 1-butene yields for these catalysts. This chapter indicates that the addition of a minority amount (10 mol%) of a dopant greatly changes the catalytic performance of Pd-catalysts during selective hydrogenation reactions. The beneficial or detrimental influence of the dopants on Pd is dependent on the specific reactant (diene or alkene) and the desired application of the reaction (*e.g.,* low alkane formation or high isomer yield).

5.5 Acknowledgements

Sonja Wilms is acknowledged for the synthesis, characterisation and testing of the M-Pd/C materials discussed in this Chapter. We thank Jan Willem de Rijk for the assistance in the 1-butene isomerisation tests.

5.6 References

1. Boucher, M. B. *et al.* Single atom alloy surface analogs in $Pd_{0.18}Cu_{15}$ nanoparticles for selective hydrogenation reactions. *Phys. Chem. Chem. Phys.* **15**, 12187-12196 (2013).
2. Kyriakou, G. *et al.* Isolated Metal Atom Geometries as a Strategy for Selective Heterogeneous Hydrogenations. *Science* **335**, 1209-1212 (2012).
3. McCue, A. J., McRitchie, C. J., Shepherd, A. M. & Anderson, J. A. Cu/Al_2O_3 catalysts modified with Pd for selective acetylene hydrogenation. *J. Catal.* **319**, 127-135 (2014).
4. Li, P. *et al.* Stable and Ordered Body-Centered Cubic PdCu Phase for Highly Selective Hydrogenation. *Small Methods* **7**, 2201356 (2023).
5. Zhao, L. *et al.* A Magnetically Separable Pd Single-Atom Catalyst for Efficient Selective Hydrogenation of Phenylacetylene. *Adv. Mater.* **34**, 2110455 (2022).
6. Hou, R., Yu, W., Porosoff, M. D., Chen, J. G. & Wang, T. Selective hydrogenation of 1,3-butadiene on PdNi bimetallic catalyst: From model surfaces to supported catalysts. *J. Catal.* **316**, 1-10 (2014).
7. Gómez, G., Belelli, P. G., Cabeza, G. F. & Castellani, N. J. A theoretical view of 1,3-butadiene selective hydrogenation toward cis-2-butene on PdNi layered catalyst. *Appl. Surf. Sci.* **353**, 820-828 (2015).
8. Méndez, F. J. *et al.* Selective hydrogenation of 1,3-butadiene in presence of 1-butene under liquid phase conditions with $NiPd/Al_2O_3$ catalysts. *Appl. Petrochemical Res.* **6**, 379-387 (2016).
9. Dasgupta, A. *et al.* Atomic control of active-site ensembles in ordered alloys to enhance hydrogenation selectivity. *Nat. Chem.* **14**, 523-529 (2022).
10. Zhou, H. *et al.* PdZn Intermetallic Nanostructure with Pd-Zn-Pd Ensembles for Highly Active and Chemoselective Semi-Hydrogenation of Acetylene. *ACS Catal.* **6**, 1054-1061 (2016).
11. Mashkovsky, I. S. *et al.* Novel Pd-Zn/C catalyst for selective alkyne hydrogenation: Evidence for the formation of Pd-Zn bimetallic alloy particles. *Mendeleev Commun.* **24**, 355-357 (2014).
12. Sarkany, A., Zsoldos, Z., Furlong, B., Hightower, J. W. & Guczi, L. Hydrogenation of 1-Butene and 1,3-Butadiene Mixtures over Pd/ZnO Catalysts. *J. Catal.* **141**, 566-582 (1993).
13. Aich, P. *et al.* Single-Atom Alloy Pd-Ag Catalyst for Selective Hydrogenation of Acrolein. *J. Phys. Chem. C* **119**, 18140-18148 (2015).
14. Pei, G. X. *et al.* Ag Alloyed Pd Single-Atom Catalysts for Efficient Selective Hydrogenation of Acetylene to Ethylene in Excess Ethylene. *ACS Catal.* **5**, 3717-3725 (2015).
15. Bukhtiyarov, A. V. *et al.* Boosting the activity of $PdAg_2/Al_2O_3$ supported catalysts towards the selective acetylene hydrogenation by means of CO-induced segregation: A combined NAP XPS and mass-spectrometry study. *Appl. Surf. Sci.* **604**, 154497 (2022).
16. Mei, D., Neurock, M. & Smith, C. M. Hydrogenation of acetylene-ethylene mixtures over Pd and Pd-Ag alloys: First-principles-based kinetic Monte Carlo simulations. *J. Catal.* **268**, 181-195 (2009).
17. González, S., Neyman, K. M., Shaikhutdinov, S., Freund, H. J. & Illas, F. On the promoting role of Ag in selective hydrogenation reactions over Pd-Ag bimetallic catalysts: A theoretical study. *J. Phys. Chem. C* **111**, 6852-6856 (2007).
18. van der Hoeven, J. E. S. *et al.* Unraveling 1-Hexene Hydrogenation over Dilute Pd-in-Au Alloys. *J. Phys. Chem. C* **126**, 15710-15723 (2022).
19. Luneau, M. *et al.* Achieving High Selectivity for Alkyne Hydrogenation at High Conversions with Compositionally Optimized PdAu Nanoparticle Catalysts in Raspberry Colloid-Templated SiO_2. *ACS Catal.* **10**, 441-450 (2020).
20. Foucher, A. C. *et al.* Influence of Pd Concentration in Au-Pd Nanoparticles for the Hydrogenation of Alkynes. *ACS Appl. Nano Mater.* **6**, 22927-22938 (2023).
21. Liu, J. *et al.* Integrated Catalysis-Surface Science-Theory Approach to Understand Selectivity in the Hydrogenation of 1-Hexyne to 1-Hexene on PdAu Single-Atom Alloy Catalysts. *ACS Catal.* **9**, 8757-8765 (2019).

22. Hugon, A., Delannoy, L., Krafft, J. M. & Louis, C. Selective hydrogenation of 1,3-butadiene in the presence of an excess of alkenes over supported bimetallic gold-palladium catalysts. *J. Phys. Chem. C* **114**, 10823-10835 (2010).
23. van der Hoeven, J. E. S. *et al.* Unlocking synergy in bimetallic catalysts by core-shell design. *Nat. Mater.* **20**, 1216-1220 (2021).
24. Studt, F. *et al.* Identification of Non-Precious Metal Alloy Catalysts for Selective Hydrogenation of Acetylene. *Science* **320**, 1320-1322 (2008).
25. Pei, G. X. *et al.* Performance of Cu-Alloyed Pd Single-Atom Catalyst for Semihydrogenation of Acetylene under Simulated Front-End Conditions. *ACS Catal.* **7**, 1491-1500 (2017).
26. Yan, H. *et al.* Single-Atom Pd_1/Graphene Catalyst Achieved by Atomic Layer Deposition: Remarkable Performance in Selective Hydrogenation of 1,3-Butadiene. *J. Am. Chem. Soc.* **137**, 10484-10487 (2015).
27. Moyes, R. B., Wells, P. B., Grant, J. & Salman, N. Y. Electronic effects in butadiene hydrogenation catalysed by the transition metals. *Appl. Catal. A Gen.* **229**, 251-259 (2002).
28. Yan, H. *et al.* Understanding the underlying mechanism of improved selectivity in Pd_1 single-atom catalyzed hydrogenation reaction. *J. Catal.* **366**, 70-79 (2018).
29. Valcárcel, A., Clotet, A., Ricart, J. M., Delbecq, F. & Sautet, P. Comparative DFT study of the adsorption of 1,3-butadiene, 1-butene and 2-cis/trans-butenes on the Pt(111) and Pd(111) surfaces. *Surf. Sci.* **549**, 121-133 (2004).
30. Van Der Hoeven, J. E. S. *et al.* Entropic Control of HD Exchange Rates over Dilute Pd-in-Au Alloy Nanoparticle Catalysts. *ACS Catal.* **11**, 6971-6981 (2021).
31. Marcella, N. *et al.* Decoding reactive structures in dilute alloy catalysts. *Nat. Commun. 2022 131* **13**, 1-9 (2022).
32. Hannagan, R. T., Giannakakis, G., Flytzani-Stephanopoulos, M. & Sykes, E. C. H. Single-Atom Alloy Catalysis. *Chem. Rev.* **120**, 12044-12088 (2020).
33. Giannakakis, G., Flytzani-Stephanopoulos, M. & Sykes, E. C. H. Single-Atom Alloys as a Reductionist Approach to the Rational Design of Heterogeneous Catalysts. *Acc. Chem. Res.* **52**, 237-247 (2019).
34. McCue, A. J. & Anderson, J. A. Recent advances in selective acetylene hydrogenation using palladium containing catalysts. *Front. Chem. Sci. Eng.* **9**, 142-153 (2015).
35. Zhang, L., Zhou, M., Wang, A. & Zhang, T. Selective Hydrogenation over Supported Metal Catalysts: From Nanoparticles to Single Atoms. *Chem. Rev.* **120**, 683-733 (2020).
36. Louis, C. & Delannoy, L. Selective hydrogenation of polyunsaturated hydrocarbons and unsaturated aldehydes over bimetallic catalysts. *Adv. Catal.* **64**, 1-88 (2019).
37. Takht Ravanchi, M., Sahebdelfar, S. & Komeili, S. Acetylene selective hydrogenation: a technical review on catalytic aspects. *Rev. Chem. Eng.* **34**, 215-237 (2018).
38. Molnár, Á., Sárkány, A. & Varga, M. Hydrogenation of carbon-carbon multiple bonds: chemo-, regio- and stereo-selectivity. *J. Mol. Catal. A Chem.* **173**, 185-221 (2001).
39. Zhou, H. *et al.* PdZn Intermetallic Nanostructure with Pd-Zn-Pd Ensembles for Highly Active and Chemoselective Semi-Hydrogenation of Acetylene. *ACS Catal.* **6**, 1054-1061 (2016).
40. Park, Y. H. & Price, G. L. Promotional Effects of Potassium on Pd/Al_2O_3 Selective Hydrogenation Catalysts. *Ind. Eng. Chem. Res.* **31**, 469-474 (1992).
41. Beerthuis, R. *et al.* Manganese oxide promoter effects in the copper-catalyzed hydrogenation of ethyl acetate. *J. Catal.* **394**, 307-315 (2021).
42. Dalebout, R. *et al.* Manganese Oxide as a Promoter for Copper Catalysts in CO_2 and CO Hydrogenation. *ChemCatChem* **14**, e202200451 (2022).
43. Melnikov, D. *et al.* Selective Hydrogenation of Acetylene over $Pd\text{-}Mn/Al_2O_3$ Catalysts. *Catalysts* **10**, 624 (2020).
44. Okamoto, H. Supplemental Literature Review of Binary Phase Diagrams: Ag-Co, Ag-Er, Ag-Pd, B-Ce, Bi-La, Bi-Mn, Cu-Ge, Cu-Tm, Er-Y, Gd-Tl, H-La, and Hg-Te. *J. Phase Equilibria Diffus.* **36**, 10-21 (2015).
45. Popov, A. A., Shubin, Y. V., Plyusnin, P. E., Sharafutdinov, M. R. & Korenev, S. V. Experimental redetermination of the Cu-Pd phase diagram. *J. Alloys Compd.* **777**, 204-212 (2019).

46. Vizdal, J., Kroupa, A., Popovic, J. & Zemanova, A. The experimental and theoretical study of phase equilibria in the Pd-Zn (-Sn) system. *Adv. Eng. Mater.* **8**, 164-176 (2006).
47. Sato, H. & Toth, R. Long-period superlattice Pd_3Mn II and its large tetragonal distortion. *Phys. Rev.* **139**, (1965).
48. Parker, L. J., Hasegawa, M., Atou, T. & Badding, J. V. High Pressure Synthesis of Alkali Metal-Transition Metal Compounds. *Rev. High Press. Sci. Technol.* **7**, 1049-1053 (1998).
49. Li, K. & Xue, D. Estimation of Electronegativity Values of Elements in Different Valence States. *J. Phys. Chem. A* **110**, 11332-11337 (2006).
50. Wu, C. Y. *et al.* Effect of Fe-based organic metal framework on the thermal decomposition of potassium nitrate and its application to the composite solid propellants. *Combust. Flame* **232**, 111556 (2021).
51. Ravanbod, M. & Pouretedal, H. R. Catalytic effect of Fe_2O_3, Mn_2O_3, and TiO_2 nanoparticles on thermal decomposition of potassium nitrate. *J. Therm. Anal. Calorim.* **124**, 1091-1098 (2016).
52. Visser, N. L. *et al.* Influence of carbon support surface modification on the performance of nickel catalysts in carbon dioxide hydrogenation. *Catal. Today* **418**, 114071 (2023).
53. Mattarozzi, F., Visser, N., de Rijk, J. W., Ngene, P. & de Jongh, P. Ligand-Free Silver Nanoparticles for CO_2 Electrocatalytic Reduction to CO. *Eur. J. Inorg. Chem.* **2022**, e202200365 (2022).
54. Bergeret, G. & Gallezot, P. Characterization of Solid Catalysts: Sections 3.1.1-3.1.3. in *Handbook of Heterogeneous Catalysis* vols 1-5 427-582 (Wiley-VCH Verlag GmbH, 2008).
55. Brandt Corstius, O. E., van der Hoeven, J. E. S., Sunley, G. J. & de Jongh, P. E. Influence of particle size in Pd-catalysed selective hydrogenation of 1,3-butadiene. *J. Catal.* **427**, 115103 (2023).
56. A. Roine. HSC Chemistry 9. Software available at www.metso.com/hsc. Metso, Pori (2023).
57. Maccoll, A. & Ross, R. A. The Hydrogen Bromide Catalyzed Isomerization of n-Butenes. I. Equilibrium Values. *J. Am. Chem. Soc.* **87**, 1169-1170 (1965).
58. Horiuti, I. & Polanyi, M. Exchange reactions of hydrogen on metallic catalysts. *Trans. Faraday Soc.* **30**, 1164 (1934).
59. Bond, G. C., Webb, G., Wells, P. B. & Winterbottom, J. M. The hydrogenation of alkadienes. Part I. The hydrogenation of buta-1,3-diene catalysed by the Noble Group VIII metals. *J. Chem. Soc.* 3218 (1965) doi:10.1039/jr9650003218.
60. Bates, A. J., Leszczynski, Z. K., Phillipson, J. J., Wells, P. B. & Wilson, G. R. The hydrogenation of akladienes. Part IV. The reaction of buta-1,3-diene with deuterium catalysed by rhodium, palladium, and platinum. *J. Chem. Soc. A Inorganic, Phys. Theor.* 2435 (1970) doi:10.1039/j19700002435.
61. Boitiaux, J. P., Cosyns, J. & Robert, E. Additive effects in the selective hydrogenation of unsaturated hydrocarbons on platinum and rhodium catalysts. II. Influence of various compounds containing phosphorus, oxygen, sulphur and chlorine on the catalytic performance of platinum catalyst. *Appl. Catal.* **49**, 235-246 (1989).

Chapter 6

Summary and outlook

6.1 Summary

This thesis covers a study on the selective hydrogenation of gaseous 1,3-butadiene (butadiene hereafter) over palladium (Pd) nanoparticle catalysts. This reaction is of essential relevance for industrial high-purity olefin production, where butadiene impurities have to be reduced down to the ppm level. Retaining a high selectivity up to complete butadiene conversion is challenging. Therefore, a full understanding of the effects of catalyst properties and reaction conditions on the catalytic performance is required. Several factors influence the catalysis, such as nanoparticle size, reaction conditions, metal composition and catalyst structure. Using different synthesis, characterisation and catalytic testing methods, we aimed to develop a better comprehension of the properties of the catalyst and reaction conditions that affect catalytic activity and selectivity. The general background of selective hydrogenation reactions is discussed in **Chapter 1**. Moreover, detailed information on the use of Pd as active metal and carbon as nanoparticle support is provided with a focus on the application in the selective hydrogenation of butadiene from an excess of propylene.

In **Chapter 2**, the influence of Pd nanoparticle size on the catalytic performance is discussed. We systematically varied the nanoparticle size of carbon-supported Pd (Pd/C) catalysts from 2 to 17 nm in diameter and studied its effect on the catalysis. The nanoparticle size determined the structure of the exposed surfaces, where small nanoparticles contain a majority of corner- and edge-sites, while larger nanoparticles expose more flat and extended terraces. The butadiene hydrogenation activity per Pd surface atom increased with nanoparticle size, from 17 s^{-1} to 34 s^{-1} at 25 °C for 2 nm to 17 nm nanoparticles. Contrarily, the propylene hydrogenation activity decreased strongly over the same range of nanoparticle sizes; from 2.6 s^{-1} to 0.4 s^{-1}, in line with the fraction of exposed corner-sites. Therefore, a size-dependent product selectivity was obtained, with a higher butene selectivity for larger nanoparticles over the full butadiene conversion range.

In **Chapter 3**, the effect of heat and mass transport limitations on activity and selectivity is described using Pd/C catalysts of similar particle size. By varying the Pd loading, a specific surface area of between 0.01 to 2.6 m^2_{Pd}/g_{cat} was obtained for different catalysts. The effective mass transport (diffusion) was varied by using different average catalyst grain sizes (between 19 and 200 μm). By comparing to the observed reaction rates, we calculated whether the external and internal heat and mass transport were sufficiently fast. The combination of catalytic results and calculations highlighted the importance of diffusion-induced concentration gradients inside catalyst grains. The observed impact of these gradients on the butene selectivity was much more severe than the impact on activity. This chapter provides guidelines for understanding the influence of catalyst structure and testing conditions for Pd-catalysed hydrogenation reactions and how to avoid attributing observations to intrinsic catalyst properties while, in reality, they are caused by internal mass transfer limitations.

In **Chapter 4**, we deal with bimetallic PdCu/C catalysts and focus on the influence of the Cu-to-Pd ratio (between 7 and 167) in Cu-rich catalysts on the catalytic performance. The Pd mass- and surface-normalised activity in bimetallic PdCu catalysts was lower than that of monometallic Pd but gradually increased with Pd content. *Operando* X-ray absorption spectroscopy showed a slight preferential clustering of Pd in the bimetallic nanoparticles, as well as electron density transfer from Cu to Pd. This changes the active site in terms of the Pd ensemble site and its electronic properties, and hence adsorption energies, which explains why the behaviour is very different from that of pure Pd. The Pd-containing catalysts showed similar isomer product compositions and high butene selectivities up to near-complete butadiene conversion. Monometallic Cu and Cu-rich (Cu:Pd≥85) catalysts showed slightly superior butene selectivity at high conversions, albeit at much lower activities. This chapter highlights the importance of tuning the Pd-concentration in Cu-rich bimetallic catalysts to combine favourable activities with high selectivities while minimising the Pd content.

In **Chapter 5**, we explore the effect of various additives (K, Mn, Cu, Zn, and Ag-based) on the performance of Pd/C catalysts. The addition of the dopants decreased the butadiene hydrogenation activity, especially at higher temperatures and conversion levels. This reduced activity was ascribed to an electron density transfer to Pd and was particularly strong for Zn- and Ag-doped catalysts. The lowest amount of alkane formation (both propane and n-butane) was observed over the undoped Pd-catalyst. Interestingly, higher 1-butene selectivities were found for the Cu-, Zn- and Ag-containing catalysts. Isomerisation tests of 1-butene showed that the addition of Cu, Zn or Ag species suppressed the 1-butene conversion relative to the butadiene conversion, which resulted in higher 1-butene yields for these catalysts. This chapter indicates that the addition of a minority amount (10 mol%) of a dopant greatly changes the catalytic performance of Pd-catalysts.

6.2 Outlook

Throughout my PhD project, more than one hundred different catalyst samples have been prepared, which were all characterised using multiple methods and examined by various catalytic tests. This research has provided answers to many questions and arguably gave rise to even more additional questions. This section offers some suggestions for future research directions and their associated challenges as a follow-up to the work presented in this thesis.

From **Chapter 2**, we learnt that corner sites on smaller Pd nanoparticles are detrimental to the butene selectivity, while terraces provide improved selectivity. By controlled synthesis methods, particles with well-defined facets can be prepared, maximising terrace site exposure and minimise the corner site fraction. However, retaining such shapes under catalytic working conditions might be challenging. Another

approach is to make large particles by core-shell design, where the core is preferentially a cheap substitute for an expensive Pd core, but is required to have no detrimental effect on the electronic properties of the catalytically active Pd shell. In an ideal scenario, the core even enhances the catalytic properties of Pd.

A concentration-activity correlation with regards to the Pd fraction was found in **Chapter 4**. For the lowest Pd concentrations (<1 at%), however, we were unable to correlate the low activity to the Pd geometry. With advanced characterisation methods, such as aberration-corrected electron microscopy or molecular probe spectroscopy, it is possible to detect isolated Pd atoms inside the Cu-host and to distinguish them from larger Pd ensembles. We note that the nature of the Pd site depends on the atmosphere, hence such experiments should preferentially be performed under *in situ* or *operando* conditions, which complicates the feasibility of the experiments.

For the dopant addition in **Chapter 5**, we found a trend in the effect on activity and selectivity based on the position of the dopant within the periodic table. These trends should be substantiated by calculations of electronic transfer or measured experimentally. *In situ* or *operando* X-ray absorption spectroscopy on these samples could be insightful into the oxidation state of these dopants and their electronic interactions with Pd. Moreover, computational assessments of which dopant species are present under reaction conditions and their electronic influence are necessary to fully understand the observed trends.

For **Chapters 4 and 5**, the use of more than one metal(-oxide) raises interesting questions on restructuring or preferential surface occupation for Pd and the secondary element. It is interesting to investigate such effects based on relevant pre-treatment conditioning, such as heating in H_2, O_2 or CO, and to correlate catalytic performance to the affinity with molecules in the reaction gas.

The strong effect of internal mass transfer limitations, observed in **Chapter 3**, should be minimised to obtain accurate structure-performance relationships in catalysis. Therefore, as a general approach, catalysts with very low Pd loadings can be used to revisit some of the investigations of intrinsic catalytic properties, including effects of size, support and additives. However, the downside of catalysts with low Pd loading is that determining the structure of the catalysts becomes increasingly more difficult due to reduced signal-to-noise ratio during characterisation experiments.

Lastly, in academic studies, including this thesis, there is often a so-called “materials and pressure gap” with respect to industry. To overcome these gaps, more complicated reaction mixtures, including CO and CH_4, and higher pressures (Table 1.1) should be tested to better resemble the typical front-end conditions in selective hydrogenation reactors. Moreover, the influence of binder materials and additives in the use of industrial catalyst bodies, such as extrudates, can be explored.

Chapter 7

Nederlandse samenvatting

Welkom in alweer het laatste hoofdstuk van dit proefschrift! Leuk dat je het bijna hebt uitgelezen (of ben je hier begonnen?). In dit hoofdstuk geef ik een bondige samenvatting van het onderzoek dat ik de afgelopen vier jaar heb gedaan. In die jaren ben ik vaak door vrienden en familie gevraagd waar ik precies aan werkte. Het was niet altijd even gemakkelijk om helder uit te leggen, vooral als ik niet precies wist wat de chemische achtergrondkennis was van degene die de vraag stelde. Ik begrijp dat de woorden "selectieve hydrogenatie met palladium katalysatoren" een verre van alledaags of tastbaar begrip zijn. In de tekst hieronder neem ik graag de tijd om, met zoveel mogelijk herkenbare voorbeelden, uit te leggen aan welk specifiek stukje binnen de scheikunde ik al die tijd heb gewerkt.

Wat is katalyse?

Wij hebben als mensen dagelijks (wellicht onbewust) te maken met verschillende scheikundige processen. Deze chemische reacties spelen een rol bij bijvoorbeeld het klaarmaken van eten, het op- en ontladen van je telefoon of bij het afbreken van alcohol door enzymen in ons lichaam. In dit proefschrift staat een specifieke tak binnen de scheikunde centraal; de katalyse. Katalyse is onlosmakelijk verbonden met het versnellen van veel chemische processen en draagt zo voor een groot gedeelte bij aan een duurzamere industrie en de wereldwijde economie. Zo wordt bij de productie van 90% van alle materialen, brandstoffen, oplosmiddelen, plastics en medicijnen ten minste één gekatalyseerde omzetting gebruikt.[1] In andere woorden: ten minste een omzetting vindt plaats met behulp van "een katalysator". Zo'n katalysator is een materiaal dat chemische reacties versnelt, ze bij lagere temperatuur laat plaatsvinden of ze in een bepaalde richting stuurt. Een bekend voorbeeld is de katalysator in elke benzineauto, waar schadelijke uitlaatgassen (zoals giftige stikstofoxides, koolstofmonoxide en roetdeeltjes) door de katalysator worden afgebroken, en weer opgebouwd tot minder schadelijke uitlaatgassen (water, stikstof en koolstofdioxide). Hierbij is het van belang dat de katalysator de reacties versnelt zonder zelf verbruikt te worden. Daardoor kunnen ze opnieuw gebruikt worden voor een volgende chemische reactie. Drie belangrijke eigenschappen van een katalysator zijn activiteit (aantal omzettingen per minuut), selectiviteit (welke omzettingen worden versneld) en stabiliteit (hoelang een katalysator effectief mee gaat).

Recente schattingen geven aan dat katalyse in direct verband kan worden gebracht met 40% van het wereldwijde bruto nationaal product (BNP, €95.4 biljoen in 2023).[2–4] Dat betekent dat katalyse bijdraagt aan een jaarlijkse waarde van €38.2 biljoen, meer dan het BNP van heel Europa (€23.2 biljoen) of de Verenigde Staten (€27.0 biljoen). Ter vergelijking heeft Nederland een BNP van €1.0 biljoen (€1.000.000.000.000). De grootste bijdrage van katalyse aan de wereldwijde economie is door de onmisbaarheid van katalysatoren in de chemische industrie. Zoals eerder genoemd, worden 90% van alle kunstmatig geproduceerde materialen gemaakt met behulp van een katalysator.[1]

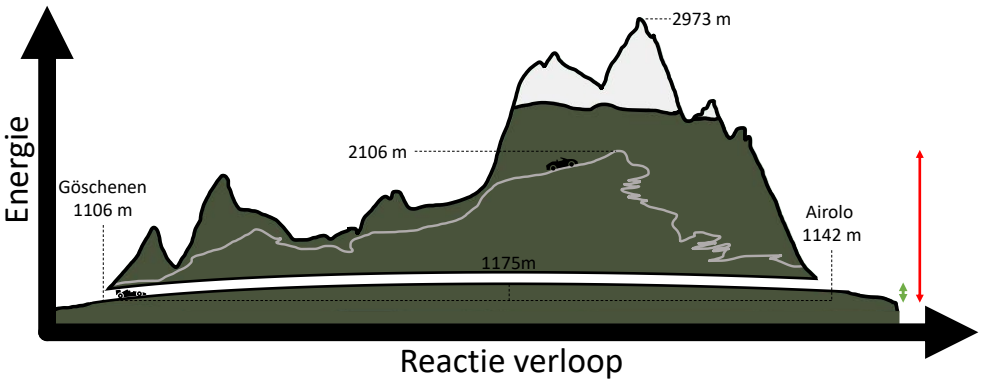

Figuur 7.1. Energielandschap. De benodigde energiebarrière om de Zwitserse Alpen te doorkruisen wordt aanzienlijk verlaagt met behulp van de Gotthardtunnel, vergelijkbaar met een chemische omzetting die door een katalysator wordt versneld.

De grootschalige toepassingen van katalyse variëren van de productie van alledaagse producten zoals kunststoffen en kleding, het maken van medicijnen tot het produceren van synthetische brandstoffen, waterstof en kunstmest. Hiermee is ook een belangrijke rol weggelegd voor de katalyse om een meer duurzame en circulaire toekomstige economie te creëren, met name via de energietransitie.

Een gekatalyseerde en niet-gekatalyseerde omzetting kunnen vergeleken worden met twee routes over de Zwitserse Alpen (Figuur 7.1). Om van Göschenen naar Airolo te komen, moet een bepaalde energiebarrière (hoogteverschil) overbrugd worden. In dit voorbeeld ligt het hoogste punt van de bergpas op exact 1000 hoogtemeters boven het beginpunt van de reis. Het kost een bepaalde hoeveelheid energie om dit hoogste punt te bereiken. Na het bereiken van het hoogste punt, komt er juist energie vrij, omdat de auto door zwaartekracht versnelt (kinetische energie) en de remschijven opwarmen (warmte-energie) bij het remmen. Na de afdaling, kom je aan in Airolo, 36 hoogtemeters boven het begin van de rit. Een katalysator verlaagt de energiebarrière van een reactie, vergelijkbaar met het verlagen van de hoogtemeters van de autotocht. Bijvoorbeeld door via de Gotthardtunnel te rijden, wordt het hoogste punt aanzienlijk verlaagd vergeleken met de bergpas, en is maar een stijging van 69 hoogtemeters nodig om dit punt te bereiken.

Het verschil tussen de energiebarrières van deze twee paden is schematisch weergegeven in Figuur 7.1 met de groene en rode pijlen. Het begin en eindpunt zijn exact hetzelfde, maar het pad daartussen is aanzienlijk gemakkelijker gemaakt. Op eenzelfde manier maakt een katalysator het mogelijk om chemische reacties te laten plaatsvinden via een ander, gemakkelijker, pad. De begin- en eindstoffen zijn hetzelfde, en ze hebben dezelfde chemische energie als via een niet-gekatalyseerd reactiepad. Maar het pad van begin- naar eindstof doorlopen is veel gemakkelijker mét de hulp van een katalysator. Naast het verlagen van de energiebarrière, kan een katalysator ook helpen in de selectiviteit. Door bepaalde reactie-routes gemakkelijk te maken, ofwel

andere juist te verhinderen, kan de selectiviteit van een chemische reactie richting een bepaald product gestuurd worden. Om terug te komen op de Alpen-metafoor, is dit te vergelijken met asfalteren van bepaalde wegen, terwijl andere gevaarlijke bergweggetjes juist worden afgesloten. Op deze manier zal het meeste verkeer zich uiteindelijk vooral via één route, richting één eindpunt, bewegen.

De selectieve reactie

De chemische reactie die in dit proefschrift is beschreven, is selectieve hydrogenatie. Met hydrogeneren wordt een proces bedoeld waarbij waterstofgas (H_2) chemisch wordt gebonden aan een waterstof-onverzadigd molecuul. Zo'n molecuul wordt daardoor meer verzadigd met waterstof atomen (H). Een bekend voorbeeld uit de voedselindustrie zijn onverzadigde vetzuren, die met hydrogeneren worden omgezet in verzadigde vetzuren. In selectieve hydrogenatie is het vereist dat de reactie specifiek is voor één bepaalde binding van een specifiek molecuul, zodat de overige bindingen en moleculen onaangetast blijven. Voorbeelden van reacties waar selectiviteit belangrijk is, is het hydrogeneren van moleculen met meerdere onverzadigde 'dubbele' koolstof-koolstof bindingen (C=C) ofwel met een drievoudige (C≡C) binding, zoals bijvoorbeeld butadieen en acetyleen in Figuur 7.2. Bij deze voorbeelden is het van belang dat slechts een enkele hydrogenatie stap plaatsvindt naar buteen of ethyleen, zonder ook een volgende stap (volledige hydrogenatie) naar butaan of ethaan. Deze selectieve reacties zijn essentieel bij de productie van medicijnen, kleur- geur- en smaakstoffen, vitamines en polymeren.[5]

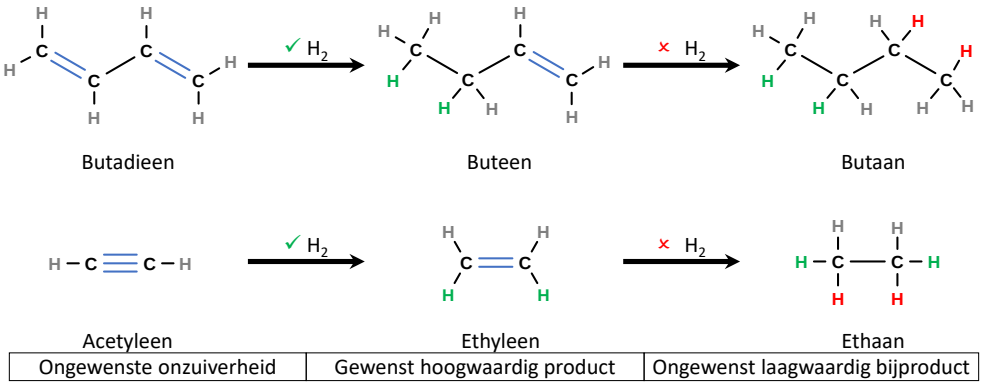

Figuur 7.2. Voorbeelden van de selectieve hydrogenatie. Schematische weergave van twee veelvoorkomende reacties: het selectief omzetten van butadieen of acetyleen naar buteen en ethyleen, zonder over-hydrogenatie naar butaan of ethaan. De moleculen zijn schematisch weergegeven met de initiële waterstof atomen in het grijs, de onverzadigde (dubbele of drievoudige) koolstof-koolstof bindingen in het blauw, de gewenste waterstoftoevoeging in het groen, en de ongewenste waterstof in het rood (over-hydrogenatie).

Een grootschalige industriële toepassing van selectieve hydrogenatie is het zuiveren van "alkeen" gasmengsels.[6] Bij de productie van deze hoogwaardige alkenen, zoals bijvoorbeeld buteen of ethyleen, wordt altijd een klein beetje ongewenst butadieen of acetyleen gevormd. De concentratie van deze onzuiverheden is minder dan ongeveer 1% in het mengsel. De kleine hoeveelheid onzuiverheid moet echter volledig uit het gasmengsel verwijderd worden, omdat anders een essentieel chemisch proces in een later stadium (de polymerisatie) ernstig wordt belemmerd. Door middel van selectieve hydrogenatie wordt de ongewenste onzuiverheid omgezet tot een gewenst hoogwaardig alkeen product (Figuur 7.2). Noodzakelijk is wel dat deze reactie zeer selectief verloopt, zodat er geen over-hydrogenatie plaatsvindt, met laagwaardige bijproducten zoals butaan en ethaan als gevolg. Bij elke hydrogenatie komt warmte vrij (het is een "exotherme" reactie). Dit maakt het nog lastiger om de reactie onder controle te houden, vooral als veel omzettingen snel achter elkaar plaatsvinden, en er veel warmte vrijkomt. Het selectief hydrogeneren van zo'n kleine (<1%) onzuiverheid uit een gasmengsel van gewenste producten, is alsof je op een chemische manier een speld (1% butadieen) uit een hooiberg (99% alkenen) probeert te halen. Echter, omdat de alkenen zelf óok gehydrogeneerd kunnen worden, waar weer warmte bij vrijkomt, is het meer vergelijkbaar met selectief een lucifer uit een hooiberg proberen te verwijderen door alleen de lucifer aan te steken, zonder dat de hooiberg eromheen vlam vat. Dit maakt selectieve hydrogenatie een zeer uitdagend wetenschappelijk vraagstuk met grootschalige industriële relevantie.

Wat zijn nanodeeltjes?

Voor katalytische omzettingen worden veelal metaal nanodeeltjes gebruikt. Voor selectieve hydrogenatie zijn metalen als koper, zilver en goud (de zogenoemde muntmetalen) bekend. Deze muntmetalen hebben een goede selectiviteit, maar de activiteit is over het algemeen erg laag. Platinagroep metalen (PGMs) zoals rhodium, palladium en platina zijn vele ordergroottes actiever dan de muntmetalen. Van de PGMs, is palladium (Pd) het meest selectief, wat het de ideale kandidaat maakt voor selectieve hydrogenatie reacties, door de combinatie van hoge activiteit en goede selectiviteit.

Een nadeel van palladium is dat het een vrij kostbaar metaal is (32.000 €/kg).[7] Daarom is het gewenst om het metaal zo effectief mogelijk te gebruiken. Dit wordt gedaan door het metaal in zogenoemde nanodeeltjes op te splitsen. Deze deeltjes van enkele nanometers (nm, 0.000000001 meter) hebben een veel groter oppervlak waar katalyse kan plaatsvinden, vergeleken met als het Pd in één enkel stuk geconcentreerd zou zijn. Ter illustratie, 1 gram Pd (dichtheid 12 g/cm^3) kan worden omvat door een bolletje van 0.54 cm in diameter met een oppervlak van 0.92 cm^2, iets minder dan een kleine postzegel. Wanneer je deze palladium doperwt opsplitst in nanodeeltjes van 5 nm, geeft dat een totaal oppervlak van ongeveer 100 m^2 voor 1 gram metaal, ongeveer de grootte van een halve tennisbaan. Kortom, door gebruik te maken van zulke nanodeeltjes wordt

het oppervlakte van dezelfde hoeveelheid Pd met ongeveer een factor 1 miljoen vergroot.[8] Om enigszins gevoel te krijgen voor hoe klein deze deeltje dan zijn, kun je je een tennisbal in je hand voorstellen. Deze tennisbal is ongeveer 100 miljoen keer (8 ordergroottes) kleiner dan de aarde (Figuur 7.3). Een tennisbal is weer 1000 keer groter dan een gemiddelde hoofdhaar (0.06 mm). Beeld je nu in dat een nanodeeltje weer 100.000 keer kleiner is dan die hoofdhaar, ofwel 100.000.000 keer kleiner dan een tennisbal. Om deze nanodeeltjes te bestuderen zijn geavanceerde meetmethodes ontwikkeld; bijvoorbeeld met elektronenmicroscopie is het mogelijk om deze nanodeeltjes te bekijken, zoals te zien is op de achterkant van dit proefschrift.

Voor deze nanodeeltjes zijn zogenoemde dragermaterialen nodig. Deze dragermaterialen zijn de fysieke ondersteuning van de nanodeeltjes, die ervoor zorgen dat ze hun kleine afmetingen behouden en niet samenklonteren tot grotere deeltjes. Idealiter hebben dragermaterialen een groot oppervlak waar de nanodeeltjes op afgezet kunnen worden. In het dragermateriaal kun je een groot oppervlak en volume creëren door het aanbrengen van veel kleine holtes of poriën, waardoor het gaat lijken op een nano-versie van een keukenspons. In dit proefschrift wordt koolstof als dragermateriaal gebruikt. Specifiek gebruiken we grafeen nanoplaatjes (GNP), die bestaan uit meerdere op elkaar gestapelde lagen grafeen, wat grafiet vormt; hetzelfde materiaal waar potloodpunten van gemaakt zijn. Deze platen (10-20 nm dik en 500-1000 nm lang) hebben een groot beschikbaar oppervlak van 500 m^2/g waar de Pd nanodeeltjes van een paar nanometer op worden afgezet. Een voordeel van koolstof als dragermateriaal, is dat het geen chemische reacties kan aangaan met de metaaldeeltjes.[9–11] Daarnaast heeft koolstof een hele hoge warmtegeleiding, wat bijdraagt aan een betere afvoer van de warmte die door de (exotherme) hydrogenatiereacties vrijkomt.[12] Voor ons vormen palladium nanodeeltjes afgezet op het koolstof dragermateriaal (de nano-potloodpunt-spons) de basis van de katalysatoren die besproken worden in dit proefschrift. De katalysator poeders worden uiteindelijk samengedrukt en gezeefd tot een hanteerbare korrelgrootte (ter grootte van fijne zandkorrels, 0.02-0.2 mm, dat is ongeveer 0.3-3 hoofdharen) die in een katalytische test opstelling geplaats kunnen worden.

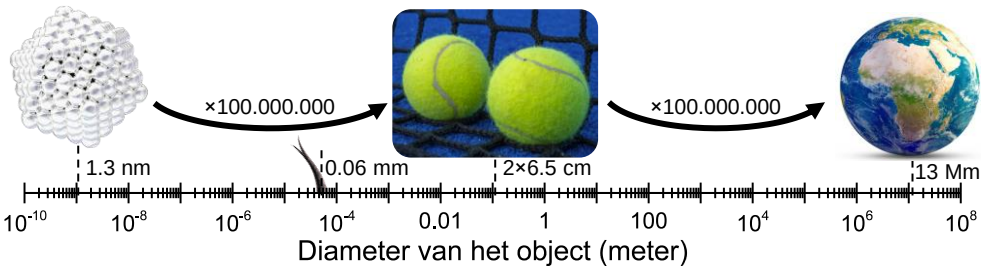

Figuur 7.3. Verschil in grootte tussen een palladium nanodeeltje, twee tennisballen en de aarde. De aarde is ongeveer 1×10^8 keer groter dan de tennisballen, die ook weer ongeveer 1×10^8 keer groter zijn dan een typisch metaal nanodeeltje.

Wat staat er in dit proefschrift?

Om chemische processen schoner, zuiniger en efficiënter te laten plaatsvinden zijn dus katalysatoren nodig. Elk proces heeft in principe een optimale katalysator en optimale reactiecondities (zoals druk, temperatuur en stroming van reactanten). Veel (scheikundige) ontdekkingen zijn het resultaat van doelgericht onderzoek, maar anderen van trial-and-error (gissen en missen) of toevalsbevindingen. Voor het ontwikkelen van betere of nieuwe katalysatoren, is het van belang om te begrijpen hoe de katalytische prestaties samenhangen met de eigenschappen van de katalysator. Daardoor kunnen katalysatoren aangepast worden voor een nog betere werking, en kunnen katalysatoren worden ontworpen voor nieuwe toepassingen. In dit proefschrift zijn verschillende katalysatoreigenschappen gecorreleerd aan de katalytische prestaties, uiteengezet in 5 hoofdstukken.

In **Hoofdstuk 1** wordt een inleiding gegeven in het onderwerp van dit proefschrift: de selectieve hydrogenatie met Pd katalysatoren (een zin die hopelijk nu meer herkenning opwekt). Dit hoofdstuk beschrijft de relevante achtergrond van de chemische reacties en de belangrijke eigenschappen van de katalysatoren, zoals de interactie die Pd heeft met de moleculen.

In de Hoofdstukken 2 t/m 5 staat beschreven wat het effect is van het variëren van verschillende katalysator materiaaleigenschappen en reactiecondities op de katalyse. Als gemeenschappelijk thema, worden in al deze hoofdstukken koolstofgedragen palladium nanodeeltjes (Pd/C) gebruikt voor het verwijderen van butadieen door middel van selectieve hydrogenatie (Figuur 7.2) uit een 100-voudige overmaat van propyleen (alkeen). Tijdens de katalyse worden activiteit en selectiviteit nauwkeurig in de gaten gehouden, als functie van temperatuur en andere reactiecondities. De resultaten worden gekoppeld aan de variaties van de eigenschappen van de katalysatoren, om zo een beter inzicht te krijgen in de werking van Pd/C tijdens selectieve hydrogenatie reacties.

In **Hoofdstuk 2** wordt het effect van de grootte van de nanodeeltjes beschreven. Hiervoor is een serie van verschillende Pd nanodeeltjes gemaakt, variërend van ongeveer 2 tot 20 nm in diameter. Met deze variatie in grootte, komt ook een variatie van hoe het oppervlak van zo'n nanodeeltje er uit ziet. Een klein nanodeeltje (Figuur 7.4A) bevat relatief veel hoek- en randpunten. Bij grotere nanodeeltjes neemt de hoeveelheid platte vlakken juist toe, en neemt de fractie hoekpunten sterk af. Deze vlakken, randen of hoekpunten hebben allemaal een andere interactie met de butadieen en propyleen moleculen, en daardoor ook een andere activiteit en selectiviteit. De katalytische experimenten lieten zien dat de activiteit voor butadieen ongeveer verdubbelt met grotere deeltjesgrootte (van 2 tot 20 nm), omdat butadieen efficiënt wordt omgezet op het platte oppervlak. Tegelijkertijd nam de activiteit voor de ongewenste propyleen hydrogenatie juist sterk af: een zesvoudige afname van 2 naar 20 nm deeltjes. Deze afname in propyleen activiteit volgde eenzelfde trend als de fractie van de hoekpunten in een nanodeeltje, wat er op wijst dat propyleen vooral over deze

hoekpunten in kleine nanodeeltjes wordt omgezet. Het verschil in activiteit van deze twee reacties resulteerde in een grootte-afhankelijke selectiviteit die veel beter was voor grotere nanodeeltjes. Kortom, grotere deeltjes zijn selectiever dan kleinere deeltjes. Je hebt alleen wel relatief meer van het dure palladium nodig om grotere deeltjes te maken.

In **Hoofdstuk 3** wordt de invloed van de reactiecondities besproken. We keken naar nanodeeltjes met vergelijkbare grootte, maar met een verschillende hoeveelheid deeltjes per gram dragermateriaal. Deze katalysatoren zijn weer onderverdeeld op basis van de "korrelgrootte" (grootte van samengeperste Pd/C deeltjes). De combinaties van de belading en korrelgrootte geven een groot variërende verhouding tussen katalytische activiteit (die toeneemt met toenemende hoeveelheid nanodeeltjes) en de diffusiesnelheid van de butadieen gasmoleculen (die afneemt met toenemende korrelgrootte). Vervolgens zijn warmtegeleiding en diffusiesnelheden voor deze katalysatoren berekend. Zo werd aangetoond dat vooral de zogenoemde "interne diffusie limitaties" een grote invloed hebben op de selectiviteit van de reactie. Door de hoge snelheid waarmee de Pd nanodeeltjes de butadieen omzetten, is de diffusiesnelheid te laag om voldoende nieuwe butadieen aan te voeren. Deze limitaties zijn te vergelijken het bewegen door een doolhof: het is gemakkelijk om langs de randen te komen en het zal er druk bezocht zijn, maar hoe dieper naar het midden van het doolhof je je begeeft, hoe langer dit duurt en hoe minder mensen dit bereiken. Hierdoor ontstaat er een concentratiegradiënt van butadieen: binnenin de katalysator korrels is minder butadieen aanwezig (Figuur 7.4B). Dit effect wordt sterker voor hogere Pd beladingen (butadieen wordt al aan rand van het doolhof snel omgezet), en grotere korrels (het doolhof wordt groter). Als deze effecten te groot worden, is in het middendeel van de katalysatorkorrel amper butadieen aanwezig. Dan hebben daar de ongewenste reacties vrij spel en neemt de totale selectiviteit af. Dit hoofdstuk beschrijft hoe met dezelfde Pd nanodeeltjes, grote verschillen in katalytische werking optraden. Deze verschillen zijn niet het gevolg van de materiaaleigenschappen van de nanodeeltjes, wat laat zien dat het van groot belang is hoe een test wordt uitgevoerd, en dat wordt gecontroleerd of het massa- en warmtetransport de reactie bij kunnen houden.

In **Hoofdstuk 4** worden nanodeeltjes bestaande uit twee metalen, namelijk Pd en koper (Cu), behandeld. In deze bimetallische ("tweemetalige") deeltjes werd de verhouding tussen Pd en Cu gevarieerd, met een Pd concentratie tussen de 0 en 13%. Door middel van röntgendiffractie en elektronenmicroscopie is aangetoond dat de Pd en Cu atomen gemengd zijn in de nanodeeltjes. Verder liet röntgenspectroscopie zien dat er een elektronische interactie is tussen Cu en Pd. De katalytische activiteit van de bimetallische deeltjes nam toe met toenemende Pd concentratie, maar bleef altijd lager dan voor een Pd katalysator zonder Cu. Ook de selectiviteit was afhankelijk van verhouding van de twee metalen, en nam iets toe voor de hogere Cu-tot-Pd verhoudingen. Deze invloed op de activiteit en selectiviteit met toenemende Pd concen-

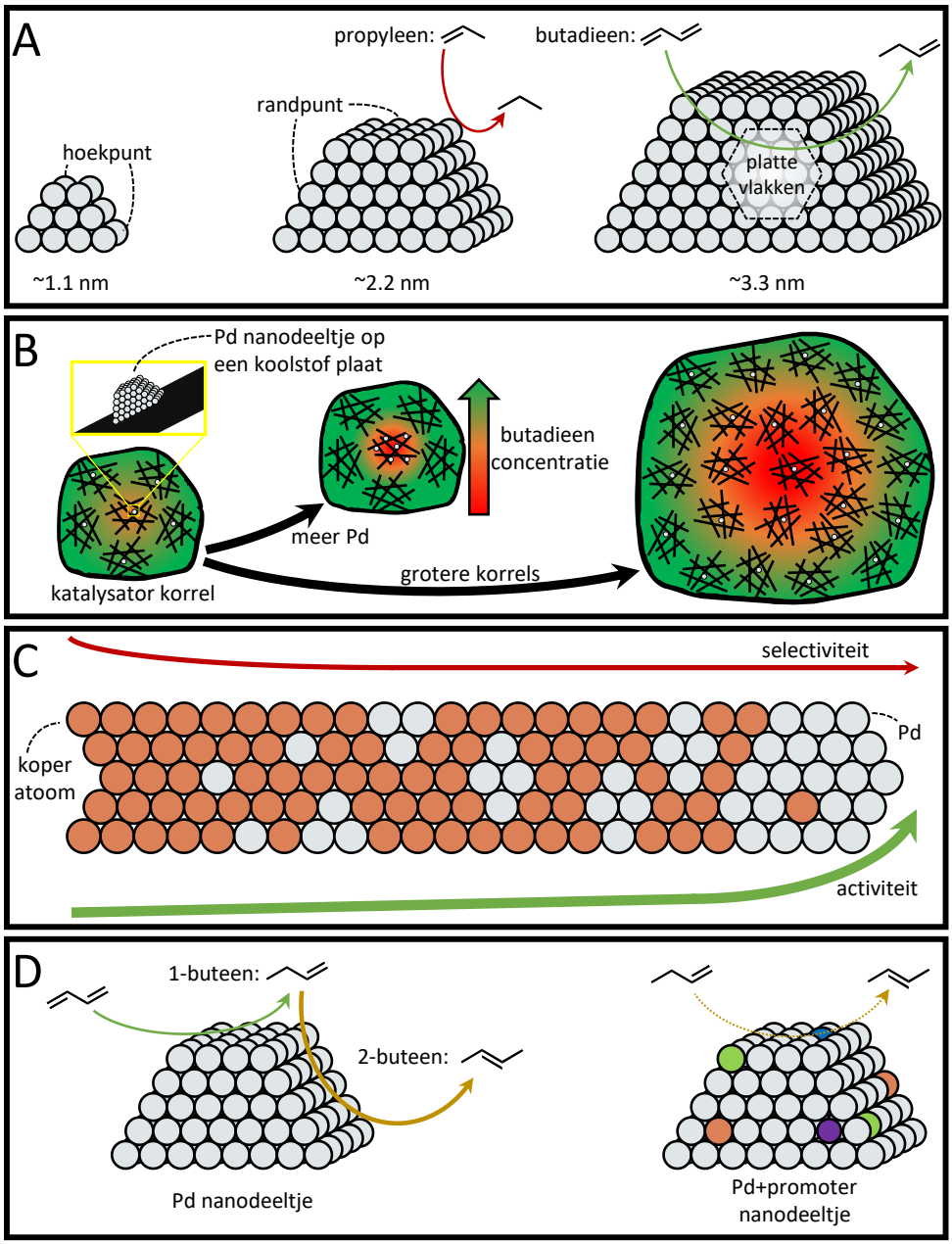

Figuur 7.4. Schematisch weergave van de experimentele hoofdstukken (2-5) uit dit proefschrift. (A) Hoofstuk 2: variatie van de deeltjesgrootte geeft een andere samenstelling van het oppervlak. (B) Hoofdstuk 3: een butadieen concentratie gradiënt ontstaat in de katalysator korrels, afhankelijk van de Pd concentratie en de korrelgrootte. (C) Met toenemende Pd-concentratie in bimetallische palladium-koper katalysatoren vormen grotere Pd-clusters, met toenemende activiteit. (D) Het toevoegen van een kleine hoeveelheid van een promoter metaal aan Pd nanodeeltjes beïnvloed de activiteit en selectiviteit.

tratie werd verklaard door een toenemende Pd clustergrootte, dat wil zeggen dat op het oppervlak van het katalytische metaaldeeltje meer Pd atomen zich naast elkaar bevonden (Figuur 7.4C).

In **Hoofdstuk 5** wordt het effect van verschillende "promoters" op de werking van Pd nanodeeltjes besproken. Hierbij werd een kleine hoeveelheid van een tweede metaal element (M) toegevoegd aan een bestaande Pd nanodeeltje. Voor het tweede metaal element zijn kalium (K), mangaan (Mn), koper (Cu), zink (Zn) en zilver (Ag) uitgekozen op basis van resultaten uit de wetenschappelijke literatuur. Onverwachts lieten alle 'gepromote' katalysatoren een lagere selectiviteit zien dan Pd/C. Ook was een hogere temperatuur nodig voor de volledige omzetting van butadieen. Interessant was dat de selectiviteit van de gevormde buteen producten wel verbeterde. Vooral met Zn- en Ag-toevoeging werd meer van het gewenste 1-buteen gemaakt, en minder 2-buteen (Figuur 7.4D). Deze verschillen in selectiviteit werden verder onderzocht met 1-buteen isomerisatie experimenten, waaruit ook bleek dat Zn- en Ag-toevoeging de sterkste invloed op de prestaties hadden.

Samenvattend; Hoofdstuk 2 benadrukt dat de vorm en grootte van een nanodeeltje uitmaakt voor welke moleculen er effectief op worden omgezet. In Hoofdstuk 3 wordt aangekaart hoe belangrijk het is om (naast de materialen) de reactiecondities zorgvuldig af te stemmen, om zinnige informatie uit de katalytische resultaten te krijgen. Hoofdstuk 4 beschrijft deeltjes met twee metalen en laat zien dat activiteit en selectiviteit van elkaar afhankelijk zijn, en dat twee niet altijd beter is dan één. Hoofdstuk 5 laat zien dat het toevoegen van een kleine hoeveelheid van een tweede metaal element de katalytische werking van Pd drastisch kan veranderen, met uiteenlopende resultaten afhankelijk van de toevoeging van verschillende elementen.

Deze inzichten leiden tot een beter begrip van Pd-gebaseerde katalysatoren voor selectieve hydrogenatie van butadieen, wat ook vertaald kan worden naar andere reacties. De meest vergelijkbare is de selectieve hydrogenatie van acetyleen, wat veel overlap in reactiecondities heeft.[13] Vandaar dat vooral effecten uit Hoofdstuk 3, ook voor acetyleen hydrogenatie een grote rol kunnen spelen. Voor hydrogenatie reacties in het algemeen, zijn Hoofstuk 4 en 5 interessant, waar de interactie van waterstof en andere reactanten op bimetallische deeltjes wordt belicht. Hier blijkt dat monometallisch Pd de meest actieve vorm is, maar dat een lagere activiteit wel kan leiden tot een betere selectiviteit. In een breder perspectief kunnen deze inzichten natuurlijk ook worden gebruikt voor andere metalen en reacties.

Referenties

1. Ma, Z. & Zaera, F. Heterogeneous Catalysis by Metals. in *Encyclopedia of Inorganic and Bioinorganic Chemistry* (Wiley, 2014). doi:10.1002/9781119951438.eibc0079.pub2.
2. Hutchings, G. *et al. Modern Developments in Catalysis*. vol. 2 (World Scientific, 2023).
3. International Monetary Fund. GDP, current prices. *World Economic Outlook* https://www.imf.org/external/datamapper/ngdpd@weo/oemdc/advec/weoworld (*October* 2023).
4. European Central Bank. Euro foreign exchange reference rates. https://www.ecb.europa.eu/stats/policy_and_exchange_rates/euro_reference_exchange_rates/html/eurofxref-graph-usd.en.html.
5. Zhang, L., Zhou, M., Wang, A. & Zhang, T. Selective Hydrogenation over Supported Metal Catalysts: From Nanoparticles to Single Atoms. *Chem. Rev.* **120**, 683-733 (2020).
6. Derrien, M. L. Chapter 18: Selective Hydrogenation Applied to the Refining of Petrochemical Raw Materials Produced by Steam Cracking. in *Studies in Surface Science and Catalysis* vol. 27 613-666 (1986).
7. Johnson Matthey. PGM prices and trading. *PGM prices and trading* https://matthey.com/products-and-markets/pgms-and-circularity/pgm-management (2023).
8. Bergeret, G. & Gallezot, P. Characterization of Solid Catalysts: Sections 3.1.1-3.1.3. in *Handbook of Heterogeneous Catalysis* vols 1-5 427-582 (Wiley-VCH Verlag GmbH, 2008).
9. Benavidez, A. D. *et al.* Improved selectivity of carbon-supported palladium catalysts for the hydrogenation of acetylene in excess ethylene. *Appl. Catal. A Gen.* **482**, 108-115 (2014).
10. De Jong, K. P. & Geus, J. W. Carbon Nanofibers: Catalytic Synthesis and Applications. *Catal. Rev. - Sci. Eng.* **42**, 481-510 (2000).
11. Gerber, I. C. & Serp, P. A Theory/Experience Description of Support Effects in Carbon-Supported Catalysts. *Chem. Rev.* **120**, 1250-1349 (2020).
12. Smith, A. W. Low-Temperature Thermal Conductivity of a Canadian Natural Graphite. *Phys. Rev.* **95**, 1095-1096 (1954).
13. Xie, K. *et al.* Catalysts for selective hydrogenation of acetylene: A review. *Mater. Today Catal.* **3**, 100029 (2023).

List of Publications and Presentations

This thesis is based on the following publications

Brandt Corstius, O.E., van der Hoeven, J.E.S., Sunley, G.J. & de Jongh, P.E. Influence of particle size in Pd-catalysed selective hydrogenation of 1,3-butadiene. *Journal of Catalysis*, 427, 115103 (2023).

Brandt Corstius, O.E., Kikkert, M., Roberts, S.T., Doskocil, E.J., van der Hoeven, J.E.S. & de Jongh, P.E. Mass transport effects in gas-phase selective hydrogenation of 1,3-butadiene over supported Pd. *Reaction Chemistry & Engineering,* Advance Article, (2024). DOI:10.1039/d4Rre00039k

Brandt Corstius, O.E., Nolten, H.L., Tierney, G.F., Xu, Z., Doskocil, E.J., van der Hoeven, J.E.S. & de Jongh, P.E. Tuneable bimetallic Pd_xCu_{100-x} catalysts for selective butadiene hydrogenation. *Catalysis Today,* under review, (2024).

Other publications by the author

De Kort, L.M., Brandt Corstius, O.E., Gulino, V., Gurinov, A., Baldus, M. & Ngene, P. Designing Highly Conductive Sodium-Based Metal Hydride Nanocomposites: Interplay between Hydride and Oxide Properties. *Advanced Functional Materials,* 33, 2209122 (2023).

Oral Presentations

15th European Congress on Catalysis (EuropaCat), 2023, Prague.
Bimetallic Pd-based catalysts for selective hydrogenation of butadiene.
Brandt Corstius, O.E., Nolten, H.L., Tierney, G.F., Xu, Z., Doskocil, E.J., van der Hoeven, J.E.S. & P.E. de Jongh

49th IUPAC World Chemistry Congress & 11th CHAINS, 2023, The Hague.
Bimetallic Pd-based catalysts for selective hydrogenation of butadiene.
Brandt Corstius, O.E., Nolten, H.L., Tierney, G.F., Xu, Z., Doskocil, E.J., van der Hoeven, J.E.S. & P.E. de Jongh

24th Netherlands' Catalysis and Chemistry Conference (NCCC), 2023, Noordwijkerhout.
Influence of palladium particle size on the selective hydrogenation of 1,3-butadiene.
Brandt Corstius, O.E., van der Hoeven, J.E.S., Roberts, S.T., Sunley, G.J. & P.E. de Jongh

27th North American Catalysis Society Meeting (NAM), 2022, New York.
Pd Particle Size Effects in Selective Hydrogenation of 1,3-butadiene.
Brandt Corstius, O.E., van der Hoeven, J.E.S., Roberts, S.T., Sunley, G.J. & P.E. de Jongh

26th Canadian Symposium on Catalysis (CSC), 2022, Vancouver
Pd Particle Size Effects in Selective Hydrogenation of 1,3-butadiene
Brandt Corstius, O.E., van der Hoeven, J.E.S., Roberts, S.T., Sunley, G.J. & P.E. de Jongh

10th Chemistry As Innovating Science (CHAINS), 2022, Veldhoven
Colloidally prepared CuPd/C catalysts for selective hydrogenation
Brandt Corstius, O.E., Nolten, H.L., Xu, Z., van der Hoeven, J.E.S. & P.E. de Jongh

Poster Presentations

23rd Netherlands' Catalysis and Chemistry Conference (NCCC), 2022, Noordwijkerhout
Palladium Particle Size Effects in Selective Hydrogenation of Butadiene and the impact of internal diffusion limitations
Brandt Corstius, O.E., van der Hoeven, J.E.S., Roberts, S.T., Sunley, G.J. & P.E. de Jongh

9th Chemistry As Innovating Science (CHAINS), 2021, Veldhoven
Palladium particle size effects in selective 1,3-butadiene hydrogenation
Brandt Corstius, O.E., van der Hoeven, J.E.S., Roberts, S.T., Sunley, G.J. & P.E. de Jongh

Acknowledgements | Dankwoord

Research is never done alone, and therefore there are several people I would like to thank for their contributions to this thesis. Some obvious ones, as they were directly involved in part of the research, and many more who indirectly aided me towards this point, where I can finally say I have finished my PhD. It has been a long journey that required not only scientific input from others, but also mentoring, motivation and perseverance from many around me.

Als eerste, **Petra**, mijn promotor, dankjewel voor de mogelijkheid mijn onderzoek te kunnen voltooien in de MCC-groep. Bedankt voor het vertrouwen dat je in me had om me een PhD plek aan te bieden, terwijl ik eigenlijk nog geen ervaring met katalyse had. Je bent onmisbaar geweest in het regelen van mijn buitenland tripjes, waaronder mijn stage in Engeland, waar ik mijn eerste katalyse ervaring kon opdoen. Het was dan ook bijzonder om je daar uit te nodigen voor een bezoekje. Ook bij terugkomst in Utrecht heb je me altijd veel vrijheid en vertrouwen gegeven om mijn eigen draai aan het onderzoek te geven. Je hebt een ontzettende passie en enthousiasme voor onderwijs én onderzoek waardoor ik erg graag met je samen heb gewerkt, zowel in het lab als in de collegezalen. Dankjewel voor de enorme hoeveelheid feedback die ik van je heb ontvangen op al mijn presentaties, publicaties, abstracts en dit proefschrift. Ik heb veel van je geleerd op zowel wetenschappelijk als persoonlijk niveau, en ik hoop dat dat wederzijds is.

Jessi, ontzettend fijn dat jij later in het project als copromotor bent aangesloten, op het begin al proactief met online meetings vanuit Boston en later in Utrecht. Je ervaring met bimetallische Pd-katalysatoren was erg waardevol voor meerdere hoofdstukken in dit proefschrift. Daarnaast heb je me veel bijgeleerd over wetenschappelijk schrijven en gedegen onderzoek doen. Je bent erg fijn om mee samen te werken, altijd attent, kritisch en scherp, je geeft veel vrijheid en goede adviezen en je vraagt ook om feedback voor jezelf. Al die eigenschappen zijn een voorbode dat je het ver gaat schoppen in je carrière.

Several researchers from BP have been of essential importance to this thesis. Thank you for the financial support for the project, but most importantly the fruitful scientific input that you have provided during our meetings. Thanks **Glenn**, for your inexhaustible curiosity for chemistry and catalysis, and for always raising the important questions (what about the water?). **Eric**, thank you for the assistance in many of the chapters in this thesis and my apologies for the overload of administration regarding the approval of many conference abstracts and research paper submissions. Thanks to **Tegan** and **Andreas** for joining our online and in-person meetings and providing valuable comments on the work. Lastly, **Zhuoran**, thank you for the clear communication in preparing, arranging, and performing the XAS measurements at APS. Dankjewel **Luc**, voor het zijn van mijn compagnon tijdens deze BP-UU samenwerking. Bedankt voor het meedenken en regelen van alle meetings en notuleren van alle (veel te snelle) suggesties die werden gegeven tijdens mijn presentaties.

Krijn, bedankt voor je interesse in mijn onderzoek en de input die je er tijdens mijn PhD op hebt gegeven. Het was ook fijn om les te geven met jou voor de klas. Met je enorme ervaring en rust die je uitstraalt ben je een genot om naar te luisteren, zowel voor studenten als werkcollegebegeleiders.

Special thanks go to **Peter**; without your enthusiasm I would not have joined MCC all those years ago for my MSc project, and who knows where I would have been by now. Many thanks for your interest in my project over the years, and always asking how my brother and parents were doing. I am happy that our work from 2019 was finally published in a journal suitable for this collaboration.

Now for my selective hydrogenation buddy, **Giorgio**. I've learned an incredible number of things from you related to the catalytic reaction we were studying. Moreover, you have always intrigued me with your engineering mindset. I will never forget when you explained to me how you performed a mass-balance calculation on your room to check if your air-conditioning was working properly. I will also never forget your face the morning after Italy won 3-0 against Turkey in the EURO2020 (which equaled 3 bottles of limoncello). I understand why I haven't seen you the days after Italy won the final. Thanks for all the help in the lab and the many laughs you gave me. I am happy to see we've both managed to finish this PhD journey.

Mijn palladium partner-in-crime, **Kristiaan**, verdient ook een eervolle benoeming. Ondanks dat je op geen een paper van mij staat als co-autheur, heb ik zeker met jou de meeste wetenschappelijk discussie gehad tijdens mijn PhD. Beiden waren we aan het zoeken hoe we palladium nou konden temmen om goede katalyse voor ons te doen. Grappig genoeg begon dit eigenlijk al 5 jaar geleden, vóor onze PhD, in Reading, waar we voor het eerste met dit wonderlijke metaal gingen werken. Dankjewel voor de vele serieuze discussies en niet serieuze momenten die we hebben gedeeld. Als je ooit nog iemand nodig hebt om je dak te dweilen of als er een deken in de douche staat, moet je maar een gil geven.

Iemand met wie ik eigenlijk mijn volledige 10 jaar in Utrecht heb gedeeld, is **Jelle**. Van de colleges in het eerste jaar, maatkolven aflezen met practicum, bubbels voor je BSc op de Rijnlaan, een 21-diner, de gele koker van de MSc uitreikingen tot nu het moment van de rode koker, overal ben je bij geweest. In die jaren hebben we veel excuses gehad om Europese hoofdsteden te bezoeken, van Londen, naar Parijs, naar Brussel, naar Amsterdam en Zürich, wat wordt de volgende?

Ik ben dan ook heel blij dat **Kristiaan** en **Jelle** mij wilden bijstaan als mijn paranimfen tijdens de verdediging van mijn proefschrift. Een waardig drietal voor een mooie dag.

Speciale dank gaat naar de studenten die ik heb mogen begeleiden tijdens mijn PhD project. Als eerste **Hidde**, je was mijn eerste student en ik wist niet goed hoe dat zou gaan, maar het is ongelooflijk goed bevallen. Onze wisselwerking was goed, en met je enorme efficiëntie en harde werken heb je zoveel gemaakt en gemeten dat het uiteindelijk niet allemaal in dit proefschrift terecht is gekomen. Ik denk dat je meer dan trots mag zijn als tweede auteur op het paper van hoofdstuk 4. Het deed me goed te zien

dat je na je stage als collega bent teruggekeerd naar Utrecht. Ook nog bedankt voor het borrelpakket op mijn laatste werkdag als bedankje voor het begeleiden van je MSc project, beter 2 jaar later dan nooit ;). Daarna kwam **Sonja**, die aan een uitdagend project begon. Met een uiterst georganiseerde aanpak, een uitgebreid literatuur-onderzoek en een strak werkplan, gingen we aan de slag. 'Helaas' werkte elke katalysator die we maakte minder goed dan Pd zelf; resultaten die een stuk moelijker op te schrijven zijn in een thesis. Desondanks heb je een prachtige thesis geschreven die grotendeels terug te vinden in hoofdstuk 5 van dit proefschrift. Je gestructureerde werken heeft het me erg makkelijk gemaakt om dit hoofdstuk af te maken, dankjewel daarvoor. Leuk om te zien dat je verder 'in mijn voetsporen' bent gegaan door de stage bij Johnson Matthey te doen. Toen ik jouw begeleider van JM later sprak op een conferentie was ook zij erg enthousiast over je! Jammer dat we elkaar net gemist hebben op de werkvloer bij je terugkeer in Utrecht. Als laatste heb ik **Marco** kort mogen begeleiden voor zijn BSc project. Het project stond al enigszins vast, maar alsnog ben je van onmiskenbare waarde geweest. Als een robot draaide je dagelijks twee katalytische testen erdoorheen, wat eigenlijk niet bij te houden was wat betreft data uitwerking. Deze grote hoeveelheid aan data heeft zijn weg gevonden in de systematisch aanpak van hoofdstuk 3, dankjewel daarvoor. Alle drie zijn jullie voorbeeldige studenten geweest en hebben jullie het mij erg gemakkelijk gemaakt. Het was altijd leuk, leerzaam en gezellig met jullie samen te werken en ik kan met zekerheid zeggen dat ik geen moment heb getwijfeld of ik het project niet beter zelf had kunnen uitvoeren.

Now there's one co-author left that has not been mentioned. Thank you, **George**, for the collaboration we've had, for the writing of beamtime proposals and arranging of the trips and detailed analysis of the XAS data. Your humor has made the long nightshifts and draining measurement days a little more doable for our little synchrotron crew consisting of you, me, Hidde and Kris. Although you could have warned Kris and me a little earlier that we were from drinking the decaf coffee during the night shifts in Diamond Light Source.

Onderzoek gaat niet zonder de grote groep aan ondersteunend personeel die we hebben bij MCC. Dankjewel **Jan Willem** voor al je hulp op het katalyse lab m.b.t het ombouwen van de set-up of oplossen van problemen. Bedankt voor de, af en toe zeer nodige, af en toe minder goed getimede, afleiding met het bespreken van verschillende bergkammen in de Alpen. Bedankt **Dennie**, voor de vele TGA-MS metingen voor mij en mijn studenten. Ik heb genoten van je humor en je snelle communicatie als er iets mis was met de XRD, zelfs als je zelf niet in Utrecht was. **Remco**, heel waardevol jou 'terug' te hebben op het lab. Dankjewel voor de onuitputbare stroom aan informatie als ik even een korte vraag kwam stellen, en alle voorbereidingen voor de XAS-metingen bij ROCK, samen met **Ad**. Met jullie beide heb ik altijd erg kunnen lachen. Dankjewel **Hans** en **Chris**, voor alles rondom het werkend houden van het elektronenmicroscopie centrum. Hans, bedankt voor de training op de TEMs, en vooral hoe snel je mij hebt toevertrouwd mijn eigen metingen te doen. Zodra er toch wat hulp nodig was stonden jij en Chris altijd klaar. Bedankt aan het secretariaat, **Ilonka** en **Silvia**, voor het begeleiden van mij en alle andere (PhD-)studenten in de groep. Jullie vangen veel van onze zorgen weg

waardoor we onze kunnen focussen op het onderzoek waar we eigenlijk mee bezig horen te zijn.

Dan blijft er nog een behoorlijke groep (oud-)collega's over die ik wil bedanken met wie ik afgelopen jaren veel zinnige en onzinnig momenten heb gedeeld. Als eerst **Suzan**, tegelijkertijd begonnen op onze eerste werkdag, en precies tegelijkertijd klaar met onze PhDs. We did it! Heel trots dat we het binnen contracttijd gedaan hebben. **Thimo**, thanks voor het gezelschap houden tijdens alle treinritten vanaf Amstel. Laat me weten als je nog eens thuisgebracht moet worden! **Jim**, bedankt vooral voor de grote hoeveelheid aan feestjes jij afgelopen jaren hebt georganiseerd. Dat heeft voor mij en veel collega's de nodige ontspanning geboden tijds stressvolle tijden! Met z'n 4en zijn we het eerste jaar Scheikunde in Utrecht begonnen en als klap op de voorpijl mochten we allemaal afgelopen Augustus naar EuropaCat in Praag. Dankjewel voor het mede mogelijk maken voor een top week, samen met **Jelle**, **Robin**, **Joris** en vele anderen.

Talking about conferences, it is of course impossible to forget the crew who joined me in a three-week-long adventure that stretched from Noordwijkerhout to Vancouver and New York City. **Francesco**, **Laura**, **Suzan**, **Nienke** and **Luc**, it was great to visit these beautiful places with you by my side. Thanks for the a-ma-zing (fake enthusiastic accent) walks in the woods of British Columbia, cycling through Central Park, birthday tequila shots on a rooftop and stunning views of Downtown Manhattan. Incredible to see all of us have graduated!

Iemand anders die ook op NAM was; **Erik**, je was de beste bureau-buurman mogelijk, vooral omdat je er eigenlijk nooit was. Wanneer je per ongeluk toch naar het DDW kwam om te werken was het altijd gezellig. Dankjewel voor het introduceren van Blender, je ziet dat de plaatjes het tot meerdere hoofdstukken hebben geschopt. Als beloning zal ik nog wat kleurrijke Excel-sheets opsturen. Joejoe.

Thanks for taking over the battery-related paper draft that remained after my MSc project, **Laura** and **Valerio**. Great to see it was finalised into such a beautiful piece of work and eventually published in a suitable journal.

Tijdens mijn tijd bij MCC heb ik meerdere borrels en feesten mogen organiseren. Dankjewel **Matt**, voor het mede opzetten van de borrelcommissie post-covid, en het beschikbaar stellen van een mooi jaarlijks budget voor onze opvolgers. Excuses voor alle boze blikken die ik je afgelopen jaren heb gegeven, het lag aan de data, niet aan jou. Samen met **Jelle** en **Sofie** hebben we ook de LIIT traditie weer tot leven gewekt, met groot succes vooral door de fantastische outfits en perfecte cocktails. Of waren we toch een ingrediënt vergeten? Een andere traditie die is opgezet, is de MOI-party van de drie (M, O en I) Chemistry and Catalysis groepen in het DDW. Thanks **Thomas** (OCC) en Thimo en Jim voor dit initiëren, wat hopelijk ook tot een traditie uitgroeit.

If you say 12:00, you say 'Lunch?', and not one minute later (except Broodje Ben Fridays, then it is 11:45), thanks to the obsessively on-time lunch crew; **Claudia**, **Juliette**, **Karan**, **Jonas**, **Just**, **Koen**, **Marta**, **Masoud, Henrik, Maaike, Matt** and many others

from MCC and ICC for the well-needed lunch breaks at M4. Apologies if I have forgotten to mention some of you.

Dan zijn we aangekomen bij de groepen die níet in Utrecht aan scheikundig onderzoek doen, en toch op een of andere manier hebben bijgedragen tot de totstandkoming van dit proefschrift. Als eerste de oudste groep, **jongens van het JvO**, ondertussen al meer dan 15 jaar onafgebroken vriendschap en vele mijlpalen samen mogen vieren. Mooi dat jullie ook bij dit feestje aanwezig zijn!

In mijn eerste werkweek als PhD ben ik op de **Parkstraat** gaan wonen en daarmee hebben de (oud-)bewoners mij een groot deel van mijn promotie daar meegemaakt. Dankjewel voor het aanhoren van mijn geklaag, het koken als ik laat thuiskwam en de verplichte ontspanning in de weekenden. Een paar van jullie zijn na mijn vertrek ook een PhD begonnen, dus blijkbaar is toch niemand afgeschrikt door mijn verhalen. Ik zal onze 10-persoons quarantaine-week niet snel vergeten.

Heren 10! Vrienden van het eerste uur in Utrecht. Dit jaar 10(!) jaar ploeggenoten en dat moet en zal gevierd worden. Thanks voor alle momenten, in voor- en tegenspoed, die we samen hebben meegemaakt. Tranen gelachen, onnozel gedaan, en ten slotte tevreden dit proefschrift afgeschreven. Op nog vele jaren kopstootjes, klaverjassen en verzaken; kortom vriendschap!

De **København** mannen, bijzonder dat we nog steeds geen andere benaming voor deze samenstelling hebben. Mooi om te zien dat we nu al jaren ons vaste eet- en kaartclubje hebben, wat ooit begon in de Deense hoofdstad heeft zich nu zelfs tot Grathem City uitgebreid, en wie weet binnenkort in San Francisco. Ooit ga ik echt leren bridgen, ik beloof het, maar tot die tijd moeten we nog maar veel excuses bedenken om samen te komen. Toet-toet!

Alle mannen van **Kampong 19** (of 23, of 21, in ieder geval kelderklasse), bedankt voor de vele woensdagavonden, iets minder zondagen en meerdere onvergetelijke weekendjes weg. Mooi ook vanuit Amsterdam nog vaak bij deze grote, maar toch hechte, groep van rare vogels (gieren) aan te mogen sluiten.

Dankjewel familie **Oostman** voor alle goede zorgen afgelopen jaren. Al vanaf mijn MSc hebben jullie interesse getoond in mijn onderzoek. Begin maart 2020, halsoverkop terug uit Parijs voor de lockdown, heb ik zelfs tijdelijk volledig onderdak gekregen bij jullie, en heb me vanaf het begin thuis gevoeld. Dankjewel voor de onvergetelijke vakantie naar Tanzania van afgelopen zomer. Zonder af en toe terug te denken aan die grote vakantie had ik het afschrijven van het proefschrift niet gehaald. Asante sana!

Dan mijn ouders, dank jullie wel. Jullie hebben mij altijd vrij gelaten om te doen en ontdekken wat ik zelf wilde, maar toch op een of andere manier de nieuwsgierigheid in mij geprikkeld om in het onderzoek te eindigen. Beiden niet chemisch opgeleid, maar toch altijd erg wetenschappelijk onderbouwd. **Pa**, bedankt voor je uitgebreide interesse in mijn onderzoek, het kritische uitvragen van de details en de toepassingen en het doorsturen van populaire wetenschappelijke krantenkoppen. **Mam**, bedankt voor je

belletjes en je moederlijke zorgen of alles wel goed ging met het proefschrift, het is uiteindelijk allemaal gelukt!

Als laatste, maar zeker niet de minste, toch wel de belangrijkste persoon van de afgelopen jaren, dankjewel **Charlotte**, voor al je steun, liefde en gezelschap. Vanaf het afschrijven van mijn BSc thesis, de keuze maken voor welk MSc project ik ging doen, tot de buitenlandstage (zelfs toen ik nog naar Amerika wilde, het werd gelukkig iets dichterbij) en uiteindelijk de PhD; overal ben je bij betrokken geweest en heb je me gesteund. Vooral ook bedankt voor de nodige schop onder m'n kont toen het leek alsof de thesis nooit af kwam. Het heeft uit uiteindelijk geholpen om op tijd klaar te zijn. We hebben laatste tijd al flink wat mijlpalen mogen vieren, en ik kan niet wachten tot de volgende avonturen die op ons pad komen. Ik hou van je!

About the Author

Oscar Brandt Corstius was born on the 1st of July 1996 in Amsterdam. He was raised in Soest and Amersfoort. For his secondary school education, Oscar went to the Stedelijk Gymnasium Johan van Oldenbarnevelt in Amersfoort, from which he graduated in 2014. That year, he started his Chemistry bachelor at Utrecht University, focusing on physical and inorganic chemistry. In 2015 and 2016, Oscar was a board member of the Science Honours Academy in the Faculty of Science. In 2017, he graduated *cum laude*, with a bachelor thesis on red-emitting materials for LEDs by upconversion luminescence in the group of prof. dr. Andries Meijerink at Condensed Matter and Interfaces. Oscar continued his studies at Utrecht University with the master programme of Nanomaterials Science in the Debye Institute. In 2019, he finished his master thesis project on the topic of 'Novel materials for solid-state-electrolytes in sodium-based batteries' under supervision of dr. Peter Ngene in the Materials Chemistry and Catalysis group. During his studies, Oscar was a teaching and lab assistant for several undergraduate and graduate courses. He also was an examination trainer in Chemistry for high school student at Stichting Studiebegeleding Leiden. Oscar joined Johnson Matthey plc at the Technology Centre in Sonning Common, United Kingdom, for an industrial internship as part of his master's degree. He graduated *cum laude* as Master of Science in September 2019.

Oscar returned to Utrecht University and started his PhD research in the Materials Chemistry and Catalysis group under the supervision of prof. dr. Petra de Jongh in October 2019. In 2021, dr. Jessi van der Hoeven joined the project as a co-promotor. During his research, Oscar worked on developing and understanding catalysts for the selective hydrogenation of butadiene. The main findings were published in peer-reviewed journals and presented at various international and national conferences on chemistry and catalysis. Besides his research, Oscar was a lab and teaching assistant for multiple bachelor and master courses. He supervised two Master thesis projects and one Bachelor thesis project during his PhD.

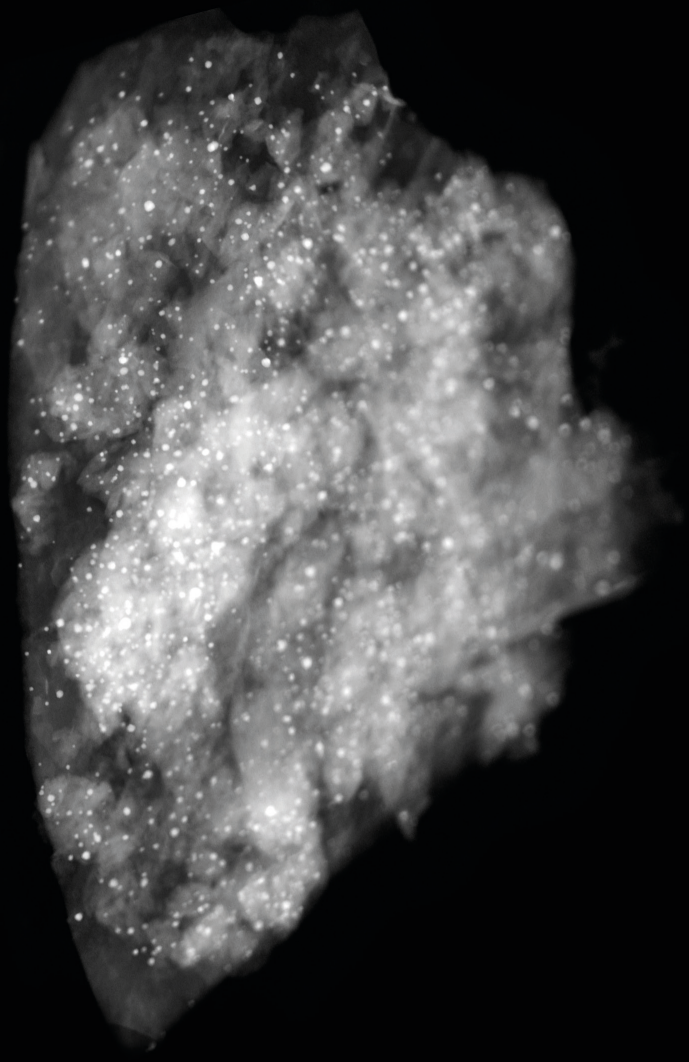

1:100 000